

University of Pardubice  
Faculty of Transport Engineering

Methodology of Thermal Stress Determination in Continuous Welded Rail

Petr Vnenk



METHODOLOGY OF THERMAL STRESS DETERMINATION  
IN CONTINUOUS WELDED RAIL

A DISSERTATION SUBMITTED TO  
THE FACULTY OF TRANSPORT ENGINEERING  
IN CANDIDACY FOR THE DEGREE OF  
DOCTOR OF PHILOSOPHY

BY  
PETR VNENK

PARDUBICE, CZECH REPUBLIC  
AUGUST 2022



Dedicated to all who listen before they speak.



7.

Whereof one cannot speak,  
thereof one must be silent.

— *Ludwig Wittgenstein*  
Tractatus Logico-Philosophicus





I hereby declare:

This thesis entitled Methodology of Thermal Stress Determination in Continuous Welded Rail was prepared separately. All the literary sources and the information I used in the thesis are listed in the bibliography.

I got familiar with the fact that the rights and obligations arising from the Act No. 121/2000 Coll., Copyright Act, apply to my thesis, especially with the fact that the University of Pardubice has the right to enter into a license agreement for use of this thesis as a school work pursuant to § 60, Section 1 of the Copyright Act, and the fact that should this thesis be used by me or should a license be granted for the use to another entity, the University of Pardubice is authorized to claim a reasonable contribution from me to cover the costs incurred during making of the thesis, according to the circumstances up to the actual amount thereof.

I am aware that my thesis will be accessible to the public in the University Library and via the Digital Library of the University of Pardubice in agreement with the article 47b of the Act No. 111/1998 Coll., on Higher Education Institutions, and on the Amendment and Supplement to some other Acts (the Higher Education Act), as subsequently amended, and with the University Pardubice's directive no. 7/2019.

This thesis was realized using the technologies of the Educational and Research Centre in Transport.

In Pardubice on 31<sup>st</sup> August 2022

Petr Vnenk  
*by own hand*



## **Study Programme**

Technique and Technology in Transport and Communications.

## **Study Field**

Transport Means and Infrastructure.

## **Supervisor**

Assoc. Prof. Bohumil Culek, Ph.D.

## **Supervising Department**

Department of Transport Structures.



## **Title**

Methodology of Thermal Stress Determination in Continuous Welded Rail

## **Annotation**

This dissertation deals with the stress determination in continuous welded rail and proposes a methodology to determine the development of the neutral temperature. It summarizes the current knowledge in this field and presents results of the performed research. The performed research covers problems of the rail temperature determination, specifically the investigation into the impact of air temperature, cloudiness and geography on the rail temperature; and problems of the continuous welded rail neutral temperature development, specifically the continuous welded rail strain monitoring and the determination of the neutral temperature development.

## **Keywords**

rail, temperature, stress, strain gauge, methodology

## **Anotace**

Tato práce se zabývá stanovením mechanického napětí v kolejnicích bezстыkové koleje a podává návrh metodiky ke stanovení vývoje neutrální teploty. Shrnuje současný stav poznání v tomto oboru a představuje výsledky provedeného výzkumu. Provedený výzkum zahrnuje témata stanovení teploty kolejnice, zejména výzkum vlivu teploty vzduchu, oblačnosti a geografie na teplotu kolejnice, a témata vývoje neutrální teploty kolejnic bezстыkové koleje, zejména sledování poměrného prodloužení kolejnic bezстыkové koleje a stanovení vývoje neutrální teploty.

## **Klíčová slova**

kolejnice, teplota, napětí, tenzometr, metodika



# Table of Contents

<b>List of Figures</b>	<b>xix</b>
<b>List of Tables</b>	<b>xxiii</b>
<b>List of Abbreviations</b>	<b>xxv</b>
<b>Acknowledgements</b>	<b>xxvii</b>
<b>Abstract</b>	<b>xxix</b>
<b>Abstrakt</b>	<b>xxxix</b>
<b>1 Introduction</b>	<b>1</b>
1.1 Motivation . . . . .	2
1.2 Research Objectives and Methodology . . . . .	2
1.3 Specifications of the Dissertation Concept . . . . .	3
<b>2 Current Knowledge</b>	<b>5</b>
2.1 History of Continuous Welded Rail . . . . .	5
2.2 Theory of Continuous Welded Rail . . . . .	5
2.3 Non-Destructive Methodologies of CWR Stress Determination . . . . .	11
2.3.1 Strain Methodologies . . . . .	11
2.3.2 Rail Shifting Methodologies . . . . .	15
2.3.3 Methodologies Based on Acoustoelastic Effect . . . . .	16
2.3.4 Methodologies Based on Magnetoelastic Effect . . . . .	20
2.3.5 Methodology Based on Steel Passive Layers Formation . . . . .	22
2.4 Rail Stresses . . . . .	22
2.4.1 Thermal Stress . . . . .	22
2.4.2 Stress from Track Operation . . . . .	23
2.4.3 Residual Stress . . . . .	24
2.4.4 Other Stresses and Stress Combinations . . . . .	25
<b>3 Rail Temperature</b>	<b>27</b>
3.1 Influence of Air Temperature and Cloudiness on Rail Temperature . . . . .	27
3.1.1 Experimental Setup . . . . .	27
3.1.2 Data Analysis . . . . .	28
3.1.3 Discussion . . . . .	32
3.2 Rail Temperature Monitoring in Selected Spots of the Czech Railway Network . . . . .	34

3.2.1	Experimental Setup . . . . .	34
3.2.2	Monitored Localities . . . . .	35
3.2.3	Data Analysis . . . . .	44
3.2.4	Discussion . . . . .	50
<b>4</b>	<b>Strain of Continuous Welded Rail</b>	<b>53</b>
4.1	Wheatstone Bridge Setup Analysis . . . . .	53
4.1.1	Experimental Setup . . . . .	53
4.1.2	Data Analysis . . . . .	55
4.1.3	Discussion . . . . .	61
4.2	Measuring Set for Diagnostics of Time-Based Development of Stress States in CWR	62
4.2.1	Technical Specifications . . . . .	63
4.3	CWR Strain Monitoring . . . . .	64
4.3.1	Monitored Localities . . . . .	65
4.3.2	Experimental Setup . . . . .	69
4.3.3	Data Collection . . . . .	69
<b>5</b>	<b>Neutral Temperature Development of Continuous Welded Rail</b>	<b>73</b>
5.1	Methodology of Non-Destructive Determination of Mechanical Stress in CWR . .	73
5.2	Data Analysis . . . . .	73
5.3	Discussion . . . . .	89
<b>6</b>	<b>Conclusions</b>	<b>99</b>
6.1	Further Research . . . . .	100
	<b>References</b>	<b>101</b>
<b>A</b>	<b>Rail Temperature Recordings</b>	<b>107</b>
<b>B</b>	<b>Measurement Uncertainty Determination</b>	<b>123</b>
B.1	Type A Evaluation of Uncertainty . . . . .	123
B.2	Type B Evaluation of Uncertainty . . . . .	124
B.2.1	Strain Gauge Uncertainty . . . . .	124
B.2.2	Uncertainty of Strain Gauge – Data Acquisition System Cable . . . . .	127
B.2.3	Data Acquisition System Uncertainty . . . . .	127
B.2.4	Uncertainty of Data Acquisition System – Personal Computer Cable . . .	128
B.2.5	Uncertainty of PC Hardware . . . . .	128
B.2.6	Uncertainty of PC Hardware . . . . .	128
B.2.7	Type B Total Evaluation of Uncertainty . . . . .	128
B.3	Combined Evaluation of Uncertainty . . . . .	128
B.4	Expanded Evaluation of Uncertainty . . . . .	129
<b>C</b>	<b>CWR Strain Recordings</b>	<b>131</b>
C.1	Chotěvice . . . . .	132



C.1.1	Daily Recordings . . . . .	132
C.1.2	Weekly Recordings . . . . .	143
C.1.3	Monthly Recordings . . . . .	154
C.2	Bezprávi . . . . .	165
C.2.1	Daily Recordings . . . . .	165
C.2.2	Weekly Recordings . . . . .	169
C.2.3	Monthly Recordings . . . . .	173
<b>D</b>	<b>Relation of Strain and Temperature</b>	<b>177</b>
D.1	Chotěvice . . . . .	178
D.2	Bezprávi . . . . .	200
<b>E</b>	<b>Development of Measured and Extrapolated Temperature Difference</b>	<b>209</b>
E.1	Chotěvice . . . . .	210
E.2	Bezprávi . . . . .	221
<b>F</b>	<b>Comparison of Temperature Differences per Cross-Sectional Profiles</b>	<b>225</b>
F.1	Chotěvice . . . . .	226
F.2	Bezprávi . . . . .	229
<b>G</b>	<b>Comparison of Standard and New Approach to the Thermal Stress Determination in CWR</b>	<b>231</b>
	<b>Annexes</b>	<b>241</b>



# List of Figures

2.1	Rail Element for the Equilibrium Investigation . . . . .	7
2.2	Relation of Longitudinal Resistance to Displacement . . . . .	8
2.3	Axial Force in Breathing Length of CWR . . . . .	9
2.4	MS-02 Extensometer for Measurement of the Longitudinal Forces in Rails . . .	11
2.5	Rail Stress Monitoring Device . . . . .	12
2.6	Layout of FBG Sensors . . . . .	13
2.7	Rail Specimen Instrumented with Strain Gauge and Optical Fibres . . . . .	14
2.8	Vortok Measure and Detect . . . . .	15
2.9	Vortok VERSE Methodology . . . . .	15
2.10	Vertical Ultrasound Measurement . . . . .	17
2.11	Horizontal Ultrasound Measurement . . . . .	17
2.12	Trajectory Plot of Particle Motion for Unstressed and Stressed Rail Steel . . .	18
2.13	Plot of Unworn 136RE Rail Study Results . . . . .	19
2.14	Plot of Worn 136RE Rail Study Results . . . . .	19
2.15	Coercivity and Remanence Measured on Milled and Scaled Surfaces of the Test Rail . . . . .	20
2.16	$dH_p(y)/dx$ for Applied Tensile Stress on a Steel Sample . . . . .	21
2.17	Thermal Stress Distribution . . . . .	23
2.18	Vertical Wheel Load Stress . . . . .	23
2.19	Residual Internal Stress in Rail . . . . .	24
2.20	Combination of Stresses in Rail . . . . .	25
3.1	Layout of the Rail Head Temperature Measurement . . . . .	28
3.2	Rail Head and Reference Temperature Record 29 <sup>th</sup> March – 12 <sup>th</sup> April 2017 . .	28
3.3	Measuring Stations of the Czech Hydrometeorological Institute . . . . .	29
3.4	Relation between Cloudiness and Temperature Difference . . . . .	30
3.5	Relation between Air Temperature and Temperature Difference . . . . .	31
3.6	Relation between Cloudiness, Air Temperature and Temperature Difference . .	32
3.7	Comparison of Measured Rail Temperature and Calculated Rail Temperature .	32
3.8	Comparison of Data from Figure 6.1 of the EN 1991-1-5 and the Analytically Calculated Data from the Measurements . . . . .	33
3.9	Card Thermometer with Built-in Data-Logger – Type Elitech ETAG-1 . . . . .	34
3.10	Card Thermometer with Built-in Data-Logger – Type Elitech TI-2S . . . . .	34
3.11	Card Thermometer Holder – Top View . . . . .	35

3.12	Card Thermometer Holder – Side View . . . . .	35
3.13	Borovnice Locality . . . . .	36
3.14	Position of the Thermometer at the Left Side of the Rail Web in the Borovnice Locality . . . . .	37
3.15	Detailed View on the Position from Figure 3.14 with the Thermometer at the Rail Foot Partly Visible . . . . .	37
3.16	Ostružná Locality . . . . .	38
3.17	Ostružná Locality – Position of a Thermometer on the Rail Bridge . . . . .	38
3.18	Ostružná Locality – Position of a Thermometer on the Embankment . . . . .	38
3.19	Position of the First Thermometer in Hradec Králové Locality . . . . .	39
3.20	Position of the Second Thermometer in Hradec Králové Locality . . . . .	39
3.21	Hradec Králové Locality – Position of a Thermometer in Pražské předměstí District . . . . .	40
3.22	Hradec Králové Locality – Position of a Thermometer in Slezské předměstí District	40
3.23	Position of the First Thermometer in Karviná Locality . . . . .	40
3.24	Position of the Second Thermometer in Karviná Locality . . . . .	41
3.25	Karviná Locality – Position of a Thermometer in Karviná-Darkov Stop . . . . .	41
3.26	Karviná Locality – Position of a Thermometer next to the Railway Crossing . .	41
3.27	Position of the First Thermometer in Harrachov Locality . . . . .	42
3.28	Position of the Other Four Thermometers in Harrachov Locality . . . . .	43
3.29	Harrachov Locality – Position of a Thermometer in Polubenský Tunnel . . . . .	43
3.30	Harrachov Locality – Position of a Thermometer in the Rock Cutting . . . . .	43
3.31	Rail Temperature Recordings in Borovnice Locality . . . . .	45
3.32	Rail Temperature Recordings in Ostružná Locality . . . . .	46
3.33	Rail Temperature Recordings in Hradec Králové Locality . . . . .	47
3.34	Rail Temperature Recordings in Karviná Locality . . . . .	48
3.35	Rail Temperature Recordings in Harrachov Locality . . . . .	49
3.36	Difference in Railway Line Azimuth of Borovnice and Hradec Králové – Slezské předměstí Localities . . . . .	50
4.1	Scheme of the Sample Geometry . . . . .	54
4.2	Steel Sample with the Half and Quarter Bridge Configurations . . . . .	54
4.3	Steel Sample Positioned in the Dynamic Stand . . . . .	55
4.4	Relation of Measured Strain and Axial Force . . . . .	56
4.5	Relation of Normal Stress and Axial Force . . . . .	56
4.6	Relation of Measured Strain and Temperature . . . . .	58
4.7	Relation of Normal Stress and Temperature . . . . .	58
4.8	Relation of Measured Strain and Temperature . . . . .	59
4.9	Relation of Normal Stress and Temperature . . . . .	59
4.10	Relation of Displacement and Temperature . . . . .	60
4.11	Relation of Measured Strain and Temperature . . . . .	60
4.12	Relation of Normal Stress and Temperature . . . . .	60

4.13	Measuring Set Track Unit . . . . .	63
4.14	Measuring Set Mobile Unit . . . . .	64
4.15	Locality Borovnice . . . . .	66
4.16	Locality Ostopovice . . . . .	67
4.17	Locality Chotěvice . . . . .	68
4.18	Locality Bezpráví . . . . .	69
4.19	Aggregated CWR Strain Record in the Chotěvice Locality in the Period of Daily Monitoring . . . . .	70
4.20	Aggregated CWR Strain Record in the Chotěvice Locality in the Period of Weekly Monitoring . . . . .	71
4.21	Aggregated CWR Strain Record in the Chotěvice Locality in the Period of Monthly Monitoring . . . . .	71
4.22	Aggregated CWR Strain Record in the Bezpráví Locality in the Period of Daily Monitoring . . . . .	71
4.23	Aggregated CWR Strain Record in the Bezpráví Locality in the Period of Weekly Monitoring . . . . .	72
4.24	Aggregated CWR Strain Record in the Bezpráví Locality in the Period of Monthly Monitoring . . . . .	72
5.1	C.VIII.1 – Daily Measurement Period Database . . . . .	74
5.2	C.VIII.1 – Complete Monitoring Period Database . . . . .	74
5.3	Scheme of a Change in the Absolute Coefficient of the Strain-Temperature Polynomial upon a Sample Pre-Stress Change . . . . .	76
5.4	Scheme of a Change in the Linear Coefficient of the Strain-Temperature Polynomial upon a Support Fixation Rigidity Change . . . . .	76
5.5	C.V.3 – Measured and Extrapolated Temperature, and Their Difference . . . . .	77
5.6	D.I – Cluster of Calculated CWR Neutral Temperature Changes . . . . .	78
5.7	D.II – Cluster of Calculated CWR Neutral Temperature Changes . . . . .	78
5.8	D.III – Cluster of Calculated CWR Neutral Temperature Changes . . . . .	78
5.9	D.IV – Cluster of Calculated CWR Neutral Temperature Changes . . . . .	78
5.10	Example of an Outlier Identification in the Case of Bezpráví CWR Strain Recordings – Day 212 . . . . .	89
5.11	Probability Density of Normal Distribution of LTCAS from the First Week of Measurements in the Chotěvice Locality . . . . .	90
5.12	Probability Density of Normal Distribution of LTCAS from All Measurements in the Chotěvice Locality . . . . .	90
5.13	Comparison of Probability Density Function for the Chotěvice Locality . . . . .	90
5.14	Probability Density of Normal Distribution of LTCAS from the First Week of Measurements in the Bezpráví Locality . . . . .	91
5.15	Probability Density of Normal Distribution of LTCAS from All Measurements in the Bezpráví Locality . . . . .	91
5.16	Comparison of Probability Density Function for the Bezpráví Locality . . . . .	91

5.17	C.VI.1 – Measured Temperature, Extrapolated Temperature, and Temperature Difference . . . . .	93
5.18	C.VI.2 – Measured Temperature, Extrapolated Temperature, and Temperature Difference . . . . .	93
5.19	D.I – Left Rail: Comparison of Standard and New Approach to the Thermal Stress Determination in CWR . . . . .	96
5.20	D.I – Right Rail: Comparison of Standard and New Approach to the Thermal Stress Determination in CWR . . . . .	96
5.21	D.II – Left Rail: Comparison of Standard and New Approach to the Thermal Stress Determination in CWR . . . . .	96
5.22	D.II – Right Rail: Comparison of Standard and New Approach to the Thermal Stress Determination in CWR . . . . .	96
5.23	D.III – Left Rail: Comparison of Standard and New Approach to the Thermal Stress Determination in CWR . . . . .	97
5.24	D.III – Right Rail: Comparison of Standard and New Approach to the Thermal Stress Determination in CWR . . . . .	97
5.25	D.IV – Left Rail: Comparison of Standard and New Approach to the Thermal Stress Determination in CWR . . . . .	97
5.26	D.IV – Right Rail: Comparison of Standard and New Approach to the Thermal Stress Determination in CWR . . . . .	97

# List of Tables

3.1	Cloudiness and Average Temperature Difference . . . . .	30
3.2	Temperature Data Collection Periods per Locality . . . . .	44
3.3	Extreme Temperature Measured per Thermometer . . . . .	44
4.1	Loading by Normal Force at Constant Temperature . . . . .	57
4.2	Thermal Loading of Sample Fixed at Both Ends . . . . .	58
4.3	Thermal Loading of Sample Fixed at Both Ends and Pre-Tensioned by Axial Force of 30 kN . . . . .	59
4.4	Thermal Loading of Sample Fixed at One End Only . . . . .	61
5.1	Chotějvice – LTCAS of the Temperature-Strain Relation . . . . .	75
5.2	Bezprávi – LTCAS of the Temperature-Strain Relation . . . . .	76
5.3	Measuring Spot D.I – CWR Neutral Temperature Changes . . . . .	79
5.4	Measuring Spot D.II – CWR Neutral Temperature Changes . . . . .	79
5.5	Measuring Spot D.III – CWR Neutral Temperature Changes . . . . .	80
5.6	Measuring Spot D.IV – CWR Neutral Temperature Changes . . . . .	80
5.7	Measuring Spot D.I – Neutral Temperature Values over Time . . . . .	81
5.8	Measuring Spot D.II – Neutral Temperature Values over Time . . . . .	81
5.9	Measuring Spot D.III – Neutral Temperature Values over Time . . . . .	82
5.10	Measuring Spot D.IV – Neutral Temperature Values over Time . . . . .	82
5.11	Measuring Spot D.I – Instant Temperature Values over Time . . . . .	83
5.12	Measuring Spot D.II – Instant Temperature Values over Time . . . . .	83
5.13	Measuring Spot D.III – Instant Temperature Values over Time . . . . .	84
5.14	Measuring Spot D.IV – Instant Temperature Values over Time . . . . .	84
5.15	Measuring Spot D.I – Left Rail: Instant Rail Temperature, Neutral Temperature and Thermal Stress . . . . .	85
5.16	Measuring Spot D.I – Right Rail: Instant Rail Temperature, Neutral Temperature and Thermal Stress . . . . .	85
5.17	Measuring Spot D.II – Left Rail: Instant Rail Temperature, Neutral Temperature and Thermal Stress . . . . .	86
5.18	Measuring Spot D.II – Right Rail: Instant Rail Temperature, Neutral Tempera- ture and Thermal Stress . . . . .	86
5.19	Measuring Spot D.III – Left Rail: Instant Rail Temperature, Neutral Temperature and Thermal Stress . . . . .	87

5.20 Measuring Spot D.III – Right Rail: Instant Rail Temperature, Neutral Temperature and Thermal Stress . . . . .	87
5.21 Measuring Spot D.IV – Left Rail: Instant Rail Temperature, Neutral Temperature and Thermal Stress . . . . .	88
5.22 Measuring Spot D.IV – Right Rail: Instant Rail Temperature, Neutral Temperature and Thermal Stress . . . . .	88



# List of Abbreviations

*In alphabetical order:*

- a. s. – *Czech: akciová společnost*, Joint-Stock Company
- AL – *Czech: akademická laboratoř*, Academic Laboratory
- AMSL – Above Mean Sea Level
- Co. – Company
- CWR – Continuous Welded Rail
- ČSM – *Czech: československá mládež*, Czechoslovak Youth
- DFJP – *Czech: Dopravní fakulta Jana Pernera*, Faculty of Transport Engineering
- ERCT – Educational and Research Centre in Transport
- FBG – Fiber Bragg Grating
- GmbH – *German: Gesellschaft mit beschränkter Haftung*, Company with Limited Liability
- HBM – Hottinger Baldwin Messtechnik
- HH – Heavy Haul
- KG – *German: Kommanditgesellschaft*, Limited Partnership Business Entity
- LTCAS – Linear Thermal Coefficient of Apparent Strain
- Ltd. – Limited Company
- MZ – *Czech: metodika zkoušky*, Test Methodology
- N – North
- NE – North-East
- NFC – Near-Field Communication
- PC – Personal Computer
- RUD – Rail Uplift Device
- S – South
- s. o. – *Czech: státní organizace*, State Company
- SW – South-West
- SŽDC – *Czech: Správa železniční dopravní cesty*, Czech Railway Infrastructure Manager
- TAČR – *Czech: Technologická agentura České republiky*, Technological Agency of the Czech Republic
- UIC – *French: Union internationale des chemins de fer*, International Union of Railways
- US – United States
- USA – United States of America



# Acknowledgements

I would like to express my gratitude to Assoc. Prof. Dr. Bohumil Culek in the first place, for his patience, guidance, and mentoring. Learning from him was a great experience for me both professionally and personally.

My gratitude belongs to Assoc. Prof. Dr. Ladislav Řoutil, too, for his mentoring and precious pieces of scientific advice.

Special gratitude belongs to Dr. Özgür Yurdakul, who spent with me many days of scientific discussions and I learned a lot from him.

Special gratitude and appreciation belongs to Assoc. Prof. Dr. Otto Plášek from Brno University of Technology, who was always open to discuss any topic that was needed and his contribution to my knowledge of railway engineering was immense.

I am very grateful to Petr Szabó from Správa železnic and Miroslav Ďurkovský from Železnice Slovenskej republiky for their valuable practical insights.

I am grateful to all members of our TAČR Zéta project research team, namely Assoc. Prof. Dr. Bohumil Culek, Assoc. Prof. Dr. Ladislav Řoutil, Dr. Özgür Yurdakul, Dr. Ondřej Sadílek, Dr. Vladimír Suchánek, Jiří Šlapák, Filip Klejch, Veronika Fričová, Zdeněk Sháněl, Karel Suchý, Miloš Šula, Tadeáš Šustr, Vojtěch Adamec, Rudolf Šudík, Akhil Avula, Anvesh Bhagirathi and Manish Kumar Labishetty. The project could never be finished and the presented work could never exist in such an extensive scope without your tireless contributions.

I would like to thank very much to Assoc. Prof. Dr. Petr Voltr and Dr. Aleš Šmejda, heads of my departments, for their great understanding and for providing me with a lot of room and support for realization of my ideas.

I am thankful to Filip Ševčík, Dr. Martin Jacura, Dr. Vladislav Borecký, Dr. Pavel Lopour, Dr. Martin Kohout, Dr. Jakub Vágner, Dr. Aleš Hába, Dr. Tomáš Michálek and Assoc. Prof. Dr. Jaromír Zelenka from whom I learned.

I am very thankful to all other members of my university departments, who were able to create a very good team, in which it was a pleasure to work.

My gratitude belongs to many people from which I learned a lot of scientific work during my study stays abroad in doctoral studies, most notably Prof. Dr.-Ing. Benno Hoffmeister, Dr.-Ing. Carl Richter, Dr.-Ing. Daniel Pak, Dr.-Ing. Hetty Bigelow, Dr.-Ing. Dominik Pyschny and Dr.-Ing. Marius Pinkawa from the RWTH Aachen University, Prof. Dr. Zdenka Popović, Assoc. Prof. Dr. Luka Lazarević and Dr. Nikola Mirković from the University of Belgrade, Prof. Dr. Władysław Koc, Prof. Dr. Piotr Chrostowski, Dr. Sławomir Grulkowski, Dr. Jacek Szmagliński, and Dr. Kamila Szwaczekiewicz from the Gdańsk University of Technology. Thanks

to all of you, I always felt like at home wherever I was.

I am very thankful to Jan Zicha, PE, who was the person that guided me to the research topic, which is elaborated in this dissertation.

I thank my friends, on whom I can always rely.

Above all, I thank my family for their endless support, care and understanding.

# Abstract

Continuous welded rail (CWR) became an integral part of railway tracks over the past decades. With expansion of the CWR into more and more railway tracks all over the world, better understanding of its behaviour and internal stress is required, and research on the CWR grows on importance. Focus on search for a non-destructive methodology of rail thermal stress determination has been one of the leading engineering tasks in the field. Studies summarizing the efforts are presented in papers and works [1, 2, 3, 4, 5, 6].

Current knowledge is summarized in the beginning of the dissertation. A brief introduction into the CWR history and theory is presented. Research into the existing methodologies and efforts to determine the CWR stress is shown and shortly discussed. The chapter concludes with a brief overview on the stress types in rail.

Investigation into some aspects of rail heating and rail temperature records are presented in the third chapter. The rail temperature investigation is crucial for the CWR stress determination and various research aims can be followed. In the first part of this chapter, empirical analysis of the cloudiness and air temperature influence is presented. Further, results of field investigation into the rail temperature are discussed. Information on the instant rail temperature in the railway network is important for a reliable determination of the rail stress or the rail neutral temperature change.

The fourth chapter comprises of research into CWR strain. The CWR strain knowledge is essential for the determination of the rail neutral temperature change. In the first part of the chapter, design of an experimental setup is analysed. A quarter bridge configuration was evaluated as the most effective one, providing sufficient precision of measurement, high resiliency in the railway track and quick installation. Functioning sample, *Measuring Set for Diagnostics of Time-Based Development of Stress States in CWR*, designed based on the analysis result is further introduced. An extensive investigation into the CWR strain measurement and further analysis conclude the chapter.

The fifth chapter introduces the *Methodology of Non-Destructive Determination of Mechanical Stress in CWR* and analyses the CWR strain data presented and discussed in the preceding chapter. A proposition of the thermal stress determination in CWR and the rail neutral temperature change is given in this chapter. The dissertation concludes with recommendations on further research. Upon resolving the questions raised by this dissertation and analysing more data, the presented approach can serve for a better and economically feasible determination of thermal stress in CWR and rail neutral temperature change over time.



# Abstrakt

Bezстыková kolej se v posledních dekáдах stala integrální součástí konstrukce železničních tratí. Spolu s tím, jak se její použití rozšiřuje do stále více kolejí po celém světě, roste potřeba lepšího pochopení jejího chování a rozložení vnitřního napětí. Proto také roste význam výzkumu bezстыkové koleje. Snaha o nalezení nedestruktivní metodiky stanovení kolejnicového napětí od tepelného působení se stala předním inženýrským úkolem v této oblasti. Studie shrnující pokusy v této oblasti jsou presentovány ve člancích a pracích [1, 2, 3, 4, 5, 6].

V úvodu disertace je shrnut současný stav poznání. Začíná stručným úvodem do historie a teorie bezстыkové koleje. Dále je sepsána rešerše existujících metodik a snah o stanovení napětí v bezстыkové koleji, která je také krátce komentována. Kapitulu uzavírá stručný přehled typů v koleji se vyskytujícími napětí.

Ve třetí kapitole je představen výzkum některých aspektů tepelného zatížení kolejnice a související teplotní záznamy. Výzkum teplot kolejnice je pro stanovení napětí v bezстыkové koleji klíčový a zároveň mohou být v rámci výzkumu sledovány různé výzkumné cíle. V první části této kapitoly je představena empirická analýza vlivu oblačnosti a teploty vzduchu na teplotu kolejnice. Dále jsou diskutovány výsledky terénního měření teploty kolejnic. Informace o aktuální teplotě kolejnice v železniční síti je důležitá pro spolehlivé stanovení napětí v kolejnici nebo změny neutrální teploty kolejnice.

Čtvrtá kapitola obsahuje výzkum poměrné deformace bezстыkové koleje. Její znalost je nezbytná pro stanovení změny neutrální teploty kolejnice. V první části kapitoly je analyzován návrh experimentální sestavy pro měření poměrné deformace bezстыkové koleje. Čtvrtmostové zapojení bylo vyhodnoceno jako nejefektivnější, neboť poskytuje dostatečnou přesnost měření v kombinaci s vysokou odolností v koleji a rychlostí instalace. Dále je představen funkční vzorek *Měřicí sestavy pro diagnostiku časového vývoje napěťových stavů v bezстыkové koleji*, jenž byl navržen v souladu s výsledky analýzy. Kapitulu uzavírá rozsáhlý výzkum poměrného prodloužení bezстыkové koleje.

V páté kapitole je představena *Metodika nedestruktivního stanovení mechanického napětí v kolejnicích bezстыkové koleje* a dále je analyzováno poměrné prodloužení bezстыkové koleje, které je představeno a diskutováno v předcházející kapitole. V páté kapitole je rovněž předložen návrh stanovení napětí od tepelného namáhání bezстыkové koleje a změny neutrální teploty kolejnice. Disertační práci uzavírají doporučení k dalšímu výzkumu. Přístup, jenž je v této práci představen, může po vyřešení otázek touto prací vznesených a analýze většího množství dat sloužit pro lepší a ekonomicky schůdné stanovování mechanického napětí v bezстыkové koleji od tepelného zatížení a změny neutrální teploty kolejnice v čase.





# Chapter 1

## Introduction

Continuous welded rail (further referred to as *CWR*) is nowadays an integral part of railway superstructure [7, 8]. It substitutes the original concept of jointed rail and is being installed into more and more railway lines all over the world every year. It offers many advantages in contrary to the jointed rail. The ride is calmer, more comfortable for passengers, wear and deterioration is reduced both at the rolling stock and the infrastructure, and safety level is increased. With these advantages, it contributes to an efficient and sustainable development of the railway network in the world and provides substantial financial savings [9, 10].

Many advantages provided by the CWR carry one problem, however. The change of rail temperature cannot be settled by rail dilation, as it is in the case of jointed track, but a thermal stress of positive or negative value occurs in the rail. In order to safely manage and control the rail stress, a way of reliable determination of the thermal stress shall be found. Many attempts to determine the instant value of the thermal stress were made over the last decades, but none of them was able to provide a satisfactory solution that would get widespread all over the world [1]. Various other attempts were done in order to simulate the problem numerically, which is a great asset to better understanding of the problem [11, 12].

This dissertation investigates new options to determine the CWR thermal stress by determination of the CWR neutral temperature change in a non-destructive way. Current knowledge is summarized in the introductory chapter and research into the aspects of the rail temperature and CWR strain development is presented in the following ones. A methodology of the CWR neutral temperature development determination, derivation of which builds upon the presented investigation, is introduced in Chapter 5. A brief conclusion and a suggestion for further research close the dissertation. Many detailed graphs from the data obtained during the research are published in the appendices.

The performed research presented in this dissertation partially builds upon research done within the scope of the research project No. TJ04000301 *Non-Destructive Determination of Mechanical Stress in Continuous Welded Rail*, of which the author was a principal investigator.

## 1.1 Motivation

Modern industry requires non-destructive monitoring of structures, as it improves the economical efficiency of the operation and maintenance. The worldwide spread of CWR emphasized the need to be informed of the thermal stress in CWR in order to prevent costly failures of railway track – track buckling and rail break [8, 13]. A methodology of direct CWR stress measurement has been investigated for decades, so far without satisfactory results [1]. At the same time, demand to gain reliable data on thermal stress in CWR has been rising as the problem became a topic all over the world. The length of railway tracks with CWR is on increase every year, and so do the average train speeds.

While research for a direct CWR stress measurement shall continue, it is necessary to investigate other approaches to get the needed data. Approaches that use indirect measurement of stress, but affordable and with a high level of accuracy, may contribute to satisfaction of the need for data. One approach of this kind is investigated in this dissertation. While some attempts were already made to use the strain gauges to monitor the CWR strain, they were usually deployed on a very limited track section [14] or a sample only [15, 16]. Large-scale deployment, in the scope presented in this dissertation, is unique.

## 1.2 Research Objectives and Methodology

Direct stress measurement in a material is a large problem of basic research. Considering the available facilities and limited resources for doctoral research, the research objectives can be summarized as follows:

1. to investigate current knowledge in the field of CWR stress determination,
2. to identify important parameters influencing rail temperature and quantify their impact,
3. to develop a methodology of non-destructive CWR thermal stress determination.

The third objective was the ultimate target, towards which a relatively extensive research and equally important partial investigation efforts aimed. The research methodology applied within the presented research can be listed as follows:

- analysis of stress, force, and strain of CWR and breathing length,
- analysis of current knowledge on CWR stress determination,
- theoretical description of rail stresses,
- derivation of impact of selected parameters on rail temperature,
- comparison of development of measured rail temperature in localities of various attributes,
- analysis of Wheatstone quarter bridge behaviour under thermal loading of a sample and comparison to half bridge behaviour,

- development and construction of a measuring set for CWR strain measurement in railway tracks under operation,
- CWR strain data analysis and synthesis,
- development of a mathematical model of CWR neutral temperature determination.

### **1.3 Specifications of the Dissertation Concept**

Some of the research results presented by this dissertation were reached in the course of investigation of the research project No. TJ04000301 *Non-Destructive Determination of Mechanical Stress in Continuous Welded Rail* supported by a grant of the programme Zeta of the Technology Agency of the Czech Republic. The research project was investigated from May 2020 until April 2022 and the author of this dissertation was its principal investigator. Since some of the project outcomes constitute completed results of applied research, they are presented as a whole among annexes to this dissertation, and only a link to the annexes is written in the particular chapters where they would logically belong. This solution was selected to keep the dissertation uncluttered and compact. Yet, these research outcomes are inherent and important parts of this dissertation.



## Chapter 2

# Current Knowledge

### 2.1 History of Continuous Welded Rail

The history of CWR and rail welding in general starts with the exothermic welding invention by Hans Goldschmidt, which was patented on 13<sup>th</sup> March 1895. The first rail welding was performed in the Essen tram tracks in 1899 [17, 18].

The tram tracks were more suitable for rail welding than the rail tracks since the track structure was closed and only the top of the rail head was open to the sun in many cases. Rail welding started, however, being used in open railway tracks soon, because of the great advantage it brought for the operation, and track and rolling stock maintenance [19].

In the 19<sup>th</sup> century, a common engineering praxis was to keep the rails only so long that the gap between the rails provided sufficient space for rail dilations. This limited the rail length significantly. A typical rail length in that time was 12 or 15 m [19]. Rail welding, together with knowledge that track structure can bear some thermal stress in rails, enabled constructions of *long rails*, which were typically 30, but sometimes also 24, 36, 45, 48 or 60 m long [19].

The first larger experiments on welding of long rails were performed in Nürnberg, Germany, in 1924. Long rails of 60, 84, 108 and 321 m length were made in this case. After the world war II, CWR was massively expanding all over the world [19].

Prof. Vaverka made the first theoretical calculations on the CWR in the former Czechoslovakia, and the first section of CWR in Czechoslovakia was established in 1954 [20, 21], while in the USA, Germany and other countries, hundreds and thousands of kilometres of tracks were welded into CWR [19].

### 2.2 Theory of Continuous Welded Rail

According to the UIC Code 720, the CWR track is defined as a *track in which the free expansion and contraction of the rails caused by temperature changes are constrained, by artificially introducing a controlled expansion into the rails prior to installation of the track fastenings* [8]. Rails of such a track can be theoretically infinitely long. However, their length is typically limited by various railway track objects and installations. Constraining longitudinal movements of rails affects especially their ability to dilate under thermal load. Axial stress, both positive and

negative, arises as a result of the longitudinal movement constraint [9].

Also according to the UIC Code 720, *resistance to longitudinal movement of the rails is secured through the clamping action of the rail fastenings and the restraining effect of the boxing ballast* [8]. In the case of a ballasted track, it can be assumed that this resistance acts on rail in each fastening node. Therefore, the further a rail element from the end of a CWR is, the higher resistance constrains its movement [9, 19].

This thesis focuses on behaviour of CWR in its confined length, where, as will be presented in this chapter, zero strain is expected. The calculation of the axial force, stress and strain of both confined length and breathing length are inherently interconnected, therefore they are presented in this section as a whole. On the other hand, all the calculations presented in this section are generally known and can be found in literature [9, 10], therefore, only the most crucial equations will be presented.

The Hooke's law for an elastic rod can be defined as

$$\varepsilon_{force} = \frac{\sigma}{E} \quad (2.1)$$

or

$$\varepsilon_{force} = \frac{N(x)}{E \cdot A}, \quad (2.2)$$

where  $\varepsilon$  is the strain,  $\sigma$  is the stress,  $E$  is the Young's modulus,  $N$  is the normal force and  $A$  is the cross sectional area. The linear thermal expansion of an elastic rod can be defined as

$$\varepsilon_{thermal} = \alpha \cdot \Delta T, \quad (2.3)$$

where  $\alpha$  is the linear temperature expansion coefficient and  $\Delta T$  is the temperature difference. The total strain is a sum of the strains from 2.1 and 2.3

$$\varepsilon = \frac{N(x)}{E \cdot A} + \alpha \cdot \Delta T. \quad (2.4)$$

Equilibrium can be investigated in the rail element as presented in Figure 2.1, where  $u$  represents the displacement,  $q$  tangential force and  $r$  resistance force.

If the strain is written as the derivative of displacement with respect to the length of rail, the total strain Equation 2.4 can be written as

$$\frac{du}{dx} = \frac{N(x)}{E \cdot A} + \alpha \cdot \Delta T. \quad (2.5)$$

Considering the significant length of the continuous welded rail, the  $N_{max}$  is reached when

$$\frac{du}{dx} = 0, \quad (2.6)$$

therefore

$$0 = \frac{N_{max}}{E \cdot A} + \alpha \cdot \Delta T \quad (2.7)$$

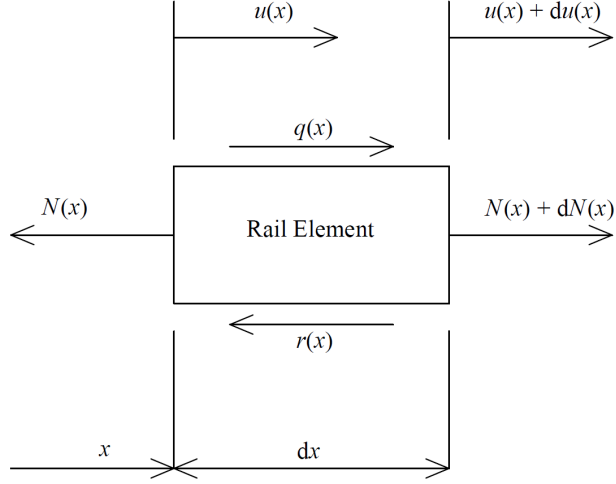


**Figure 2.1** – Rail Element for the Equilibrium Investigation

and

$$N_{max} = -E \cdot A \cdot \alpha \cdot \Delta T. \quad (2.8)$$

Disregarding the area change through rail wearing, we can see that the axial force in CWR is a function of the temperature change. Substituting the relation of force and stress

$$N_{max} = \sigma_{max} \cdot A \quad (2.9)$$

into Equation 2.8 we get an equation for  $\sigma_{max}$  as

$$\sigma_{max} = -E \cdot \alpha \cdot \Delta T. \quad (2.10)$$

The equilibrium condition for the forces in Figure 2.1 can be written as

$$N(x) + dN(x) - N(x) + q(x)dx - r(x)dx = 0 \quad (2.11)$$

$$dN(x) = (r(x) - q(x))dx \quad (2.12)$$

$$\frac{dN(x)}{dx} = r(x) - q(x), \quad (2.13)$$

which is the fundamental differential equation of the axial stress in a rail.

Modification of Equation 2.5 and its derivative gives

$$\frac{N(x)}{E \cdot A} = \frac{du}{dx} - \alpha \cdot \Delta T \quad (2.14)$$

and

$$\frac{dN(x)}{dx} = \frac{d^2u}{dx^2} \cdot E \cdot A, \quad (2.15)$$

respectively. Substitution of Equation 2.15 into 2.13 results in

$$\frac{d^2u}{dx^2} \cdot E \cdot A = r(x) - q(x). \quad (2.16)$$

If we do not consider tangential forces, Equation 2.16 reduces into

$$\frac{d^2u}{dx^2} \cdot E \cdot A - r(x) = 0, \quad (2.17)$$

which is a second order homogenous differential equation. To investigate the longitudinal displacement of a rail  $u$ , we have to find out the relation of longitudinal resistance  $r$  on the displacement  $u$ . According to [9], plastic and elastic shear resistance is considered. Comparison of these assumptions is presented in Figure 2.2.

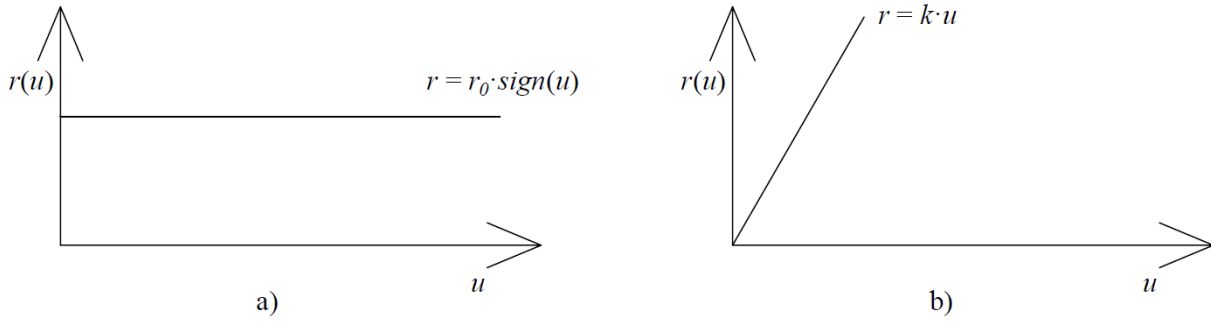


**Figure 2.2** – Relation of Longitudinal Resistance to Displacement: a) Plastic Shear Resistance, b) Elastic Shear Resistance

Empirical experience shows that for longer, homogenous sections of CWR, the longitudinal resistance acts closer to the plastic shear resistance model, whereas for shorter sections, like CWR on bridges, the elastic shear resistance model is more suitable. In the following calculation, only the plastic shear resistance model will be presented. More information to the elastic one can be found in literature [9, 10].

For solution of the differential equation 2.17, two situations can be considered [22]. One occurs if  $u = 0$ , then  $r(x) = 0$  and

$$\frac{d^2u}{dx^2} \cdot E \cdot A = 0, \quad (2.18)$$

which leads to the Equation 2.8, which is valid for the central, confined length of the CWR. The other situation, valid for breathing lengths at each end of the CWR, proceeds from  $u \neq 0$ , thus  $r(x) = -r_0 \cdot \text{sign}(\Delta T)$ , then

$$E \cdot A \cdot \frac{d^2u}{dx^2} = r(x) \quad (2.19)$$

$$\frac{d^2u}{dx^2} = \frac{r(x)}{E \cdot A} \quad (2.20)$$

$$\frac{du}{dx} = \frac{r(x) \cdot x}{E \cdot A} + C_1 \quad (2.21)$$



$$u = \frac{r(x) \cdot x^2}{2 \cdot E \cdot A} + C_1 \cdot x + C_2. \quad (2.22)$$

Boundary conditions are  $u(l_{bl}) = 0$ , where  $l_{bl}$  is the breathing length of the CWR, and

$$R_x = E \cdot A \cdot \varepsilon = E \cdot A \cdot \left( \frac{du}{dx} - \alpha \cdot \Delta T \right), \quad (2.23)$$

where  $R_x = -R_0 \cdot \Delta T$ , and it is the resistant force in a rail joint or a rail expansion device.

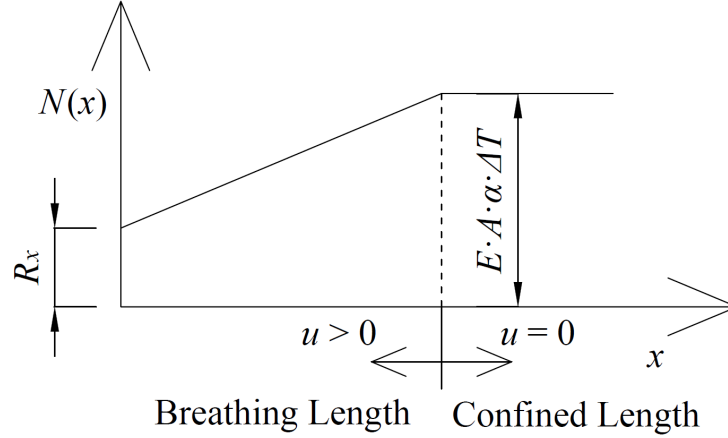


**Figure 2.3** – Axial Force in Breathing Length of CWR;  $R_x$  – Resistant Force in a Rail Joint or Rail Expansion Device,  $u$  – Displacement,  $E \cdot A \cdot \alpha \cdot \Delta t$  – Axial Force in Confined Length of CWR

The breathing length of rail can be calculated as follows [22]:

$$R_x + \int_0^{l_{bl}} r(x) dx = -E \cdot A \cdot \alpha \cdot \Delta T \quad (2.24)$$

$$R_x + [r(x) \cdot x]_0^{l_{bl}} = -E \cdot A \cdot \alpha \cdot \Delta T \quad (2.25)$$

$$R_x + r(x) \cdot l_{bl} = -E \cdot A \cdot \alpha \cdot \Delta T \quad (2.26)$$

$$l_{bl} = \frac{-E \cdot A \cdot \alpha \cdot \Delta T - R_x}{r(x)}, \quad (2.27)$$

and upon substitution of the second boundary condition from Equation 2.23

$$\frac{du}{dx}(0) = \frac{R_x}{E \cdot A} + \alpha \cdot \Delta T = \frac{r(x) \cdot 0}{E \cdot A} + C_1 \quad (2.28)$$

$$C_1 = \frac{R_x}{E \cdot A} + \alpha \cdot \Delta T. \quad (2.29)$$

Applying the first boundary condition upon substitution of Equation 2.29 into 2.22

$$u(l_{bl}) = \frac{r(x) \cdot l_{bl}^2}{2 \cdot E \cdot A} + \left( \frac{R_x}{E \cdot A} + \alpha \cdot \Delta T \right) \cdot l_{bl} + C_2 = 0 \quad (2.30)$$

$$C_2 = -\frac{r(x) \cdot l_{bl}^2}{2 \cdot E \cdot A} - \left( \frac{R_x}{E \cdot A} + \alpha \cdot \Delta T \right) \cdot l_{bl} = 0. \quad (2.31)$$

The longitudinal displacement of rail  $u$  can be calculated by substitution of the constants of integration into Equation 2.22

$$u = \frac{r(x) \cdot x^2}{2 \cdot E \cdot A} + \left( \frac{R_x}{E \cdot A} + \alpha \cdot \Delta T \right) \cdot x - \frac{r(x) \cdot l_{bl}^2}{2 \cdot E \cdot A} - \left( \frac{R_x}{E \cdot A} + \alpha \cdot \Delta T \right) \cdot l_{bl} \quad (2.32)$$

$$u = \frac{r(x) \cdot x^2}{2 \cdot E \cdot A} - l_{bl} \cdot \frac{r(x) \cdot x}{E \cdot A} - \frac{r(x) \cdot l_{bl}^2}{2 \cdot E \cdot A} + \frac{r(x) \cdot l_{bl}^2}{E \cdot A} \quad (2.33)$$

$$u = \frac{r(x) \cdot x^2}{2 \cdot E \cdot A} - l_{bl} \cdot \frac{r(x) \cdot x}{E \cdot A} - \frac{r(x) \cdot l_{bl}^2}{2 \cdot E \cdot A} + \frac{r(x) \cdot l_{bl}^2}{E \cdot A} \quad (2.34)$$

$$u = \frac{r(x) \cdot x^2}{2 \cdot E \cdot A} - \frac{r(x) \cdot x \cdot l_{bl}}{E \cdot A} + \frac{r(x) \cdot l_{bl}^2}{2 \cdot E \cdot A} \quad (2.35)$$

$$u = \frac{r(x)}{2 \cdot E \cdot A} \cdot (x - l_{bl})^2, \quad (2.36)$$

which is the general equation for calculating displacement along the breathing length of the CWR. Calculation of stress and force in the breathing length can be performed as

$$\sigma = E \cdot \varepsilon = E \cdot \left( \frac{du}{dx} - \alpha \cdot \Delta T \right) = E \cdot \left( \frac{r(x) \cdot x}{E \cdot A} + \frac{R_x}{E \cdot A} + \alpha \cdot \Delta T \right) \quad (2.37)$$

$$\sigma = \frac{r(x) \cdot x + R_x}{A} \quad (2.38)$$

$$N(x) = r(x) \cdot x + R_x, \quad (2.39)$$

where  $r(x) = -r_0 \cdot \text{sign}(\Delta T)$ .

The advantages of CWR reside in the absolute elimination of the problem of rail head running edge interruption, except interruptions caused by other reasons – like in a flat diamond crossing. On the contrary, other problems, like formation of higher axial stress in rails that contributes to a higher risk of rail breaks and track buckling occurrences, emerged [9, 10].

Many railway infrastructure managers deal with this problem currently [8]. The general approach lays in the ability to determine the axial stress in rail using non-destructive methodologies. Based on a thorough research dealing with measurement methodologies of axial stress in rail and presented in Section 2.3, it is shown that no methodology fulfilling the criteria set by Kish and Samavedam in 1987 is known at the moment. Kish and Samavedam set the criteria as follows [23]:

- it is portable and not permanently fixed to a rail,
- it measures the absolute value of force, not the relative changes,

- it is independent on residual stress in rail,
- the actual neutral temperature of rail can be estimated with accuracy of  $\pm 5^{\circ}\text{F}$ .

## 2.3 Non-Destructive Methodologies of CWR Stress Determination

In this section, current knowledge in the area of non-destructive methodologies to determine the internal stress in CWR is presented.

Many methodologies have been developed in purpose to determine the internal stress in CWR. The approach varies not only in its destructiveness in relation to the tested rail but in its ability to provide useful results, too. All these methodologies can be divided into five basic categories: strain methodologies, rail shifting methodologies, methodologies based on acoustoelastic effect, methodologies based on magnetoelastic effect and methodology based on steel passive layers formation.

### 2.3.1 Strain Methodologies

Strain methodologies of CWR stress measurement work on the simple mechanical assumption of change of a relative distance between two points of material, rail in this case. In Newton's mechanics, a relatively stiff rail behaves according to the Hook's law if unfastened. However, even the fastening systems ensure only a certain level of rigidity and, provided the axial force in rail is sufficient enough, a strain can be observed even at fastened rail sections. As of now, some solutions using strain are available as presented below.

#### Research of the Gdańsk University of Technology

This research was carried out in the mid-seventies at the Gdańsk University of Technology, Poland. A strain sensor with accuracy of 0.001 mm was applied for a measurement on a 200 mm long rail section. Next to the CWR measurement spot, a reference rail section was placed. This reference rail section was set free to lengthen and shorten. It was able to observe soon that the stress varies over different sections of the rail even if the temperature of the rail was the same at the measured locations.



**Figure 2.4** – MS-02 Extensometer for Measurement of the Longitudinal Forces in Rails [24]

It is believed that this effect is caused by a slip of rail in the fastening points. Such a slip can be derived by several sources like tangential forces of traffic, but also by exposure of some parts of rail to the sun and location of some parts of rail in a completely shady place. Such a different exposure to the sun results in a difference of the daily mean temperature and, subsequently, to a stress gradient in the rail.

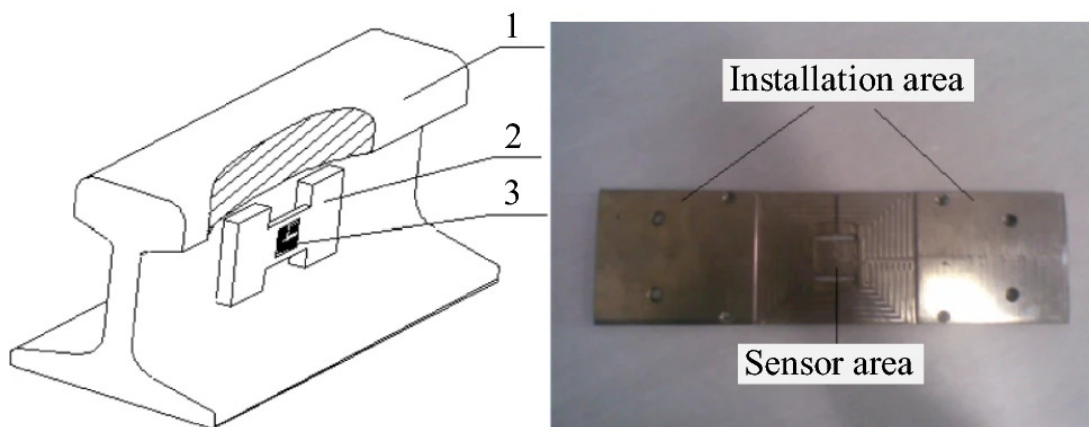
This revealing is a good asset of the measurement. The methodology itself, however, is not suitable for commercial use as it is very costly, time demanding and requires a reference rail to be placed at the measurement spot. Nevertheless, it can well serve as a reference for calibration of other methodologies [24].

### The Calibrated Length of Rail Methodology

This methodology, which has supposedly been applied in China since 1982, consists of length comparison of a freely placed 50 m long steel strip with a selected rail section originally of the same length [25]. The principle of this methodology, however, appears to be the same like in the research of the Gdansk University of Technology, only modified for a bigger span. Author’s daring claim that this methodology is the only one in the world without *fatal* shortcomings and can be operated widely does not match the state of the research in this area after the publication date, because much of research has been emerging in this field.

### Strain Gauge Measurements

Strain gauge measurements have been applied to detect the rail strain. An Australian study [14] shows the use of a strain-gauge-based device with integrated thermometer to monitor a neutral temperature development over time. Constraints of this study reside in presenting the measuring devices generally as black boxes, only with information that strain gauges are included, in a very limited deployment of eight devices only, out of which two were claimed inaccurate. On the other hand, the approach is similar as the one in the dissertation and the work can contribute to searching for a viable solution based on this system.



1. Rail; 2 Steel plate; 3 Full-bridge strain gauge

Figure 2.5 – Rail Stress Monitoring Device [15]

A detailed description of a strain gauge device for CWR strain measurement is presented in a Chinese study [15]. In this study, a full bridge configuration of strain gauges is used. The configuration was, however, installed on a steel plate which is attached to a rail. Moreover, only results from laboratory testing are provided.

### Measurement with Bi-directional FBG Strain Sensors

Strain measurement on a rail web in longitudinal and vertical direction using optic FBG sensors is another interesting approach [26, 27]. In general, this measurement resembles strain gauge measurements. However, the advantage of FBG sensors is the possibility to measure even temperature, apart from the mere strain. Moreover, it is characterized by its longer durability in relation to the strain gauge sensors. Provided the sensor is attached to the rail web prior to the CWR installation (i.e. at the rail neutral temperature or known rail tension), it keeps measuring the deformation as long as the sensor works. This can be theoretically reached using strain gauges only, although the durability appears as an important factor here. [26].

Measurement using FBG sensors has been done in China. The layout was placed on a bridge as presented in Figure 2.6.

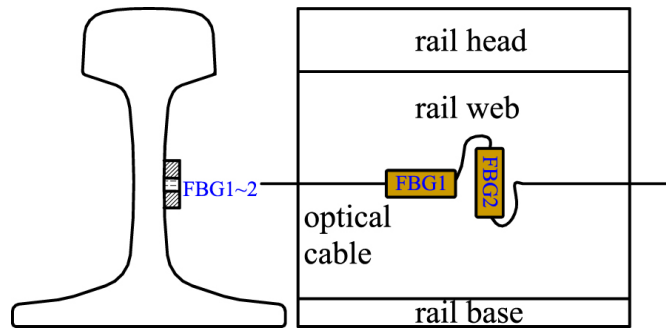


**Figure 2.6** – Layout of FBG Sensors [26]

Assuming the basic equation of force-stress relation

$$F = \sigma \cdot A, \quad (2.40)$$

we get a modified equation when other force, in this case the bridge influence, is applied.

In combination with Equation 2.1, it results in

$$F = E \cdot A \cdot \varepsilon_f - E \cdot A \cdot \alpha \cdot \Delta T, \quad (2.41)$$

where  $E$  is the Young's modulus,  $A$  is the cross-sectional area of rail, and  $\varepsilon_f$  is the strain induced by additional force of train-bridge interaction.

When the  $\varepsilon_f$  is distributed into two perpendicular strains, along with the layout of FBG sensors, we can introduce

$$\varepsilon_x = \varepsilon_f \quad (2.42)$$

and

$$\varepsilon_y = (\mu + 1) \cdot \alpha \Delta T - \mu \cdot \varepsilon_f. \quad (2.43)$$

Incorporation of Equation 2.42 and 2.43 into 2.41 results in

$$F = E \cdot A \cdot \frac{\varepsilon_x - \varepsilon_y}{\mu + 1}, \quad (2.44)$$

where  $\varepsilon_x$  and  $\varepsilon_y$  are the strains measured by FBG sensors placed in the horizontal and vertical direction, respectively, as shown in Figure 2.6 [26].

Other experiments with fiber-optic sensors were conducted by Barker, Hoult and Zhang [28].

### Measurement with Brillouin Optical Time-Domain Reflectometry

An option to use the optic sensor resides in the Brillouin Optical Time-Domain Reflectometry. This approach was adopted in a study published in 2018 [16]. The results show good applicability under laboratory conditions, but a need of calibration in the case of field measurements. More investigation in this methodology could provide a better understanding on its practical applicability.



**Figure 2.7** – Rail Specimen Instrumented with Strain Gauge and Optical Fibres [16]

### VORTOK Measure and Detect

Another option to measure strain can be reached by using the Measure and Detect sensor produced by the VORTOK Ltd. company. A simple sensor that is able to measure variety of parameters is made ready to be screwed into a drilled hole in a rail web. The manufacturer does not share any detailed information of what principles this device uses. It looks, however, like a piezoelectric sensor with accessories that is incorporated into a screw-in dowel.

This robust shape most probably predicts a strain methodology with a long durability. A disadvantage of this methodology is a need for calibration. After the calibration is made, either by fastening of the device on a stress-free rail or by using another calibration methodology, the value of internal stress in a rail can be obtained in a stable manner. The options to set up an automatic data transmission via email or wi-fi even from a moving train make this sensor a user-friendly device [29].

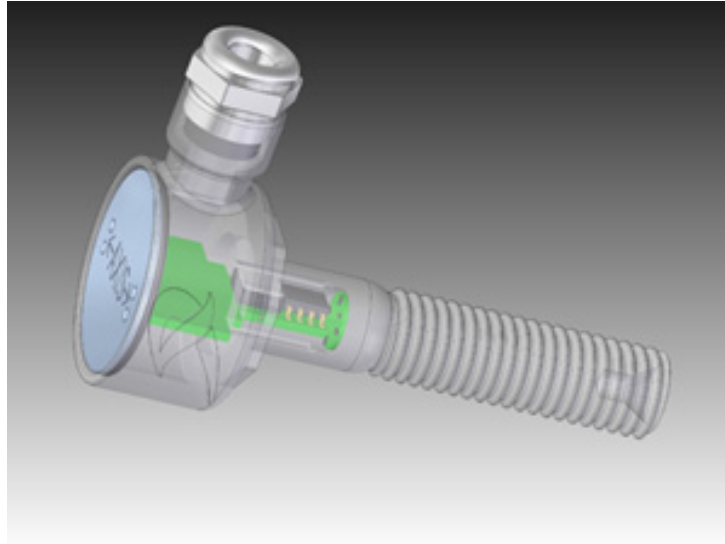


**Figure 2.8** – Vortok Measure and Detect [29]

### 2.3.2 Rail Shifting Methodologies

The rail shifting methodologies use the principle of bending stiffness dependence on the axial tension in rail. Provided the rail is in tension, the higher force is necessary to be applied to laterally shift the rail, the higher the axial force in the rail is. Apparently, these methodologies are viable only when the rail is in tension, otherwise a failure by buckling may appear.

#### **VERSE Methodology**

This methodology has been presented by the VORTOK Ltd. company from the United Kingdom. It is a development of the Rail Uplift Device (RUD) presented by Kish and Samavedam [30]. In the first place, the rail shall be released from all fastenings in the length of 30 m. Afterwards, the central part of the unfastened section of the rail shall be lifted into a certain height. The force that is applied to move the rail is related to the axial force in the rail.



**Figure 2.9** – Vortok VERSE Methodology [31]

Wide use of this methodology is restricted by some disadvantages. The most obvious one is the limitation to the tensile stress in the measured rail. The operator needs to be sure that there is a tensile stress as problems with re-installation of the rail into the original position could occur, leave apart the danger of operator's injury or material damage. Another disadvantage is the need to unfasten the rail in the length of 30 m. This operation requires additional time and subsequently prolongs the track closure. Moreover, in the case the measured section is situated in a curve, the re-installation of the rail can be difficult, too, as the condition of a tensile stress in the rail is inevitable.

Even though the disadvantages are important, this methodology appears to be one of the most widely spread to measure the CWR stress nowadays. The manufacturer produces their own device for the rail lifting and stress measurement. The light aluminium design of this device enables easy transport, manipulation and operation [31].

### **Use of Tamping Machine**

In a paper published in 2009, scientists at the Gdańsk University of Technology look into a possibility to use a tamping machine for the stress measurement in CWR. The tamping machine is capable to shift rails in both vertical and horizontal directions when adjusting the railway track geometry. The goal of this research was to use this movement to estimate the stress in CWR. The principle of this measurement is similar like at the VERSE methodology, including the disadvantages. However, the disturbing signal produced by the operation of tamping machine turned out to be too high and the attempts to get some CWR stress data were unsuccessful [32].

Other studies on the use of standard measuring cars were conducted, too [33].

### **2.3.3 Methodologies Based on Acoustoelastic Effect**

The acoustoelastic effect is a physical effect of change of sound velocity based on a change of stress in elastic continuum. For measurements, ultrasound is typically used. The definition, however, can cover vibration, as mechanical waves, too. In such a case, vibrometer is used as a measurement tool.

It is always necessary to execute a calibration measurement on the site with known temperature and stress as the sound velocity in rail is not dependent only on the stress, but on the steel microstructure, too. This calibration measurement can be performed either prior to the CWR installation, or once the CWR is installed. However, in the latter only when the rail is cut, unfastened and welded again. As a consequence, similar disadvantage like at the strain methodologies emerges, which means the need to start the measurement at the neutral temperature. The advantage, on the contrary, is in a possible high durability of ultrasound sensors and their attachment to the measurement place.

### **Jacek Szelażek's Measurements**

Jacek Szelażek has worked out two ultrasound measurement procedures in the nineties of the twentieth century. In the first procedure, the ultrasound signal is emitted vertically from the top of the rail head to the bottom of the rail foot where it reflects off and moves back to the receiver,



which can be the same device as the emitter. The second procedure uses separate emitter and receiver and those are placed to the side of the rail head horizontally next to each other. The signal moves through the rail head lengthwise, in this case.

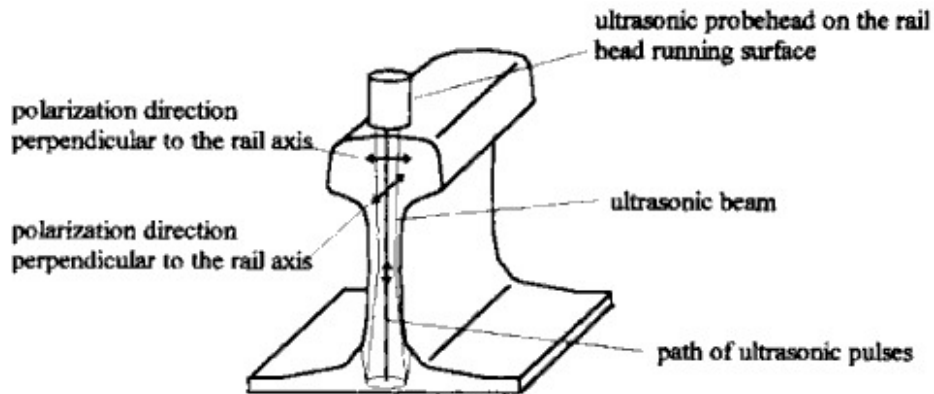


**Figure 2.10** – Vertical Ultrasound Measurement [34]

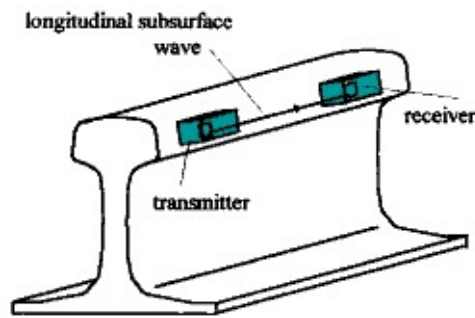


**Figure 2.11** – Horizontal Ultrasound Measurement [34]

The first procedure proved as inapplicable, as the signal dispersed due to the uneven rail head profile. The major cause of this unevenness is the rail head wear. Placing the signal receiver to the bottom of the rail foot did not improved the results and, moreover, the signal path was reduced to one half.

The second procedure appeared more promising, but even at this measurement, disturbances appeared and the results were influenced by strong dispersion [34].

### **Research of the University of Florence**

In 2007, Italian scientists worked out the second procedure of Jacek Szelażek. This procedure was tested for 2 years and appeared viable. However, it shared all the common disadvantages of the ultrasound methodologies and the necessity to perform a calibration measurement in situ [35].

### **Measurement of Stresses Using the Polarization of Rayleigh Surface Waves**

Two US researches work with measurement of polarization of the Rayleigh surface waves. The measurement of dependence of the Rayleigh surface waves polarization on the change of rail

stress turned out not just to be more robust than the measurement of dependence of the Rayleigh surface waves velocity on the change of rail stress, but also to be easier to detect.

Michael D. A. Junge's work deals with general measurement of stress in material based on the Rayleigh surface waves [36]. Stefan Hurlebaus' report deals with application of this procedure on the rail stress research. On the page 42, the author presents that the polarization of the Rayleigh surface waves is dependent on the value of the axial force in rail and that a further research is recommended [37].

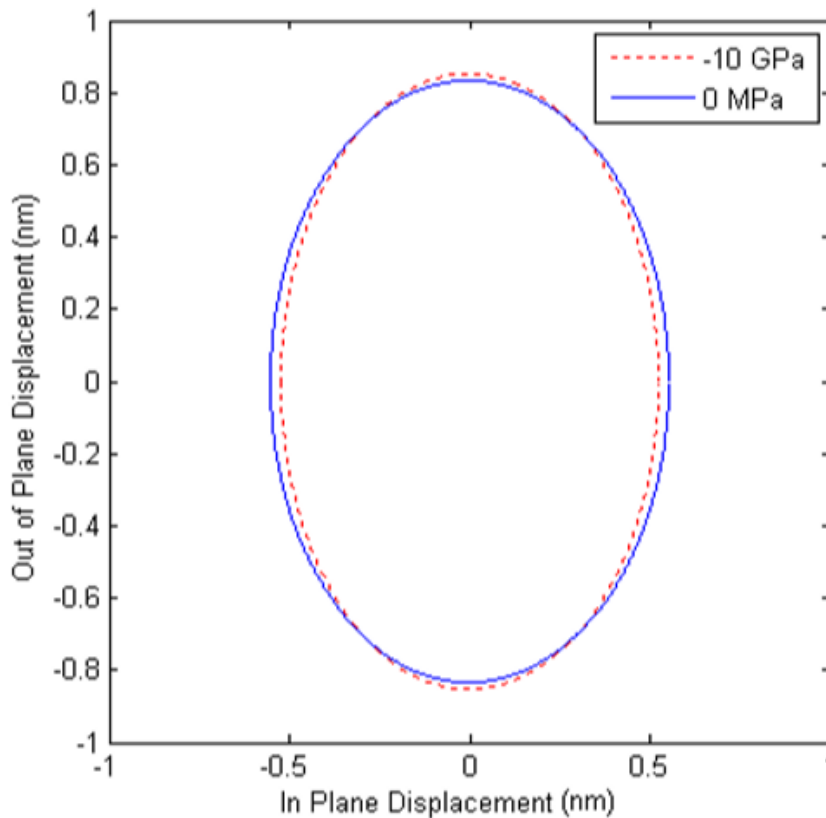


**Figure 2.12** – Trajectory Plot of Particle Motion for Unstressed and Stressed Rail Steel [37]

### Vibration Measurement

More publications deal with vibration measurement of the internal rail stress. The results of the rail stress determination from wave lengths of a vibrating sensor seem well under laboratory conditions when a steel bar or a new rail is used. In the case of worn rail, and this is very important for practical application, it is possible to get certain results, but these results are not that clear like in the previous cases. When performing a field measurement, the results of measurement on a worn rail are much worse.

In case it is possible to diminish the problems, this methodology can have a good perspective [23, 38, 39, 40]. A research team at the University of Illinois in Urbana-Champaign and the University of Utah recently built upon the work in new updates [41].

In the following figures, a difference in accuracy of measurement on unworn and worn rail is clearly visible.

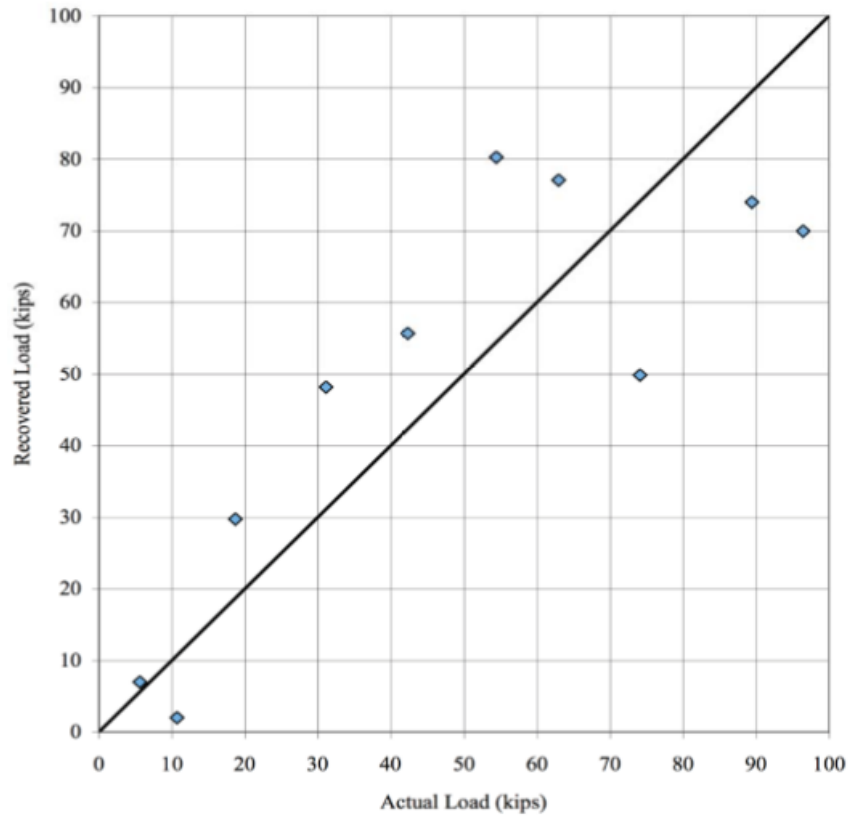


**Figure 2.13** – Plot of Unworn 136RE Rail Study Results [23]

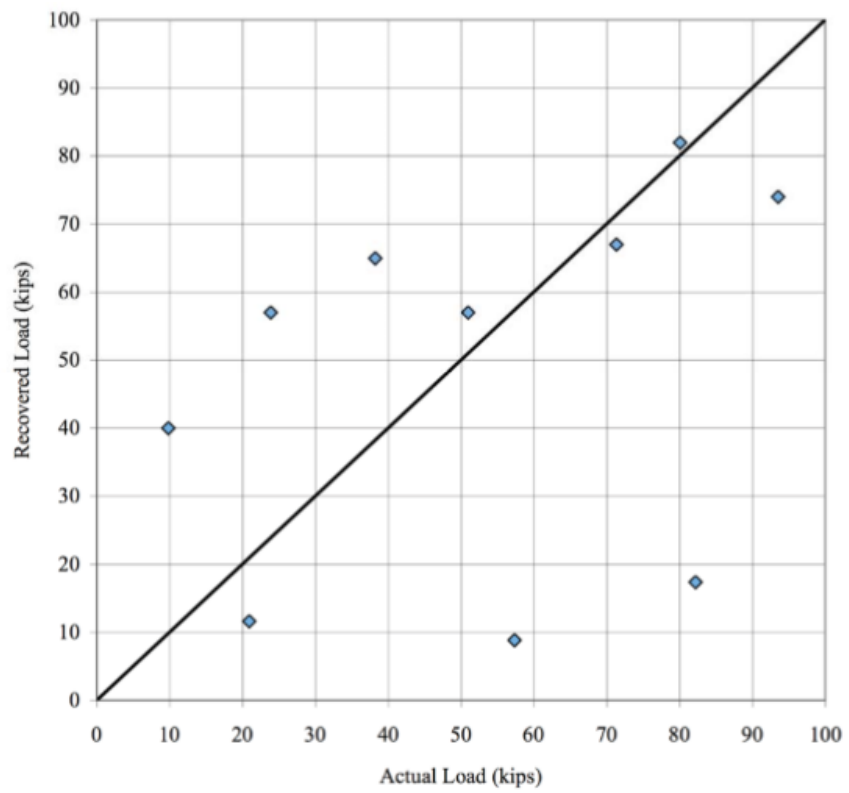


**Figure 2.14** – Plot of Worn 136RE Rail Study Results [23]

### 2.3.4 Methodologies Based on Magnetoelastic Effect

The magnetoelastic effect is the inverse magnetostrictive effect. It is presented as a change of the magnetic susceptibility in relation to the change of stress in material. The magnetoelastic effect is also known as the Villari effect.

#### Measurement of Magnetic Hysteresis

In the nineties, D. Utrata tested the possibility of application of the magnetoelastic effect on the rail stress measurement. He measured the dependence of coercivity and remanence of the magnetic field in rail on different surface conditions, like scaled rail surface, or milled rail surface. However, the comparison of the obtained data showed various results based on the input type of rail.

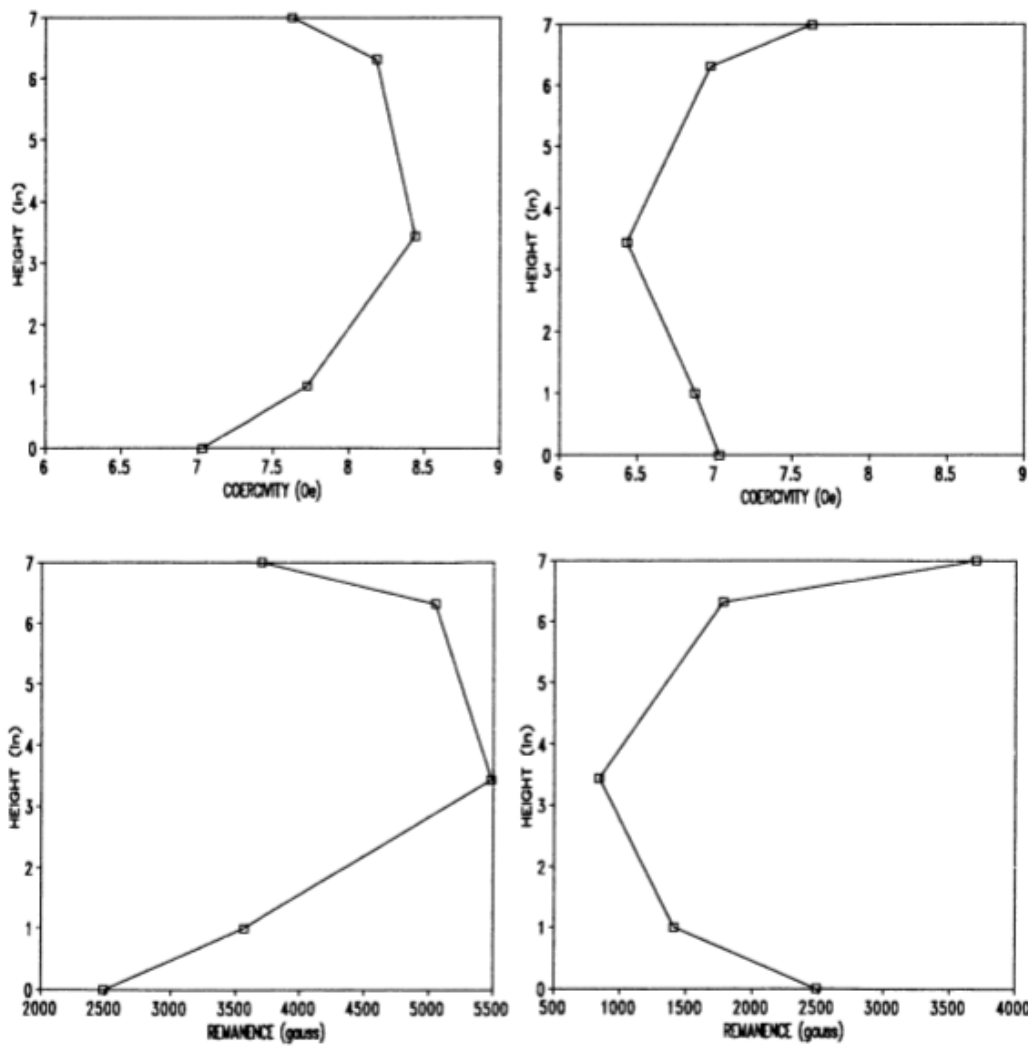


**Figure 2.15** – Coercivity (top) and Remanence (bottom) Measured on Milled (left) and Scaled (right) Surfaces of the Test Rail [42]

Surprisingly, the only data that match were on the milled running surface and scaled base underside. D. Utrata assumes, that either a calibration measurement or a new approach to the data interpretation has to be delivered in order to make this methodology applicable.

A. Wegner needed 400 calibration sensors to run a measurement of a 3 meters long rail using the hysteresis methodology, which does not contribute to its viability [23, 42].

### Measurement of Magnetic Barkhausen Effect

Japanese scientists Tsuchima and Enokinozo have studied the reaction of the Barkhausen noise on the stress in a steel plate. It is possible to get some relation from the graphs of the mutual dependence. However, the authors found it difficult to estimate the influence of time and get a value of the stress. Additionally, they suggest application of the chaos theory to get a better interpretation of the results [43].

Measurement using the Barkhausen noise together with measurement of the magnetic permeability is used by the Elektro-Thermit GmbH & Co. KG. company to determine the internal rail stress. Their methodology requires calibration on a rail test sample. Their product has been awarded a certificate of the railway infrastructure manager of Denmark, the Banedanmark. On the contrary, the manufacturer appears not interested in the sale of their product and only offers to perform a measurement in the required section by themselves [24, 44].

Czech company Pirell also presents an instrument to measure and evaluate the stress level in rail. Similarly to the above mentioned company, a railway infrastructure manager, České Dráhy (Author's note: this happened before České Dráhy was divided into České Dráhy, a. s. and Správa železnic, s. o. – the current major Czech railway infrastructure manager), has approved the instrument for the use on their railway network. However, as it is in other methodologies using the effect of the Barkhausen noise or the magnetic hysteresis, a thorough calibration on many samples is necessary to be made before the measurement is commenced [45].

### Metal Magnetic Memory Measurement

Collective of authors from the University of Nanjing have carried out an experiment of measuring the effect called Metal Magnetic Memory on a steel test sample. Contrary to the Barkhausen noise, this effect does not require external magnetization of the sample.

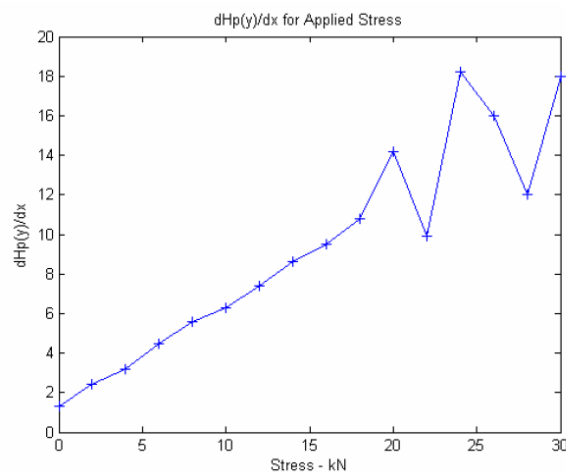


**Figure 2.16** –  $dHp(y)/dx$  for Applied Tensile Stress on a Steel Sample [46]; See the Linear Dependence in the Elastic Region

The effect is activated anywhere in the natural magnetic field of the Earth. When the loading increases, the rotation of the Weiss magnetic domains in metals raises the value of the magnetic flux around the central point and this increases the gradient of the magnetic flux which is in the elastic region linearly dependent on the stress in the sample. Graph of the linear dependence of the magnetic flux gradient on the stress in a steel sample as measured by Wang, et. al. [46] is presented in Figure 2.16. The linear dependence in the elastic region is completely sufficient, because the rail geometry deformation emerges earlier than the plastic deformation in the axial direction of the rail [46].

### 2.3.5 Methodology Based on Steel Passive Layers Formation

Provided the stress could be evaluated from a surface layer of rail only, i. e. there was a mutual relation between the surface stress and the stress in the core of the rail, another possible methodology emerges. The research of F. Navaï has shown that when a steel sample is a subject of a normal sulphuric acid bath at a room temperature and is passivated under a voltage of 450 mV, the anodic current density varies based on the straining of the sample. Additionally, it is presented that the magnitude of oxidation is higher on the tensile stressed surface than on the compressive stressed surface. If a plausible benchmarking is possible to be made, this methodology can provide an additional way to determine the level of stress in a rail [47].

## 2.4 Rail Stresses

Rail is a heavily loaded element of a railway track. Many stresses of various types and intensity act on rails in tracks under operation and purpose of the rail is to transfer these stresses to the fastening nodes and sleepers in a less demanding way of acting [10].

The influence and causes of the thermal stress were introduced in Section 2.2, therefore only a shorter section is dedicated to this phenomenon within this chapter. Stresses in the rail foot centre are the most critical for estimation of the rail strength and fatigue fracture occurrence, thus their description will be more detailed. Stresses in the rail head, other stresses and a combination of stresses are addressed in this chapter, too. All information from this chapter are generally known and reader can get more detailed information e. g. in [9, 10].

### 2.4.1 Thermal Stress

It is expected that the thermal stress acts in the normal direction and is distributed evenly across the cross section of rail [10], as presented in Figure 2.17.

The actual volume of the stress depends only on the temperature difference in the confined length of the CWR as it is shown in Equation 2.8, or on more parameters in the breathing length of the CWR as it is shown in Equation 2.39. The stress can reach both tension, in cold, and compression, in hot temperatures. Under the state of tension and along with the bending stress in the rail foot, it adversely contributes to the fatigue strength, as described in the following section.

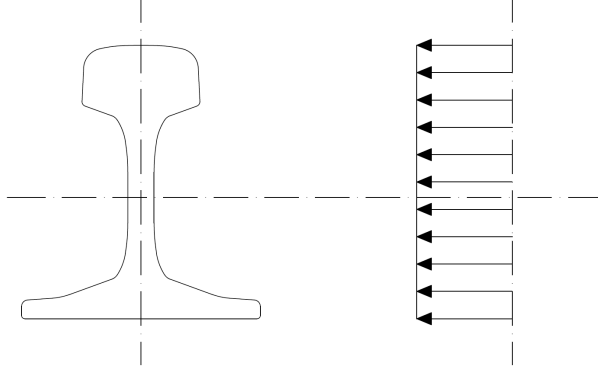


**Figure 2.17** – Thermal Stress Distribution, retrieved from [10]

### 2.4.2 Stress from Track Operation

One of the major stress sources for rails is the stress from vertical wheel load of track operation. It can be represented as a superposition of the standard bending stress and the rail head bending stress caused by significant indents of the rail shape in the level of rail web [10]. The stresses, including the combined bending stress, are presented in Figure 2.18.

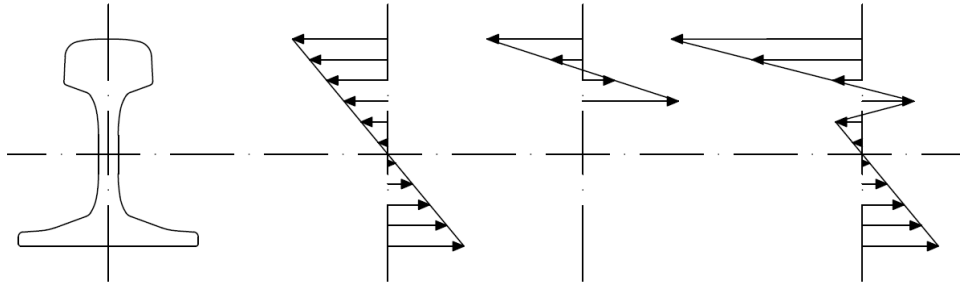


**Figure 2.18** – Vertical Wheel Load Stress, retrieved from [10]

According to [9], the mean value of the rail bending stress can be calculated as

$$\sigma_{mean} = \frac{Q}{A} \cdot \frac{A \cdot \sqrt[4]{I_y}}{4 \cdot W_{yf}} \cdot \sqrt[4]{\frac{4 \cdot E \cdot a}{k_d}} \quad (2.45)$$

where  $Q$  is the effective wheel load,  $A$  is the rail cross-sectional area,  $I_y$  is the moment of inertia,  $W_{yf}$  is the section modulus of rail relative to the rail foot,  $E$  is the modulus of elasticity of rail steel,  $a$  is the sleeper spacing, and  $k_d$  is the spring constant of discrete support [9].

The vertical wheel load additionally causes a shear stress in the rail head, which can contribute to fatigue failures of the rail head [9].

Lateral wheel forces contribute to the stress from track operation not only in curves but a straight track, too, as the sinus movement of the wheelset periodically acts on both rails [10].

Wheel flats can contribute with an impact of 400 to 800 MPa in the vertical direction, based on the train speed and weight. In the same way, rail defects can cause dynamic impacts of force when a train is passing over them [10].

Other stress from track operation arises from train acceleration and braking forces. This acts on rail in the longitudinal direction, therefore it may locally increase the effect in the same

way as the thermal stress [10].

Rolling contact stress is a very local one, but reaches extremely high values in the range of 1 to 2.5 GPa. In the case of two contact points between a wheel and a rail, stress and wear of the rail is the highest. According to [9], the mean contact stress (in MPa) can be calculated as

$$q_{mean} = \sqrt{\frac{\pi \cdot E}{64 \cdot (1 - \nu^2)} \cdot \frac{Q}{r \cdot b}} \quad (2.46)$$

and maximum shear stress (in MPa) as

$$\tau_{max} \cong 0.3 \cdot q_{mean}, \quad (2.47)$$

where  $Q$  is the effective wheel load [kN],  $r$  is the wheel radius [mm],  $2b$  is the width of rail contact area [mm],  $E$  is the modulus of elasticity and  $\nu$  is the Poisson's ratio [9].

It is important to add that the stresses from track operations typically act in a dynamic way, therefore significantly contributing to the fatigue of the rail as described in Section 2.4.4.

### 2.4.3 Residual Stress

The process of rail production loads newly produced rail by stresses caused by roller straightening and uneven rail cooling. A significant tension occurs in the rail head and mostly rail foot of new rail, whereas a compression occurs in the rail web. Under operational loading, the surface and subsurface layer of the running edge of the head is forged so that the tension decreases and compression emerges in this area [10]. The course of the residual internal stress is presented in Figure 2.19.

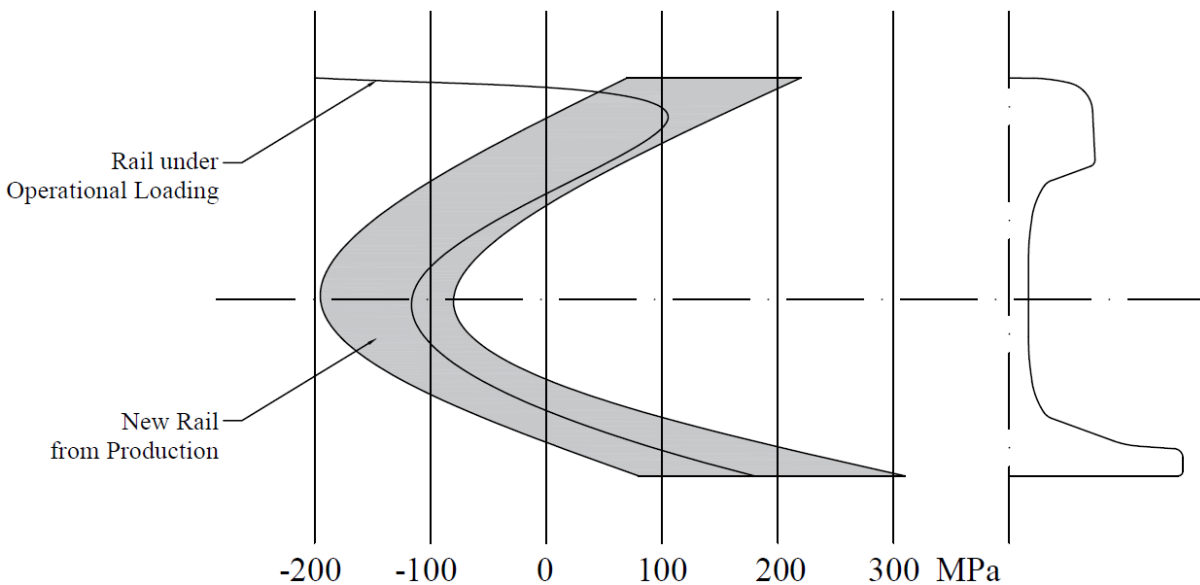


**Figure 2.19** – Residual Internal Stress in Rail, retrieved from [10]



## 2.4.4 Other Stresses and Stress Combinations

Among other significant stresses, the stress from track maintenance vehicles shall be mentioned. These vehicles, like track relaying machine, tamping machine and ballast cleaning machine, move with rails at their work and therefore induce an additional stress caused by a significant change in rail position, often in a short longitudinal section. This stress can reach hundreds of MPa [10].

Wheels of smaller radii, typical for some track maintenance vehicles, can additionally cause a very high local stress leading to a plastic deformation of the rail head. The load of wheels of smaller radii is therefore limited [10].

A combination of stresses with a focus on the cyclic character of some of them is presented in Figure 2.20 from [48].

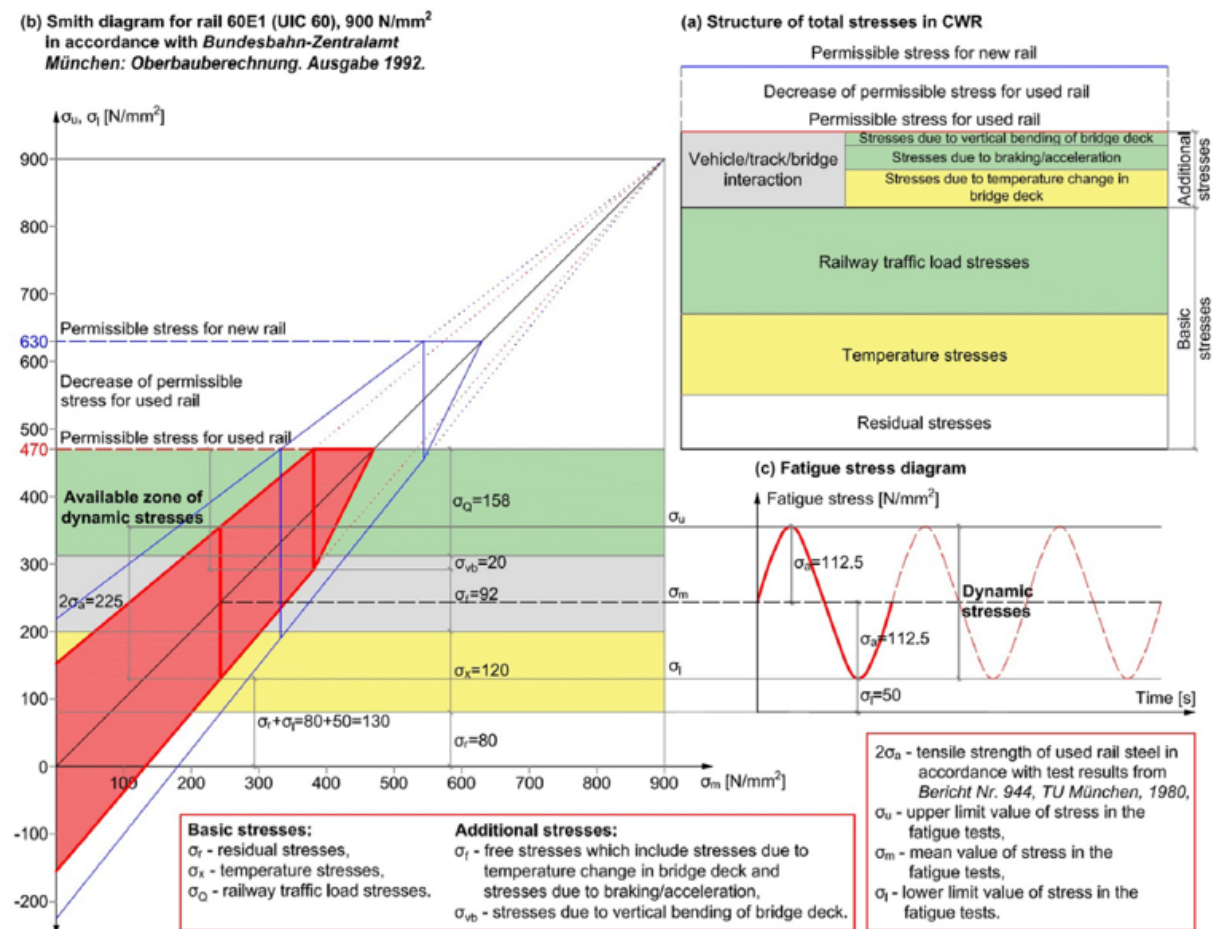


Figure 2.20 – Combination of Stresses in Rail, retrieved from [48]



# Chapter 3

## Rail Temperature

In this chapter, investigation into the influence of selected parameters on the rail temperature will be presented.

### 3.1 Influence of Air Temperature and Cloudiness on Rail Temperature

Rail in a railway track is exposed to various atmospheric effects which influence the rail temperature. Among the effects of the highest impact, air temperature and cloudiness can be involved [49]. Based on the second law of thermodynamics, there is a heat transfer among the rail and the ambient air until an equilibrium is reached if another body does not enter the thermodynamic system. This effect can be observed on very cloudy days, or later in the night when the sun doesn't heat the rail any more. The sun transfers the heat to the rail by thermal heating and this effect has a significant impact on the rail temperature. Clouds can limit the amount of thermal energy transferred from the sun to the rail, but they can never wholly intermit this effect. Research in this chapter follows the work presented in [50, 51].

There are other atmospheric effects that can influence the rail temperature in a track, like precipitation, wind speed, or air humidity; and other environmental effects like the cleanliness of the ballast bed, the colour of the ballast grains, or the material of sleepers. It would be interesting to investigate into the influence of these parameters, however, measurement described in this section deals with the influence of air temperature and cloudiness only. This measurement was performed in the area of Educational and Research Centre in Transport (ERCT) in Spring 2017.

#### 3.1.1 Experimental Setup

A hole of 6 mm diameter and 40 cm depth was drilled into the centre of head of a 120 cm long 60E2 rail sample. This rail sample was placed on a ballast bed at the narrow gauge experimental track in the ERCT, Pardubice. A 2-channel data-logger Comet System S0121 and a temperature probe Pt1000 were acquired to measure and store the measured data. The Pt1000 probe was put into the drilled hole and the data-logger was set to log the temperature from the probe every full hour and was buried into a case next to the rail sample. The setup is shown in Figure 3.1.



**Figure 3.1** – Layout of the Rail Head Temperature Measurement

### 3.1.2 Data Analysis

The temperature data from the probe in the rail head were recorded. The record of the first two weeks of measurement is presented in Figure 3.2.

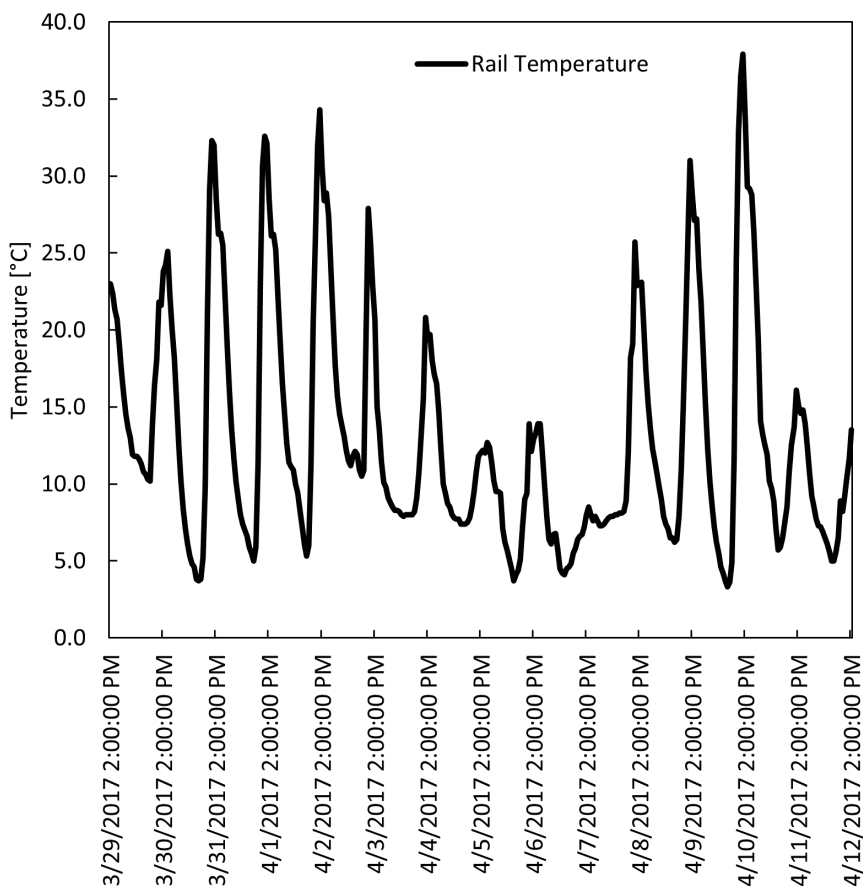


**Figure 3.2** – Rail Head and Reference Temperature Record 29<sup>th</sup> March – 12<sup>th</sup> April 2017

The Czech Hydrometeorological Institute operates a network of measuring stations that cover the whole area of the Czech Republic as can be seen in Figure 3.3. The air temperature data are measured every full hour, the cloudiness data are measured in a quantity named tenths of cloudiness and are measured daily at 7 a.m., 2 p.m. and 9 p.m. Cloudiness 0/10 means that the sky is clear, cloudiness 10/10 means that it is fully cloudy, every 1/10 of cloudiness in between marks 10 % more clouds covering the sky. The data of air temperature and cloudiness from the H3PARD01 measuring station located in the airport of Pardubice, approximately 5.1 km from the location of the rail, were obtained.

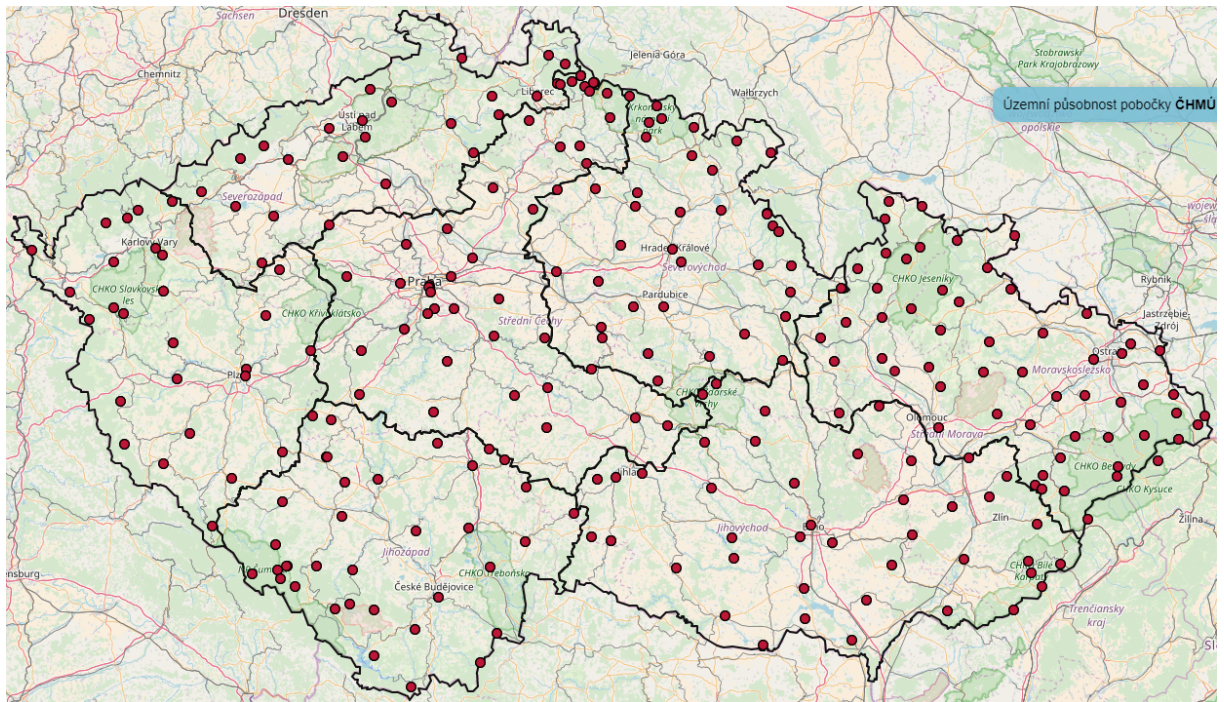


**Figure 3.3** – Measuring Stations of the Czech Hydrometeorological Institute [52]

Out of the data recorded in the measurement setup and obtained from the Czech Hydrometeorological Institute in the period from 1<sup>st</sup> April to 30<sup>th</sup> September 2017, a relation between cloudiness, air temperature and rail temperature was derived. Due to the constraints given by only three cloudiness measurements per day, data of 549 measurements in total entered the calculations. The average value of difference between the rail temperature and air temperature (further in this section referred to as *temperature difference*) is used in the following calculations.

### Impact of Cloudiness on Temperature Difference

In the first phase, impact of cloudiness on the temperature difference was determined. The average values of the temperature difference are presented in Table 3.1.

Arrangement of these data into a chart and adding a logarithmic trend line is presented in Figure 3.4.

Cloudiness	Average Temperature Difference [°C]
100 %	4.769
90 %	7.769
80 %	8.357
70 %	9.533
60 %	9.838
50 %	10.769
40 %	11.082
30 %	10.767
20 %	13.900
10 %	11.860
0 %	11.325

**Table 3.1** – Cloudiness and Average Temperature Difference

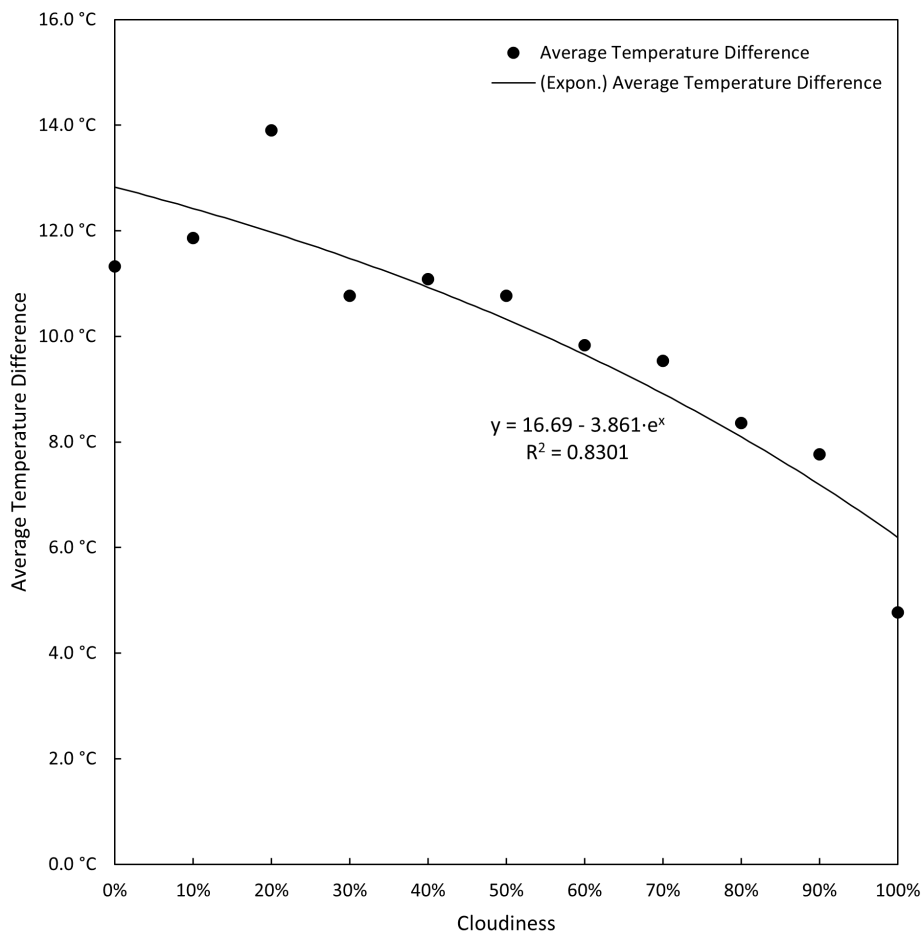


**Figure 3.4** – Relation between Cloudiness and Temperature Difference

Equation of the trend line from Figure 3.4 is

$$y = 16.69 - 3.861 \cdot e^x, \quad (3.1)$$

where  $x$  is the cloudiness [-] and  $y$  is the average temperature difference.

### Impact of Air Temperature on Temperature Difference

Following the previous calculation, the impact of the air temperature on the temperature difference was studied. For this purpose, only data from measurements with 100 % cloudiness entered the calculation to minimize the influence by the sun radiation. In Figure 3.5, a weak correlation in the relation of air temperature and temperature difference can be seen.

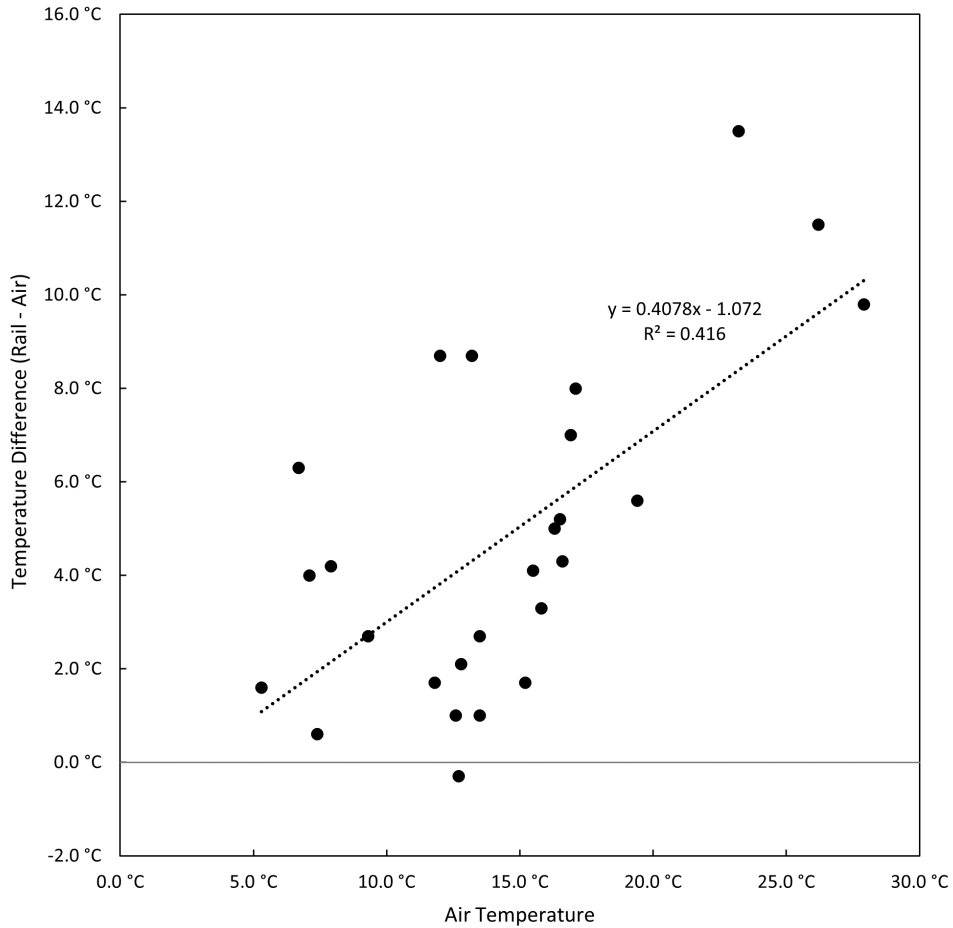


**Figure 3.5** – Relation between Air Temperature and Temperature Difference

A linear trend line can be obtained out of this dataset using the least squares methodology. The equation of this trend line is

$$y = 0.4078 \cdot t - 1.072, \quad (3.2)$$

where  $t$  is the air temperature.

Combining Equations 3.1 and 3.2, we can obtain the relation of cloudiness, air temperature, and temperature difference; and subsequently the relation of cloudiness, air temperature and rail temperature. The resulting equation is

$$y = 1.4078 \cdot t - 3.861 \cdot e^x + 9.4938, \quad (3.3)$$

where  $t$  is the air temperature and  $x$  is the cloudiness [-].

Spatial diagram of Equation 3.3 is shown in Figure 3.6.

Finally, application of Equation 3.3 on the calculation of the rail temperature results in a good correlation among the measured data and the calculated prediction. The correlation coefficient for the population of values measured in the period from 1<sup>st</sup> April to 30<sup>th</sup> September 2017 is 0.923. Figure 3.7 shows the measured rail temperature data (black line) and the calculated prediction of the rail temperature (red line) for the investigated period.

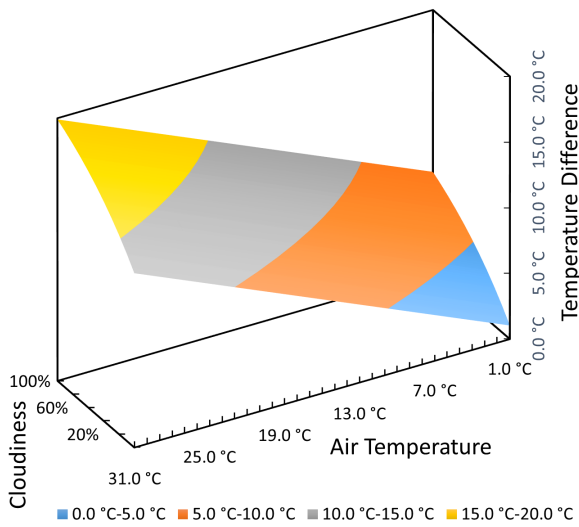


**Figure 3.6** – Relation between Cloudiness, Air Temperature and Temperature Difference

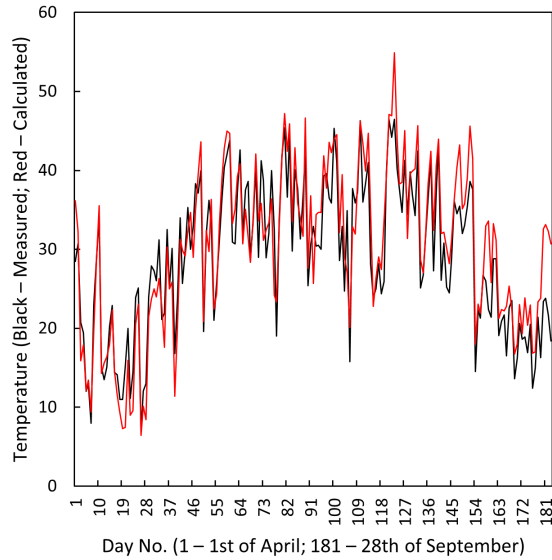


**Figure 3.7** – Comparison of Measured Rail Temperature (blue line) and Calculated Rail Temperature (grey line)

### 3.1.3 Discussion

The presented data show that the rail temperature can be reasonably well estimated by a combination of a set of parameters. Using well selected parameters, a sufficiently accurate instant value of rail temperature can be reached. In this chapter, only two basic parameters – air temperature and cloudiness – were selected, and a limited data gathered. Yet, the results show a decently good correlation. With a larger database and a larger set of parameters investigated, a good system of rail temperature estimation can be established for the Czech Republic, and potentially for other countries.

An interesting correlation can be made in comparison with the Eurocode EN 1991-1-5 – Thermal actions [53]. This Eurocode includes a graph of a bridge structure temperature related to the ambient air temperature in both uniform temperature component and temperature difference component. The uniform temperature component of the Type 1 bridge deck (steel deck) can be compared to the uniform temperature component of a rail investigated in this chapter. Comparison of data from Figure 6.1 of the Eurocode and the analytically calculated data from the measurement is presented in Figure 3.8.

The population for the analytical calculation was somewhat limited, with data for the temperature range of 5 – 28 °C only. Therefore, the calculated values are limited by this range.



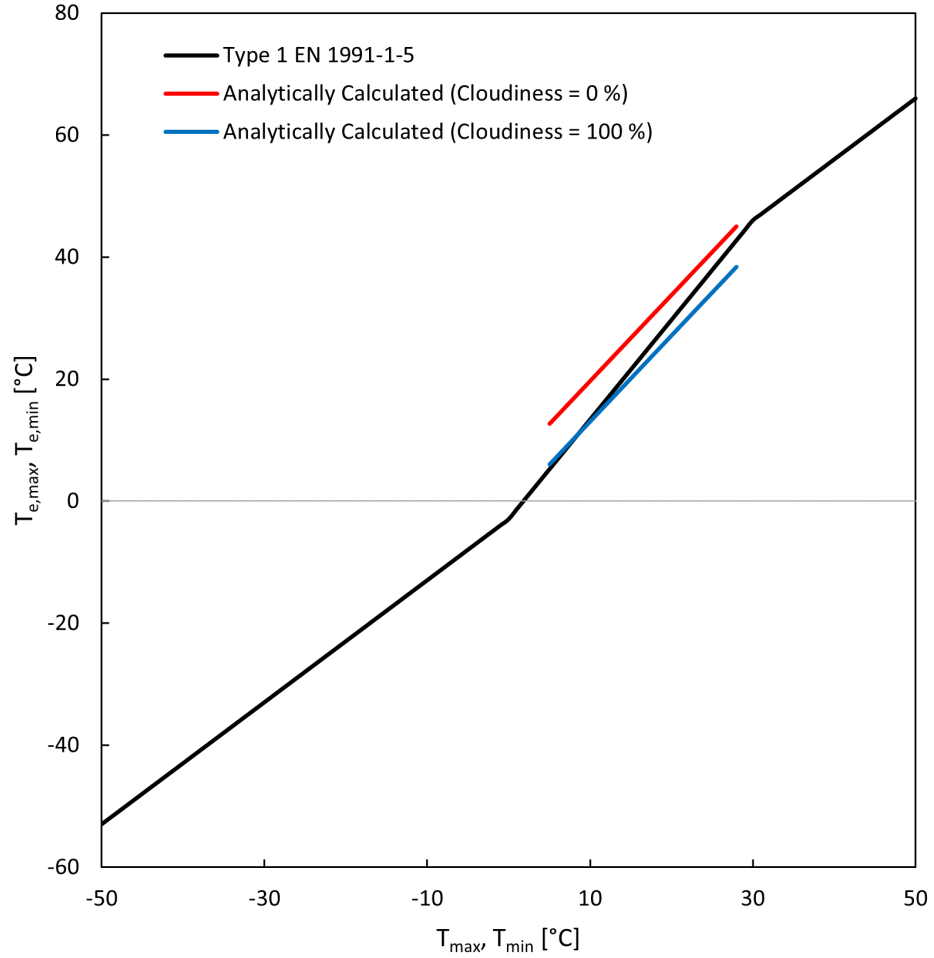


**Figure 3.8** – Comparison of Data from Figure 6.1 of the EN 1991-1-5 [53] and the Analytically Calculated Data from the Measurements

On the other hand, cloudiness data were available. This enabled to calculate the lower and upper boundaries in this temperature range based on the cloudiness level. The lower boundary (represented by the blue line) shows the calculated uniform temperature component of a rail under cloudiness = 100 %, based on Equation 3.3 for  $x = 1$ ; and upper boundary (red line) shows the calculated uniform temperature component of a rail under cloudiness = 0 %, based on Equation 3.3 for  $x = 0$ . A good correlation among the uniform temperature components of a bridge deck according to the Eurocode and the uniform temperature component of a rail was found.

Rail temperature is a crucial quantity to investigate the neutral temperature change, as will be claimed further in the dissertation. Even though it can be relatively easily monitored by autonomous thermometers (a development of one type of such a thermometer was a part of the research project No. TJ04000301 *Non-Destructive Determination of Mechanical Stress in Continuous Welded Rail*), it may be more efficient to make use of the existing network of hydrometeorological measuring stations and, with an intake of the existing data, estimate the rail temperature mathematically. Apart from other reasons, it shall reduce the amount of instruments being installed in the railway tracks.

Among other important parameters which may have an impact on rail temperature, precip-

itation and wind speed seem as the most important ones. The landscape, with scaling up to the ecotope level, may be of a great importance, too. Further research on the parameters and their impact on the rail temperature shall be investigated in the future.

### 3.2 Rail Temperature Monitoring in Selected Spots of the Czech Railway Network

Operated railway lines are never built in laboratory conditions. Except for the impact of particular atmospheric effects, as those studied in the previous section of this chapter, the full combination of factors that create the particular ecotope of a spot can be investigated, too. An extensive research into the thermal conditions of selected localities in the Czech railway network was done. This research is summarized in this section. This research was a part of investigation of the research project No. TJ04000301 *Non-Destructive Determination of Mechanical Stress in Continuous Welded Rail*.

#### 3.2.1 Experimental Setup

Rail temperature measurements were performed by card thermometers with adjustable interval of recording and built-in data-logger. The thermometers were purchased in more orders, therefore two types were used in total (the older type was substituted by the newer one in the market and not available any more). The older type of the thermometer which was used for the measurements was the type of Elitech ETAG-1 and the newer type Elitech TI-2S. The thermometers are shown in Figures 3.9 and 3.10.



Figure 3.9 – Card Thermometer with Built-in Data-Logger – Type Elitech ETAG-1



Figure 3.10 – Card Thermometer with Built-in Data-Logger – Type Elitech TI-2S

Both types of thermometers store data into a built-in memory with the capacity of 4000, respectively 3840 values. The data can be downloaded into a cell phone via an NFC chip and exported in a *.csv* file. The principle of work of both thermometers is very similar, therefore, no specification on which type was used at which measuring spot is provided further in this section.

The thermometers were attached from bottom to the rail foot between two sleepers (except for the Borovnice locality, see below). A plastic holder with a magnetic system to hold the temperature probe adjoining to the rail surface was developed by undergraduate students Karel Suchý and Tadeáš Šustr collaborating on the research project. The holder is presented in Figures 3.11 and 3.12.



**Figure 3.11** – Card Thermometer Holder – Top View



**Figure 3.12** – Card Thermometer Holder – Side View

### 3.2.2 Monitored Localities

The selection of monitoring localities was done in collaboration with representatives of Správa železnic, s. o., the Czech national railway infrastructure manager. Five localities were selected in total:

- Borovnice,
- Ostružná,
- Hradec Králové,
- Karviná, and
- Harrachov.

A closer description of the localities follows.

## A. Borovnice

The rail temperature measurement in the Borovnice locality was combined with the CWR strain measurement described in Section 4.3. Four thermometers were attached to the rails, with three of them at the same spot into different positions – one was attached at the left side of the rail web, one at the rail foot from below the rail, and one at the right side of the rail web. Only these three are used in this analysis. All of them on the same rail. The railway line, as visible in Figure 3.13, is constructed nearly in the east-west orientation. This means the left side of the rail web faces towards the south-southwest and is predominantly exposed to sunshine on sunny days, and the right side of the rail web faces towards the north-northeast and is in shade over the majority of daytime. The railway track in this locality is at an altitude of approximately 500 m AMSL. A map of the locality is shown in Figure 3.13 and the attached thermometers in Figures 3.14 and 3.15.

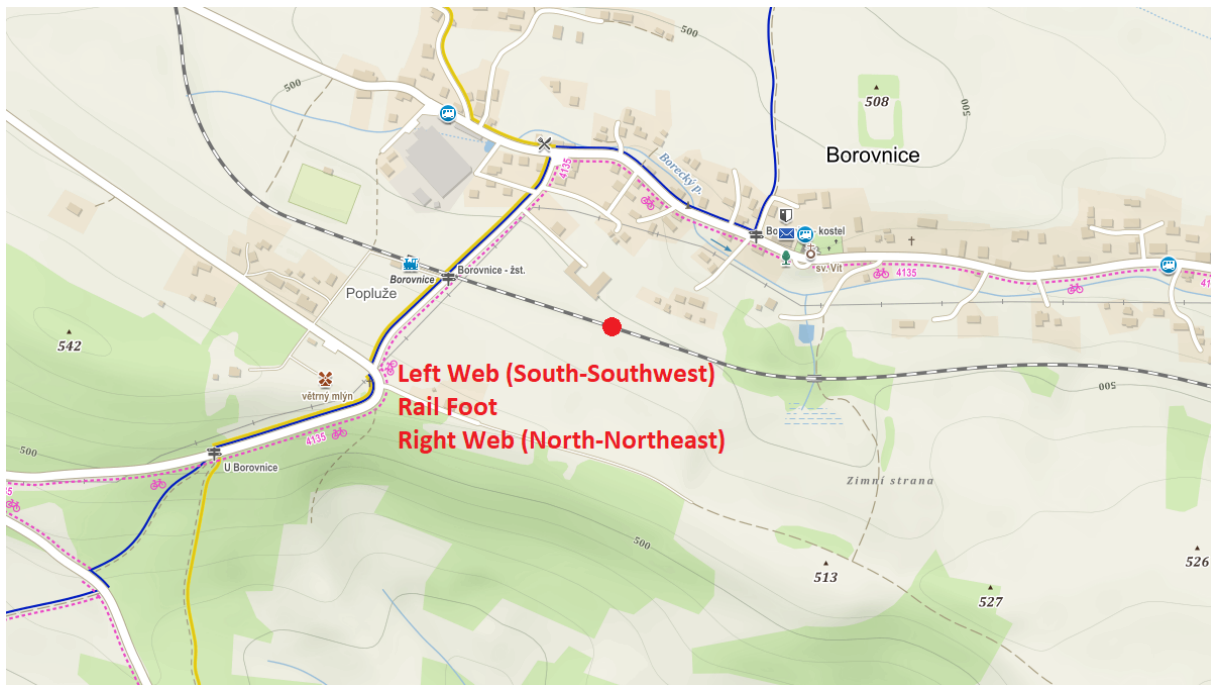


Figure 3.13 – Borovnice Locality



**Figure 3.14** – Position of the Thermometer at the Left Side of the Rail Web in the Borovnice Locality



**Figure 3.15** – Detailed View on the Position from Figure 3.14 with the Thermometer at the Rail Foot Partly Visible

## **B. Ostružná**

Two thermometers were installed in the Ostružná locality. One thermometer was attached to a rail on a bridge across the II/369 road from Branná to Ostružná and the other one was attached to a rail on an embankment next to the bridge in a distance of approximately 100 m. Both thermometers were attached to the rail foot from below the rail. The railway track in this section is in a horizontal curve and vertical slope. At the positions of the thermometers, the orientation of the rail is approximately east-west. The railway track in this locality is at an altitude of approximately 670 m AMSL. A map of the locality is shown in Figure 3.16 and the positions of the thermometers in Figures 3.17 and 3.18.



**Figure 3.16** – Ostružná Locality



**Figure 3.17** – Ostružná Locality – Position of a Thermometer on the Rail Bridge (Thermometer from the bottom of the Rail Foot), Author Miloš Šula

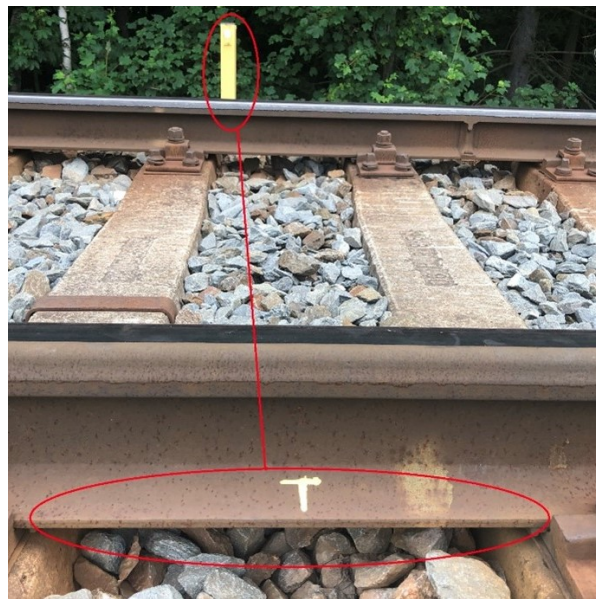


**Figure 3.18** – Ostružná Locality – Position of a Thermometer on the Embankment (Thermometer from the bottom of the Rail Foot), Author Miloš Šula

### C. Hradec Králové

Another two thermometers were installed in the Hradec Králové locality. One thermometer was attached to a rail foot in the railway line from Pardubice to Hradec Králové in the Pražské předměstí district. The railway track is in a straight section in this locality and its orientation is approximately north-south. The altitude of the railway track is approximately 230 m AMSL. A map of this thermometer position is shown in Figure 3.19 and its position in Figure 3.21.



**Figure 3.19** – Position of the First Thermometer in Hradec Králové Locality

The other thermometer in the Hradec Králové locality was attached to a rail foot in the railway line from Hradec Králové to Týniště nad Orlicí in the Slezské předměstí railway station. The railway track is in a straight section here and its orientation is approximately east-west. The altitude of the railway track is approximately 235 m AMSL. A map of this thermometer position is shown in Figure 3.20 and its position in Figure 3.22.



**Figure 3.20** – Position of the Second Thermometer in Hradec Králové Locality



**Figure 3.21** – Hradec Králové Locality – Position of a Thermometer in Pražské předměstí District (Thermometer from the bottom of the Rail Foot), Author Dr. Vladimír Suchánek



**Figure 3.22** – Hradec Králové Locality – Position of a Thermometer in Slezské předměstí District (Thermometer from the bottom of the Rail Foot), Author Dr. Vladimír Suchánek

#### D. Karviná

Other two thermometers were installed in the Karviná locality. Both of them were installed on a railway track of the Bohumín – Český Těšín railway line. One thermometer was installed at the former Karviná-Darkov railway stop. The railway track is in a straight section and its orientation is from north-west to south-east. The altitude of the railway track is approximately 230 m AMSL. A map of this thermometer position is shown in Figure 3.23 and its position in Figure 3.25.



**Figure 3.23** – Position of the First Thermometer in Karviná Locality



The other thermometer in the Karviná locality is placed approximately 2.8 km from the first one in the direction of Český Těšín. Its location is just next to the level crossing of the railway line and the road II/475. The railway track orientation is from north-west to south-east again. The altitude of the railway track is approximately 240 m AMSL. A map of this thermometer position is shown in Figure 3.24 and its position in Figure 3.26.



**Figure 3.24** – Position of the Second Thermometer in Karviná Locality



**Figure 3.25** – Karviná Locality – Position of a Thermometer in Karviná-Darkov Stop (Thermometer from the bottom of the Rail Foot)



**Figure 3.26** – Karviná Locality – Position of a Thermometer next to the Railway Crossing (Thermometer from the bottom of the Rail Foot)

## E. Harrachov

A set of thermometers was installed in the Harrachov locality, because it offers various geographical locations and structural specifications within a relatively short section with similar weather conditions. The set comprises of six thermometers, five of them used for the analysis within this dissertation as one of the set was experiencing technical problems. One of the five thermometers is installed in the Polubenský Tunnel on the Tanvald – Harrachov railway line, but relatively close – approximately 50 m – from the tunnel portal. The railway track in this location is in a steep slope of more than 50 ‰. The altitude of the railway track is approximately 660 m AMSL in the position of the thermometer. A map of this thermometer position is shown in Figure 3.27 and its position in Figure 3.29.

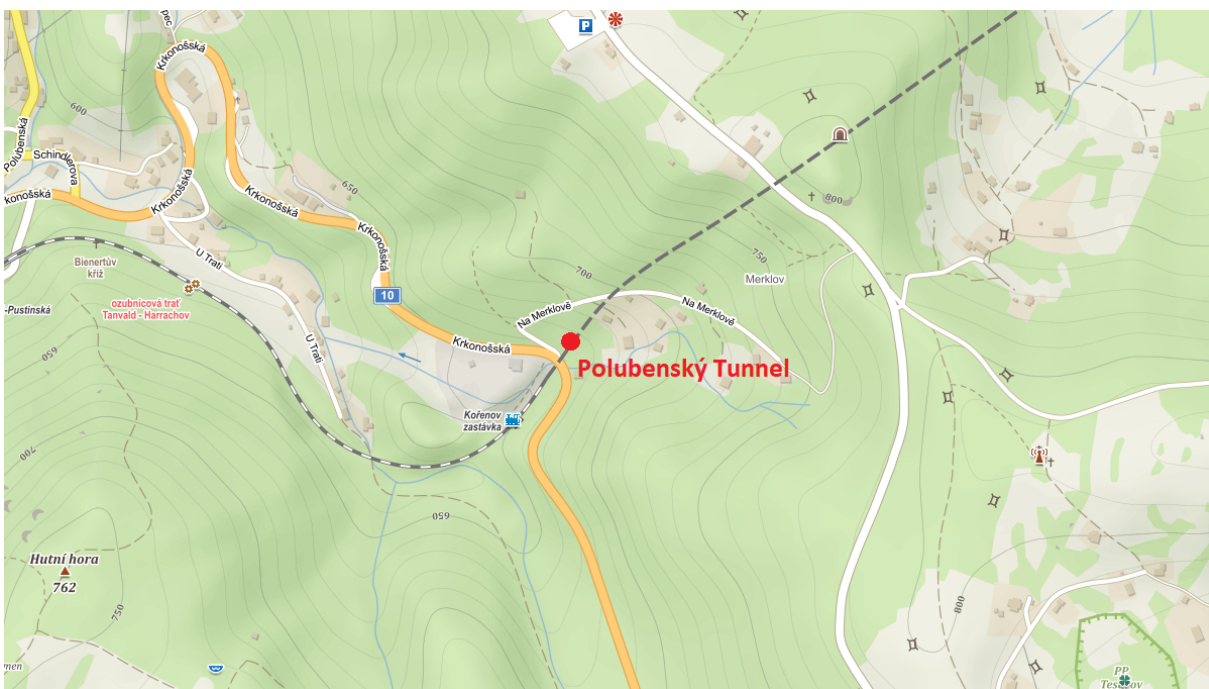


**Figure 3.27** – Position of the First Thermometer in Harrachov Locality

The other thermometers were installed on the same line further in the direction of the Harrachov station. One thermometer was attached to a rail on the Jizera bridge. This bridge spans over the Jizera river and its orientation is east-west, another one is attached to a rail on the embankment next to the Jizera bridge, the next one is placed in a rock cutting which is oriented from north-west to south-east and finally, the last one is positioned in the Harrachov station in the same orientation. The altitude of the railway track is 700 – 740 m AMSL in the section of these four thermometers. For a better overview, position of the thermometers are depicted in Figure 3.28 and, for illustration, the position of the thermometer in a rock cutting in Figure 3.21.

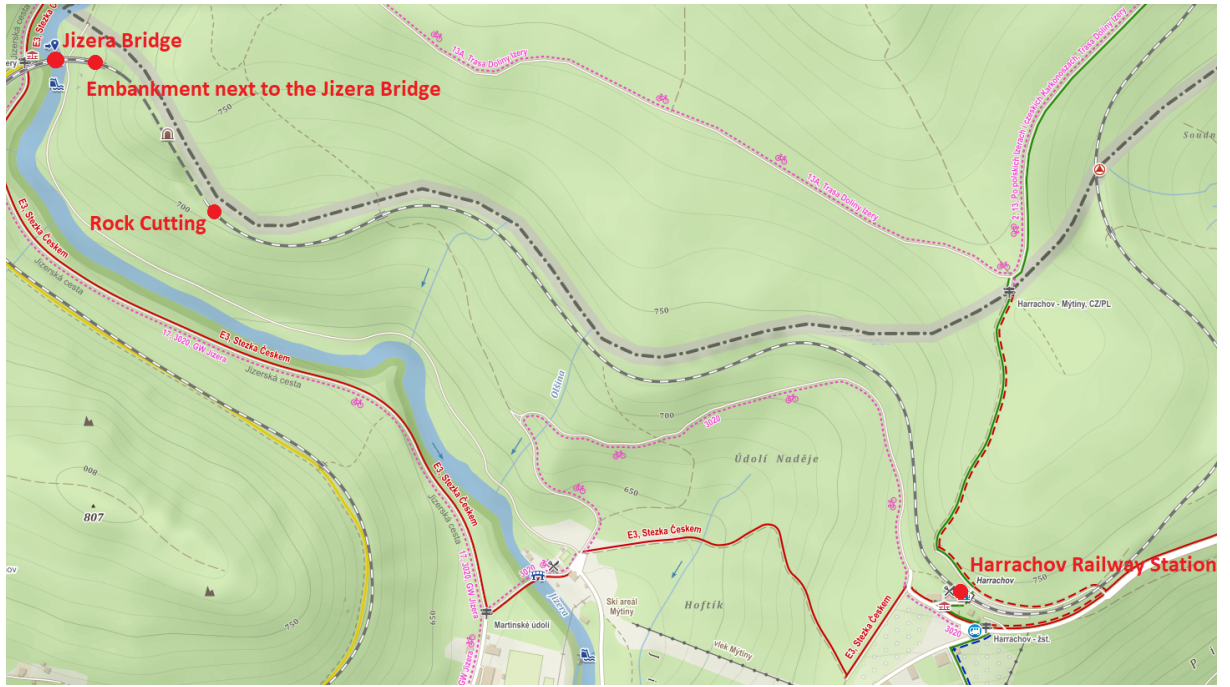


**Figure 3.28** – Position of the Other Four Thermometers in Harrachov Locality



**Figure 3.29** – Harrachov Locality – Position of a Thermometer in Polubenský Tunnel (Thermometer from the bottom of the Rail Foot), Author Dr. Vladimír Suchánek



**Figure 3.30** – Harrachov Locality – Position of a Thermometer in the Rock Cutting (Thermometer from the bottom of the Rail Foot), Author Dr. Vladimír Suchánek

### 3.2.3 Data Analysis

The data collected from the data loggers were processed in Microsoft Excel and graphs of the temperature records were produced. Summarized graphs from all thermometers within a locality are presented in this section. Graphs of particular thermometers are presented in Appendix A.

The following table summarizes the periods of data collection in each locality.

Locality	Start of Measurement	End of Measurement
A. Borovnice	5 <sup>th</sup> June 2021	26 <sup>th</sup> October 2021
B. Ostružná	5 <sup>th</sup> August 2021	24 <sup>th</sup> October 2021
C. Hradec Králové	16 <sup>th</sup> August 2021	27 <sup>th</sup> October 2021
D. Karviná	25 <sup>th</sup> December 2021	1 <sup>st</sup> April 2022
E. Harrachov	14 <sup>th</sup> July 2021	5 <sup>th</sup> July 2022

**Table 3.2** – Temperature Data Collection Periods per Locality

The following table summarizes the minimum and maximum temperature recorded by each thermometer.

Locality	Thermometer	Minimum Temperature	Maximum Temperature
A. Borovnice	Left Web	−4.5 °C	56.9 °C
	Rail Foot	−4.0 °C	48.3 °C
	Right Web	−4.2 °C	49.7 °C
B. Ostružná	Bridge	−3.1 °C	42.0 °C
	Embankment	−1.6 °C	31.4 °C
C. Hradec Králové	Pražské předměstí	−2.0 °C	41.0 °C
	Slezské předměstí	−1.9 °C	42.2 °C
D. Karviná	Karviná-Darkov Stop	−13.3 °C	31.0 °C
	Next to the Railway Crossing	−14.3 °C	37.0 °C
E. Harrachov	Polubenský Tunnel	−4.8 °C	14.8 °C
	Jizera bridge	−19.5 °C	38.1 °C
	Embankment	−12.4 °C	46.5 °C
	Rock Cutting	−9.4 °C	38.3 °C
	Harrachov Railway Station	−10.1 °C	45.8 °C

**Table 3.3** – Extreme Temperature Measured per Thermometer

## A. Borovnice

The record from Borovnice compares the temperature measurements in various positions on a rail. The presented data were recorded in the period of 5<sup>th</sup> June 2021 – 26<sup>th</sup> October 2021. While the record low temperatures are on a similar level, the record high temperatures are significantly higher on the left side of the rail web (in the sun). On 19<sup>th</sup> June 2021, 56.9 °C was measured as the extreme high temperature within the monitored period on the left side of the rail web, while 47.8 °C was measured on the rail foot and 48.5 °C on the right web. The recorded values from all thermometers in Borovnice are presented in Figure 3.31.

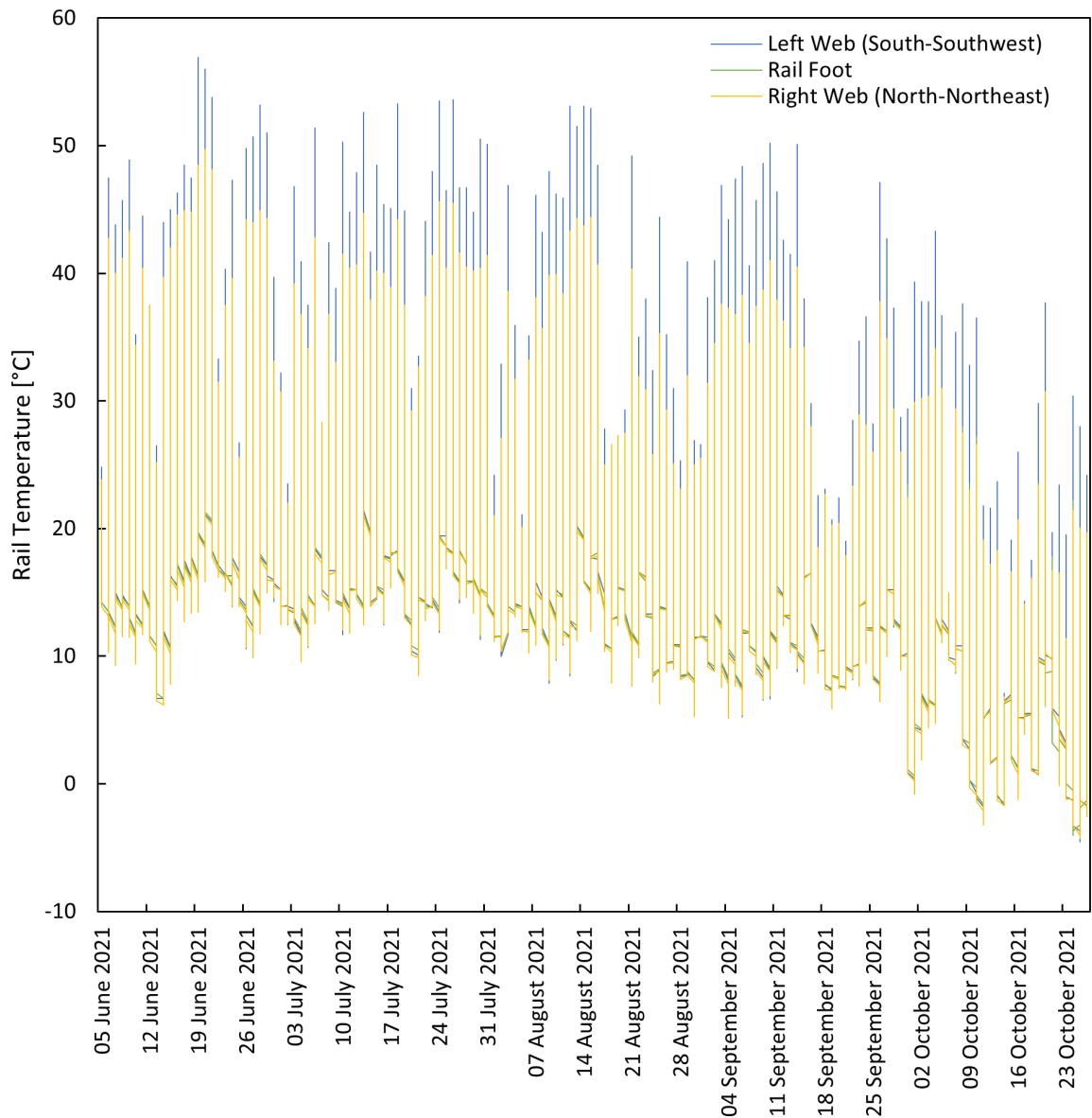


**Figure 3.31** – Rail Temperature Recordings in Borovnice Locality

## B. Ostružná

The record from Ostružná shows a difference among a rail on a bridge and on an embankment of similar geographical orientation. The presented data were recorded in the period of 5<sup>th</sup> August 2021 – 24<sup>th</sup> October 2021. Higher amplitudes of temperature are recorded on the bridge with the record high temperature of 42 °C on 14<sup>th</sup> August 2021 and the record low of –3.1 °C on 24<sup>th</sup> October 2021. On the embankment, the record high temperature of 31.4 °C was measured on 15<sup>th</sup> August 2021 and the record low of –1.6 °C on 24<sup>th</sup> October 2021, too. All the recorded values from the Ostružná locality are presented in Figure 3.32.

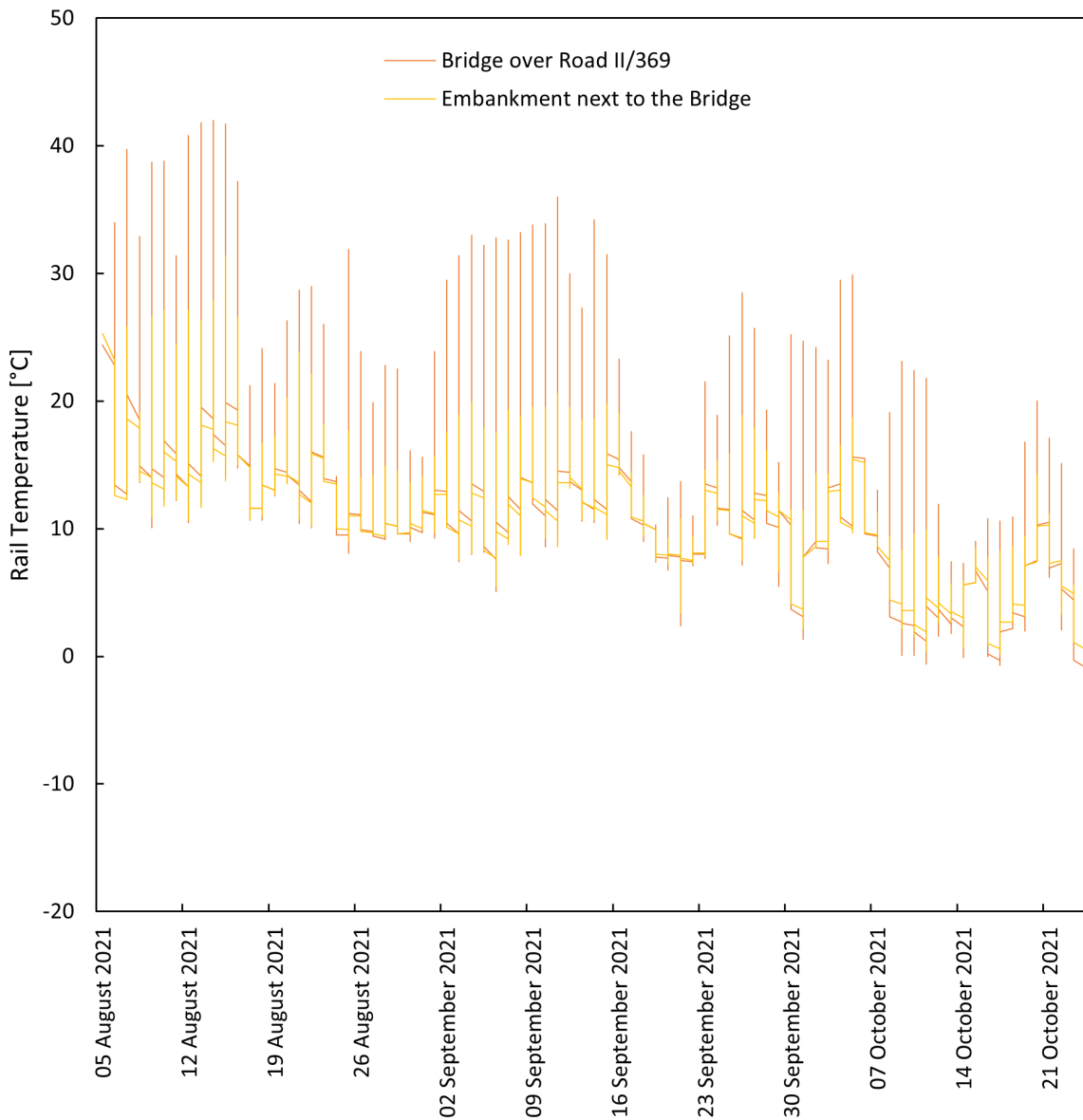


**Figure 3.32** – Rail Temperature Recordings in Ostružná Locality

### C. Hradec Králové

The record from Hradec Králové shows a difference among a rail oriented in the approximately north-south direction and a rail oriented in the east-west direction. The presented data were recorded in the period of 16<sup>th</sup> August 2021 – 27<sup>th</sup> October 2021. Slightly higher amplitudes of temperature seem to appear on the railway track with the north-south orientation, although the record high temperature of 42.2 °C was recorded in the east-west railway track in the Slezské předměstí district on 10<sup>th</sup> September 2021. The record low temperature of –2 °C was recorded in the north-south railway track in the Pražské předměstí district on 24<sup>th</sup> October 2021. All the recorded values from the Hradec Králové locality are presented in Figure 3.33.

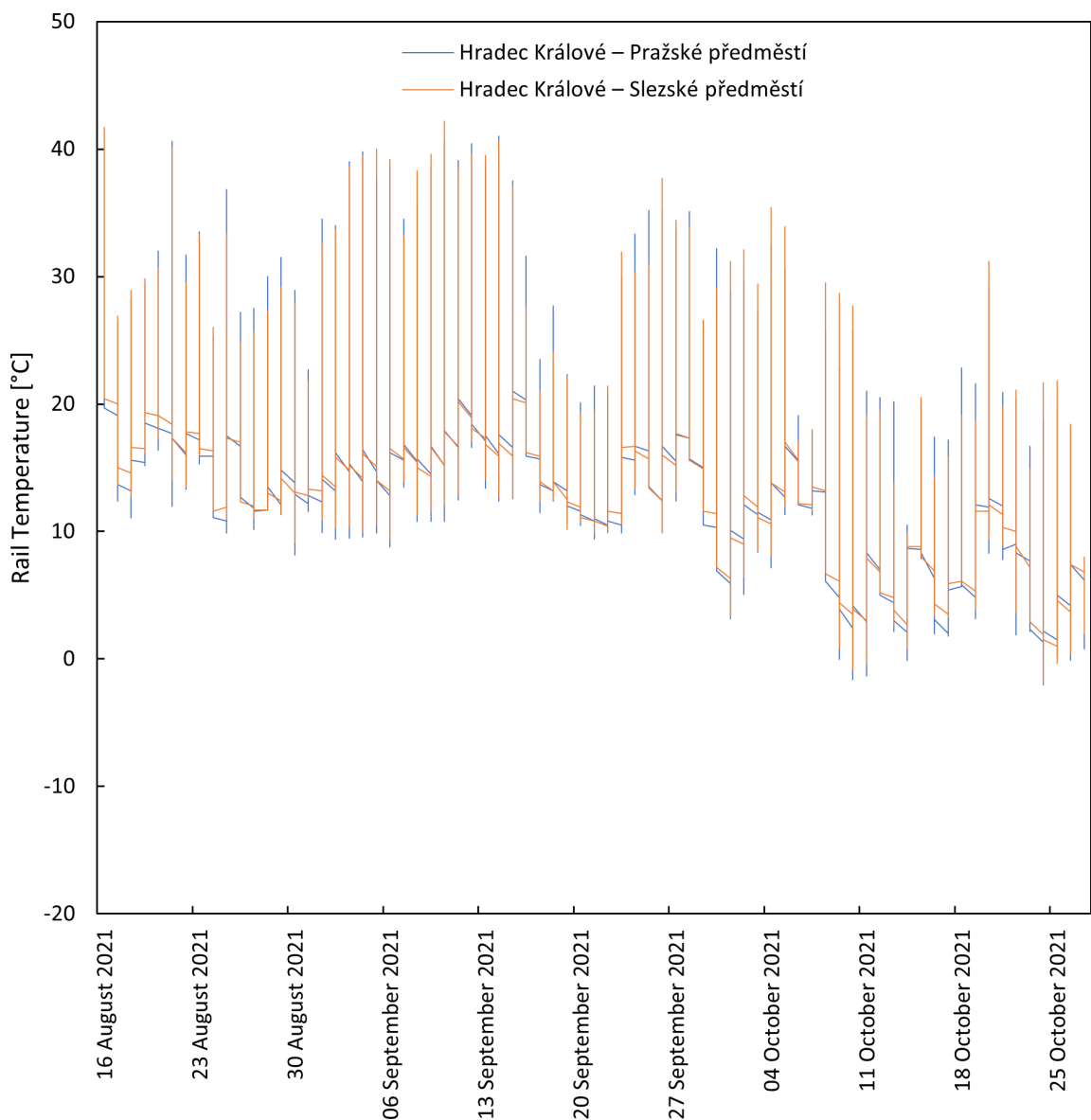


**Figure 3.33** – Rail Temperature Recordings in Hradec Králové Locality

## D. Karviná

The record from Karviná shows a slightly higher amplitudes in the position near to a railway crossing next to the former ČSM Sever coal mine. The record high temperature measured in this position was 37 °C on 23<sup>rd</sup> March 2022, the record low  $-14.3$  °C on 26<sup>th</sup> December 2021. Presented data were recorded in the period of 25<sup>th</sup> December 2021 – 1<sup>st</sup> April 2022. All the recorded values from the Karviná locality are presented in Figure 3.34.

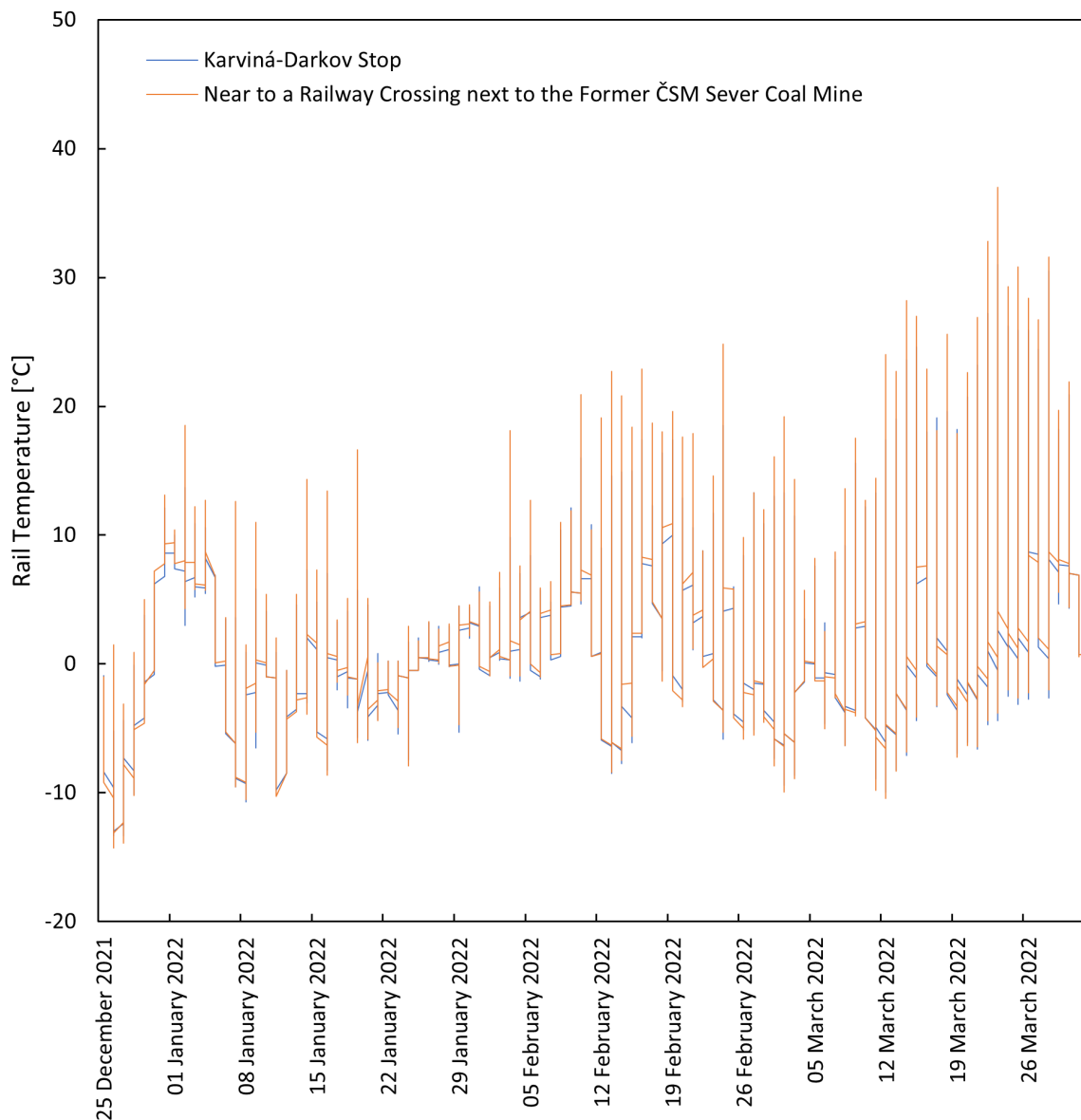


**Figure 3.34** – Rail Temperature Recordings in Karviná Locality



## E. Harrachov

The Harrachov locality data cover the longest period: 14<sup>th</sup> July 2021 – 5<sup>th</sup> July 2022. The first thermometer is placed in a tunnel, but only 50 m from its portal. The record high temperature of 14.8 °C was measured on 1<sup>st</sup> July 2022 and the record low of –4.8 °C on 25<sup>th</sup> December 2021. The second one, placed on the Jizera bridge, shows the record high value of 38.1 °C on 27<sup>th</sup> June 2022 and the record low of –19.5 °C on 26<sup>th</sup> December 2021. The third one, placed on embankment next to the bridge, shows the record high value of 46.5 °C on 27<sup>th</sup> June 2022 and the record low of –12.4 °C on 26<sup>th</sup> December 2021. The fourth one, placed in the rock cutting, stopped recording on 23<sup>rd</sup> February 2022. It shows the record high temperature of 38.3 °C on 26<sup>th</sup> July 2021 and the record low of –9.4 °C on 26<sup>th</sup> December 2021. The fifth one, placed at the Harrachov station, shows the record high value of 45.8 °C on 27<sup>th</sup> June 2022 and the record low of –10.1 °C on 26<sup>th</sup> December 2021. All the records are presented in Figure 3.35.

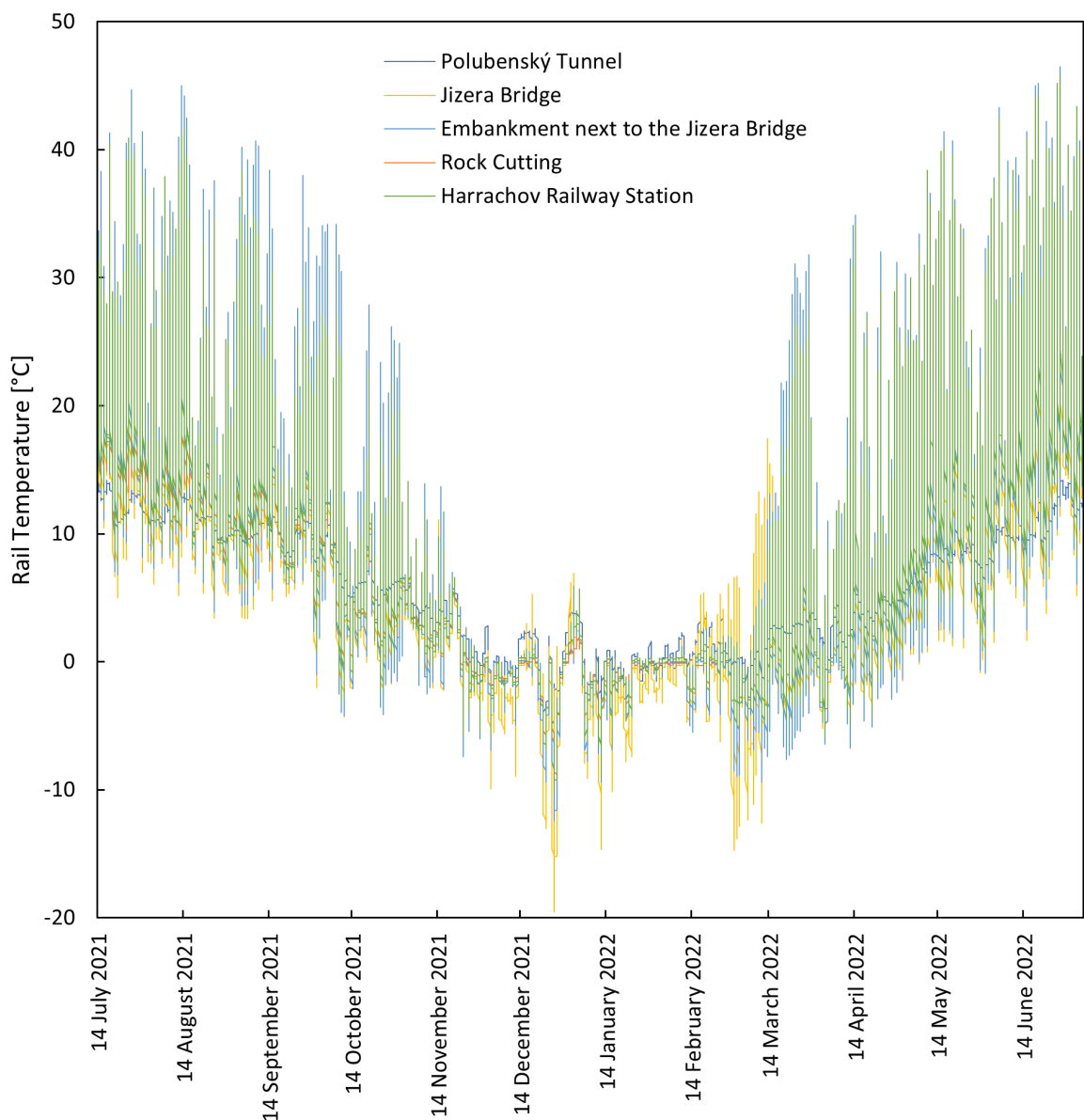


**Figure 3.35** – Rail Temperature Recordings in Harrachov Locality



The lower intensity of rail traffic in Borovnice can be among other reasons of this effect, as the passing vehicles may provide both a while of shade and a cooling air stream to prevent the rail from reaching the top heat over the period of a sunny day. A more valid explanation has to be given by a further research.

The data from Ostružná show that the mass of soil in the embankment provides a more stable environment for a day/night temperature change than a relatively tinier bridge structure, which can be cooled from below, too. No extreme temperature values were recorded in this locality.

The data from Hradec Králové were expected to show a difference between a temperature record on a rail aligned in the north-south orientation and in the east-west orientation. Such a difference has not been proved. However, it is important to note that only two thermometers were placed into this locality and both were attached to places relatively far from each other. Moreover, the situation may vary here in the case of the rail web, as the south face of the rail web in the Slezské předměstí district is significantly more exposed to sunshine than the north face, while the web sites in the Pražské předměstí district share the exposition to sunshine evenly.

The values recorded in Karviná show the influence of vegetation in the railway track vicinity on the rail temperature. The forest, which surrounds the railway tracks in the former Karviná-Darkov station significantly decreases the record high temperatures in comparison to the ones measures in the relatively open space area of the railway crossing next to the former ČSM Sever coal mine. The ballast bed in both sections is relatively clear. For this reason, no impact of a ballast bed covered by bituminous coal powder fouling could be recorded.

The data from Polubenský Tunnel in the Harrachov locality show the minimum difference between the record high and the record low temperature – less than 20 °C. This is expected and, if the thermometer was placed further in the tunnel tube, even more equal course could be expected. However, no more thermometers were attached further in the tunnel and therefore no more data is available from there.

The thermometer attached on the Jizera bridge recorded significantly lower recorded temperatures than others, reaching the record low as of  $-19.5$  °C. These values are in a clear support of what can be observed in the case of the bridge over the II/369 road near Ostružná. The circulating air cools down the structure and the rail and enables reaching significantly lower extremes than in the case of embankments. In the case of the Jizera bridge, the effect might be even underpinned by the geography of a mountain valley and the fact that the bridge spans across a river as a water body instead of only a road.

The temperatures recorded on the embankment next to the Jizera bridge show significantly higher values than those ones recorded on the next-standing bridge. This is a difference from what was recorded in Ostružná, where the thermometer on the bridge recorded more extreme values on both sides of the spectrum. Here the low amplitudes are on the same level as on the bridge or higher, and the high amplitudes are higher than the ones on the bridge. This leads to an assumption that the bridge acts as a local cool spot in the railway track and this may result in various implications, like a possibility of decrease of the rail neutral temperature in this position.

One more interesting fact can be observed from the data obtained at the embankment next to the Jizera bridge: After a period of freezing the measured temperature does not rise over 0 °C. The reason of this behaviour seems to reside in freezing the thermometer (possibly with a layer of snow) to the rail and therefore keeping the snow melting temperature. The warmer periods in this time was probably so short that the warmth was unable to deliver the necessary latent heat of fusion and the snow and ice packed to the track superstructure did not melt and prevented the thermometer (and the rail!) from increasing its temperature over 0 °C. After a sufficient period of warm weather, the snow and ice melted and the rail could experience higher temperatures again.

The thermometer in the rock cutting stopped logging the temperature on 23<sup>rd</sup> February 2022, the provided data is, therefore, limited. Yet, the same effect of freezing up in snow and ice can be observed. The record high temperatures are higher than in the case of the Jizera bridge, but lower than in the case of the embankment next to the bridge and the Harrachov railway station. This is assumed to be caused by the specific geographic location of the rock cutting which keeps a relatively cooler climate and sunshine is limited in this environment.

Finally, the records from the Harrachov railway station show a similar progress as the records from the embankment next to the bridge. An interesting comparison can be seen in the months of September/October and March. The temperature recorded in the Harrachov railway station is significantly lower than the temperature on the embankment next to the Jizera bridge. No investigation on this difference was made as of yet, but a local influence on the specific sun rays angle in this time of year is assumed to be the cause.

In comparison of the values from different localities mutually, the clear influence of bridges on the record low temperatures is apparent. It is not unequivocal in the record high temperatures, however. A more closed environment, like a tunnel and a rock cutting helps to reduce the range of recorded temperatures. An interesting role is played by the packed ice and snow, as their ability to prevent the rail temperature rise over 0 °C even if the air temperature rises may be an influencing factor on the yearly average rail temperature, especially if the heat waves are short (i. e. the positive and negative temperatures are changing frequently). A vegetation surrounding helps reduce the record high rail temperatures significantly, too.

## Chapter 4

# Strain of Continuous Welded Rail

Under optimum conditions, no permanent strain is expected in CWR after stress-controlled welding, according to the theory of CWR. Under such assumption, the neutral temperature shall correspond to the tensioning temperature and shall remain constant over time [9]. In reality however, various reasons can cause an occurrence of permanent strain in CWR [8]. Among such reasons, the lateral displacement of track in a curve, the longitudinal displacement of rail in a fastening node, or the deterioration of track geometry can be considered. If such a displacement occurs, strain is to be detected in the rail.

In this chapter, an investigation into the strain detection in CWR is described. The analysis of an experimental setup under laboratory conditions is presented in the first section. A description of experimentally developed measuring set follows. Finally, an extensive CWR Strain Monitoring, which has been realised within the scope of investigation of the TAČR Zéta Project TJ04000301 *Non-Destructive Determination of Mechanical Stress in Continuous Welded Rail* is presented.

### 4.1 Wheatstone Bridge Setup Analysis

Two types of the Wheatstone bridge configurations were considered for the purpose of the track installation: the half bridge and the quarter bridge configuration, the latter bringing advantages in the laboriousness of the installation [55]. A comparison laboratory measurement was performed to find out possible drawbacks and constraints of the quarter bridge configuration. The measurement was repeated at an interval of one week with virtually the same results reached. Without loss of generality, only one of the measurements are presented in this section.

#### 4.1.1 Experimental Setup

A half bridge with one active and one dummy strain gauge, and a quarter bridge configuration of the Wheatstone bridge were installed on an S355 steel sample 200 mm long, 25 mm wide and 10 mm thick. The geometry of the sample is presented in Figure 4.1.

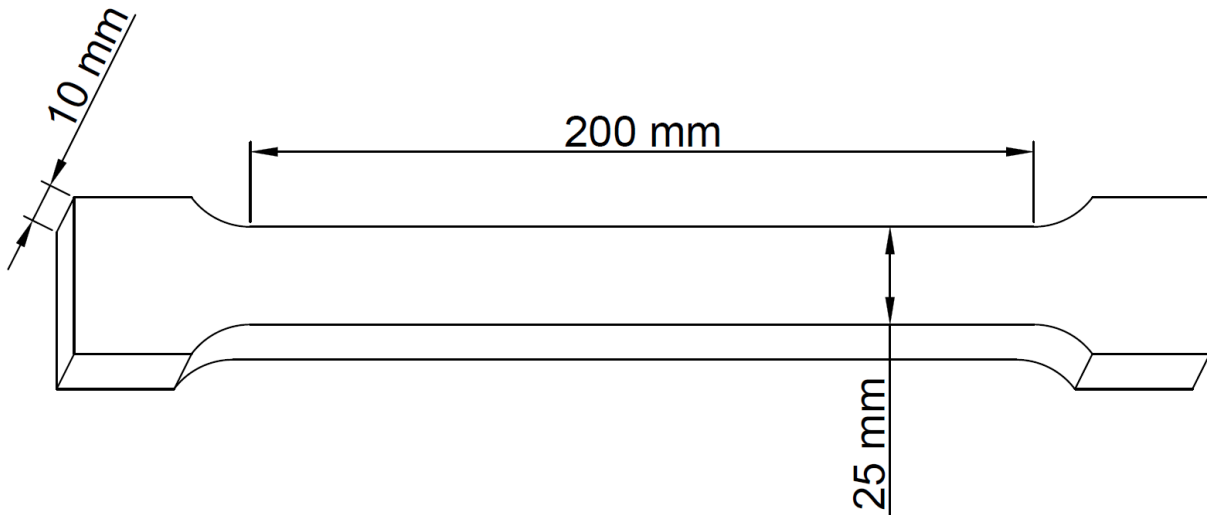


**Figure 4.1** – Scheme of the Sample Geometry

At both ends, the steel sample was widened to hold better in the clamp jaws of the dynamic stand of the ERCT. All strain gauges were of the same type – HBM K-CLY4-0060-1-350-4-050-Y, i. e. with the nominal resistance of  $350 \Omega$ , temperature compensation for ferritic steel, 4-wire cable and RJ11 connector [56]. The sample is shown in Figure 4.2. Please note that the quarter bridge strain gauge and the active strain gauge of the half bridge configuration are placed next to each other into the same cross-section of the sample, whereas the strain gauge placed closer to the end of the sample is the dummy one of the half bridge configuration.

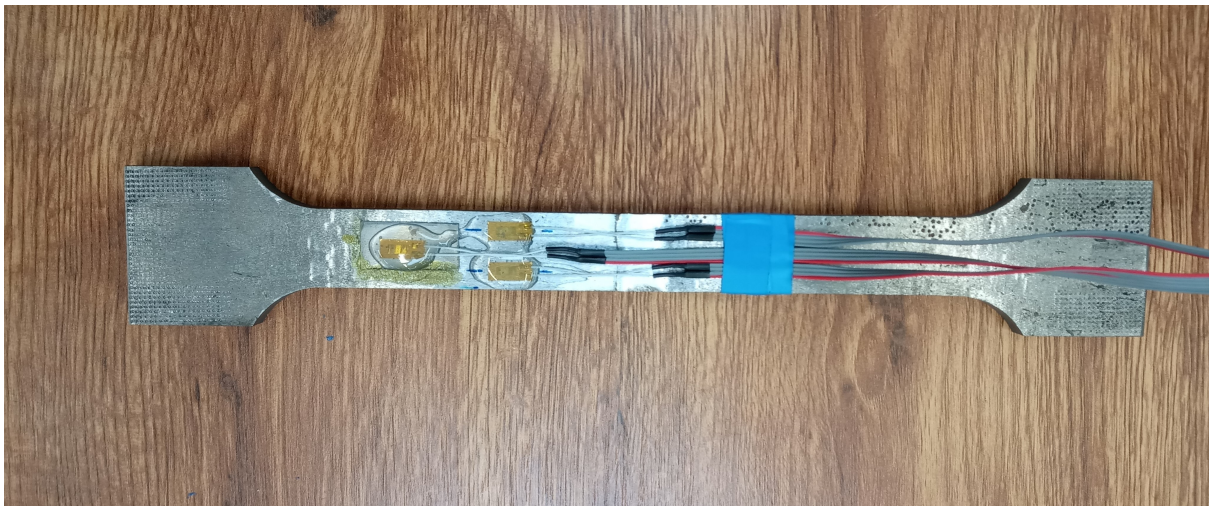


**Figure 4.2** – Steel Sample with the Half and Quarter Bridge Configurations

The sample was placed into the clamp jaws of a dynamic stand with the strain gauges facing down for the heating purposes described further in the paragraph. The strain gauges were connected into the HBM QuantumX MX840A data acquisition system and the data were recorded into the Catman Easy software. The dynamic stand enabled both position-controlled and force-controlled displacement of clamp jaws. The heating of the sample was performed manually using a hairdryer. The hairdryer was moved over the length of the steel sample aiming at the top side at a constant speed there and back to ensure as unilateral thermal loading as

possible. Positioning of the steel sample in the clamp jaws of the dynamic stand is visible in Figure 4.3. The steel sample was loaded by a linear hydraulic actuator INOVA AH 100 – 40 M062 with a force transducer GTM Series K 100 and a Messotron LVDT sensor of the WLG type.

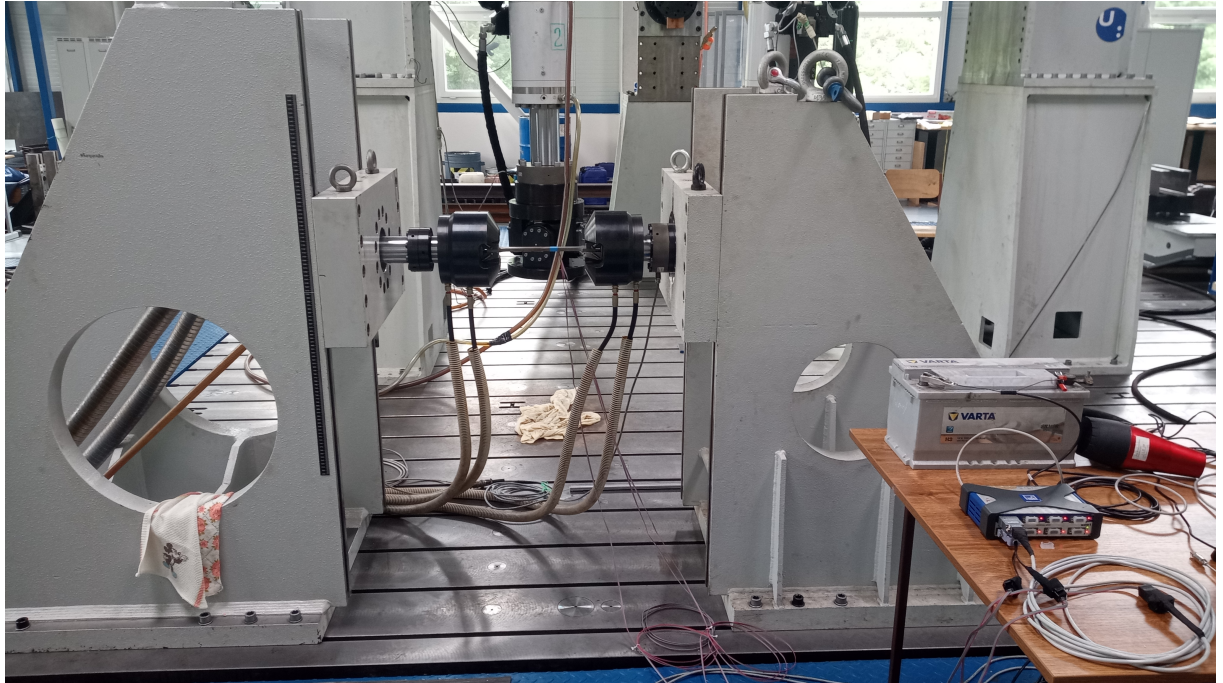


**Figure 4.3** – Steel Sample Positioned in the Dynamic Stand

#### 4.1.2 Data Analysis

Four tests were performed in the laboratory in order to compare the performance of the quarter and half bridge configurations. In the first test, the steel sample was loaded by an axial force under constant temperature. This test was performed to calibrate the strain gauges based on the analytical calculations of stress and strain applied by the axial force. In the second and third test, the sample was fixed at both ends and uniformly heated, while strain was monitored at both strain gauge configurations. The difference of those tests resided in the stress state of the sample: in the second test, the sample was free of normal stress (except for the stress emerging from the thermal loading during the test); in the third test, a pre-tension by the axial force of 30 kN was applied to the test before the thermal loading commenced and released after the cool off of the sample. Finally, in the fourth test, the sample was fixed at one side and thermally loaded, while not only strain was monitored by the strain gauges, but the displacement of the free end of the sample was monitored by the dynamic stand control unit.

#### **Loading by Normal Force at Constant Temperature**

The first test was performed without a change of temperature of the sample. The sample was loaded with a gradually increasing force from 1 to 30 kN and released back to 0 kN. The value of force was controlled by the dynamic stand control unit. The measured values of strain in

relation to the axial force is presented in Figure 4.4 and the values of normal stress in relation to the axial force is presented in Figure 4.5.

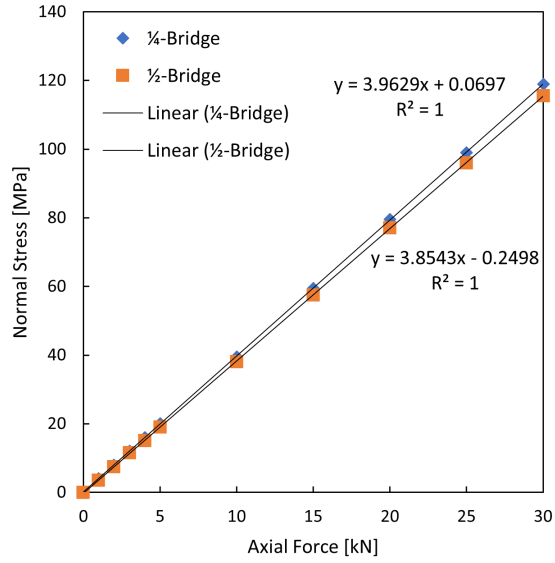
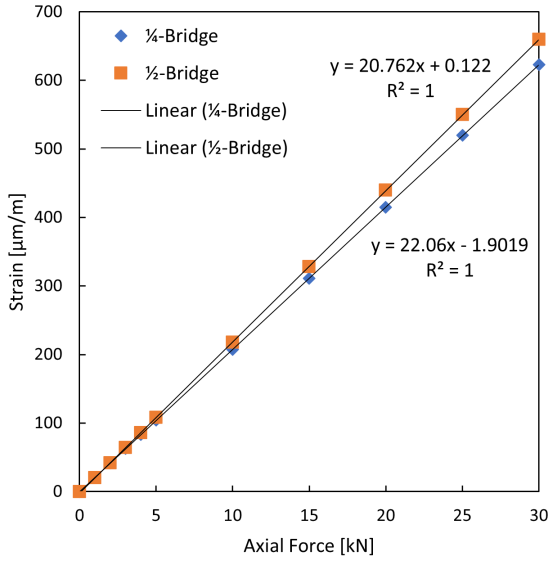


**Figure 4.4** – Relation of Measured Strain and Axial Force

**Figure 4.5** – Relation of Normal Stress (Calculated from Measured Strain) and Axial Force

The normal stress values were calculated according to Equations 4.1 and 4.2 to match the expected stress in the sample analytically calculated using Equation 4.3.

$$\sigma_{quarter} = \frac{\varepsilon \cdot E}{1.1} \quad (4.1)$$

$$\sigma_{half} = \frac{\varepsilon \cdot E}{1.2} \quad (4.2)$$

$$\sigma_{analytical} = \varepsilon \cdot E. \quad (4.3)$$

The selection of coefficients of adjustment 1.1 and 1.2 is discussed in Subsection 4.1.3.



The measured data are presented in the following Table.

Normal Force [kN]	Strain [ $\mu\text{m}\cdot\text{m}^{-1}$ ]		Normal Stress [MPa]	
	Quarter Bridge	Half Bridge	Quarter Bridge	Half Bridge
0	0	0	0.0	0.0
1	21	20	4.0	3.5
2	42	42	8.0	7.5
3	63	64	12.0	11.5
4	83	86	16.0	15.0
5	104	108	20.0	19.0
10	207	218	39.5	38.0
15	311	328	59.5	57.5
20	415	440	79.5	77.0
25	520	550	99.0	96.0
30	623	660	119.0	115.5

**Table 4.1** – Loading by Normal Force at Constant Temperature

#### Thermal Loading of Sample Fixed at Both Ends

The steel sample was fixed at both ends by jaw clamps. This position was controlled by the dynamic stand control unit. The sample was subsequently uniformly heated by a hairdryer. Initial temperature of the sample was 23.8 °C. The sample was heated up to 62.1 °C and then naturally cooled off to 25.9 °C. Temperature of the sample was periodically measured by a contact thermometer. At each temperature measurement, the axial force was recorded by the dynamic stand control unit and the strain by strain gauges. The strain was then recalculated into the normal stress according to Equations 4.1 and 4.2. The relation of strain and temperature is presented in Figure 4.6 and the relation of normal stress and temperature is presented in Figure 4.7.

After cool off to 25.9 °C, the axial force dropped to  $-1.97$  kN, the strain measured at quarter bridge to  $-43 \mu\text{m}\cdot\text{m}^{-1}$ , at half bridge to  $-24 \mu\text{m}\cdot\text{m}^{-1}$ , the calculated normal stress in both strain gauge configurations to  $-8.5$  MPa.

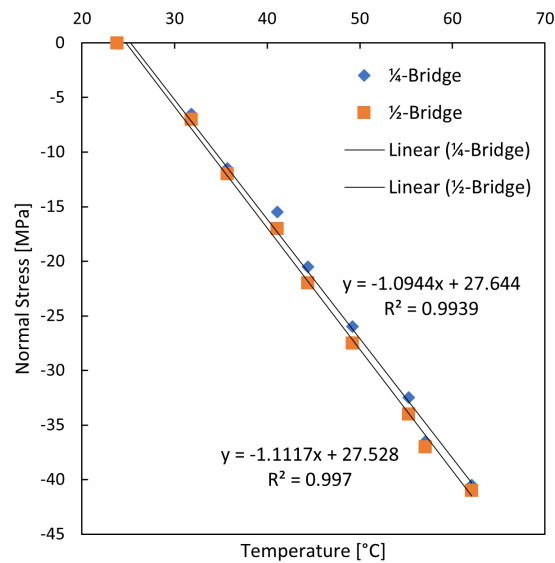
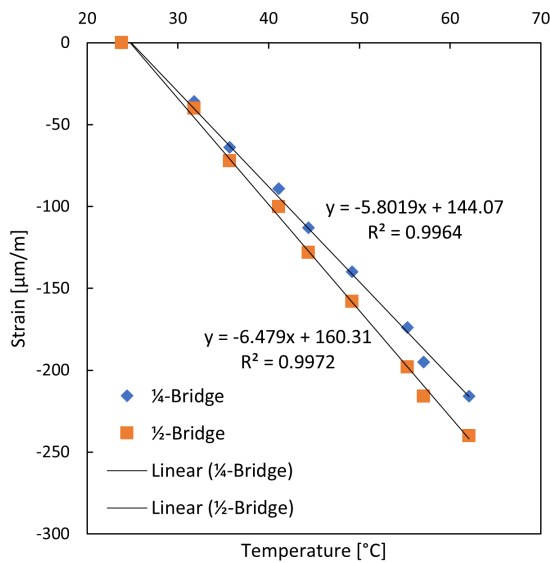


**Figure 4.6** – Relation of Measured Strain and Temperature

**Figure 4.7** – Relation of Normal Stress (Calculated from Measured Strain) and Temperature

The measured data are presented in the following Table.

Temperature [°C]	Force [kN]	Strain [ $\mu\text{m}\cdot\text{m}^{-1}$ ]		Normal Stress [MPa]	
		Quarter Bridge	Half Bridge	Quarter Bridge	Half Bridge
23.8	0.0	0	0	0.0	0.0
31.8	-1.8	-36	-40	-6.5	-7.0
35.7	-3.2	-64	-72	-11.5	-12.0
41.1	-4.6	-89	-100	-15.5	-17.0
44.4	-5.5	-113	-128	-20.5	-22.0
49.2	-6.8	-140	-158	-26.0	-27.5
55.3	-8.4	-174	-198	-32.5	-34.0
57.1	-9.1	-195	-216	-36.5	-37.0
62.1	-10.1	-216	-240	-40.5	-41.0
25.9	-2.0	-43	-48	-8.5	-8.5

**Table 4.2** – Thermal Loading of Sample Fixed at Both Ends

### Thermal Loading of Sample Fixed at Both Ends and Pre-Tensioned by Axial Force of 30 kN

This test ran in a similar way like the previous one except for the sample being prestressed by the axial force of 30 kN. The position (strain) of the sample was controlled by the dynamic stand control unit and the sample was uniformly heated by a hairdryer. The initial temperature of the sample was 22.7 °C. The sample was heated up to 61.5 °C and then naturally cooled off to 26.7 °C. The relation of strain and temperature is presented in Figure 4.8 and the relation of normal stress and temperature is presented in Figure 4.9.

Please note that the marks at the horizontal axis depict the values measured before prestressing and after releasing of the axial force.

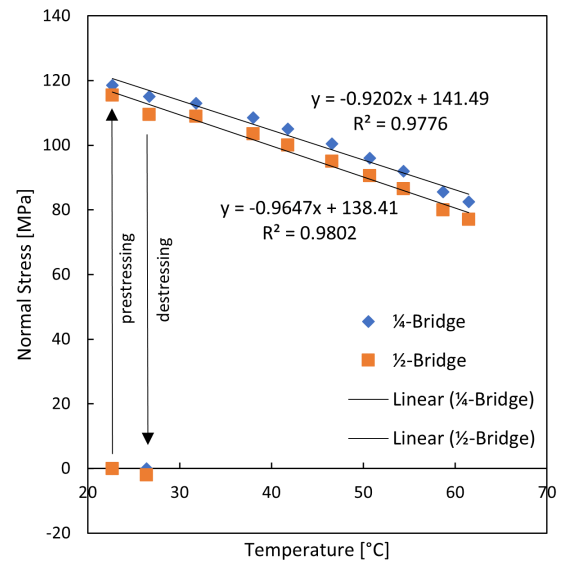
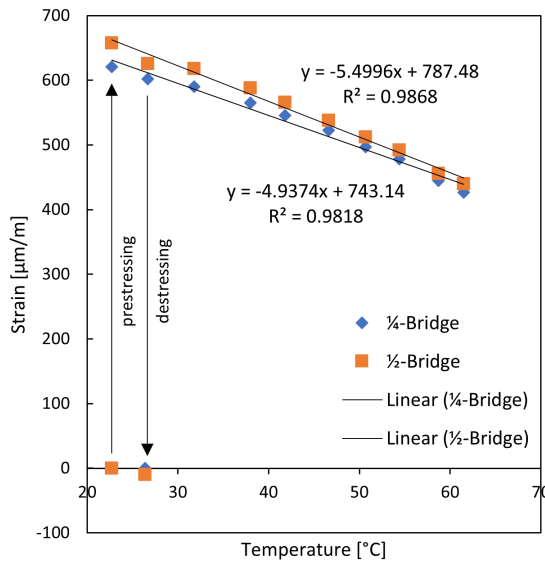


**Figure 4.8** – Relation of Measured Strain and Temperature

**Figure 4.9** – Relation of Normal Stress (Calculated from Measured Strain) and Temperature

The measured data are presented in the following Table.

Temperature [°C]	Force [kN]	Strain [ $\mu\text{m}\cdot\text{m}^{-1}$ ]		Normal Stress [MPa]	
		Quarter Bridge	Half Bridge	Quarter Bridge	Half Bridge
22.7	0.0	0	0	0.0	0.0
22.7	30.0	621	658	118.5	115.5
31.8	28.0	590	618	113.0	109.0
38.0	26.6	565	588	108.5	103.5
41.8	25.6	546	566	105.0	100.0
46.6	24.6	523	538	100.5	95.0
50.7	23.5	497	512	96.0	90.5
54.4	22.6	478	492	92.0	86.5
58.7	21.5	445	456	85.5	80.0
61.5	20.4	427	440	82.5	77.0
26.7	29.2	602	626	115.0	109.5
26.4	0.0	0	-10	0.0	-2.0

**Table 4.3** – Thermal Loading of Sample Fixed at Both Ends and Pre-Tensioned by Axial Force of 30 kN

### Thermal Loading of Sample Fixed at One End Only

The sample was fixed into the dynamic stand clamp jaws at both ends, but the control unit was set to keep the axial force at zero kN, therefore the sample was free to expand under thermal loading and the dilation of the sample was monitored by recording of the clamp jaw position.

The initial temperature of the sample was 25.6 °C. The sample was heated up to 57.3 °C. The relation of displacement of the sample and temperature is presented in Figure 4.10, the relation of strain and temperature is presented in Figure 4.11, and the relation of normal stress and temperature is presented in Figure 4.12.

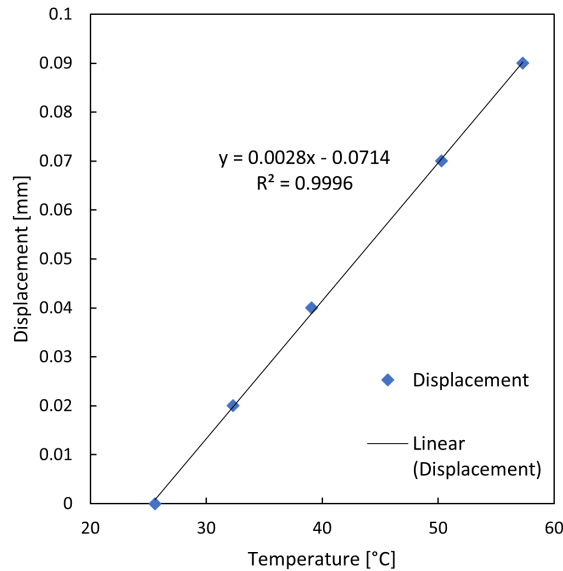


**Figure 4.10** – Relation of Displacement and Temperature

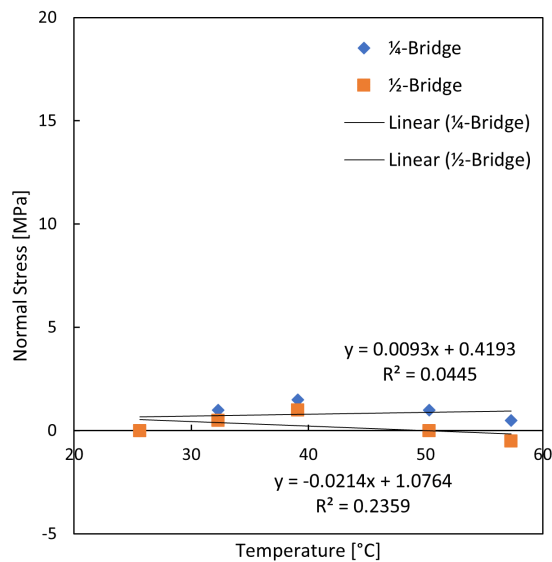
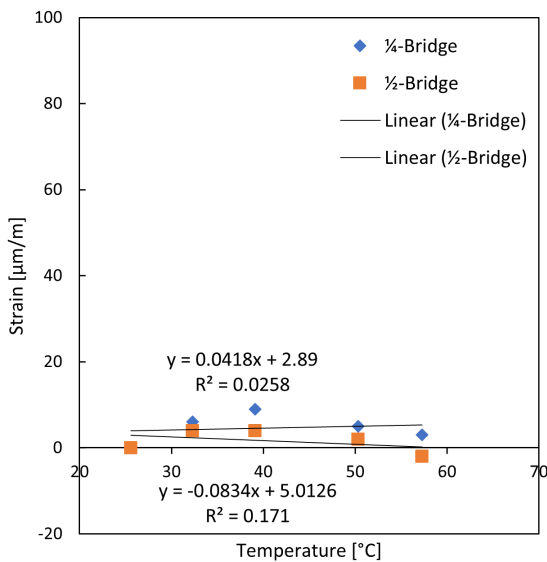


**Figure 4.11** – Relation of Measured Strain and Temperature

**Figure 4.12** – Relation of Normal Stress (Calculated from Measured Strain) and Temperature

The measured data are presented in the following Table.

Temp. [°C]	Def. [mm]	Strain [ $\mu\text{m}\cdot\text{m}^{-1}$ ]		Normal Stress [MPa]	
		Quarter Bridge	Half Bridge	Quarter Bridge	Half Bridge
25.6	0.00	0	0	0.0	0.0
32.3	0.02	6	4	1.0	0.5
39.1	0.04	9	4	1.5	1.0
50.3	0.07	5	2	1.0	0.0
57.3	0.09	3	-2	0.5	-0.5

**Table 4.4** – Thermal Loading of Sample Fixed at One End Only (Temp. – Temperature, Def. – Deformation)

### 4.1.3 Discussion

The tests performed in the laboratory have shown that the use of the quarter bridge configuration of the Wheatstone bridge provides sufficient precision of measurement and is applicable to the field measurement of strain in track. The application of the quarter bridge configuration can be used regardless of the pre-stressing of the sample. The thermal load test with one end of the sample fixed only shows that the thermal self-compensation of the strain gauge compensates for the vast majority of the thermal-induced strain in the tested sample. The not compensated part, which is the non-linear part according to the instructions of manufacturer, causes a very low impact and can be negligible, at least in the early stages of the field investigation.

The record of strain measured under loading by the axial force and constant temperature presented in Figure 4.4 shows in the case of the quarter bridge configuration the slope coefficient of 20.762. This value very well corresponds to the mathematical parameter of the relation among strain and the axial loading force, which can be written as

$$\varepsilon = \frac{1}{E \cdot A} \cdot N, \quad (4.4)$$

where  $\varepsilon$  is the strain,  $E$  is the Young's modulus,  $A$  is the cross-sectional area and  $N$  is the axial loading force.

If  $E$  is considered 200 GPa, the parameter, which is the first multiplier in Equation 4.4, equals 20. Considering the strain measured by the half bridge is multiplied by two, since the measured value was lower due to incorrect settings of the data processing programme, the slope coefficient would reach approximately 22. These results lead to the necessity to divide the measured strain by 1.1 in the case of the quarter bridge or 1.2 in the case of the half bridge configuration to reach the perfect fit to the analytical value. Among the reasons that cause this discrepancy, imperfections of the tested sample or displacement in the hydraulic clamp jaws could be considered, but this question remains unresolved until the date of submission of this thesis.

Very important results come out of the thermal loading test, as this type of loading is crucial in the field measurements. The slope coefficients presented in Figure 4.6 reach values  $-5.8$  for

the quarter bridge and  $-6.5$  for the half bridge configurations and in the test after prestressing, i. e. in Figure 4.8 –4.9 for quarter bridge and  $-5.5$  for half bridge. This results into two questions: 1. Why is the slope coefficient negative? 2. Why does it reach such a value? And a subsequent question: 2.1 What is the actual value of the slope coefficient?

The test of thermal loading of the sample fixed at one end gives the solution to the Question 1. If there was no thermal compensation in the strain gauge, the expansion of the sample would have to be recorded by the strain of the strain gauge. Since virtually no strain was recorded, the thermal compensation successfully compensated for the vast majority of the strain and, therefore proves the self-compensation of the strain gauge. If the sample is heated with both sides fixed, the strain gauge expects the sample, and the strain gauge itself, would expand, but it does not, therefore it experiences the same behaviour as if the sample had expanded by thermal loading and then was pushed back to its original length, thus experiencing negative strain.

This explanation leads to the idea that the slope coefficient shall equal  $-\alpha$ , i. e. approximately  $-11.5 \cdot 10^{-6} \text{ K}^{-1}$  for the rail steel. However, as mentioned before, the measured value equals approximately  $-5$  or  $-6$  at the measurement in laboratory conditions and in the case of sample fixed at both ends. If the coefficients 1.1 and 1.2 from Equations 4.1 and 4.2 are applied, which can be performed without loss of generality, the values for the quarter bridge and half bridge are the same at both tests and they are approximately  $-5.35$  in the case of the test without pre-stressing and  $-4.5$  in the case of the test with the prestressing of 30 kN. Since the laboratory conditions allowed for a very high level of support fixing, investigation into the Questions 2 and 2.1 are yet to be done and these questions remain unresolved at the time of submission of this thesis.

## 4.2 Measuring Set for Diagnostics of Time-Based Development of Stress States in CWR

A measuring set was developed for practical measurements of the CWR strain in railway tracks under operation [57]. The measuring set had to meet the following criteria:

- not limit the railway track operation in any way,
- not interfere with the railway track circuits,
- enable quick measurement, so that it is realisable even in a track section with high intensity of operations,
- enable easy installation,
- provide high precision of measured data,
- withstand all natural and operation effects in the railway track,
- enable track maintenance.

A measuring set meeting the above listed criteria and comprising of a track and mobile unit was developed. The track unit is relatively simple for installation and relatively cheap, which is important because every track unit can be used only for one measuring spot. The mobile unit, on the contrary, contains a relatively expensive data acquisition system, but it isn't fixed to the rail, is easily transferable, and can be used for measurement at unlimited number of measuring spots.

The measuring set uses the quarter bridge strain gauge configuration, which is sufficient for field investigation as follows from Section 4.1, easy to install and less prone to damage than the half bridge installation [57].

#### 4.2.1 Technical Specifications

The measuring set is composed out of a track (Figure 4.13) and a mobile (Figure 4.14) unit.



**Figure 4.13** – Measuring Set Track Unit

The track unit contains a K-CLY4-0060-1-350-4-050-Y strain gauge type produced by HBM, a polypropylene tube of length of 150 mm and outer diameter of 40 mm, and a polyurethane foam cube of an edge length of 50 mm. The strain gauge is connected to the investigated rail at its neutral axis with the main axis of the strain gauge being parallel to the neutral axis of the rail. The corresponding area of the rail surface must be cleaned from rust and unevenness and degreased. The strain gauge is attached by the 1-Z70 fast-acting superglue and, after drying, painted over by the 1-PU140 polyurethane lacquer, both produced by HBM. After the covering material is dry, the strain gauge is covered by the 1-ABM75 aluminium foil coated with kneadable putty produced by HBM, too. The polypropylene tube is attached to the lower part of the rail web by a pair of cable ties and cable ties holders and the Chemopren Extreme glue. The strain gauge conductors with RJ male connector are placed into the polypropylene tube closed from



**Figure 4.14** – Measuring Set Mobile Unit

one end, while the other end of the tube is plugged by the polyurethane foam cube. The mobile unit contains an MX840A data acquisition system and a SCM-SG350 quarter bridge adaptor produced by HBM, a connecting cable and an RJ11 female connector produced by ENCITECH. Mechanical deformation is measured directly by the MX840A data acquisition system.

Instructions to install and use the measuring set are closely described in the methodology [58] and in the measuring set documentation [57], both of which were created as a direct outcome of the research project No. TJ04000301 *Non-Destructive Determination of Mechanical Stress in Continuous Welded Rail* and are attached as annexes to this dissertation.

### 4.3 CWR Strain Monitoring

An extensive CWR Strain Monitoring was performed within the scope of investigation of the TAČR Zéta Project TJ04000301 *Non-Destructive Determination of Mechanical Stress in Continuous Welded Rail*. The measuring set [57], which was an outcome of the mentioned research project, was used for the purpose of this monitoring.

The CWR Strain Monitoring took place at tracks of the Czech railway network. The localities involved in the monitoring were selected upon discussions with representatives of *Správa železnic*, the Czech national railway infrastructure manager, and based on the plans of track superstructure maintenance which involved CWR welding.

The data of strain, including the apparent strain described in Section 4.1 under laboratory measurements with sample fixed at both ends, were recorded using the introduced measuring set [57]. At each measurement, the rail temperature in the vicinity of the involved strain gauge was recorded, too.

The methodology [58] was composed out of the measurements. This methodology was an-



other outcome of the above-mentioned research project and is an annex to this dissertation [58].

#### **4.3.1 Monitored Localities**

There were four localities where the field monitoring of CWR strain took or has been taking place:

- A. Borovnice,
- B. Ostopovice,
- C. Chotěvice, and
- D. Bezpráví.

A closer description of the localities follows.

## A. Borovnice

The locality of Borovnice was the first one to perform the CWR strain measurement. It is located on the Pardubice – Liberec railway line in km 73.1 – 73.6. The monitored section is shown in Figure 4.15.

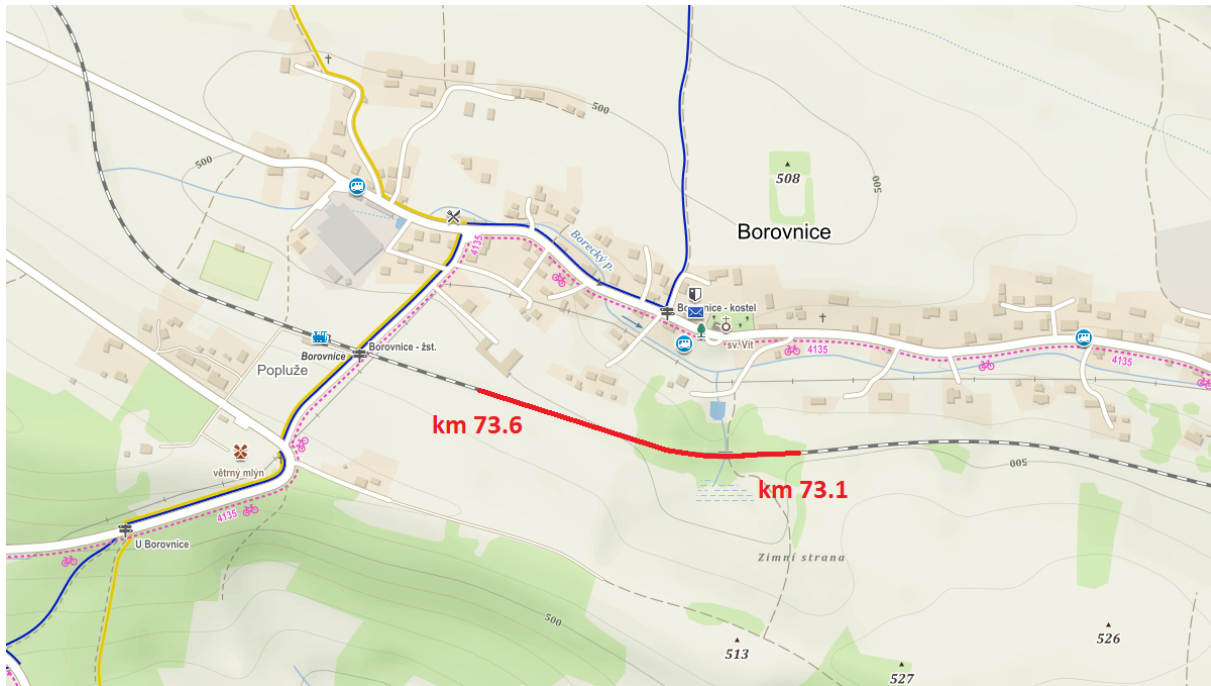


**Figure 4.15** – Locality Borovnice

The horizontal alignment of the monitored section contains one circular curve of 545 m radius with transition curves and a straight track section. The curved part contains a masonry bridge with a ballast bed and is in a forest. The straight section lies between fields and is open to the sun. The track in the monitored section lies in the east-west orientation, with a slight north-west orientation in the direction of Liberec.

There were 48 measuring spots of the measuring set track unit installed in three subsections of 16 spots. There were spaces of approximately 150 m between the subsections, and each subsection comprised of four profiles of four measuring spots as recommended in the methodology [58]. The purpose of this division was to cover three specific positions within the monitored section: a transition curve in a relatively deep forest, a circular curve in a sparse forest and a straight section fully open to the sun over the whole day.

For measurements in this section, the half bridge configuration of strain gauges were originally used. This was later changed into the quarter bridge configuration as the noise grew into an unacceptable level and the quarter bridge configuration of the measuring set was developed. For this reason, the data from this locality will not be further discussed in this dissertation. However, the monitoring in the Borovnice locality served very well to the development of both, the measuring set and the methodology, as the first field research locality.

## B. Ostopovice

The locality of Ostopovice was the first one to perform the CWR strain measurement using the quarter bridge strain gauge configuration and the second one to perform the CWR strain field measurement totally. It is located in the track No. 1 on the Střelice – Brno railway line in km 146.9 – 147.4. The monitored section is shown in Figure 4.16.



**Figure 4.16** – Locality Ostopovice

The horizontal alignment of the monitored section contains one circular curve of a large radius with transition curves and a following straight track section. The curved part is in cutting and the line converts into an embankment in the straight section. Whole the section is in a deforested area and lies in the east-west orientation with ends of the section aiming to the south-west and south-east due to the curve in the section.

There were 16 measuring spots installed in the monitored section. The number was limited due to a very limited time reserved for the installation. The measuring spots were distributed into four profiles of four spots in each profile. The stationing of the profiles was: km 146.953, km 147.053, km 147.153 and km 147.400, with the latest being in the straight section. The purpose of this distribution was to monitor a possible different behaviour in the curve and in the straight section.

The quarter bridge configurations were applied in this locality for the first time. However, due to troubles in the information exchange, the measuring set track units were destroyed during the track maintenance. For this reason, the data from this locality will not be further discussed in this dissertation, too.

### C. Chotěvice

The locality of Chotěvice was the third one to perform the CWR strain measurement. It is located on the Velký Osek – Trutnov railway line in km 112.0 – 112.5. The monitored section is shown in Figure 4.17.

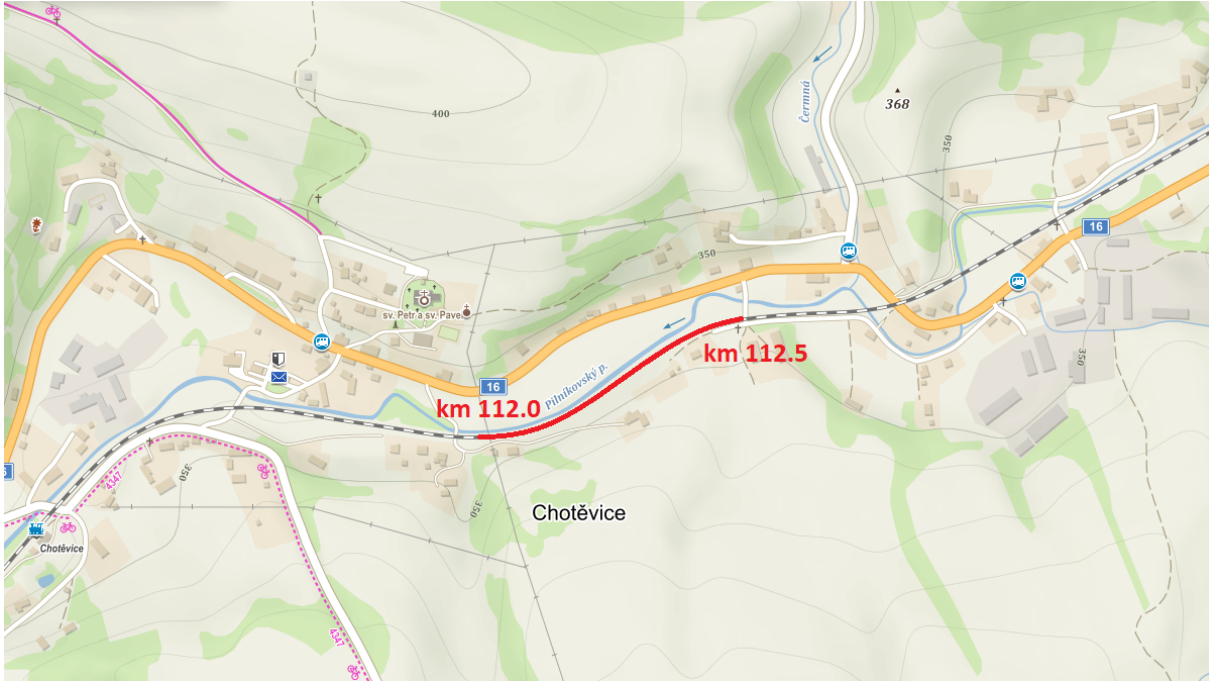


**Figure 4.17** – Locality Chotěvice

The horizontal alignment of the monitored section contains two circular curves with transition curves and a short intermediate straight section. The radii of the circular curves are 300 m, and 297 m, respectively. The length of the intermediate straight section is 26 m. The vicinity of the monitored section varies by length with approximately the first half of the section being shadowed by vegetation while the other half being largely exposed to sunshine. The section is placed in the east-west and south-west–north-east orientation.

There were 44 measuring spots installed in the monitored section, always four measuring spots per profile in eleven profiles in total. The spacing of the profiles is 50 m, with the exception of profiles No. VI and VII, which are placed next to each other in the distance of 0.6 m (the neighbouring space between sleepers). The purpose of this distribution was to record data in this section uniformly, and the reason to place two profiles of strain gauges to the neighbouring spaces between sleepers was to investigate a potential different strain in a very local area.

The quarter bridge configurations of strain gauges were used in this locality, too. The recorded data from this locality will be discussed further in the text.

## D. Bezprávi

The locality of Bezprávi was the fourth one to perform the CWR strain measurement. It is located in the track No. 1 on the Olomouc – Prague railway line in km 260.8 – 261.4. The monitored section is shown in Figure 4.17.

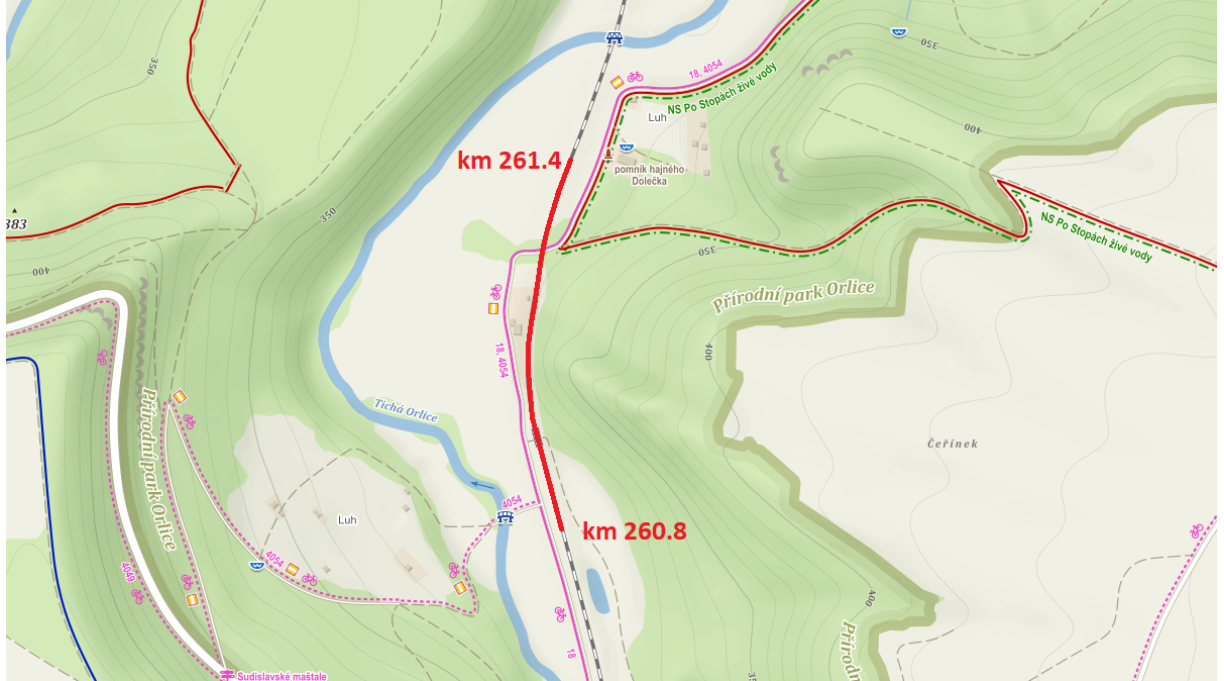


Figure 4.18 – Locality Bezprávi

The horizontal alignment of the monitored section is presented in the Strain Gauge Installation Scheme, which is a part of an annex to this dissertation, therefore not described here in the text. The central part of this section with the two central profiles is protected from the sunshine from the east, while the beginning and the end of the section is open to the sun over the majority of the day. The section is placed in the north-south orientation.

There were 16 measuring spots installed in the monitored section. The number was limited due to a very limited time reserved for the installation. The measuring spots were distributed evenly into four profiles of four spots in each profile. The spacing of the profiles is 160 m. The purpose of this distribution was to record data in this section uniformly.

Even in this locality, the quarter bridge configurations of strain gauges were applied. Recorded data from this locality will be discussed further in the text.

### 4.3.2 Experimental Setup

The experimental setup is closely described in the annexes (the measuring set documentation [57] and the methodology [58]), therefore not here duplicated.

### 4.3.3 Data Collection

The strain gauge installation in all localities was performed closely before the stress-controlled rail welding was scheduled. The rails were in their position on sleepers in all the cases. At least

one measurement was performed just before the welding, when the rails were in a stress-free state (released from fastenings and on rollers) and at least one measurement was performed just after the tensioning temperature was reached (either by rail pre-tensioning with the use of hydraulic device, or by rail heating). The tensioning temperature, rail strain, and other important data related to rail welding were noted. With this information, the measured values at the time of welding serve as a reference to other measurements of the CWR strain.

Apart from other purposes, the rail strain data of the state prior pre-tensioning and after pre-tensioning serve well to investigate the potential unevenness of the rail pre-tensioning. Discussion on this effect is, however, beyond the scope of this dissertation.

The CWR strain measurements using the measuring set [57] are quick, but not autonomous, and only one measuring spot can be monitored at a time. Therefore, a schedule of measurements was prepared for all the monitored localities. The typical schedule was set as a series of measurements with the daily frequency lasting for approximately one week. This was followed by the weekly frequency lasting for the first month after the CWR welding and the monthly frequency lasting for the first year after the CWR welding. This schedule was set to cover the hypothetical development of a neutral temperature change in the CWR over the time (see the more detailed description in Section 4.5 of the annexed methodology [58]) and not overload the research group members.

The detailed calculation of measurement uncertainties is provided in Appendix B, with the type B total evaluation of uncertainty reaching  $6.36 \mu\text{m}\cdot\text{m}^{-1}$ .

The detailed records of the measured strain at each measuring spot in Chotěvice and Bezprávi localities are presented in Appendix C. An aggregated record of all measuring spots within a locality is presented in Figures 4.19 to 4.24.

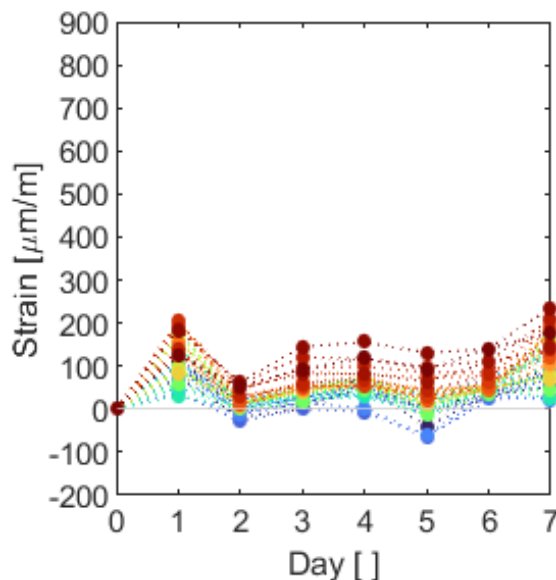


**Figure 4.19** – Aggregated CWR Strain Record in the Chotěvice Locality in the Period of Daily Monitoring

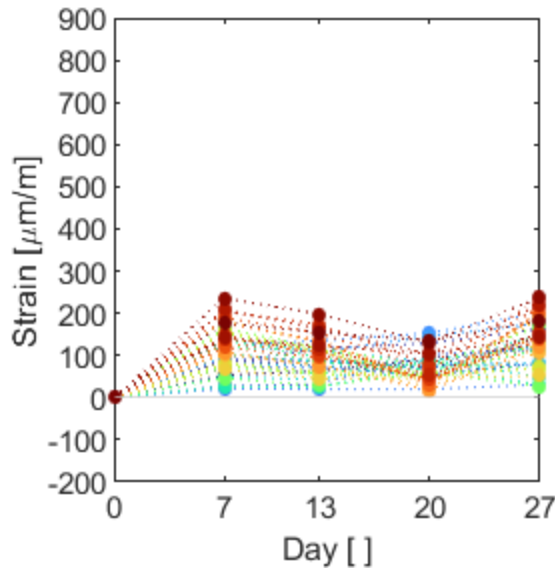


**Figure 4.20** – Aggregated CWR Strain Record in the Chotěvice Locality in the Period of Weekly Monitoring

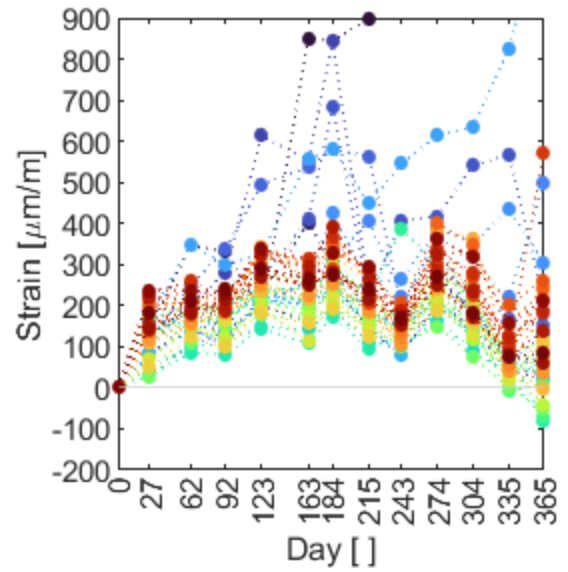


**Figure 4.21** – Aggregated CWR Strain Record in the Chotěvice Locality in the Period of Monthly Monitoring

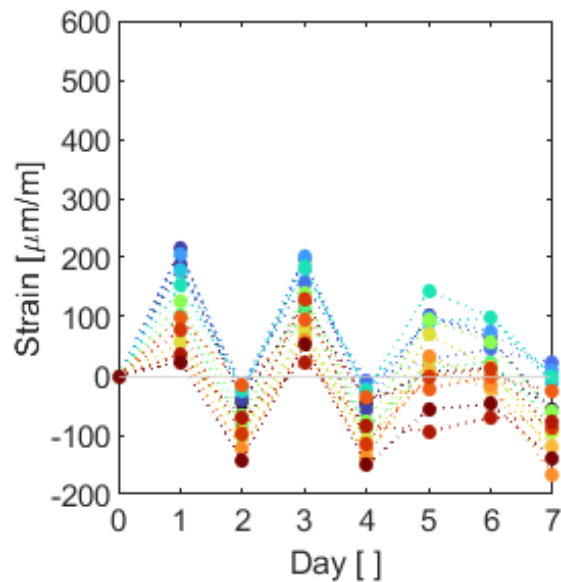


**Figure 4.22** – Aggregated CWR Strain Record in the Bezprávi Locality in the Period of Daily Monitoring

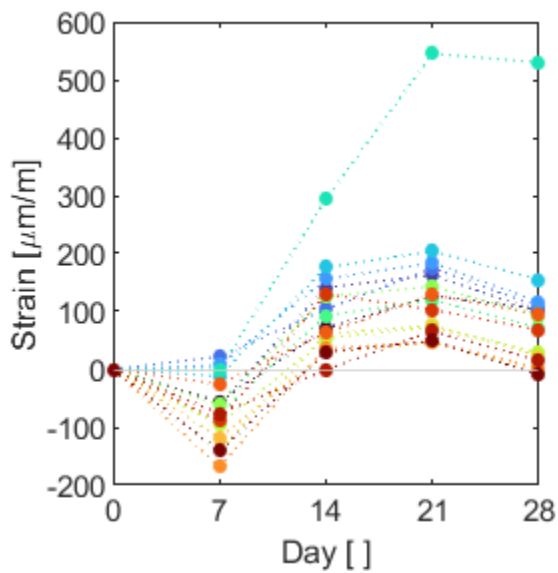


**Figure 4.23** – Aggregated CWR Strain Record in the Bezprávi Locality in the Period of Weekly Monitoring

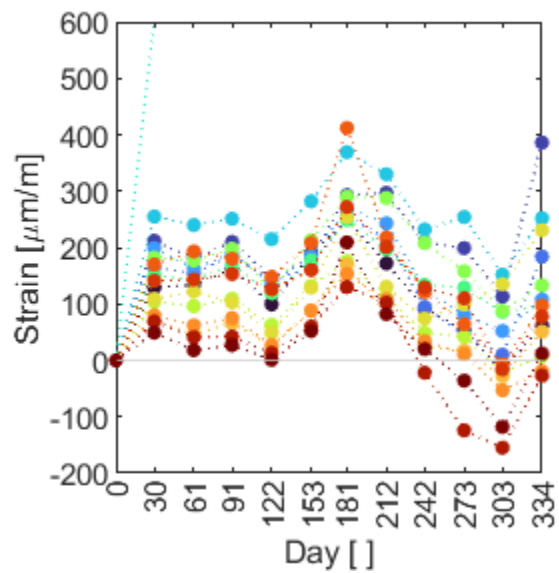


**Figure 4.24** – Aggregated CWR Strain Record in the Bezprávi Locality in the Period of Monthly Monitoring



## Chapter 5

# Neutral Temperature Development of Continuous Welded Rail

Considering the elastic behaviour of rail under thermal loading, it can be assumed that in order to change the rail neutral temperature, a rail strain shall occur. If the rail strain is measured, it shall be proportional to the change of the neutral temperature. In this chapter, an approach to the determination of this change is presented.

### 5.1 Methodology of Non-Destructive Determination of Mechanical Stress in CWR

The methodology [58] was developed as an outcome of the research project No. TJ04000301 *Non-Destructive Determination of Mechanical Stress in Continuous Welded Rail* and is attached as an annex to this dissertation. A procedure of determination of the stress from thermal loading (the neutral temperature change) is described in the methodology [58]. Since the methodology was released before the release of this dissertation, it does not contain all the ideas written in the dissertation. The data analysis continues as new data are being obtained from the ongoing monitoring and the methodology will be updated as further conclusions will be made.

### 5.2 Data Analysis

The measured CWR strain data contain both the rail strain and the apparent strain as described in the previous chapters. In order to get the real strain data, the impact of the apparent strain proportional to the rail temperature shall be removed from the measured strain data. According to the user instructions of the strain gauge manufacturer, the self-compensation of strain gauges compensates for the linear part of the thermal impact, leaving the non-linear part uncompensated. However, in Figures 4.6 to 4.9, it could be seen that the non-linear part can be neglected without loss of generality at this moment of analysis.

The relations of strain and temperature for each measuring spot can be plotted for various datasets. Datasets of the daily measurement period database, i. e. the data from typically the first week of measurements, when the measurements were performed on a daily basis, and

datasets of the complete measurement period are applied in this case. As an example, it can be seen in the case of the measuring spot C.VIII.1 presented in Figures 5.1 and 5.2. All relations of the strain and temperature are presented in Appendix D.

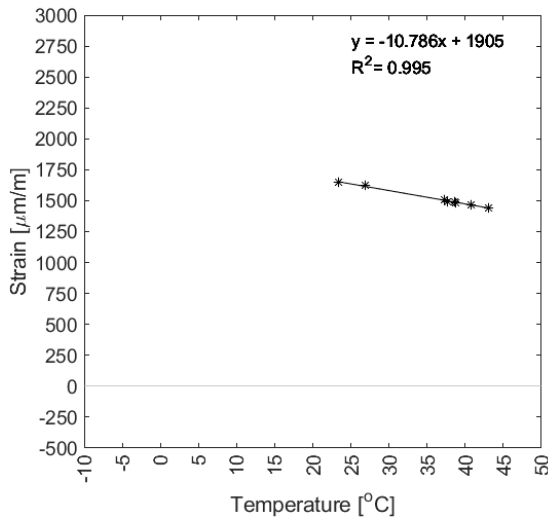


**Figure 5.1** – C.VIII.1 – Daily Measurement Period Database

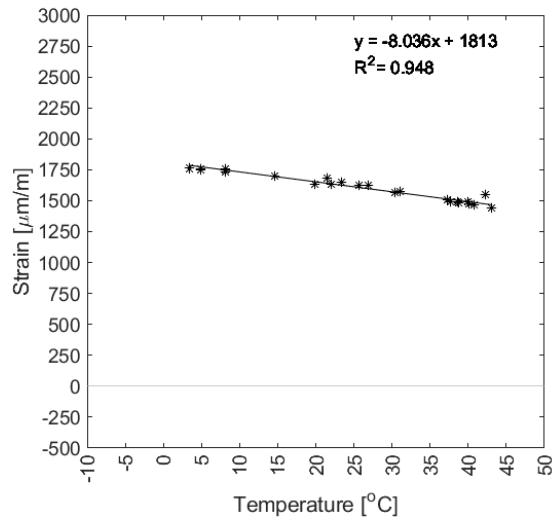


**Figure 5.2** – C.VIII.1 – Complete Monitoring Period Database

The question on the database selection is discussed further in the discussion to this chapter. A linear trend line is attached to each graph. This trend line is calculated in the shape of a linear polynomial:

$$y = a \cdot x + b, \quad (5.1)$$

where  $a$  is the slope coefficient.

The slope coefficient  $a$  represents the linear impact of the apparent strain proportional to the rail temperature (further referred to as *linear thermal coefficient of the apparent strain*, or *LTCAS*) and is always negative. The absolute value, however, varies. The following tables summarize the LTCAS of the temperature-strain relation per particular measuring spots, calculated from both datasets – the data from the daily frequency measurements from the first week after installation (further referred to as *LTCAS week*), and the data from all measurements performed within one year after the installation (further referred to as *LTCAS all*). Except for the LTCAS values, the tables summarize the respective coefficients of determination  $R^2$  to both *LTCAS week* and *LTCAS all*, and the *LTCAS difference* calculated as

$$LTCAS_{difference} = LTCAS_{all} - LTCAS_{week}. \quad (5.2)$$

Measuring Spot	LTCAS Week	$R^2$	LTCAS All	$R^2$	LTCAS Difference
C.I.1	-10.408	0.781	-24.231	0.574	-13.823
C.I.2	-6.872	0.439	-11.429	0.813	-4.557
C.I.3	-11.464	0.699	-6.923	0.808	4.541
C.I.4	-11.691	0.737	-26.314	0.919	-14.623
C.II.1	-6.507	0.774	-10.829	0.349	-4.322
C.II.2	-1.753	0.108	-15.475	0.715	-13.722
C.II.3	-5.219	0.587	-7.127	0.743	-1.908
C.II.4	-0.659	0.014	-6.446	0.204	-5.787
C.III.1	-13.335	0.417	-5.224	0.119	8.111
C.III.2	-12.340	0.393	-3.020	0.008	9.320
C.III.3	-14.161	0.435	-7.054	0.694	7.107
C.III.4	-12.914	0.495	-7.834	0.629	5.080
C.IV.1	-9.302	0.976	-7.085	0.893	2.217
C.IV.2	-3.223	0.673	-3.927	0.819	-0.704
C.IV.3	-6.987	0.930	-6.122	0.889	0.865
C.IV.4	-1.893	0.348	-4.366	0.642	-2.473
C.V.1	-9.308	0.950	-7.377	0.645	1.931
C.V.2	-4.971	0.853	-6.593	0.833	-1.622
C.V.3	-8.695	0.959	-6.961	0.959	1.734
C.V.4	-3.494	0.670	-5.461	0.868	-1.967
C.VI.1	-10.412	0.981	-7.167	0.940	3.245
C.VI.2	-4.884	0.841	-5.062	0.831	-0.178
C.VI.3	-9.466	0.953	-6.615	0.865	2.851
C.VI.4	-4.606	0.838	-4.959	0.892	-0.353
C.VII.1	-10.200	0.978	-6.289	0.886	3.911
C.VII.2	-4.950	0.873	-4.682	0.828	0.268
C.VII.3	-8.998	0.956	-6.197	0.914	2.801
C.VII.4	-3.996	0.803	-3.800	0.701	0.196
C.VIII.1	-10.786	0.995	-8.036	0.948	2.750
C.VIII.2	-5.976	0.949	-6.307	0.962	-0.331
C.VIII.3	-10.631	0.991	-8.510	0.781	2.121
C.VIII.4	-6.583	0.953	-6.497	0.981	0.086
C.IX.1	-9.506	0.981	-8.475	0.932	1.031
C.IX.2	-7.127	0.934	-6.354	0.821	0.773
C.IX.3	-9.740	0.983	-8.633	0.796	1.107
C.IX.4	-6.546	0.920	-6.626	0.617	-0.080
C.X.1	-9.214	0.990	-8.049	0.921	1.165
C.X.2	-6.784	0.943	-6.251	0.390	0.533
C.X.3	-9.675	0.979	-8.174	0.937	1.501
C.X.4	-6.598	0.925	-6.380	0.848	0.218
C.XI.1	-9.746	0.867	-8.179	0.942	1.567
C.XI.2	-6.566	0.762	-6.484	0.915	0.082
C.XI.3	-10.140	0.762	-7.042	0.785	3.098
C.XI.4	-6.791	0.601	-6.333	0.858	0.458

**Table 5.1** – Chotěvice – LTCAS of the Temperature-Strain Relation

Measuring Spot	LTCAS Week	$R^2$	LTCAS All	$R^2$	LTCAS Difference
D.I.1	-8.294	0.953	-6.341	0.924	1.953
D.I.2	-10.828	0.954	-7.410	0.673	3.418
D.I.3	-7.574	0.918	-6.128	0.873	1.446
D.I.4	-9.742	0.937	-6.449	0.866	3.293
D.II.1	-10.501	0.809	-10.168	0.843	0.333
D.II.2	-9.822	0.685	-37.690	0.417	-27.868
D.II.3	-8.698	0.714	-7.985	0.865	0.713
D.II.4	-9.559	0.652	-8.929	0.828	0.630
D.III.1	-6.913	0.909	-6.867	0.958	0.046
D.III.2	-8.606	0.958	-7.272	0.648	1.334
D.III.3	-7.000	0.941	-6.268	0.933	0.732
D.III.4	-8.656	0.983	-7.084	0.954	1.572
D.IV.1	-5.245	0.776	-8.143	0.883	-2.898
D.IV.2	-8.114	0.733	-7.256	0.827	0.858
D.IV.3	-5.634	0.911	-5.320	0.802	0.314
D.IV.4	-8.750	0.877	-6.038	0.798	2.712

**Table 5.2** – Bezprávi – LTCAS of the Temperature-Strain Relation

The experiments presented in Section 4.1 proved that the LTCAS of a sample fixed at both ends remains constant under a changing temperature of the sample if the non-linearity is neglected, and an assumption can be made that only the absolute member of the Polynomial 5.1 changes if a pre-stress (e. g. by a change of the relative distance of fixed supports) is applied. Additionally, an assumption that the LTCAS of a freely expandable member is zero can be made from the experiments presented in Section 4.1. It is interpreted in the following schemes:

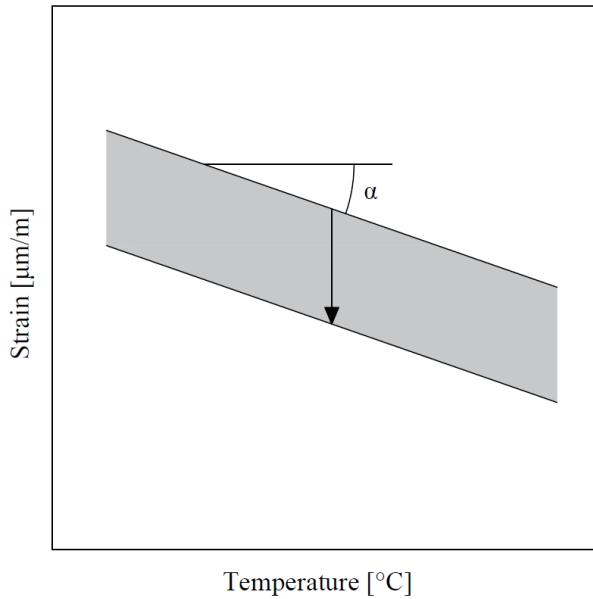


**Figure 5.3** – Scheme of a Change in the Absolute Coefficient of the Strain-Temperature Polynomial upon a Sample Pre-Stress Change

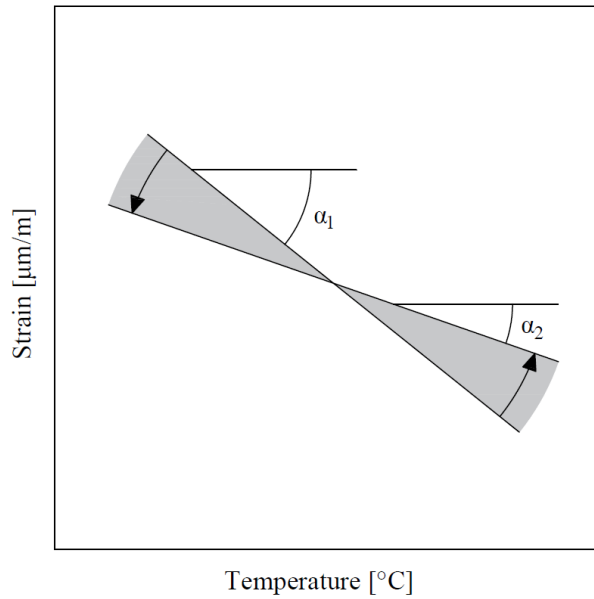


**Figure 5.4** – Scheme of a Change in the Linear Coefficient of the Strain-Temperature Polynomial upon a Support Fixation Rigidity Change

The index at the LTCAS indicates the coefficient value before (1) and after (2) change. Please note that the change can occur in both directions and the arrows are used for an illustrative purpose only. Both changes (the LTCAS indicated as  $\alpha$ ) presented in Figures 5.3 and 5.4 can occur contemporaneously.

As a result of these assumptions, an extrapolated rail temperature can be determined. If Polynomial 5.1 is written with quantities as

$$\varepsilon = a \cdot T + b, \quad (5.3)$$

where  $\varepsilon$  is the strain,  $a$  is the LTCAS, and  $T$  is the temperature, the extrapolated rail temperature is given by equation

$$T = \frac{\varepsilon - b}{a}. \quad (5.4)$$

Please note that this Equation applies the different LTCAS of the particular measuring spots as the denominator, therefore effectively removes its impact from the volume of the calculated rail temperature.

If the daily measurement period database (LTCAS week) is put into the calculation, the graphs depicted in Appendix E are obtained. In these graphs, the measured and extrapolated temperature, and the difference of these values are presented for each particular measuring spot. The day zero is the day of stress-controlled rail welding. An example of this graph for the C.V.3 measuring spot is in Figure 5.5.

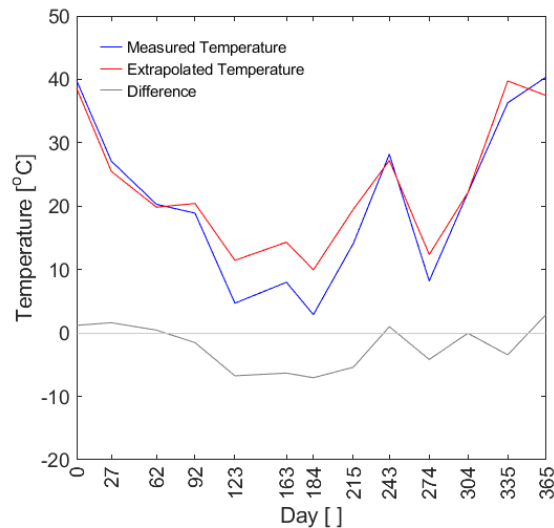


**Figure 5.5** – C.V.3 – Measured and Extrapolated Temperature, and Their Difference

It can be further assumed that the measured values of strain contain the real strain, the apparent strain, other impacting factors and noise. If the values of the extrapolated temperature express the impact of the apparent strain, the values of difference of the measured and extrapolated temperature contain only the change of the rail neutral temperature, other impacting factors and noise. The impact of the other factors is unknown by the date of submission of this dissertation, however, no evidence is found that it is significant.

Since the day zero represents the data obtained on the day of rail welding after the welding, it can be postulated that **the values of the measured and extrapolated temperature difference represent the determination of the neutral temperature development in continuous welded rail over time, with zero being the tensioning (installation) temperature.** Yet, it has to be taken into account that some outlying values may be caused by a failure of the probes or other reasons, and other factors influencing the neutral temperature may lurk in the curve of the temperature difference.

The values of the CWR neutral temperature change (measured and extrapolated temperature difference) clustered per cross-sectional profiles are presented in Appendix F. An example of the CWR neutral temperature change clusters for measuring spots in the Bezprávi locality is presented in Figures 5.6 – 5.9.

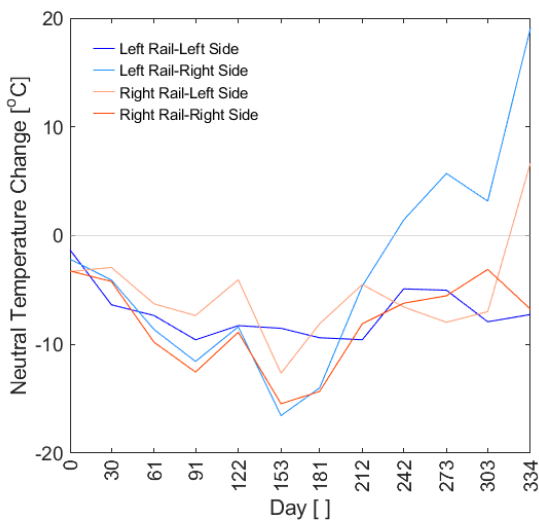


**Figure 5.6 – D.I – Cluster of Calculated CWR Neutral Temperature Changes**

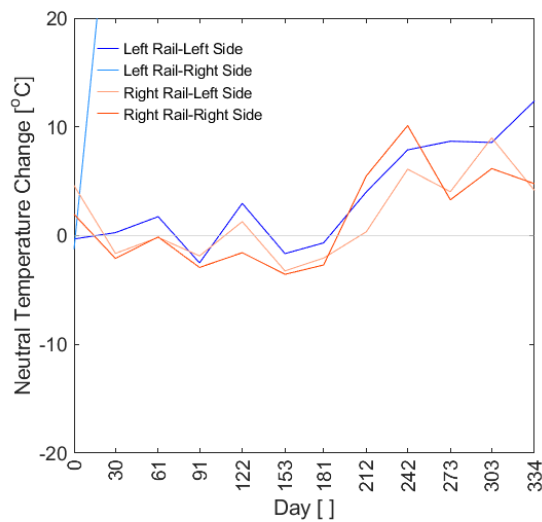


**Figure 5.7 – D.II – Cluster of Calculated CWR Neutral Temperature Changes**

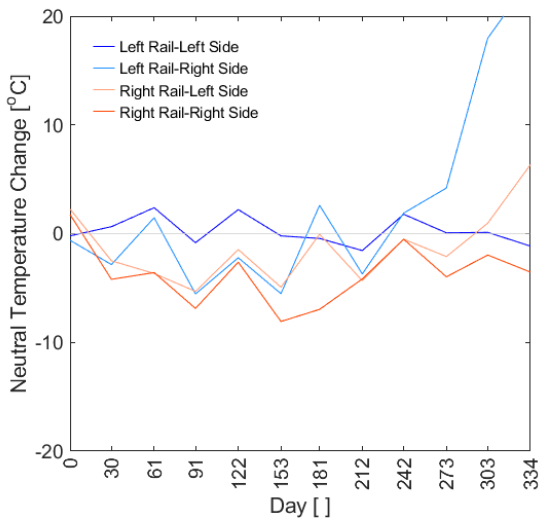


**Figure 5.8 – D.III – Cluster of Calculated CWR Neutral Temperature Changes**

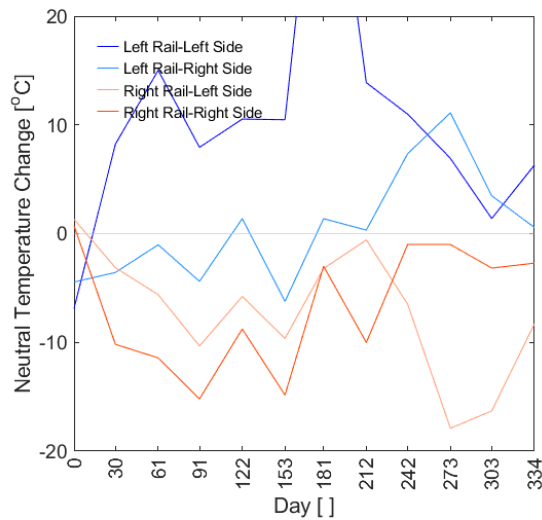


**Figure 5.9 – D.IV – Cluster of Calculated CWR Neutral Temperature Changes**

The values presented in Figures 5.6 – 5.9 are summarized in Tables 5.3 – 5.6.

Day	Date	D.I.1 [°C]	D.I.2 [°C]	D.I.3 [°C]	D.I.4 [°C]
0	1 <sup>st</sup> September 2021	-1.3	-2.2	-3.3	-3.2
30	1 <sup>st</sup> October 2021	-6.4	-4.1	-2.9	-4.2
61	1 <sup>st</sup> November 2021	-7.4	-8.6	-6.3	-9.8
91	1 <sup>st</sup> December 2021	-9.6	-11.1	-7.3	-12.5
122	1 <sup>st</sup> January 2022	-8.3	-8.4	-4.1	-8.9
153	1 <sup>st</sup> February 2022	-8.5	-16.5	-12.7	-15.5
181	1 <sup>st</sup> March 2022	-9.4	-14.0	-8.1	-14.3
212	1 <sup>st</sup> April 2022	-9.6	-4.6	-4.5	-8.1
242	1 <sup>st</sup> May 2022	-4.9	1.4	-6.6	-6.2
273	1 <sup>st</sup> June 2022	-5.0	5.7	-8.0	-5.5
303	1 <sup>st</sup> July 2022	-7.9	3.2	-7.0	-3.1
334	1 <sup>st</sup> August 2022	-7.3	19.1	6.7	-6.8

**Table 5.3** – Measuring Spot D.I – CWR Neutral Temperature Changes

Day	Date	D.II.1 [°C]	D.II.2* [°C]	D.II.3 [°C]	D.II.4 [°C]
0	1 <sup>st</sup> September 2021	-0.3	-1.2	4.6	2.0
30	1 <sup>st</sup> October 2021	0.3	37.1	-1.6	-2.1
61	1 <sup>st</sup> November 2021	1.7	63.5	-0.2	-0.1
91	1 <sup>st</sup> December 2021	-2.5	63.7	-1.9	-2.9
122	1 <sup>st</sup> January 2022	3.0	87.5	1.3	-1.6
153	1 <sup>st</sup> February 2022	-1.7	102.5	-3.2	-3.6
181	1 <sup>st</sup> March 2022	-0.7	118.3	-2.1	-2.7
212	1 <sup>st</sup> April 2022	4.0	130.3	0.4	5.5
242	1 <sup>st</sup> May 2022	7.9	131.3	6.1	10.1
273	1 <sup>st</sup> June 2022	8.7	130.5	4.0	3.3
303	1 <sup>st</sup> July 2022	8.6	136.6	9.0	6.2
334	1 <sup>st</sup> August 2022	12.4	135.8	4.2	4.8

**Table 5.4** – Measuring Spot D.II – CWR Neutral Temperature Changes; \*It is necessary to consider D.II.2 as an outlier – see Figure 5.10

Day	Date	D.III.1 [°C]	D.III.2 [°C]	D.III.3 [°C]	D.III.4 [°C]
0	1 <sup>st</sup> September 2021	-0.2	-0.6	2.3	1.8
30	1 <sup>st</sup> October 2021	0.6	-2.8	-2.5	-4.2
61	1 <sup>st</sup> November 2021	2.4	1.5	-3.7	-3.6
91	1 <sup>st</sup> December 2021	-0.8	-5.5	-5.3	-6.9
122	1 <sup>st</sup> January 2022	2.2	-2.2	-1.5	-2.6
153	1 <sup>st</sup> February 2022	-0.2	-5.5	-4.9	-8.1
181	1 <sup>st</sup> March 2022	-0.4	2.6	-0.1	-7.0
212	1 <sup>st</sup> April 2022	-1.6	-3.7	-4.3	-4.2
242	1 <sup>st</sup> May 2022	1.8	1.9	-0.5	-0.5
273	1 <sup>st</sup> June 2022	0.1	4.2	-2.1	-4.0
303	1 <sup>st</sup> July 2022	0.1	18.0	1.0	-2.0
334	1 <sup>st</sup> August 2022	-1.1	23.4	6.3	-3.5

**Table 5.5** – Measuring Spot D.III – CWR Neutral Temperature Changes

Day	Date	D.IV.1* [°C]	D.IV.2 [°C]	D.IV.3 [°C]	D.IV.4 [°C]
0	1 <sup>st</sup> September 2021	-6.9	-4.4	1.3	0.7
30	1 <sup>st</sup> October 2021	8.2	-3.6	-3.1	-10.2
61	1 <sup>st</sup> November 2021	15.0	-1.0	-5.6	-11.4
91	1 <sup>st</sup> December 2021	7.9	-4.4	-10.3	-15.2
122	1 <sup>st</sup> January 2022	10.5	1.4	-5.8	-8.8
153	1 <sup>st</sup> February 2022	10.5	-6.2	-9.6	-14.8
181	1 <sup>st</sup> March 2022	43.1	1.4	-3.2	-3.0
212	1 <sup>st</sup> April 2022	13.9	0.3	-0.6	-10.0
242	1 <sup>st</sup> May 2022	11.0	7.4	-6.5	-1.0
273	1 <sup>st</sup> June 2022	6.9	11.1	-17.9	-1.0
303	1 <sup>st</sup> July 2022	1.4	3.5	-16.3	-3.2
334	1 <sup>st</sup> August 2022	6.3	0.6	-8.3	-2.7

**Table 5.6** – Measuring Spot D.IV – CWR Neutral Temperature Changes; \*It is necessary to consider D.IV.1 as an outlier

Out of the data presented in Tables 5.3 – 5.6, the development of neutral temperature can be determined. The tensioning temperature in this section was 23 °C. In the following analysis, the data from the left and right side of rail will be averaged. In general, a difference can occur even in the left and right side of a rail – e. g. under thermal stress – that can cause slight lateral bending with inflection in the fastening nodes. A detailed analysis of bending of adjacent rail sections needs to be done to investigate this effect, however. Upon averaging the data from the left and right rail, the development of neutral temperature in measuring spots in the Bezprávi locality can be summarized as presented in Tables 5.7 – 5.10.



Day	Date	Left Rail [°C]	Right Rail [°C]
0	1 <sup>st</sup> September 2021	21.3	19.7
30	1 <sup>st</sup> October 2021	17.8	19.4
61	1 <sup>st</sup> November 2021	15.0	15.0
91	1 <sup>st</sup> December 2021	12.4	13.1
122	1 <sup>st</sup> January 2022	14.7	16.5
153	1 <sup>st</sup> February 2022	10.5	8.9
181	1 <sup>st</sup> March 2022	11.3	11.8
212	1 <sup>st</sup> April 2022	15.9	16.7
242	1 <sup>st</sup> May 2022	21.3	16.6
273	1 <sup>st</sup> June 2022	23.3	16.3
303	1 <sup>st</sup> July 2022	20.6	18.0
334	1 <sup>st</sup> August 2022	28.9	23.0

**Table 5.7** – Measuring Spot D.I – Neutral Temperature Values over Time

Day	Date	Left Rail* [°C]	Right Rail [°C]
0	1 <sup>st</sup> September 2021	22.7	26.3
30	1 <sup>st</sup> October 2021	23.3	21.1
61	1 <sup>st</sup> November 2021	24.7	22.9
91	1 <sup>st</sup> December 2021	20.5	20.6
122	1 <sup>st</sup> January 2022	26.0	22.9
153	1 <sup>st</sup> February 2022	21.3	19.6
181	1 <sup>st</sup> March 2022	22.3	20.6
212	1 <sup>st</sup> April 2022	27.0	25.9
242	1 <sup>st</sup> May 2022	30.9	31.1
273	1 <sup>st</sup> June 2022	31.7	26.7
303	1 <sup>st</sup> July 2022	31.6	30.6
334	1 <sup>st</sup> August 2022	35.4	27.5

**Table 5.8** – Measuring Spot D.II – Neutral Temperature Values over Time; \*Because of the Outlying Values of D.II.2, the D.II.1 Values are Considered Only and Not Averaged

Day	Date	Left Rail [°C]	Right Rail [°C]
0	1 <sup>st</sup> September 2021	22.6	25.0
30	1 <sup>st</sup> October 2021	21.9	19.7
61	1 <sup>st</sup> November 2021	24.9	19.4
91	1 <sup>st</sup> December 2021	19.8	16.9
122	1 <sup>st</sup> January 2022	23.0	21.0
153	1 <sup>st</sup> February 2022	20.1	16.5
181	1 <sup>st</sup> March 2022	24.1	19.5
212	1 <sup>st</sup> April 2022	20.4	18.8
242	1 <sup>st</sup> May 2022	24.8	22.5
273	1 <sup>st</sup> June 2022	25.1	20.0
303	1 <sup>st</sup> July 2022	32.0	22.5
334	1 <sup>st</sup> August 2022	34.1	24.4

**Table 5.9** – Measuring Spot D.III – Neutral Temperature Values over Time

Day	Date	Left Rail* [°C]	Right Rail [°C]
0	1 <sup>st</sup> September 2021	18.6	24.0
30	1 <sup>st</sup> October 2021	19.4	16.3
61	1 <sup>st</sup> November 2021	22.0	14.5
91	1 <sup>st</sup> December 2021	18.6	10.2
122	1 <sup>st</sup> January 2022	24.4	15.7
153	1 <sup>st</sup> February 2022	16.8	10.8
181	1 <sup>st</sup> March 2022	24.4	19.9
212	1 <sup>st</sup> April 2022	23.3	17.7
242	1 <sup>st</sup> May 2022	30.4	19.3
273	1 <sup>st</sup> June 2022	34.1	13.6
303	1 <sup>st</sup> July 2022	26.5	13.3
334	1 <sup>st</sup> August 2022	23.6	17.5

**Table 5.10** – Measuring Spot D.IV – Neutral Temperature Values over Time; \*Because of the Outlying Values of D.IV.1, the D.IV.2 Values are Considered Only and Not Averaged

The instant rail temperature measurement was performed in the same time as the CWR strain measurement. The rail temperature, measured at each particular measuring spot, can be averaged for measuring spots on each rail, too. The instant rail temperature is presented in Tables 5.11 – 5.14.

Day	Date	Left Rail [°C]	Right Rail [°C]
0	1 <sup>st</sup> September 2021	30.8	31.1
30	1 <sup>st</sup> October 2021	9.7	9.7
61	1 <sup>st</sup> November 2021	8.1	7.8
91	1 <sup>st</sup> December 2021	2.5	2.4
122	1 <sup>st</sup> January 2022	11.5	11.6
153	1 <sup>st</sup> February 2022	0.2	0.0
181	1 <sup>st</sup> March 2022	-7.7	-7.6
212	1 <sup>st</sup> April 2022	1.3	1.4
242	1 <sup>st</sup> May 2022	15.5	15.3
273	1 <sup>st</sup> June 2022	20.5	20.5
303	1 <sup>st</sup> July 2022	26.1	26.0
334	1 <sup>st</sup> August 2022	16.9	16.7

**Table 5.11** – Measuring Spot D.I – Instant Temperature Values over Time

Day	Date	Left Rail [°C]	Right Rail [°C]
0	1 <sup>st</sup> September 2021	28.4	28.2
30	1 <sup>st</sup> October 2021	4.8	4.9
61	1 <sup>st</sup> November 2021	7.8	7.4
91	1 <sup>st</sup> December 2021	2.5	2.5
122	1 <sup>st</sup> January 2022	11.4	11.5
153	1 <sup>st</sup> February 2022	0.3	0.2
181	1 <sup>st</sup> March 2022	-7.0	-6.9
212	1 <sup>st</sup> April 2022	1.5	1.5
242	1 <sup>st</sup> May 2022	14.6	14.5
273	1 <sup>st</sup> June 2022	13.2	12.9
303	1 <sup>st</sup> July 2022	22.9	23.0
334	1 <sup>st</sup> August 2022	17.2	16.9

**Table 5.12** – Measuring Spot D.II – Instant Temperature Values over Time

Day	Date	Left Rail [°C]	Right Rail [°C]
0	1 <sup>st</sup> September 2021	19.5	19.9
30	1 <sup>st</sup> October 2021	4.9	4.8
61	1 <sup>st</sup> November 2021	7.8	7.4
91	1 <sup>st</sup> December 2021	2.8	2.7
122	1 <sup>st</sup> January 2022	12.5	12.5
153	1 <sup>st</sup> February 2022	0.0	-0.1
181	1 <sup>st</sup> March 2022	-6.5	-6.6
212	1 <sup>st</sup> April 2022	1.5	1.5
242	1 <sup>st</sup> May 2022	13.9	13.7
273	1 <sup>st</sup> June 2022	13.2	13.0
303	1 <sup>st</sup> July 2022	22.7	22.4
334	1 <sup>st</sup> August 2022	17.0	16.7

**Table 5.13** – Measuring Spot D.III – Instant Temperature Values over Time

Day	Date	Left Rail [°C]	Right Rail [°C]
0	1 <sup>st</sup> September 2021	21.9	21.6
30	1 <sup>st</sup> October 2021	5.0	5.0
61	1 <sup>st</sup> November 2021	7.4	7.4
91	1 <sup>st</sup> December 2021	2.8	2.6
122	1 <sup>st</sup> January 2022	11.7	12.1
153	1 <sup>st</sup> February 2022	0.0	0.1
181	1 <sup>st</sup> March 2022	-6.2	-6.0
212	1 <sup>st</sup> April 2022	1.5	1.6
242	1 <sup>st</sup> May 2022	17.3	17.7
273	1 <sup>st</sup> June 2022	23.7	24.2
303	1 <sup>st</sup> July 2022	31.7	31.4
334	1 <sup>st</sup> August 2022	17.0	16.8

**Table 5.14** – Measuring Spot D.IV – Instant Temperature Values over Time

The knowledge of instant values of the rail temperature and neutral temperature can provide the determination of the thermal stress in the CWR according to Equation 2.10. The values of the instant rail temperature, instant neutral temperature and instant thermal stress in each rail in measuring spots in Bezpráví are presented in Tables 5.15 – 5.22.

Day	Date	Instant Rail Temperature [°C]	Instant Neutral Temperature [°C]	Instant Thermal Stress [MPa]
0	1 <sup>st</sup> September 2021	30.8	21.3	−23.0
30	1 <sup>st</sup> October 2021	9.7	17.8	19.5
61	1 <sup>st</sup> November 2021	8.1	15.0	16.7
91	1 <sup>st</sup> December 2021	2.5	12.4	24.0
122	1 <sup>st</sup> January 2022	11.5	14.7	7.7
153	1 <sup>st</sup> February 2022	0.2	10.5	24.8
181	1 <sup>st</sup> March 2022	−7.7	11.3	45.9
212	1 <sup>st</sup> April 2022	1.3	15.9	35.3
242	1 <sup>st</sup> May 2022	15.5	21.3	13.9
273	1 <sup>st</sup> June 2022	20.5	23.3	6.9
303	1 <sup>st</sup> July 2022	26.1	20.6	−13.2
334	1 <sup>st</sup> August 2022	16.9	28.9	29.0

**Table 5.15** – Measuring Spot D.I – Left Rail: Instant Rail Temperature, Neutral Temperature and Thermal Stress

Day	Date	Instant Rail Temperature [°C]	Instant Neutral Temperature [°C]	Instant Thermal Stress [MPa]
0	1 <sup>st</sup> September 2021	31.1	19.7	−27.5
30	1 <sup>st</sup> October 2021	9.7	19.4	23.5
61	1 <sup>st</sup> November 2021	7.8	15.0	17.3
91	1 <sup>st</sup> December 2021	2.4	13.1	25.7
122	1 <sup>st</sup> January 2022	11.6	16.5	11.9
153	1 <sup>st</sup> February 2022	0.0	8.9	21.6
181	1 <sup>st</sup> March 2022	−7.6	11.8	46.8
212	1 <sup>st</sup> April 2022	1.4	16.7	37.0
242	1 <sup>st</sup> May 2022	15.3	16.6	3.2
273	1 <sup>st</sup> June 2022	20.5	16.3	−10.3
303	1 <sup>st</sup> July 2022	26.0	18.0	−19.4
334	1 <sup>st</sup> August 2022	16.7	23.0	15.1

**Table 5.16** – Measuring Spot D.I – Right Rail: Instant Rail Temperature, Neutral Temperature and Thermal Stress

Day	Date	Instant Rail Temperature [°C]	Instant Neutral Temperature [°C]	Instant Thermal Stress [MPa]
0	1 <sup>st</sup> September 2021	28.4	22.7	-13.8
30	1 <sup>st</sup> October 2021	4.8	23.3	44.6
61	1 <sup>st</sup> November 2021	7.8	24.7	40.9
91	1 <sup>st</sup> December 2021	2.5	20.5	43.5
122	1 <sup>st</sup> January 2022	11.4	26.0	35.2
153	1 <sup>st</sup> February 2022	0.3	21.3	50.8
181	1 <sup>st</sup> March 2022	-7.0	22.3	70.8
212	1 <sup>st</sup> April 2022	1.5	27.0	61.6
242	1 <sup>st</sup> May 2022	14.6	30.9	39.3
273	1 <sup>st</sup> June 2022	13.2	31.7	44.6
303	1 <sup>st</sup> July 2022	22.9	31.6	20.9
334	1 <sup>st</sup> August 2022	17.2	35.4	43.9

**Table 5.17** – Measuring Spot D.II – Left Rail: Instant Rail Temperature, Neutral Temperature and Thermal Stress

Day	Date	Instant Rail Temperature [°C]	Instant Neutral Temperature [°C]	Instant Thermal Stress [MPa]
0	1 <sup>st</sup> September 2021	28.2	26.3	-4.6
30	1 <sup>st</sup> October 2021	4.9	21.1	39.2
61	1 <sup>st</sup> November 2021	7.4	22.9	37.3
91	1 <sup>st</sup> December 2021	2.5	20.6	43.7
122	1 <sup>st</sup> January 2022	11.5	22.9	27.4
153	1 <sup>st</sup> February 2022	0.2	19.6	46.9
181	1 <sup>st</sup> March 2022	-6.9	20.6	66.5
212	1 <sup>st</sup> April 2022	1.5	25.9	59.0
242	1 <sup>st</sup> May 2022	14.5	31.1	40.1
273	1 <sup>st</sup> June 2022	12.9	26.7	33.2
303	1 <sup>st</sup> July 2022	23.0	30.6	18.3
334	1 <sup>st</sup> August 2022	16.9	27.5	25.5

**Table 5.18** – Measuring Spot D.II – Right Rail: Instant Rail Temperature, Neutral Temperature and Thermal Stress

Day	Date	Instant Rail Temperature [°C]	Instant Neutral Temperature [°C]	Instant Thermal Stress [MPa]
0	1 <sup>st</sup> September 2021	19.5	22.6	7.5
30	1 <sup>st</sup> October 2021	4.9	21.9	41.1
61	1 <sup>st</sup> November 2021	7.8	24.9	41.4
91	1 <sup>st</sup> December 2021	2.8	19.8	41.1
122	1 <sup>st</sup> January 2022	12.5	23.0	25.3
153	1 <sup>st</sup> February 2022	0.0	20.1	48.6
181	1 <sup>st</sup> March 2022	-6.5	24.1	73.9
212	1 <sup>st</sup> April 2022	1.5	20.4	45.6
242	1 <sup>st</sup> May 2022	13.9	24.8	26.4
273	1 <sup>st</sup> June 2022	13.2	25.1	28.8
303	1 <sup>st</sup> July 2022	22.7	32.0	22.6
334	1 <sup>st</sup> August 2022	17.0	34.1	41.4

**Table 5.19** – Measuring Spot D.III – Left Rail: Instant Rail Temperature, Neutral Temperature and Thermal Stress

Day	Date	Instant Rail Temperature [°C]	Instant Neutral Temperature [°C]	Instant Thermal Stress [MPa]
0	1 <sup>st</sup> September 2021	19.9	25.0	12.3
30	1 <sup>st</sup> October 2021	4.8	19.7	35.9
61	1 <sup>st</sup> November 2021	7.4	19.4	28.9
91	1 <sup>st</sup> December 2021	2.7	16.9	34.3
122	1 <sup>st</sup> January 2022	12.5	21.0	20.4
153	1 <sup>st</sup> February 2022	-0.1	16.5	40.1
181	1 <sup>st</sup> March 2022	-6.6	19.5	63.0
212	1 <sup>st</sup> April 2022	1.5	18.8	41.7
242	1 <sup>st</sup> May 2022	13.7	22.5	21.2
273	1 <sup>st</sup> June 2022	13.0	20.0	16.8
303	1 <sup>st</sup> July 2022	22.4	22.5	0.2
334	1 <sup>st</sup> August 2022	16.7	24.4	18.6

**Table 5.20** – Measuring Spot D.III – Right Rail: Instant Rail Temperature, Neutral Temperature and Thermal Stress

Day	Date	Instant Rail Temperature [°C]	Instant Neutral Temperature [°C]	Instant Thermal Stress [MPa]
0	1 <sup>st</sup> September 2021	21.9	18.6	-8.1
30	1 <sup>st</sup> October 2021	5.0	19.4	34.8
61	1 <sup>st</sup> November 2021	7.4	22.0	35.2
91	1 <sup>st</sup> December 2021	2.8	18.6	38.2
122	1 <sup>st</sup> January 2022	11.7	24.4	30.6
153	1 <sup>st</sup> February 2022	0.0	16.8	40.5
181	1 <sup>st</sup> March 2022	-6.2	24.4	73.8
212	1 <sup>st</sup> April 2022	1.5	23.3	52.7
242	1 <sup>st</sup> May 2022	17.3	30.4	31.5
273	1 <sup>st</sup> June 2022	23.7	34.1	25.1
303	1 <sup>st</sup> July 2022	31.7	26.5	-12.6
334	1 <sup>st</sup> August 2022	17.0	23.6	15.9

**Table 5.21** – Measuring Spot D.IV – Left Rail: Instant Rail Temperature, Neutral Temperature and Thermal Stress

Day	Date	Instant Rail Temperature [°C]	Instant Neutral Temperature [°C]	Instant Thermal Stress [MPa]
0	1 <sup>st</sup> September 2021	21.6	24.0	5.8
30	1 <sup>st</sup> October 2021	5.0	16.3	27.4
61	1 <sup>st</sup> November 2021	7.4	14.5	17.1
91	1 <sup>st</sup> December 2021	2.6	10.2	18.4
122	1 <sup>st</sup> January 2022	12.1	15.7	8.8
153	1 <sup>st</sup> February 2022	0.1	10.8	25.7
181	1 <sup>st</sup> March 2022	-6.0	19.9	62.5
212	1 <sup>st</sup> April 2022	1.6	17.7	38.9
242	1 <sup>st</sup> May 2022	17.7	19.3	3.8
273	1 <sup>st</sup> June 2022	24.2	13.6	-25.7
303	1 <sup>st</sup> July 2022	31.4	13.3	-43.8
334	1 <sup>st</sup> August 2022	16.8	17.5	1.7

**Table 5.22** – Measuring Spot D.IV – Right Rail: Instant Rail Temperature, Neutral Temperature and Thermal Stress

A similar analysis can be made for every measuring spot.



### 5.3 Discussion

The records presented in Figures 4.19 to 4.24 show that a majority of measuring spots evince a similar development of the measured strain, with only some seem to escape into outlying values. The low amount of outliers among the measured data attest to a good efficacy of the selected methodology. The outlying values shall be considered not to enter the statistical evaluations as there can be various mechanical or other disruptions causing the issue. Since many strain gauges were installed in all the monitored localities, enough data is provided to identify the outliers. An example of an outlier identification is provided in Figure 5.10. In the data from Day 212 of the Bezprávi CWR strain recordings, the relative strain value is clearly out of the whiskers and far from the 1.5 multiplication of the interquartile range.

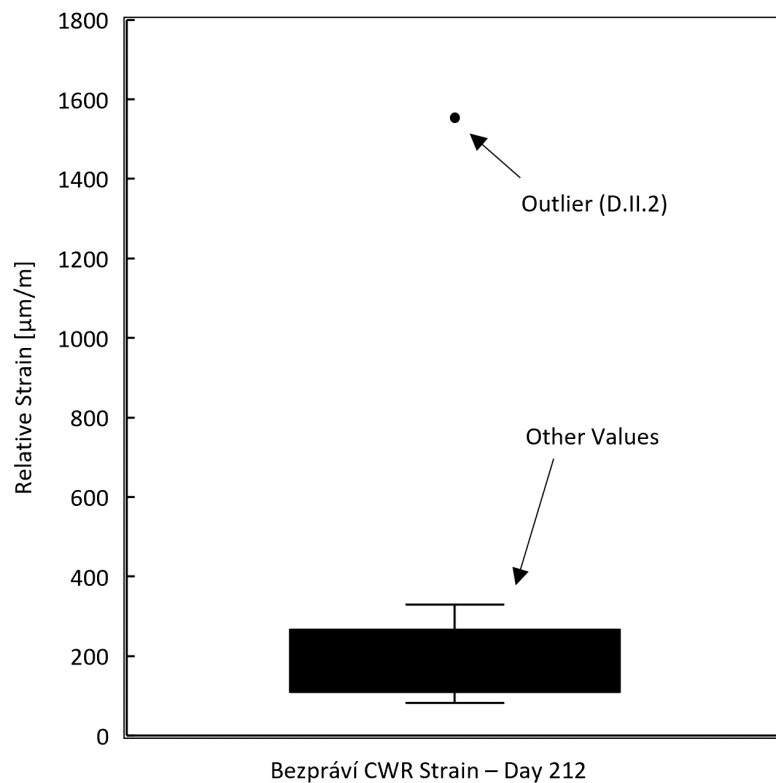
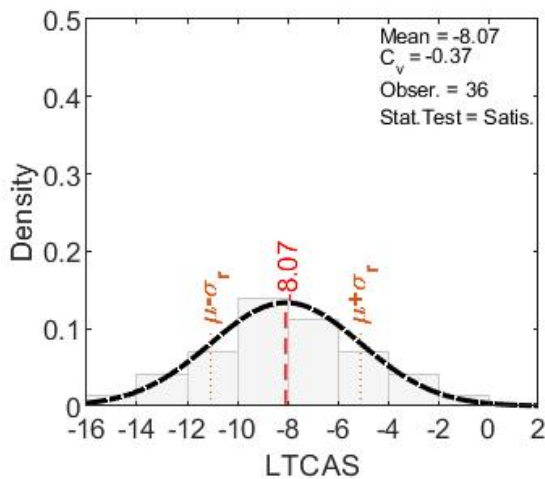


**Figure 5.10** – Example of an Outlier Identification in the Case of Bezprávi CWR Strain Recordings – Day 212

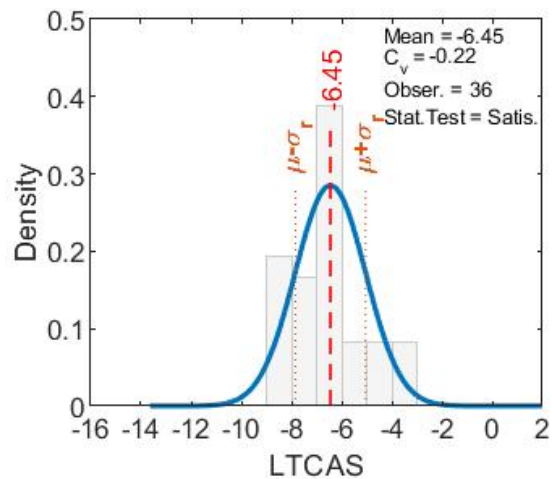
The crucial point of the neutral temperature development determination is the setting of the LTCAS for the calculation of the extrapolated temperature. Experimentally, the LTCAS can be obtained from a test on a sample under a known fixation of the supports. This is, however, impossible to simulate in the track. If the rail fastenings or the track alignment deteriorates over time and change the magnitude of fixation of the supports, it may cause the change of the LTCAS (as presented in Figures 5.3 and 5.4) and thus improperly omit a change of the rail neutral temperature. It can be assumed that the accuracy of the LTCAS determination increases with shortening of the time needed to obtain the coefficient. This is, because a lower deterioration of the rail fastenings and the track alignment can be expected just after welding

than if the data collection is spread over a longer period, where the construction site transport and other impacts can play a role. On the other hand, the more measurements are performed, the more values are obtained and the higher accuracy of the measured data can be determined.

The LTCAS values calculated for measurements in Chotěvice and Bezprávi localities were presented in Tables 5.1 and 5.2. The statistical analysis of the LTCAS values can indicate why the CWR strain measurements in a short period after rail welding is desired. It can be illustrated in Figures 5.11 – 5.16.



Legend for Figure 5.11:  
 - Hist. Week Data (light grey bar)  
 - Normal Distribution (black dashed line)  
 - Mean Value (red dashed line)  
 - Prominent Range (dotted line)



Legend for Figure 5.12:  
 - Hist. All Data (light grey bar)  
 - Normal Distribution (blue solid line)  
 - Mean Value (red dashed line)  
 - Prominent Range (dotted line)

**Figure 5.11** – Probability Density of Normal Distribution of LTCAS from the First Week of Measurements in the Chotěvice Locality

**Figure 5.12** – Probability Density of Normal Distribution of LTCAS from All Measurements in the Chotěvice Locality

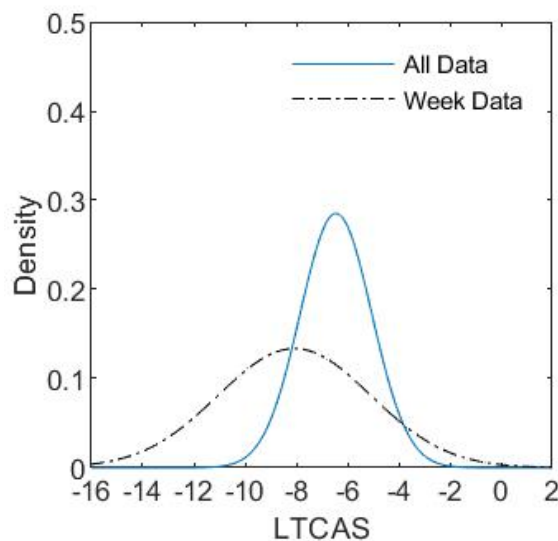


**Figure 5.13** – Comparison of Probability Density Function for the Chotěvice Locality

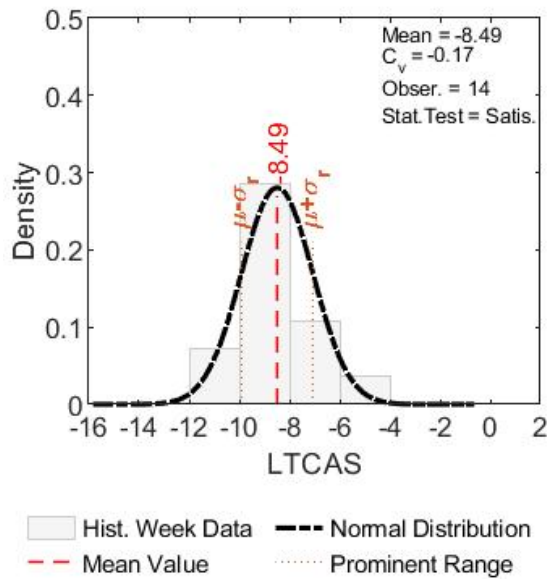


**Figure 5.14** – Probability Density of Normal Distribution of LTCAS from the First Week of Measurements in the Bezprávi Locality

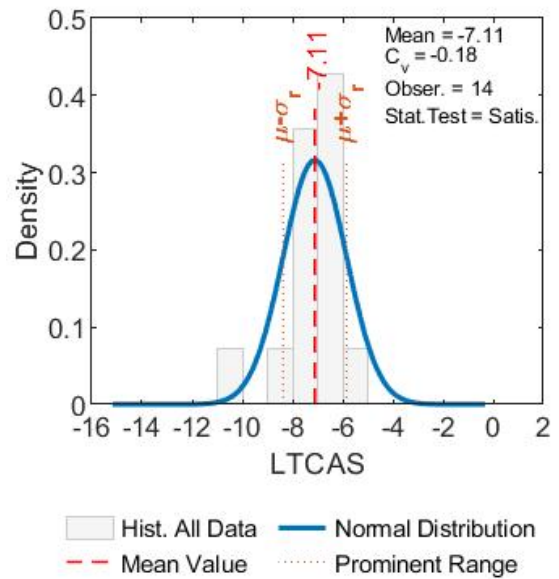


**Figure 5.15** – Probability Density of Normal Distribution of LTCAS from All Measurements in the Bezprávi Locality

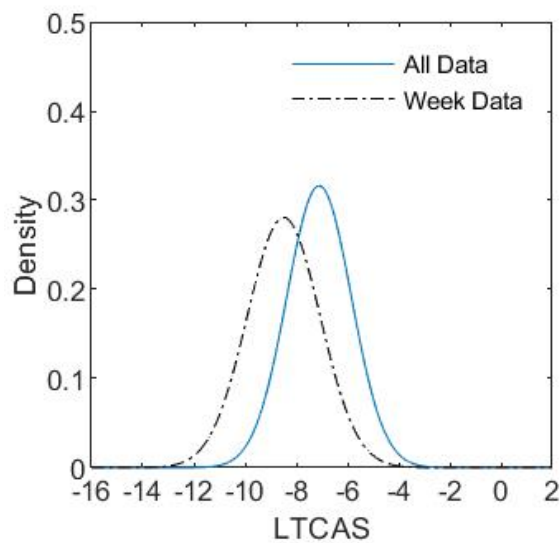


**Figure 5.16** – Comparison of Probability Density Function for the Bezprávi Locality

As presented in Figures 5.11 – 5.16, the LTCAS mean values grow with the growing number of measurements over time. The statistics available from our measurements is limited and more investigation is needed to verify this effect, but the change of the LTCAS mean value towards zero corresponds to the hypothesis of the CWR fixation deterioration over time [59, 60]. In Chapter 4.1, it was shown that the LTCAS (slope coefficient) is zero in the case of a freely expandable sample and reaches some constant value if the sample is fixed at both sides. An area of a semi-rigid fixation lies between these two values. The same principle can be considered

for a railway track. It can be assumed that the fixation of rails (through fastenings) slightly deteriorate over time and this corresponds to the slight increase (as the values are presented in the negative scale) of the LTCAS towards zero.

It is necessary to note that a change of the mean value occurs if the number of samples grows in a population. Considering the normal distribution, however, the direction of the change can occur to both sides of the original value. In the datasets created from the measured data, the change was towards zero.

For the completeness of the description, it is necessary to mention that the standard deviation decreases with a growing number of samples in the population, as expected. An interesting difference can be seen among the standard deviation of the Chotěvice and Bezprávi data, with a significantly lower standard deviation of the latter. This is caused by the weather conditions in the first week of measurements. In Chotěvice, the first week of measurements was in the end of July and the weather was stable – hot and sunny – all days of the week. In Bezprávi, the first week of measurements was in the beginning of September and the weather was changeable with the temperature varying day by day. This difference provided us with a larger span of rail temperatures that resulted in smaller standard deviation of the normal distribution.

The measurements performed on a daily basis are used as a dataset for the estimation of the LTCAS in this dissertation. This database was selected because the volume of the dataset seems sufficient for the intention of the LTCAS determination on one hand and seem acceptable in the terms of the data collection period length on the other hand. Based on the ideas formulated in the previous paragraphs, it is recommended to obtain as many as possible, but at least ten, values of strain in a shortest possible period, but with a maximum reachable rail temperature change (to be able to construct a reasonable trend line and obtain a reliable LTCAS). An automated data collection system would make the most comfortable way, but a measurement according to the methodology [58] can be used, too. In the latter, it is recommended to perform the measurement at least over the evening and morning within the first 24 hours after the stress-controlled rail welding and collect at least ten values of strain.

The data presented in Appendix E start at the day zero, which is the day of stress-controlled rail welding, after the welding or at least tensioning. The advantage of this approach is that the values of the measured and extrapolated temperature difference visualised by a grey line show directly the assumed determination of the CWR neutral temperature change. An example of this data is presented in Figures 5.17 and 5.18.

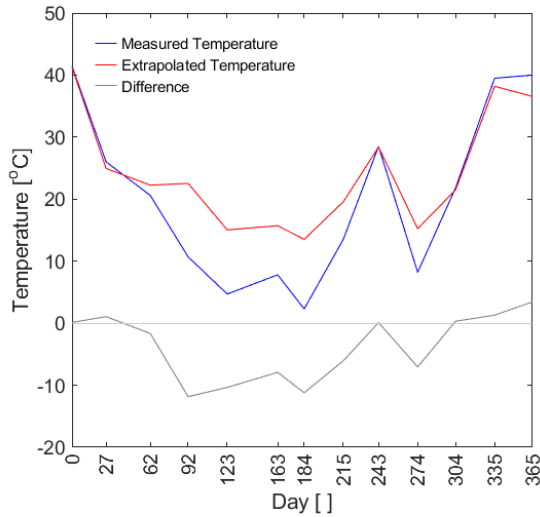


**Figure 5.17** – C.VI.1 – Measured Temperature, Extrapolated Temperature, and Temperature Difference

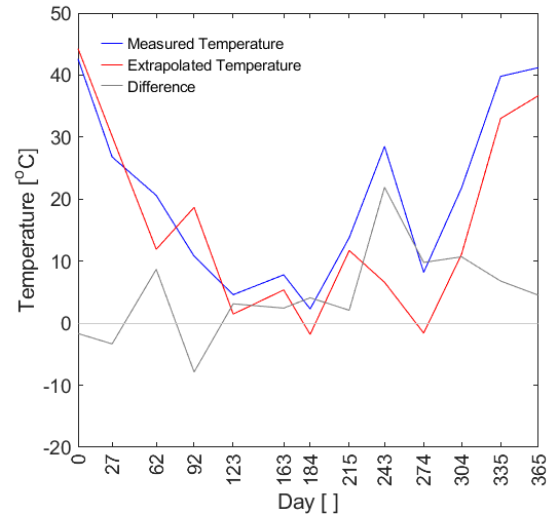


**Figure 5.18** – C.VI.2 – Measured Temperature, Extrapolated Temperature, and Temperature Difference

Another point which requires elaboration is the initial value of the measured and extrapolated temperature difference, which is different from zero in many cases. This is not an error. This is a result of a relatively long period of data collection for the LTCAS determination dataset. In the case of the presented experiments, the period was typically one week, some deterioration might have occurred and the coefficient of determination was somewhat different from one. If the data collection was performed in a shorter period, the deterioration might be lower and the coefficient of determination higher. In a thought experiment, if the data collection was performed in such a short period that no deterioration occurred and the supports could be considered as fully fixed, the coefficient of determination would reach one (leave apart the non-linear part) and the values of the measured and extrapolated temperature difference would start at zero on the day zero.

The clustered data presented in Appendix F are more illustrative to discuss the particular results of the rail monitoring. Notable effects can be seen in the comparison of the general behaviour of the development of the curve clusters. The curve clusters of the Bezprávi locality (D), except for the cluster D.IV, seem evolving in a very similar shape. Moreover, they show lower amplitudes than the ones at the Chotěvice locality (C), which can be caused by a stronger track elements: 60E2 rail in Bezprávi to 49E1 rails in Chotěvice, fastening system Vossloh W 30 HH in Bezprávi to W 14 in Chotěvice, etc.

In a closer discussion on the data from Chotěvice presented in Appendix F, following can be mentioned: The data from the profile C.I do not provide valuable outcomes as three out of four measuring set track units were destroyed by the track maintenance on 2<sup>nd</sup> March 2022. The data from the profiles C.II and C.III need to be taken with a lower reliability as the measured values tended not to be fully stable at all measurements. The data from the other profiles show a slight to moderate increase of the neutral temperature in the summer period after the winter period of stability or a slight drop of the neutral temperature. Please note the values measured on the Day 243. These values were recorded after track tamping was performed on 2<sup>nd</sup> March 2022.

A change of the neutral temperature is clearly visible in this measurement, most notably in the cross-sectional profiles C.V, C.VI, and C.VII, which are located in an intermediate straight section between two curves or (profile C.V) in a transition curve. This effect shall be a subject to further studies.

Another way of the neutral temperature development results presentation is the visualisation of the thermal stress in rails. The example analysis for the Bezpráví locality measuring spots presented in the end of Section 5.2 can be visualized by Figures 5.19 – 5.26. For a better mutual comparison of the presented values, the graphs are composed to a rectangular array without legend and in a small size. The full scale figures are presented in Appendix G.

In Figures 5.19 – 5.26, the red line corresponds to the instant rail temperature in Tables 5.15 – 5.22 and represents the thermal stress if neutral temperature was considered constant in the level of the tensioning temperature (23 °C in the case of the Bezpráví locality). The green line corresponds the instant neutral temperature in Tables 5.15 – 5.22 and represents the neutral temperature change over time (in this graphs, however, expressed in the equivalent stress according to Equation 2.10). The difference coloured as the grey area represents the actual level of the thermal stress in the particular measuring spot of the CWR if the new approach to the determination of the neutral temperature change over time according to this dissertation is adopted.

Presentation of the results in the form of graphs shown in Figures 5.19 – 5.26 can be done under several constraints, which must be kept in mind for interpretation. First of all, the values corresponding to the instant rail temperature (marked by the red line) and the values corresponding to the neutral temperature change (marked by the green line) were not measured continuously, therefore only the discrete values in the particular days of measurement are calculated. The discrete points were connected for a better visualisation of the discussed effect. The instant rail temperature (marked by the red line) changes cyclically every day and a correct visualisation would include the cycles, but the measurements were performed on a monthly basis in the discussed period. Therefore, the intraday change of the instant rail temperature cannot be shown.

Several important effects can be seen in Figures 5.19 – 5.26 separately and in their mutual comparison:

- **The neutral temperature change in the left and right rail of the same measuring spot show a similar trend.** In both rails of the D.I measuring spot, a decrease of the neutral temperature (and the equivalent stress) is visible in the first half of the monitored period and an increase follows in the second half. In both rails of the D.II measuring spot, the neutral temperature remains relatively constant or experiences a very limited decrease in the first half of the monitored period and increases above its original value in the second half. The D.III measuring spot shows a similar trend, too.
- **The neutral temperature change is different in different measuring spots.** The distance between each measuring spot is 160 m (as can be seen from the drawing in the annex). Whereas in the middle of the monitoring period, the neutral temperature seems to be on a similar level to the tensioning temperature in the case of the D.II and D.III

measuring spots, a clear decrease of the neutral temperature is visible in the D.I measuring spot. Neutral temperature returns to the level of the tensioning temperature at the end of the measuring period in the D.I measuring spot, but increases to higher levels in the case of the D.II measuring spot. In the case of the D.III measuring spot, the increase is not so significant, as it is in the case of D.II.

- **The neutral temperature seems to adjust itself to the yearly temperature cycles into a certain extent.** This effect helps to decrease the thermal stress in the times of extreme instant rail temperature values and prevents CWR from more frequent failures.

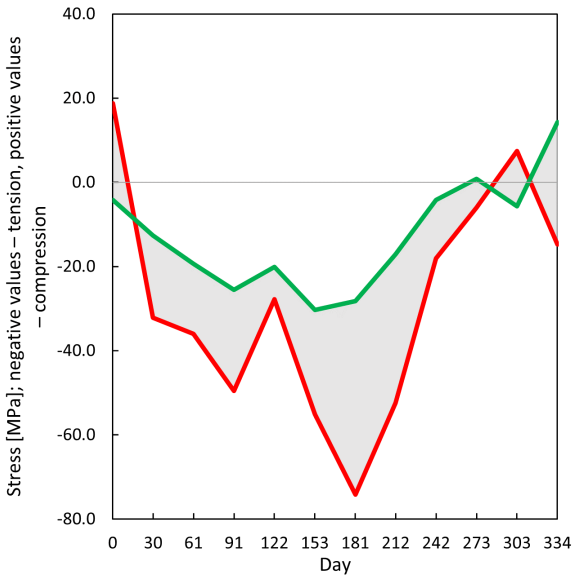


**Figure 5.19** – D.I – Left Rail: Comparison of Standard and New Approach to the Thermal Stress Determination in CWR

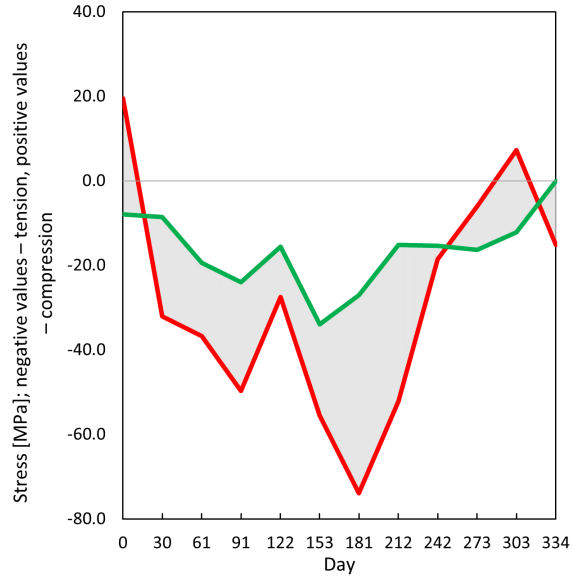


**Figure 5.20** – D.I – Right Rail: Comparison of Standard and New Approach to the Thermal Stress Determination in CWR

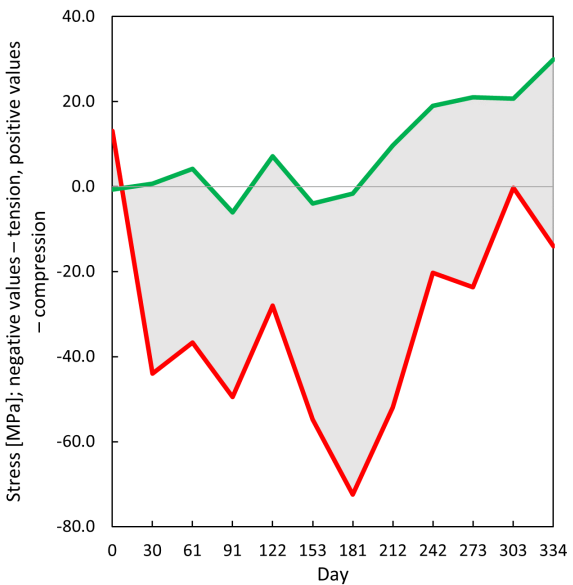


**Figure 5.21** – D.II – Left Rail: Comparison of Standard and New Approach to the Thermal Stress Determination in CWR

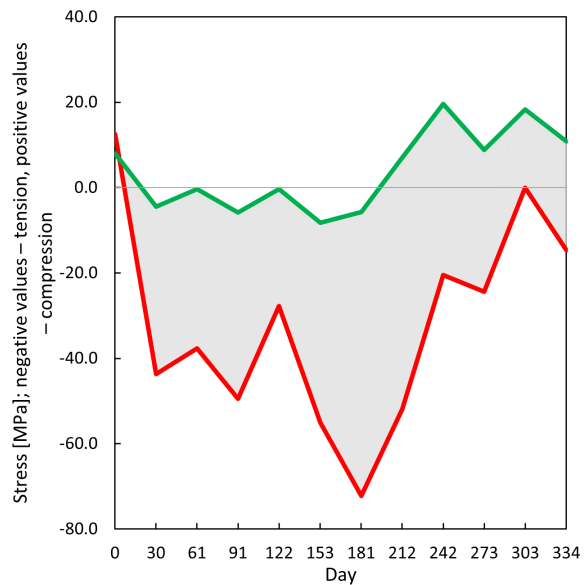


**Figure 5.22** – D.II – Right Rail: Comparison of Standard and New Approach to the Thermal Stress Determination in CWR



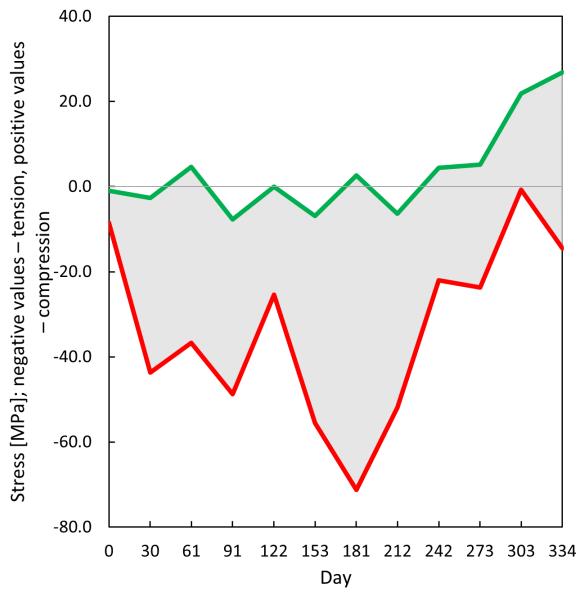


**Figure 5.23** – D.III – Left Rail: Comparison of Standard and New Approach to the Thermal Stress Determination in CWR

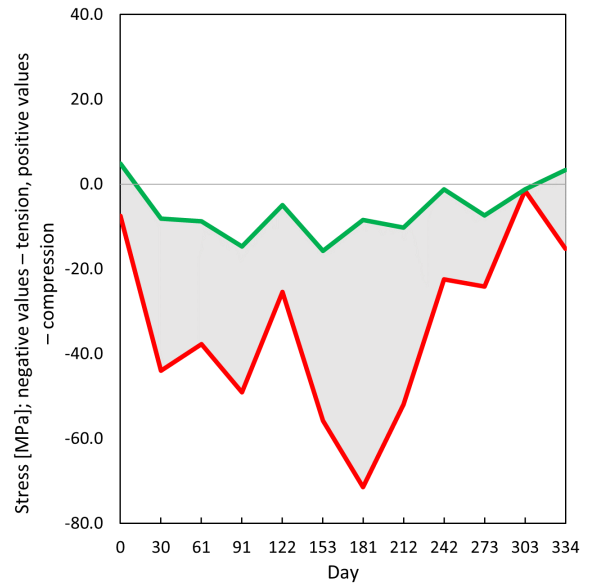


**Figure 5.24** – D.III – Right Rail: Comparison of Standard and New Approach to the Thermal Stress Determination in CWR

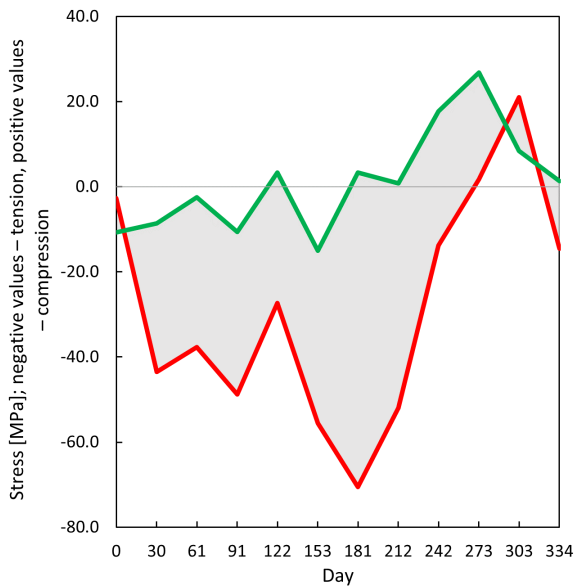


**Figure 5.25** – D.IV – Left Rail: Comparison of Standard and New Approach to the Thermal Stress Determination in CWR

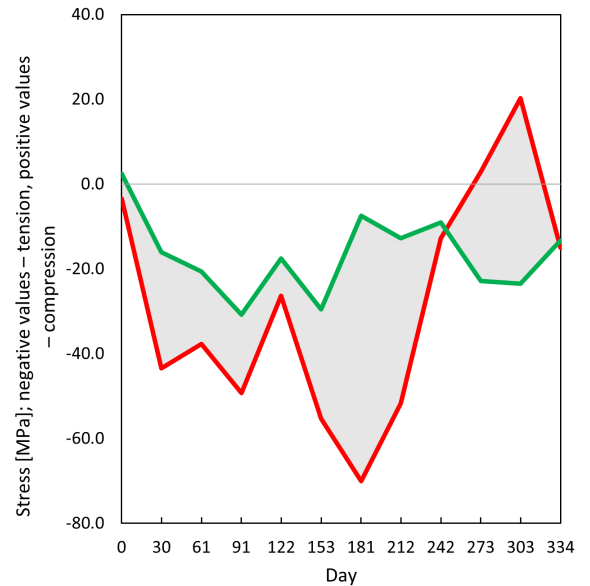


**Figure 5.26** – D.IV – Right Rail: Comparison of Standard and New Approach to the Thermal Stress Determination in CWR



## Chapter 6

# Conclusions

The problem of determination of the instant value of the neutral temperature in the CWR is an up-to-date topic all over the world. Many attempts have been made to develop a non-destructive direct methodology of the normal rail stress measurement, so far without an appreciable success. The proposed dissertation deals with this problem searching for a development of a methodology using the state-of-the-art technology that is affordable and easy to deploy, and presents research results that provide an insight into the CWR behaviour, propose a methodology for the determination of the neutral temperature change and the calculation of the thermal stress in the CWR, and charts a way of investigation to gain a better knowledge on the development of the neutral temperature in the CWR.

The opening chapters of this dissertation present a short introduction to the CWR, rail stresses, and the problem of the neutral temperature determination. Chapter 3 presents the research results in the area of the rail temperature measurement, which is important for the further work on the neutral temperature determination. A short analysis of two critical parameters that have an impact on the rail temperature, i. e. the air temperature and cloudiness, is given, and a comparison to the Eurocode is presented. Further, an extensive investigation into the rail temperature development in selected localities in the Czech Republic is presented. Various parameters connected to the railway track position are identified as factors influencing the rail temperature. A railway track location on a bridge across a river is identified as the most prone one to the extreme cold temperatures, whereas the south-west orientation of rail on a sunny plain is identified as the most prone to the extreme hot temperatures. A specific impact of snow cover of a railway track is discussed in this section, too.

Chapter 4 focuses on an investigation into the strain monitoring of the CWR. The laboratory measurement setup is analysed in the first section. In this section, a self-compensation attribute of the strain gauges used in the tests is proven and further questions regarding the slope coefficient are raised. A comparison of the half bridge and quarter bridge configurations of strain gauges is performed and the quarter bridge configuration is recommended for the field measurements. A functioning sample *Measuring Set for Diagnostics of Time-Based Development of Stress States in CWR*, which follows the first section is briefly introduced (with the full documentation available in the annexes) in the second section. The third section presents a large-scale extensive CWR strain monitoring that was performed in several localities across

the Czech Republic in the past years. The CWR strain data of the investigated sections are the outcomes of this monitoring.

Chapter 5 follows the CWR strain monitoring with research ideas that were elaborated from the obtained data, presents the *Methodology of Non-Destructive Determination of Mechanical Stress in CWR* (with the full text available in the annexes), and embraces the ideas into the methodology to form a proposal of determination of the neutral temperature change in CWR and a new approach to the thermal stress calculation. A hypothesis of an important role of the LTCAS is presented and applied in the example of two measuring spots monitored within the scope of the extensive CWR strain measurement presented in Chapter 4. A change of neutral temperature within the interval of  $\langle 8.9; 28.9 \rangle^{\circ}\text{C}$  in the case of the measuring spot D.I rails,  $\langle 19.6; 35.4 \rangle^{\circ}\text{C}$  in the case of the measuring spot D.II rails,  $\langle 16.5; 34.1 \rangle^{\circ}\text{C}$  in the case of the measuring spot D.III rails, and  $\langle 10.2; 34.1 \rangle^{\circ}\text{C}$  in the case of the measuring spot D.IV rails with the tensioning temperature of  $23^{\circ}\text{C}$  in all spots is calculated. Figures visualising the results of the new approach to the CWR neutral temperature determination and thermal stress calculation are introduced in the discussion.

## 6.1 Further Research

The performed research opened several questions that need to be addressed and problems with a potential to be solved by further research. This section summarizes the topics of further research in both major aims of this dissertation – the rail temperature and CWR strain monitoring.

Research on the rail temperature estimation based on a set of more parameters and quantification of their impact shall be made. The combined influence of natural parameters on the rail temperature shall be studied in order to create a parametric mathematical model predicting the rail temperature based on public weather information. This would provide an alternative approach to the rail temperature determination from the direct measurement provided by the proposed thermometer in the paragraph above. Yet, both research aims may well complement each other.

The risk rail temperature index shall be determined and a rail temperature prediction model for the whole railway network shall be made based on and in succession of the work by Mr. Ďurkovský [49]. A map of the rail network with local temperature extremes and the risk rail temperature index can be created.

Measures to prevent rails from extreme heating, beyond those already existing in the world, shall be investigated.

Longitudinal displacement of rails in railway tracks shall be investigated and parameters of this displacement identified and quantified. A parametric model of the longitudinal displacement of rails shall be created.

Finding answers to the questions on the LTCAS (slope coefficient) value and its stability formulated in Subsection 4.1.3 shall be targeted. The CWR strain monitoring and verification of the interpreted data on the change of the CWR neutral temperature shall continue with a possible update of the *Methodology of Non-Destructive Determination of Mechanical Stress in Continuous Welded Rail*.

# References

1. VNENK, Petr; CULEK, Bohumil. Measurement Methods of Internal Stress in Continuous Welded Rail. In: Prague: Czech Technical University in Prague, 2017, pp. 91–96. ISBN 978-80-01-06297-5. ISSN 2336-5382. Available from DOI: 10.14311/APP.2017.11.0091.
2. GRULKOWSKI, Sławomir. *Badanie i Analiza Procesu Regulacji Geometrycznej Toru Kolejowego*. Gdańsk, 2008. Dissertation. Politechnika Gdańska.
3. JOHNSON, Erland. *Measurement of forces and neutral temperatures in railway rails – an introductory study* [online]. Borås, 2004 [visited on 2022-08-29]. Available from: <https://www.diva-portal.org/smash/get/diva2:962265/FULLTEXT01.pdf>. Report. Swedish National Testing and Research Institute.
4. VNENK, Petr; CULEK, Bohumil. Long-Term Measurements in the Neutral Temperature Identification Problems in Continuous Welded Rail. In: Budapest: Budapest University of Technology and Economics, 2017, pp. 173–178. ISBN 978-963-313-258-6.
5. MIRKOVIĆ, Nikola; BRAJOVIĆ, Ljiljana; MALOVIĆ, Miodrag; VNENK, Petr. Measurement Methods for Residual Stress in CWR. In: Berlin: Springer, 2019, vol. 982, pp. 346–355. ISBN 978-3-030-19755-1. ISSN 2194-5357. Available from DOI: 10.1007/978-3-030-19756-8\_32.
6. ŠMEJDA, Aleš; VNENK, Petr; BORKOVCOVÁ, Anna; BORECKÝ, Vladislav; LOPOUR, Pavel; ŠEVČÍK, Filip. Diagnostika a průzkum drážního tělesa. In: Prague: Agentura VI-ACO, 2020, pp. 27–30.
7. SPRÁVA ŽELEZNIČNÍ DOPRAVNÍ CESTY, S. O. *SŽDC S 3/2 Bezстыková kolej*. 2013.
8. UIC. *Code 720 Laying and Maintenance of CWR Track*. Paris, 2005.
9. ESVELD, Coenraad. *Modern Railway Track*. 2nd ed. Delft: MRT-Productions, 2001. ISBN 90-800324-3-3.
10. LICHTBERGER, Bernhard. *Track Compendium*. 2nd ed. Hamburg: DVV Media Group, 2011. ISBN 978-3-7771-0421-8.
11. LIM, Nam-Hyoung; PARK, Nam-Hoi; KANG, Young-Jong. Stability of continuous welded rail track. *Computers and Structures*. 2003, vol. 81. Available also from: [https://www.researchgate.net/publication/229270238\\_Stability\\_of\\_continuous\\_welded\\_rail\\_track](https://www.researchgate.net/publication/229270238_Stability_of_continuous_welded_rail_track).

12. KISH, Andrew; SAMAVEDAM, Gopal. *Track Buckling Prevention: Theory, Safety Concepts, and Applications*. U.S. Department of Transportation, 2013. Available from eprint: <https://www.fra.dot.gov/Elib/Document/3036>. U. S. Department of Transportation, March 2013, [2017-07-25].
13. BALUCH, Henryk. Wykolejenia pociągów związane ze stanem nawierzchni i metody ich badań. *XXIV Konferencja Naukowo-Techniczna Awarie Budowlane*. 2009. Available also from: [http://www.awarie.zut.edu.pl/files/ab2009/referaty/00\\_referaty\\_prob\\_lemowe/02\\_Baluch\\_H\\_Wykolejenia\\_pociagow\\_zwiazane\\_ze\\_stanem\\_nawierzchni\\_i\\_metody\\_ich\\_badan.pdf](http://www.awarie.zut.edu.pl/files/ab2009/referaty/00_referaty_prob_lemowe/02_Baluch_H_Wykolejenia_pociagow_zwiazane_ze_stanem_nawierzchni_i_metody_ich_badan.pdf).
14. MANDAL, Nirmal Kumar; LEES, Mitchell. An Investigation into Monitoring Rail Stress in Continuously Welded Rails Through Stress-Free Temperature. *Conference on Railway Engineering, Melbourne, Australia*. 2016. Available also from: [https://www.researchgate.net/publication/303805601\\_AN\\_INVESTIGATION\\_INTO\\_MONITORING\\_RAIL\\_STRESS\\_IN\\_CONTINUOUSLY\\_WELDED\\_RAILS\\_THROUGH\\_STRESS-FREE\\_TEMPERATURE](https://www.researchgate.net/publication/303805601_AN_INVESTIGATION_INTO_MONITORING_RAIL_STRESS_IN_CONTINUOUSLY_WELDED_RAILS_THROUGH_STRESS-FREE_TEMPERATURE).
15. LIU, Ganzhong; LIU, Hao; WEI, Anqi; XIAO, Jieling; WANG, Ping; LI, Shaozheng. A new device for stress monitoring in continuously welded rails using bi-directional strain method. *Journal of Modern Transportation*. 2018, vol. 26, pp. 179–188. ISSN 2662-4745. Available from DOI: 10.1007/s40534-018-0164-z.
16. GU, Lijuan; ZHANG, Liang; BAO, Xiaoyi; ZHANG, Merrina; ZHANG, Chengxian; DONG, Yongkang. Detection of Thermal Strain in Steel Rails with BOTDA. *Applied Sciences*. 2018, vol. 8, no. 2013. ISSN 2076-3417. Available from DOI: 10.3390/app8112013.
17. LONSDALE, C. P. *Thermite rail welding: history, process developments, current practices and outlook for the 21st century*. Available also from: <http://citeseerx.ist.psu.edu/viewdoc/download?doi=10.1.1.546.5448&rep=rep1&type=pdf>. Proceedings of the AREMA 1999 Annual Conference Chicago, IL, 1999.
18. ELEKTRO-THERMIT GMBH & CO. KG. *Wir machen das lückenlose Gleis* [online]. 2008 [visited on 2022-08-27]. Available from: [https://www.elektro-thermit.de/fileadmin/et/user\\_upload/PDF/ET-Broschueren-Upload/ET-Imagebroschuere-deutsch-21.pdf](https://www.elektro-thermit.de/fileadmin/et/user_upload/PDF/ET-Broschueren-Upload/ET-Imagebroschuere-deutsch-21.pdf).
19. WATTMANN, J. *Längskräfte im Eisenbahngleis*. Darmstadt: Otto Elsner Verlagsgesellschaft, 1957.
20. SZABÓ, Petr. Novelizace předpisu SŽDC S3/2 Bezstyková kolej. In: Prague: Správa železniční dopravní cesty, 2012, pp. 118–130. Available also from: <https://www.spravazeleznic.cz/documents/50004227/50157246/c02-szabo-szdc-sb.pdf>.
21. VALEHRACH, Jan (ed.). *Ústav železničních konstrukcí a staveb: Historie* [online]. 2022 [visited on 2022-08-27]. Available from: <https://www.zel.fce.vutbr.cz/historie/>.
22. PLÁŠEK, Otto. *Lecture notes from Otto Plášek lectures*. 2022.

23. KOOB, Michael J. *The Development of a Vibration Technique for Estimation of Neutral Temperature in Continuously Welded Railroad Rail*. 2005. Available also from: [http://railtec.illinois.edu/CEE/images/pdf/Thesis/Koob%20MS%20thesis%20\(final\).pdf](http://railtec.illinois.edu/CEE/images/pdf/Thesis/Koob%20MS%20thesis%20(final).pdf). Champaign, Illinois, University of Illinois at Urbana-Champaign.
24. KOC, Władysław; WILK, Andrzej; CHROSTOWSKI, Piotr; GRULKOWSKI, Sławomir. Określanie wartości sił podłużnych w szynach toru bezстыkowego. *Problemy Kolejnictwa*. 2014, vol. 163. Available also from: [http://www.problemykolejnictwa.pl/images/PDF/163\\_3.pdf](http://www.problemykolejnictwa.pl/images/PDF/163_3.pdf).
25. XING-HAN, Liu. The "Calibrated Length of Rail" Method for Measuring Rail Temperature Stress. *AREMA Proceedings of the 2000 Annual Conference*. 2000. Available also from: [https://www.arena.org/files/library/2000\\_Conference\\_Proceedings/00006.pdf](https://www.arena.org/files/library/2000_Conference_Proceedings/00006.pdf).
26. WANG, Ping; XIE, Kaize; SHAO, Liyang; YAN, Lianshan; XU, Jingmang; CHEN, Rong. Longitudinal Force Measurement in Continuous Welded Rail with Bi-directional FBG Strain Sensors. *Smart Materials and Structures*. 2016, vol. 25. Available also from: <http://iopscience.iop.org/article/10.1088/0964-1726/25/1/015019>.
27. SHAO, Li-Yang; ZHANG, Meng; XIE, Kaize; ZHANG, Xinpu; WANG, Ping; YAN, Lianshan. The Longitudinal Force Measurement of CWR Tracks with Hetero-Cladding FBG Sensors: A Proof of Concept. *Sensors*. 2016, vol. 16, no. 2184. ISSN 1424-8220. Available from DOI: 10.3390/s16122184.
28. BARKER, Christian; HOULT, Neil A.; ZHANG, Merrina. Development of an Axial Strain Measurement System for Rails. *Journal of Performance of Constructed Facilities*. 2020, vol. 35. ISSN 0887-3828. Available from DOI: 10.1061/(ASCE)CF.1943-5509.0001559.
29. VORTOK, LTD. *Vortok Measure and Detect*. Vortok, 2012. Available from eprint: <http://www.vortok.com/rail-stress-management/vortok-measure-and-detect-2>. Vortok, [2016-06-07].
30. KISH, Andrew; SAMAVEDAM, Gopal. Continuous Welded Rail Track Buckling Safety Assurance Through Field Measurements of Track Resistance and Rail Force. *Transportation Research Record*. 1991. Available also from: <http://onlinepubs.trb.org/Onlinepubs/trr/1991/1289/1289-004.pdf>. 1289.
31. VORTOK, LTD. *VERSE*. Vortok, 2012. Available from eprint: <http://www.vortok.com/rail-stress-management/verse>. Vortok, [2016-05-31].
32. KOC, Władysław; WILK, Andrzej. Investigations of Methods to measure longitudinal forces in continuous welded rail tracks using the tamping machine. *Journal of Rail and Rapid Transit*. 2009, vol. 223, no. 1. Available also from: <http://journals.sagepub.com/doi/abs/10.1243/09544097JRRT204>.
33. ATAPIN, Vitaly; BONDARENKO, Alexey; SYSYN, Mykola; GRÜN, Dimitri. Monitoring and Evaluation of the Lateral Stability of CWR Track. *Journal of Failure Analysis and Prevention*. 2022, vol. 22, pp. 319–332. ISSN 1547-7029. Available from DOI: 10.1007/s11668-021-01307-3.

34. SZELAŻEK, Jacek. *Monitoring of Thermal Stresses in Continuously Welded Rails with Ultrasonic Technique*. NDTnet, 1998. Available from eprint: <http://www.ndt.net/article/dresd97/szelazek/szelazek.htm>. NDTnet, 1. June 1998, [2016-05-30].
35. VANGI, Dario; VIRGA, Antonio. A Practical Application of Ultrasonic Thermal Stress Monitoring in Continuous Welded Rail. *Experimental Mechanics*. 2007, vol. 47. Available also from: <https://link.springer.com/article/10.1007/s11340-006-9016-6>.
36. JUNGE, Michael Dominic Alexander. *Measurement of Applied Stresses Using the Polarization of Rayleigh Surface Waves*. 2003. Available also from: [https://smartech.gatech.edu/bitstream/handle/1853/5337/junge\\_michael\\_d\\_a\\_200312\\_ms.pdf](https://smartech.gatech.edu/bitstream/handle/1853/5337/junge_michael_d_a_200312_ms.pdf). Atlanta, Georgia, School of Civil and Environmental Engineering, Institute of Technology.
37. HURLEBAUS, Stefan. *Determination of Longitudinal Stress in Rails*. 2011. Available also from: <http://onlinepubs.trb.org/Onlinepubs/IDEA/FinalReports/Safety/S15Report.pdf>. College Station, Texas, Transportation Research Board of the National Academies.
38. WEAVER, Richard. *Vibration Measurement of Rail Stress*. 2006. Available also from: [http://onlinepubs.trb.org/onlinepubs/archive/studies/idea/finalreports/highspeedrail/hsr-48final\\_report.pdf](http://onlinepubs.trb.org/onlinepubs/archive/studies/idea/finalreports/highspeedrail/hsr-48final_report.pdf). Champaign, Illinois, Transportation Research Board of the National Academies.
39. PARCHAŃSKI, Józef. Pomiary naprężenia osiowego w szynach kolejowych metoda analizy czestotliwości drgań swobodnych. *Zeszyty Naukowe Politechniki Śląskiej*. 1995, vol. 144. Available also from: [http://delibra.bg.polsl.pl/Content/40990/BCPS\\_45013\\_1995\\_Pomiary-naprzenia-o.pdf](http://delibra.bg.polsl.pl/Content/40990/BCPS_45013_1995_Pomiary-naprzenia-o.pdf). Seria: Elektryka.
40. DAMLJANOVIĆ, Vesna; WEAVER, Richard L. Laser vibrometry technique for measurement of contained stress in railroad rail. *Journal of Sound and Vibration*. 2005, vol. 282, no. 1, pp. 341–366. ISSN 0022-460X. Available from DOI: <http://dx.doi.org/10.1016/j.jsv.2004.02.055>.
41. POPOVICS, John S.; DERSCH, Marcus S.; ZHU, Xuan. *Vibration-based Longitudinal Rail Stress Estimation Exploiting Acoustic Measurement and Machine Learning* [online]. Washington, 2020 [visited on 2022-08-29]. Available from: <https://onlinepubs.trb.org/onlinepubs/IDEA/FinalReports/Safety/Safety41.pdf>. report. Transportation Research Board.
42. UTRATA, D.; STROM, A.; NEGLEY, M. Stress Measurement in Railroad Rail Using Ultrasonic and Magnetic Technique. *Review of Progress in Quantitative Nondestructive Evaluation*. 1995, vol. 14. Available also from: <http://lib.dr.iastate.edu/cgi/viewcontent.cgi?article=2577&context=qnde>.
43. TSUCHIDA, Yuji; ENOKINOZO, Masato. Stress Evaluation by Chaotic Characteristics of Barkhausen Noise. *AIP Conference Proceedings*. 2003, vol. 657, no. 1545. Available from DOI: [10.1016/j.conbuildmat.2021.122713](https://doi.org/10.1016/j.conbuildmat.2021.122713).



44. WEGNER, Alfred. Stress-Free Temperature Monitoring Using Different Measuring Technologies – Experiences and Assessment. *Proceedings of 10th International Heavy Haul Association Conference*. 2013. Available also from: [http://www.mav-thermit.hu/fileadmin/downloads/4.1/Paper\\_IHHC\\_2013\\_SFT\\_Wegner.pdf](http://www.mav-thermit.hu/fileadmin/downloads/4.1/Paper_IHHC_2013_SFT_Wegner.pdf).
45. ŠIROKÝ, Michal; VOLTNER, Jaroslav. Měření upínací teploty přístrojem RailScan. *Nová železniční technika*. 2002, vol. 1.
46. WANG, Ping; ZHU, Shougao; TIAN, Gui Yun; WANG, Haitao; WILSON, John; WANG, Xin. Stress Measurement Using Magnetic Barkhausen Noise and Metal Magnetic Memory Testing. *Measurement Science and Technology*. 2010, vol. 21. Available also from: <http://iopscience.iop.org/article/10.1088/0957-0233/21/5/055703>.
47. NAVAĪ, F. Effects of Tensile and Compressive Stresses on the Passive Layers Formed on a Type 302 Stainless Steel in a Normal Sulphuric Acid Bath. *Journal of Materials Science*. 1995, vol. 30. Available also from: <https://link.springer.com/article/10.1007/BF00356115>.
48. MIRKOVIĆ, Nikola; BRAJOVIĆ, Ljiljana; POPOVIĆ, Zdenka; TODOROVIĆ, Goran; LAZAREVIĆ, Luka; PETROVIĆ, Miloš. Determination of temperature stresses in CWR based on measured rail surface temperatures. *Construction and Building Materials*. 2021, vol. 284, no. 122713. ISSN 0950-0618. Available from DOI: 10.1016/j.conbuildmat.2021.122713.
49. ĎURKOVSKÝ, Miroslav. Continuous Measurement of Rail Temperature 24/7. In: BALLA, Ágnes (ed.). Budapest: InnoRail Kiadó és Konferencia Kft., 2019, pp. 1069–1103. ISBN 978-615-81512-0-7. Available also from: <http://innorail2019.hu/wp-content/uploads/2019/12/Miroslav-DURKOVSKY-Continuous-measurement-of-rail-temperature-247-temperature-mode-of-rail.pdf>. [2022-08-13].
50. CULEK, Bohumil jr.; CULEK, Bohumil. Determination of Non-Traffic Loads of the Czech Railway Bridges. In: Pardubice: University of Pardubice, 2005, pp. 74–78. ISBN 80-7194-769-5.
51. CULEK, Bohumil jr.; CULEK, Bohumil. Response traffic and non-traffic loads of the steel railway bridges from the lifetime point of view. In: Parma: University of Parma, 2005, pp. 250–251. ISBN 3-9501554-3-0.
52. CZECH HYDROMETEOROLOGICAL INSTITUTE. *Meteorological Stations*. Czech Hydrometeorological Institute. Available also from: [http://portal.chmi.cz/files/portal/docs/poboc/OS/stanice/ShowStations\\_CZ.html](http://portal.chmi.cz/files/portal/docs/poboc/OS/stanice/ShowStations_CZ.html). Czech Hydrometeorological Institute, [2018-08-24].
53. CEN. *Eurocode 1: Actions on structures – Part 1-5: General Actions – Thermal actions*. Brussels, 2003.
54. ŘÍHA, Tomáš. Zařízení pro měření vnitřní teploty kolejnic. In: *Juniorstav 2012 – Sborník anotací* [print]. 1st ed. Vysoké učení technické v Brně, Fakulta stavební: Vysoké učení technické v Brně, Fakulta stavební, 2012, chap. 89991, pp. 230–230.

55. WINDOW, A. L. (ed.). *Strain Gauge Technology*. 2nd ed. Barking, Essex, United Kingdom: Elsevier Science Publishers Ltd., 1992. ISBN 1-85166-864-0.
56. HOTTINGER BALDWIN MESSTECHNIK GMBH. *Strain Gauges: First choice for strain measurements* [online]. Hottinger Baldwin Messtechnik GmbH [visited on 2022-08-27]. Available from: <https://www.hbm.cz/wp-content/uploads/S01265.pdf>.
57. VNENK, Petr et al. *Measuring set for diagnostics of time-based development of stress states in continuous welded rail*. Pardubice. Functioning Sample, TJ04000301-V2. Available also from: [https://dfjp.upce.cz/sites/default/files/public/pevn0935/funkcni\\_vzorek\\_1\\_en\\_175469.pdf](https://dfjp.upce.cz/sites/default/files/public/pevn0935/funkcni_vzorek_1_en_175469.pdf).
58. VNENK, Petr; YURDAKUL, Özgür; ŠLAPÁK, Jiří; SUCHÁNEK, Vladimír; SADÍLEK, Ondřej; KLEJCH, Filip; CULEK, Bohumil; ŘOUTIL, Ladislav. *Methodology of Non-Destructive Determination of Mechanical Stress in Continuous Welded Rail*. Pardubice. Certified Methodology, TJ04000301-V1. Available also from: [https://dfjp.upce.cz/sites/default/files/public/pevn0935/methodology\\_complete\\_188550.pdf](https://dfjp.upce.cz/sites/default/files/public/pevn0935/methodology_complete_188550.pdf).
59. PĚTIOKÝ, Marek; CULEK, Bohumil; VNENK, Petr. Měření napjatosti pružných svěrek v provozu. In: Brno: Vysoké učení technické v Brně, 2018, pp. 357–365. ISBN 978-80-86433-69-1.
60. CULEK, Bohumil; PĚTIOKÝ, Marek; SCHMIDOVÁ, Eva; TOMEK, Petr; VNENK, Petr. Fatigue Behaviour of Vossloh SKL14 Tension Clamps. In: Zürich: IABSE, 2021, pp. 1555–1563. ISBN 978-3-85748-176-5.
61. CULEK, Bohumil. *Tenzometrické měření ocelových konstrukcí*. Pardubice, 2007. Unverzita Pardubice, Doprávní fakulta Jana Pernera, Zkušební laboratoř AL DFJP.

## Appendix A

# Rail Temperature Recordings

The rail temperature recordings from particular thermometers attached to the rail in the selected localities in the Czech Republic are presented in this appendix. The thermometers automatically logged the measured temperature at an interval of one hour into the built-in data-logger.

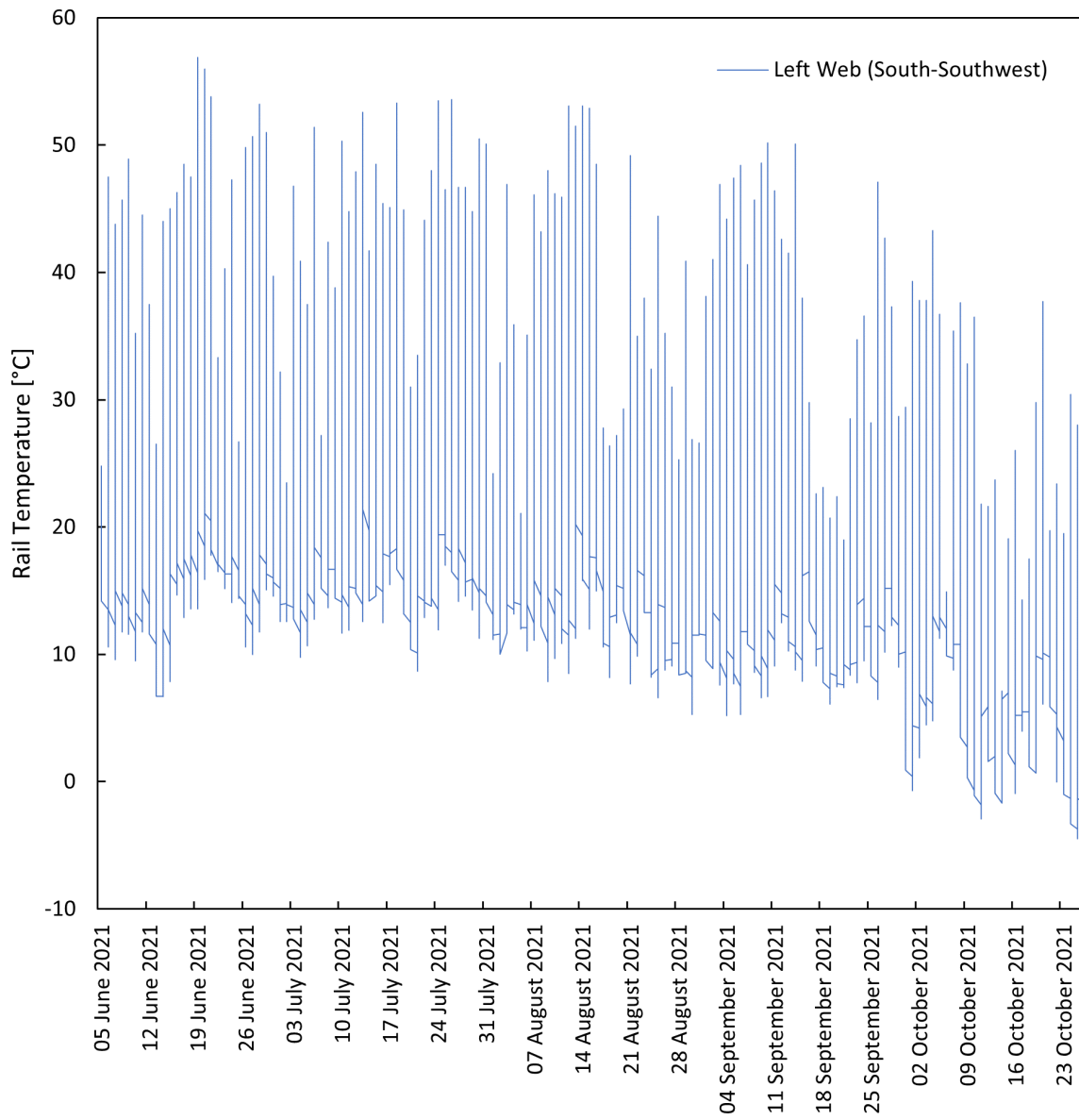


**Figure A.1** – Rail Temperature Recordings in Locality Borovnice – Left Web (S-SW)

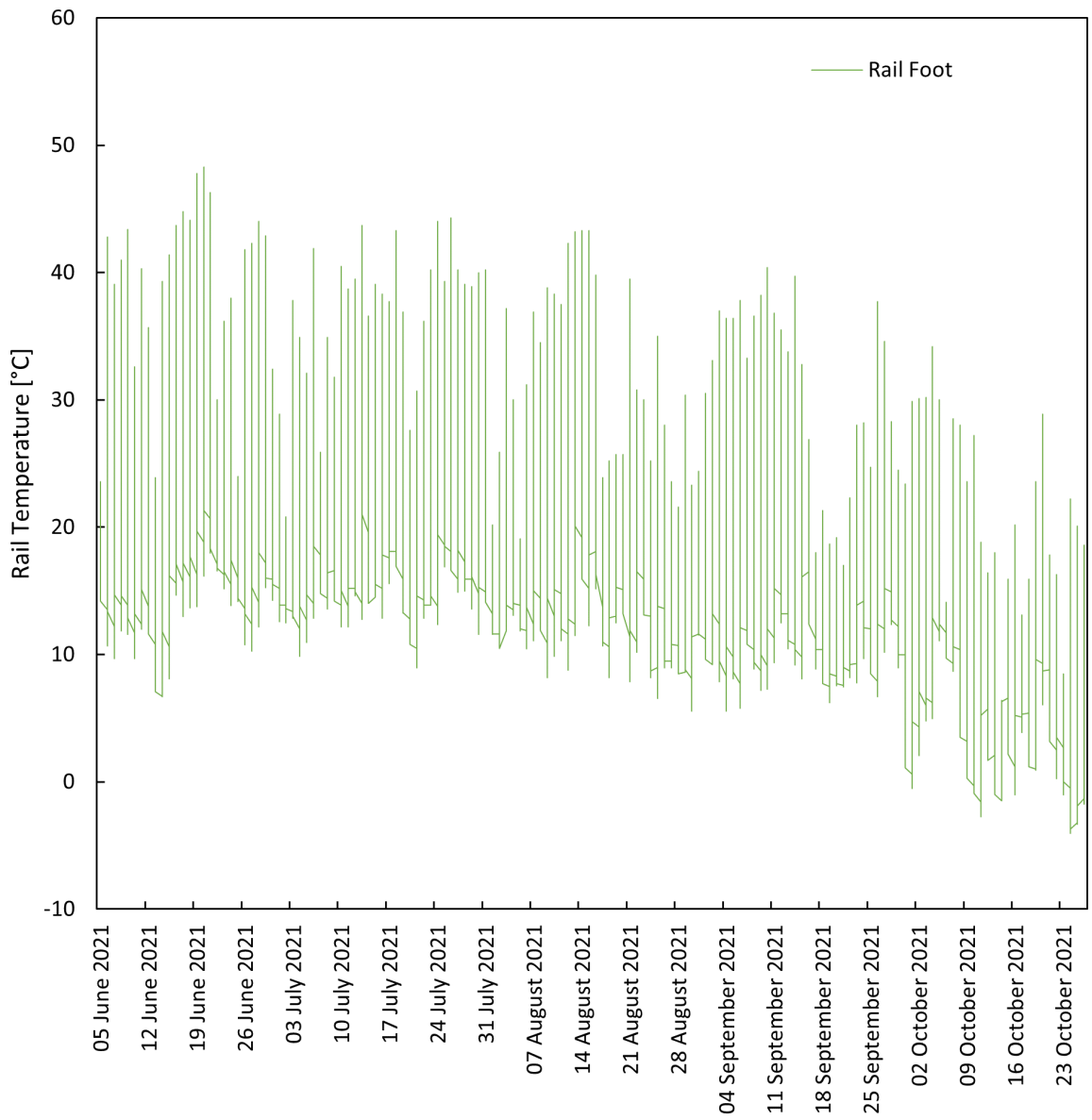


**Figure A.2** – Rail Temperature Recordings in Locality Borovnice – Rail Foot

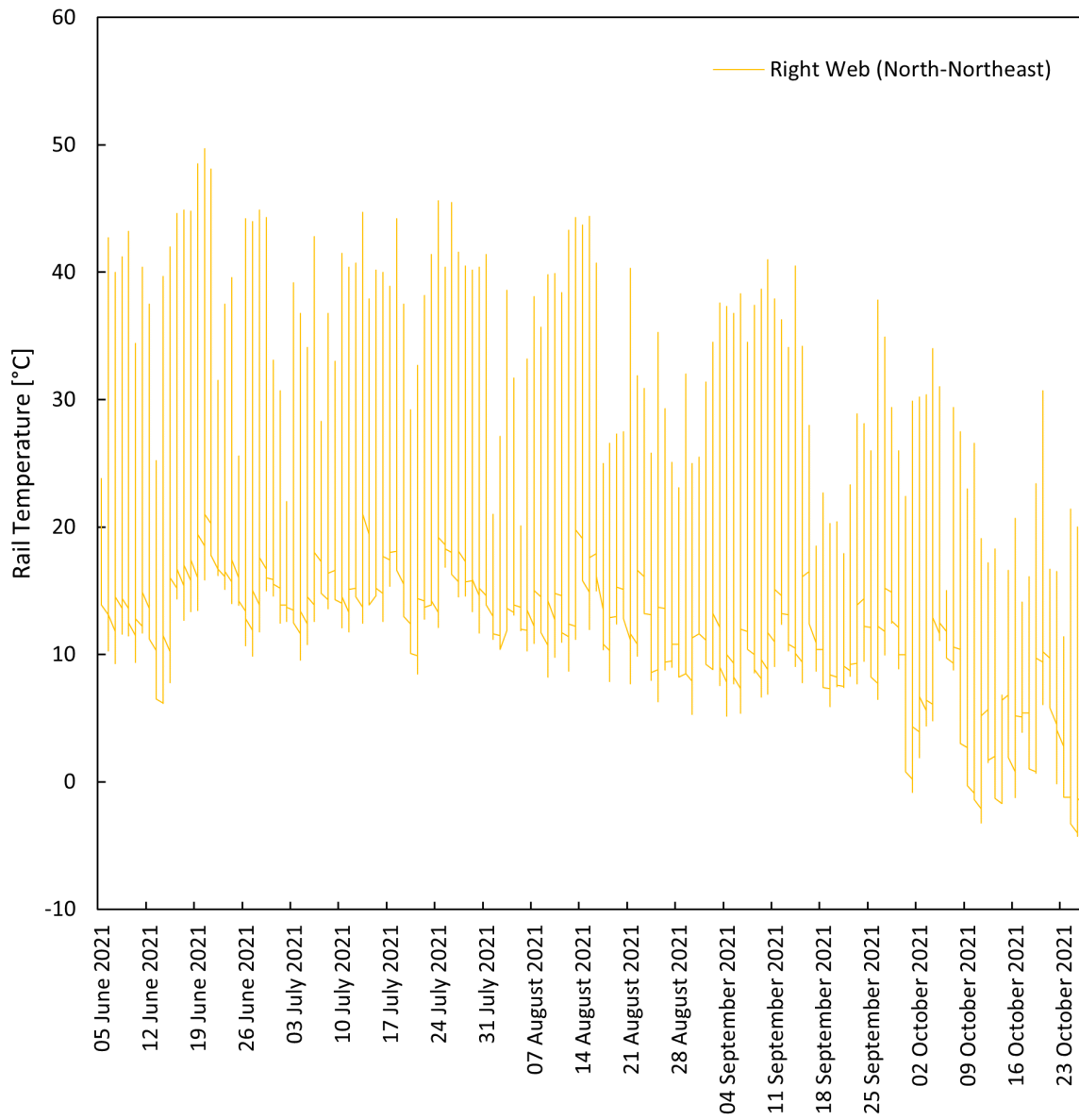


**Figure A.3** – Rail Temperature Recordings in Locality Borovnice – Right Web (N-NE)

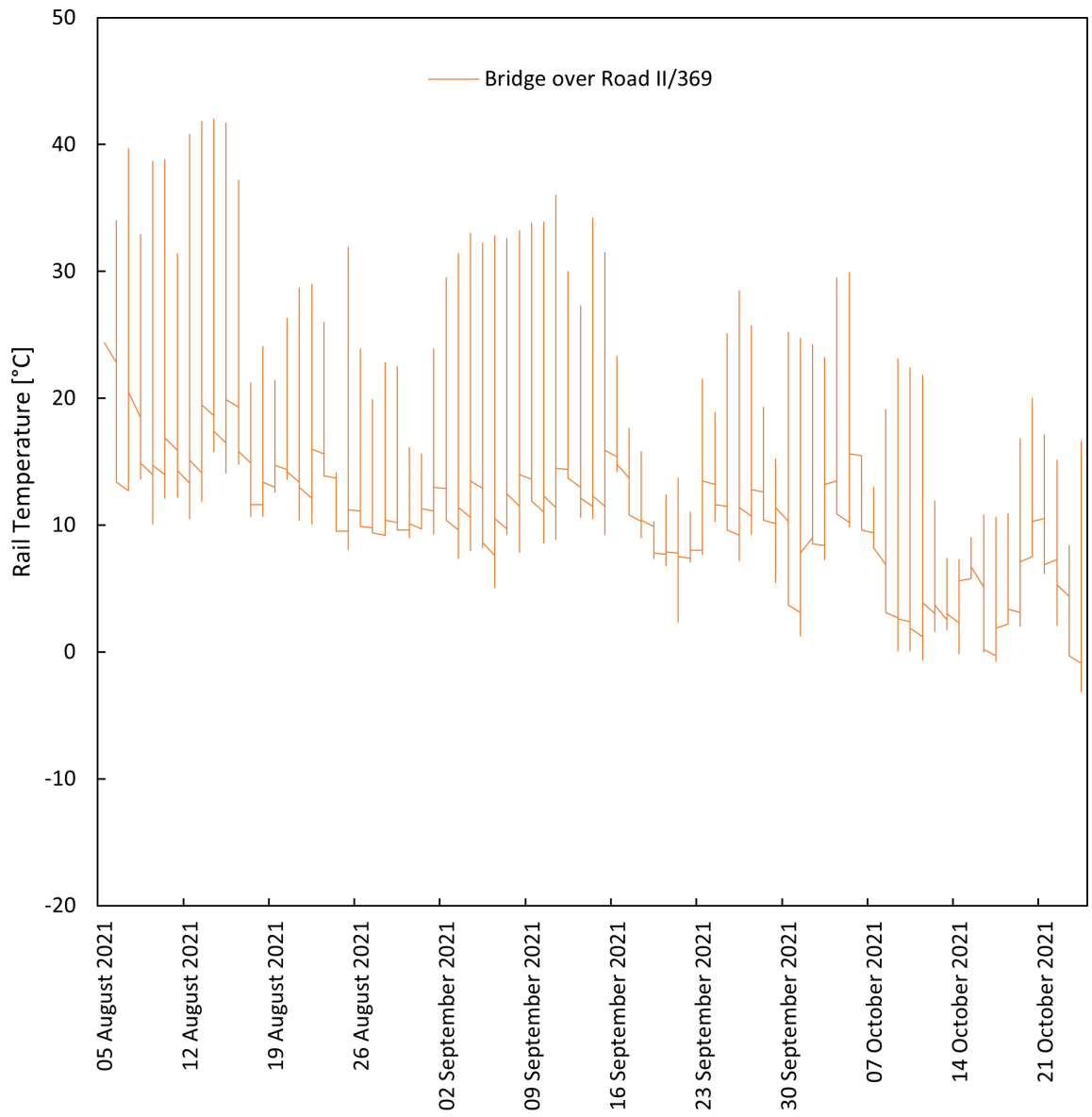
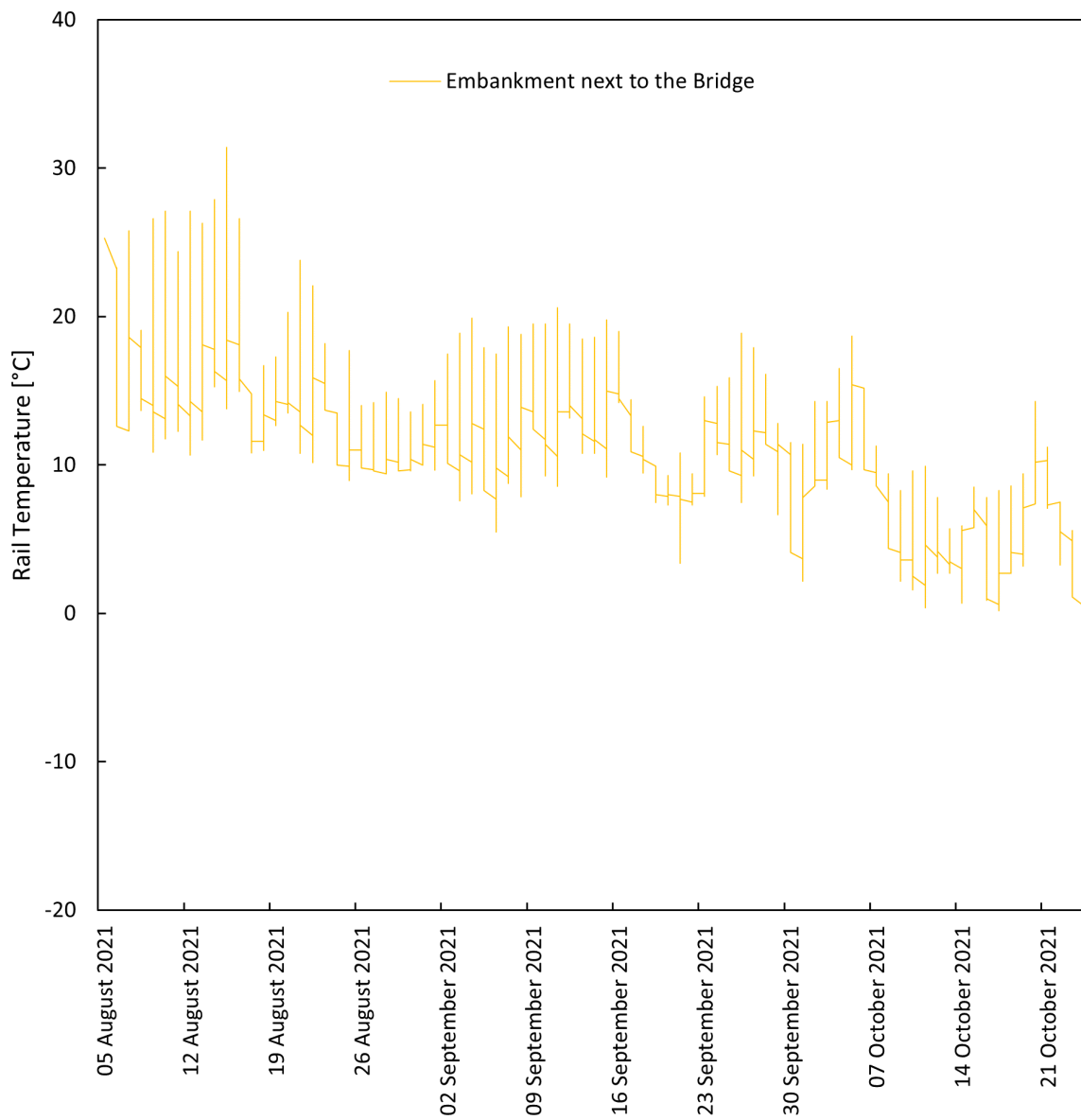
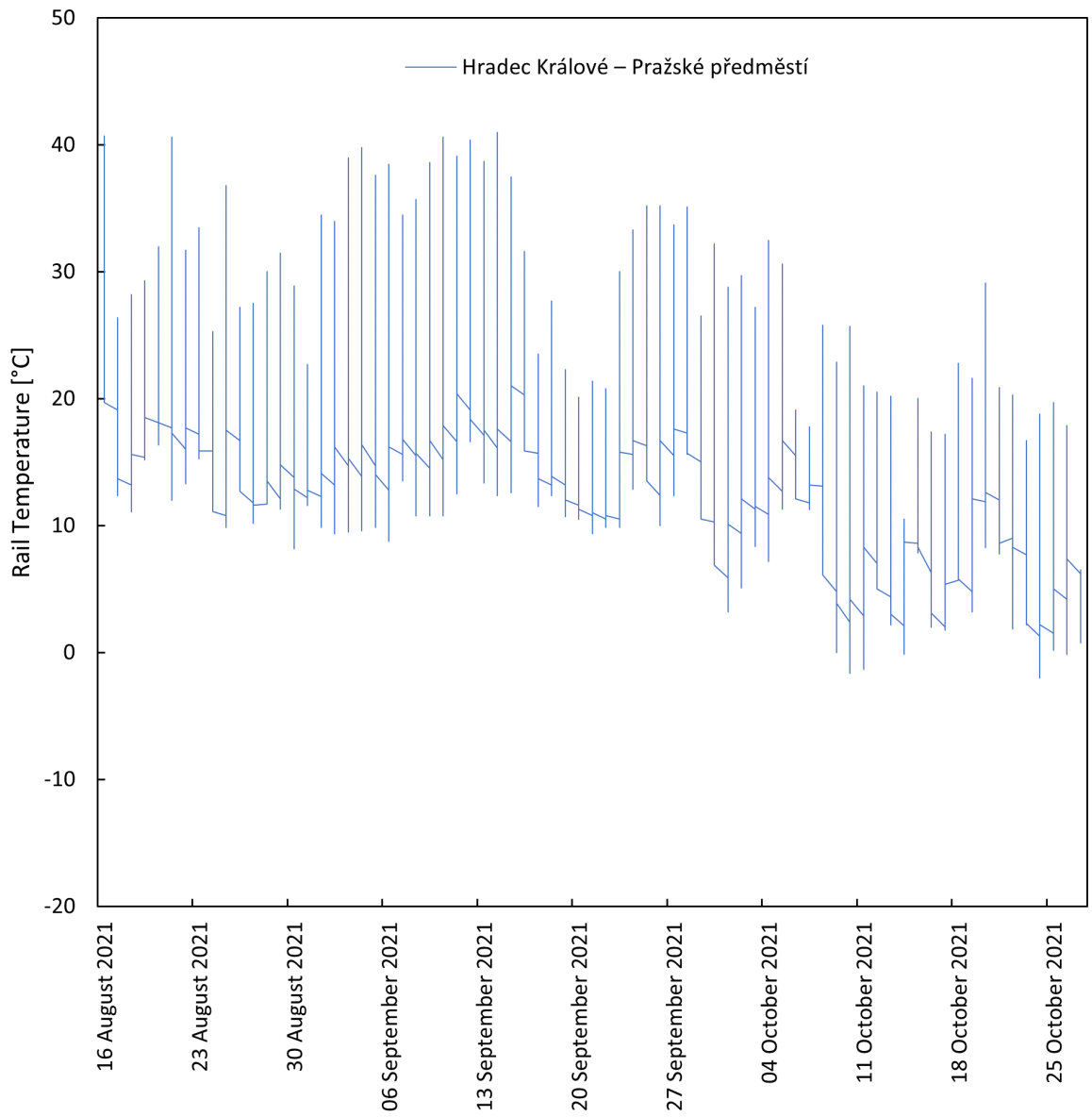


Figure A.4 – Rail Temperature Recordings in Locality Ostružná – Bridge over Road II/369



**Figure A.5** – Rail Temperature Recordings in Locality Ostružná – Embankment next to the Bridge





**Figure A.6** – Rail Temperature Recordings in Locality Hradec Králové – Pražské předměstí

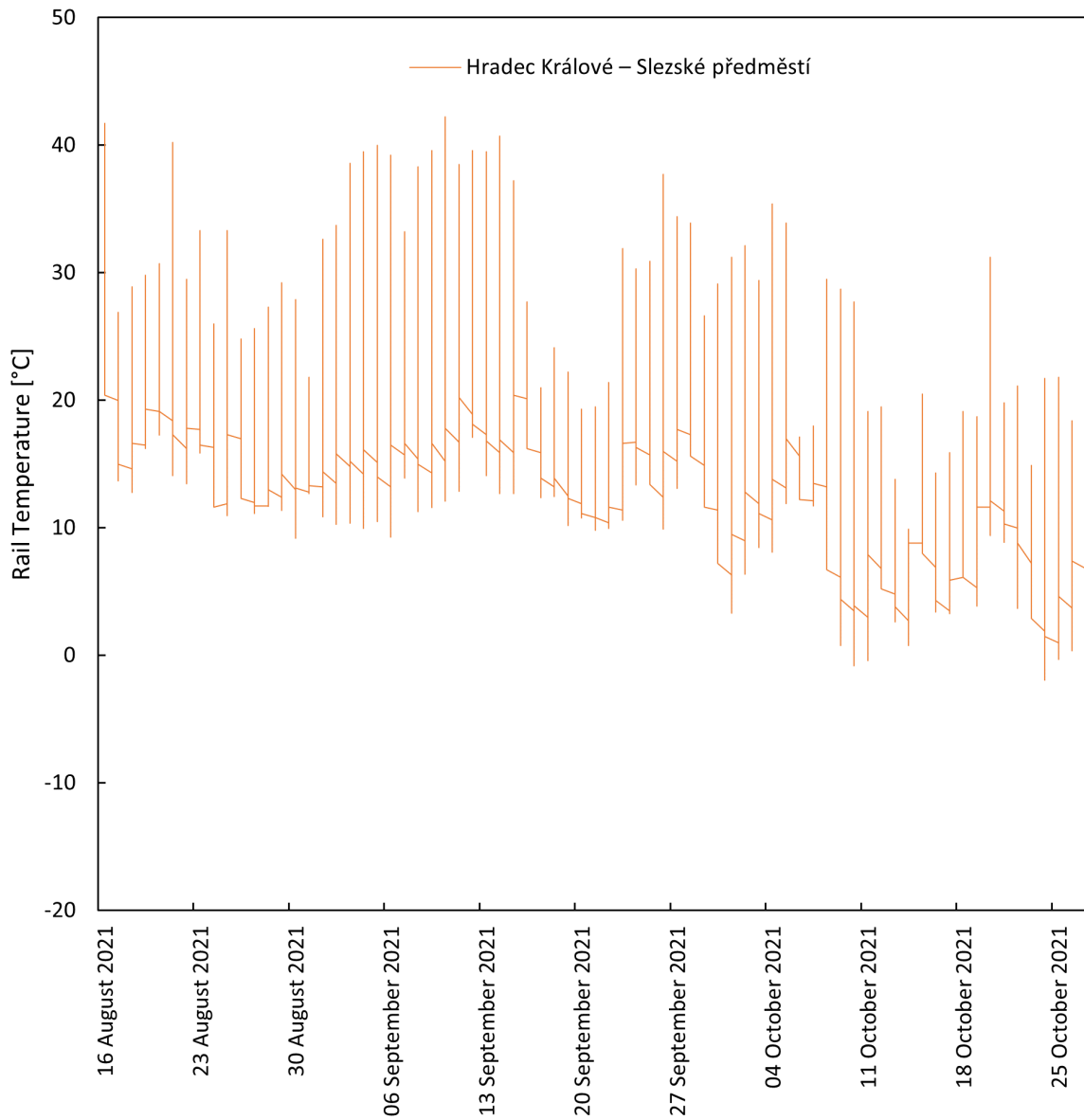


**Figure A.7** – Rail Temperature Recordings in Locality Hradec Králové – Slezské předměstí

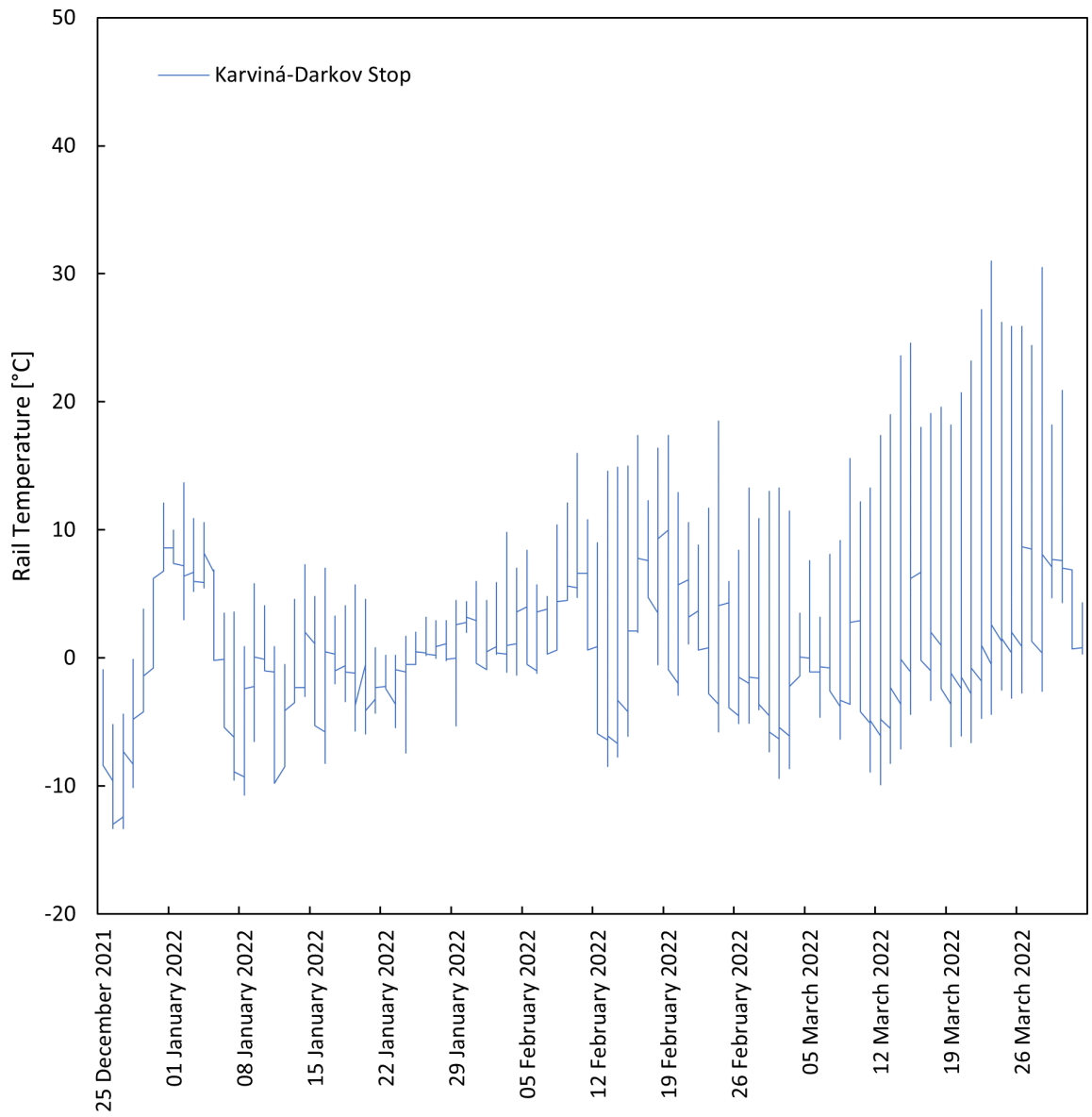


**Figure A.8** – Rail Temperature Recordings in Locality Karviná – Karviná-Darkov Stop

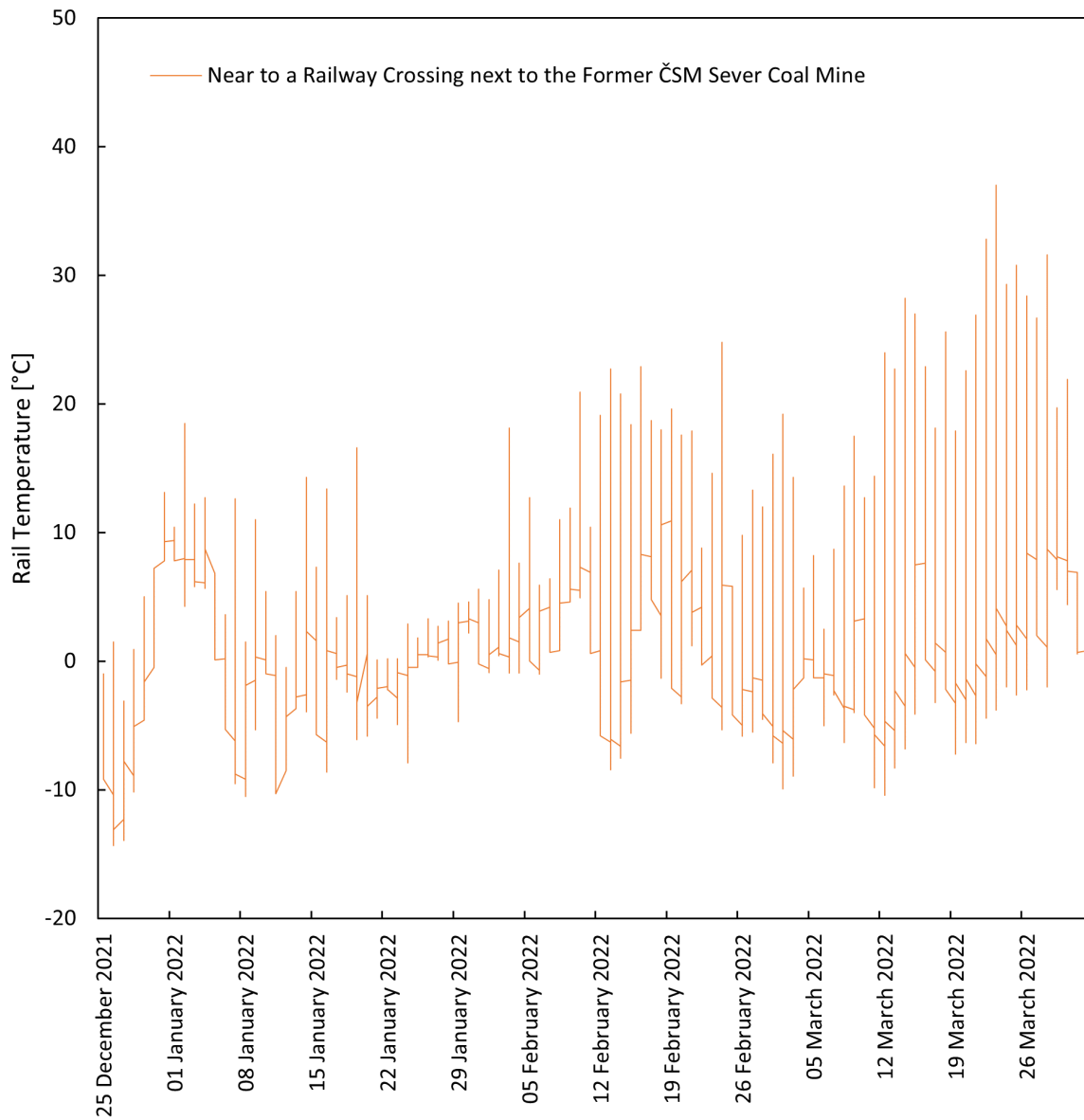


**Figure A.9** – Rail Temperature Recordings in Locality Karviná – Near to a Railway Crossing next to the Former ČSM Sever Coal Mine

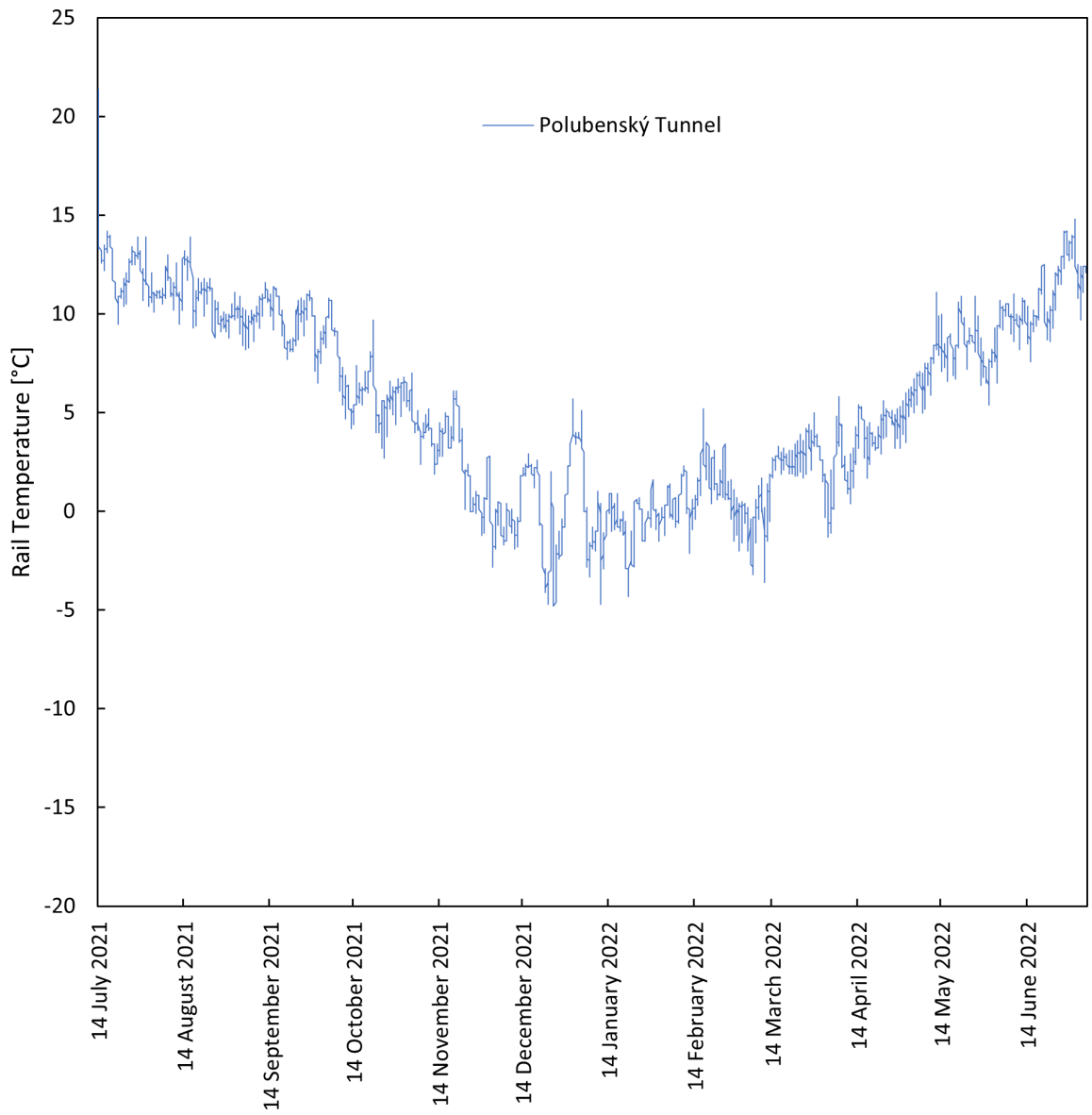


Figure A.10 – Rail Temperature Recordings in Locality Harrachov – Polubenský Tunnel

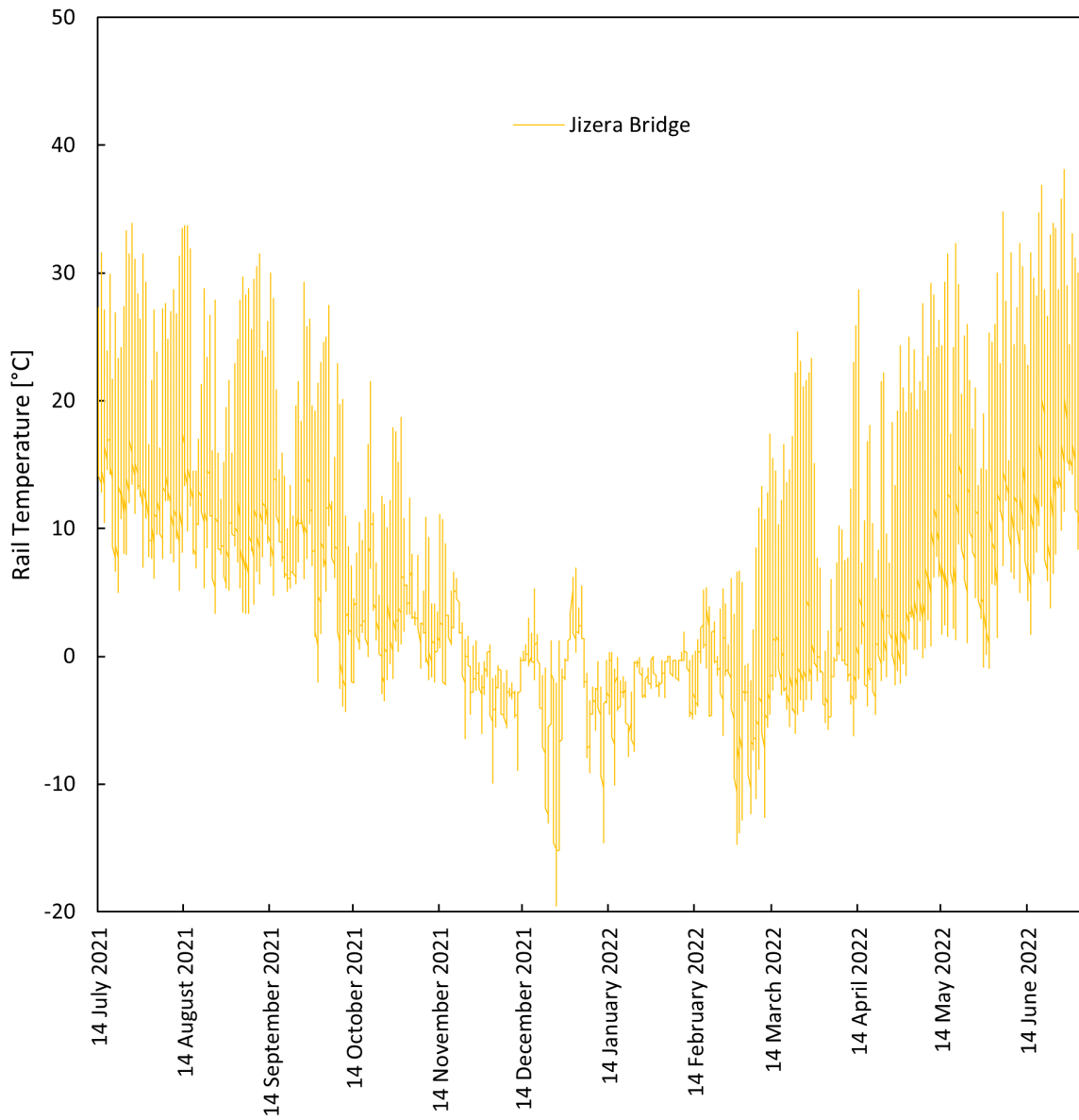
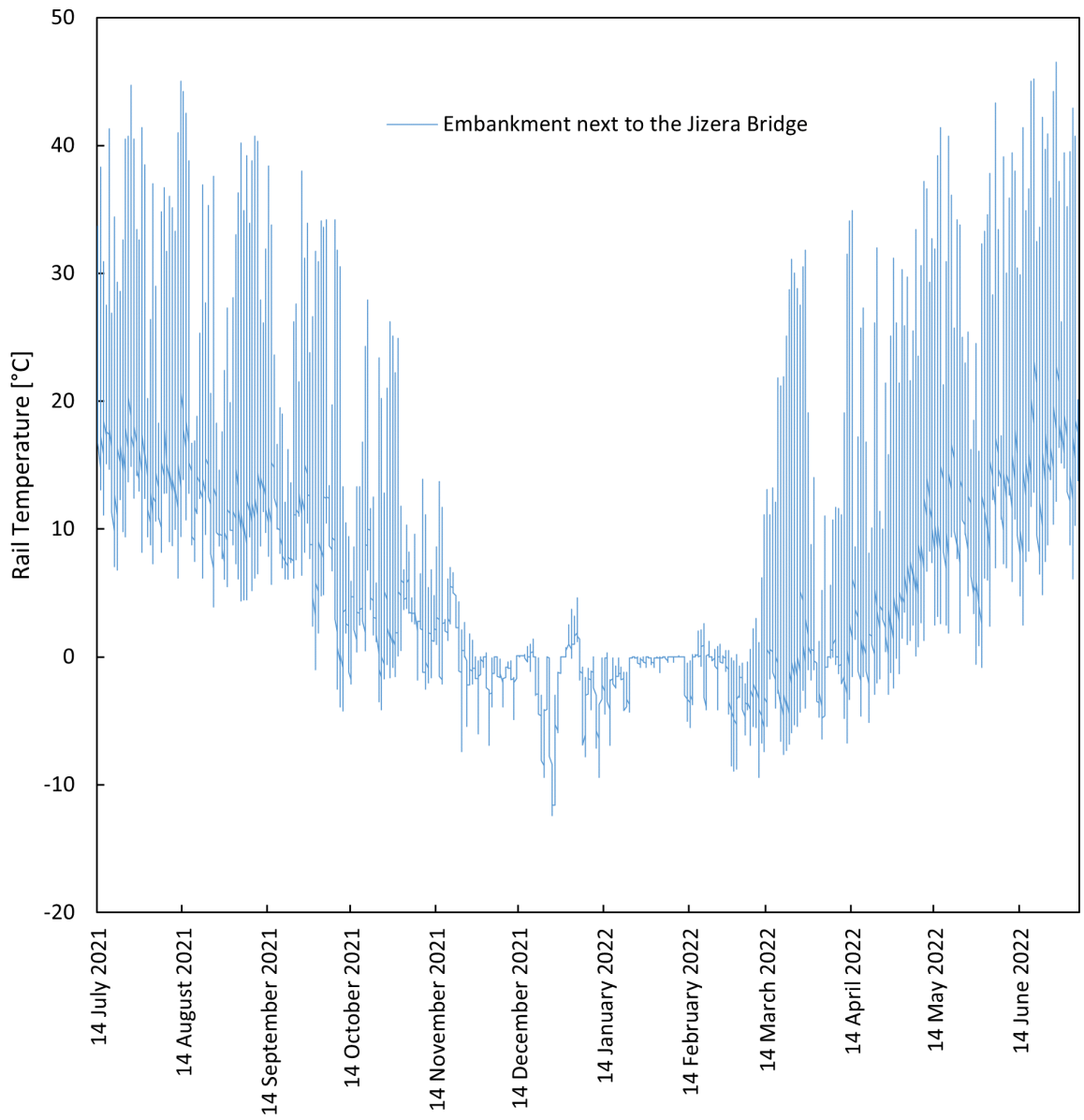


Figure A.11 – Rail Temperature Recordings in Locality Harrachov – Jizera Bridge



**Figure A.12** – Rail Temperature Recordings in Locality Harrachov – Embankment next to the Jizera Bridge

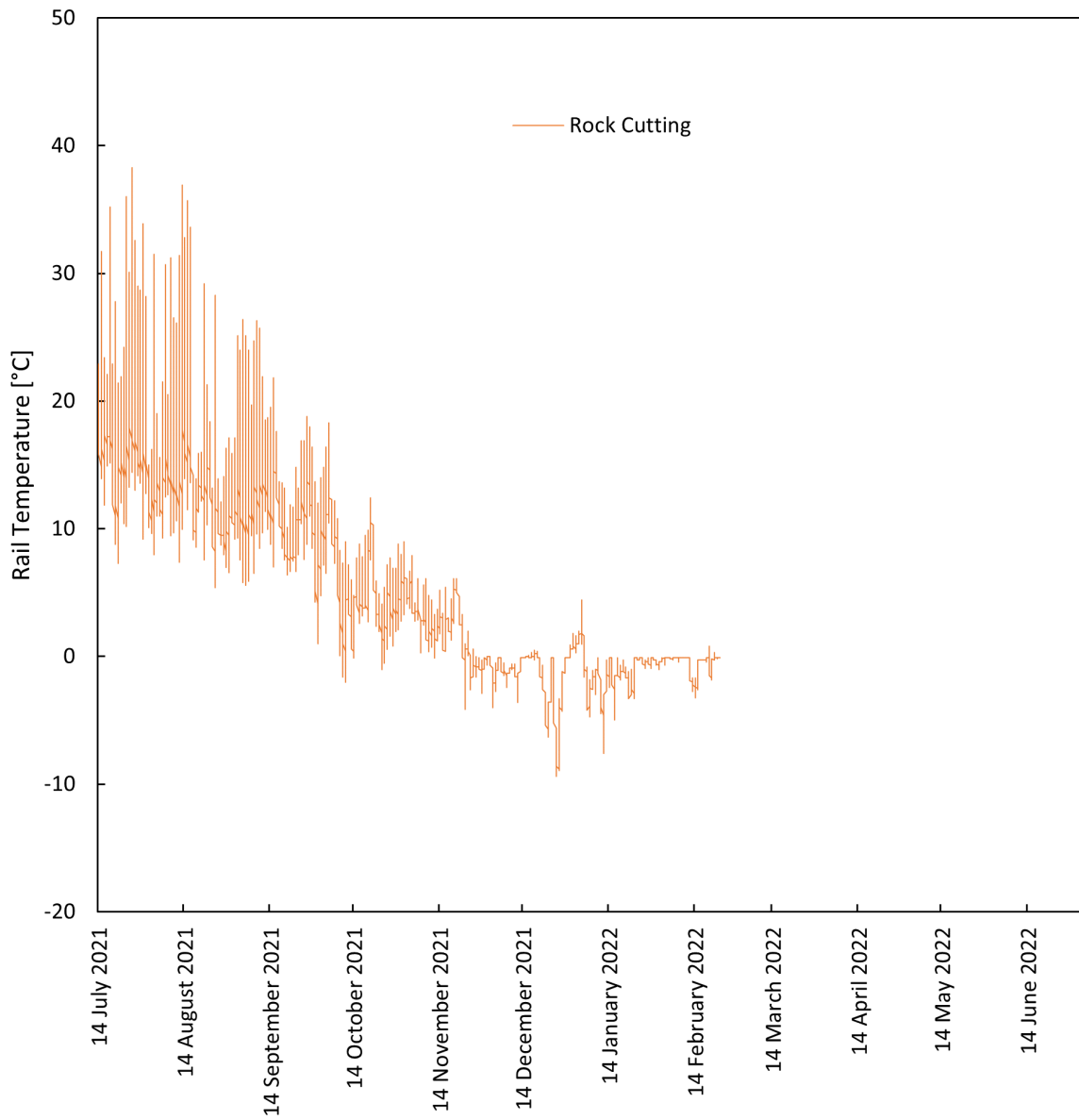


Figure A.13 – Rail Temperature Recordings in Locality Harrachov – Rock Cutting



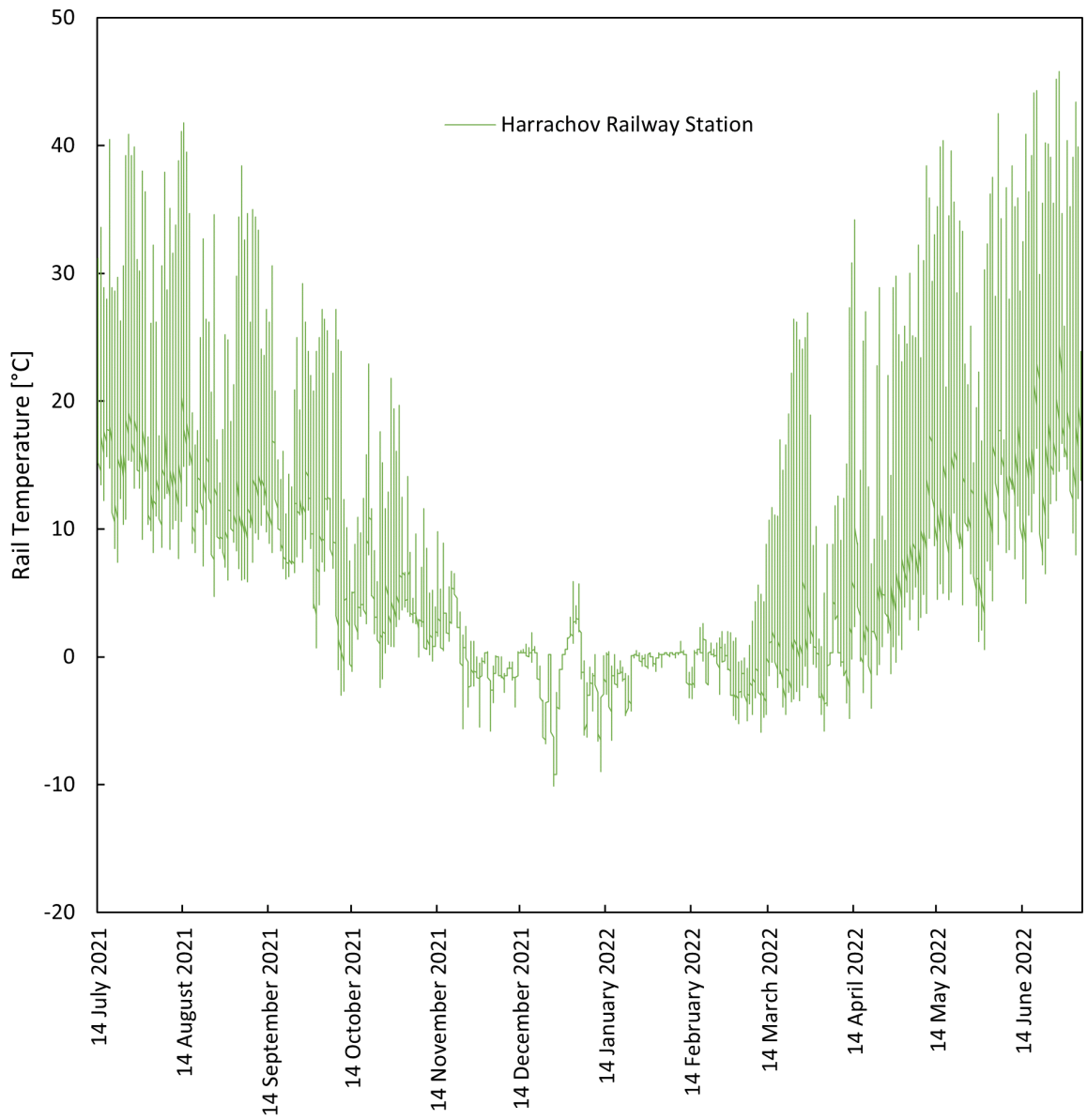


Figure A.14 – Rail Temperature Recordings in Locality Harrachov – Harrachov Railway Stop



## Appendix B

# Measurement Uncertainty Determination

All the measurement uncertainty calculation in this section is determined based on the calculations in the document on strain gauge measurements of steel structures published at the Testing laboratory AL DFJP as the Document No. AL MZ 5-1 [61]. The calculation is performed for the half-bridge configuration of strain gauges, because the use of the quarter-bridge configuration in the CWR strain measurements is based on a half-bridge configuration of the Quantum MX840A data acquisition system with the use of SCM-SG350 adaptor.

The measurement uncertainty is calculated for all parameters entering the measurement of strain  $\varepsilon$ . The following equation is applied to calculate the quantity [61]:

$$\varepsilon = \left(1 + \frac{\Delta R}{R}\right)^{\frac{1}{K_d}} - 1, \quad (\text{B.1})$$

where  $K_d$  is the gauge factor,  $\Delta R$  is the strain gauge resistance change, and  $R$  is the strain gauge resistance.

### B.1 Type A Evaluation of Uncertainty

The type A evaluation of uncertainty directly depends on repeated measured values. This was usually not the case in the presented CWR strain monitoring. Nevertheless, it is possible to perform a repeated set of measurements and the type A evaluation of uncertainty is calculated based on [61]

$$u_{Ax} = s_{\bar{x}} = \sqrt{\frac{\sum_{i=1}^n (x_i - \bar{x})^2}{n \cdot (n - 1)}}, \quad (\text{B.2})$$

where  $u_{Ax}$  is the type A evaluation of uncertainty,  $s_{\bar{x}}$  is the corrected sample standard deviation, and  $\bar{x}$  is the mean value defined as

$$\bar{x} = \frac{\sum_{i=1}^n x_i}{n}. \quad (\text{B.3})$$

## B.2 Type B Evaluation of Uncertainty

The following type B evaluations of uncertainty shall be considered in the case of strain measurement [61]:

- strain gauge uncertainty, which can be further divided into:
  - strain gauge geometry uncertainty,
  - measuring spot surface quality uncertainty,
  - strain gauge adhesive uncertainty,
  - strain gauge resistance uncertainty,
  - strain gauge factor uncertainty,
  - strain gauge thermal deformation uncertainty,
  - strain gauge lateral deformation uncertainty,
- uncertainty of strain gauge – data acquisition system cable,
- data acquisition system uncertainty,
- uncertainty of data acquisition system – personal computer cable,
- uncertainty of PC hardware,
- uncertainty of PC software.

### B.2.1 Strain Gauge Uncertainty

The strain gauge uncertainty can be evaluated based on technical standards of strain gauge producers, the HBM company, where the accuracy of its evaluation is guaranteed.

#### Strain Gauge Geometry Uncertainty

The strain gauge geometry uncertainty can be evaluated based on the accuracy of the strain gauge attachment on the particular spot of the measured structure, i. e. the CWR in the case of the CWR strain measurements. The spot for the strain gauge attachment is always marked with horizontal lines showing the level of the neutral axis in the rail as described in the annexed methodology [58]. By this marking, the strain gauge geometry uncertainty is significantly reduced. The strain gauge geometry uncertainty can be generally caused by a shift in the horizontal and vertical direction, and a rotation by an angle [61].

Since the purpose of the CWR strain measurement does not require the strain gauges being placed into the neutral axis precisely – the stress from the thermal loading is expected to be evenly distributed along the cross section of the rail – the strain gauge geometry uncertainty caused by a shift in the horizontal and vertical direction, considering the admissible level of shift from the horizontal and vertical axis of 5 mm, is negligible.

The admissible level of rotation of the strain gauge is  $3^\circ$ . This is set based on experience [61]. The analytical equation of the strain gauge geometry uncertainty by rotation of an angle is

$$u_{B1\alpha} = \frac{\varepsilon \cdot \left(\frac{1}{\cos \alpha} - 1\right)}{3}, \quad (\text{B.4})$$

where  $\varepsilon$  is the measured strain,  $\alpha$  is the defined admissible level of uncertainty by rotation of an angle ( $\alpha = 3$ ), and 3 is the coefficient set upon the assumption of the normal distribution of the measurement deviation probability.

The maximum admissible strain for the strain gauge type described in the methodology [58] is  $\varepsilon_{max} = 20\,000 \mu\text{m}\cdot\text{m}^{-1}$ , but in the measurements performed, the measured strain never exceeded  $4\,000 \mu\text{m}\cdot\text{m}^{-1}$ . The strain gauge geometry uncertainty by rotation of an angle is then

$$u_{B1\alpha} = \frac{4\,000 \mu\text{m} \cdot \text{m}^{-1} \cdot \left(\frac{1}{\cos 3^\circ} - 1\right)}{3} = 1.83 \mu\text{m} \cdot \text{m}^{-1}. \quad (\text{B.5})$$

The complete strain gauge geometry uncertainty is calculated as

$$u_{B1} = \sqrt{(u_{B1y})^2 + (u_{B1x})^2 + (u_{B1\alpha})^2}, \quad (\text{B.6})$$

however, since the  $u_{B1y}$  and  $u_{B1x}$  values are negligible, the strain gauge geometry uncertainty for the CWR strain measurement is

$$u_{B1} = \sqrt{(u_{B1\alpha})^2} = 1.83 \mu\text{m} \cdot \text{m}^{-1}. \quad (\text{B.7})$$

### Measuring Spot Surface Quality Uncertainty

The measuring spot surface quality uncertainty is caused when the rust removal from CWR does not leave the surface smooth but with some level of unevenness. The general equation to calculate the material loss in a ground groove is [61]

$$y = l_{sg} \cdot \tan \alpha, \quad (\text{B.8})$$

where  $y$  is the depth of groove,  $l_{sg}$  is the length of the strain gauge, and  $\alpha$  is the angle of the uneven surface as depicted in Figure B.1.

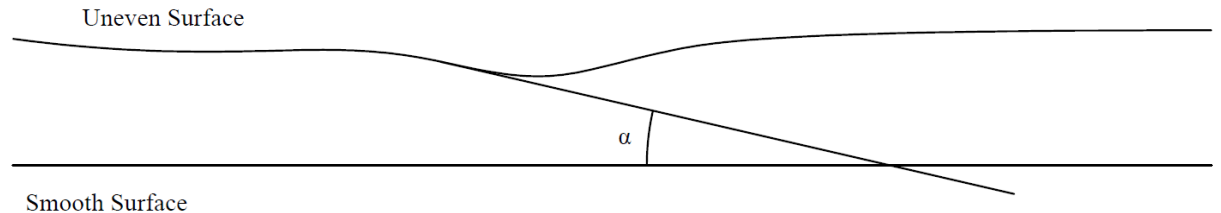


**Figure B.1** – Uneven Surface of the Measuring Spot, according to [61]

The admissible unevenness is as low as  $0.5^\circ$ . The length of strain gauges used and recommended by the annexed methodology [58] is 6 mm.

The admissible depth of groove is then [61]

$$y = 6 \text{ mm} \cdot \tan 0.5^\circ = 0.052 \text{ mm}. \quad (\text{B.9})$$

The measurement uncertainty is therefore by several orders of magnitude lower than the actual measurement values, it can be therefore neglected and set as

$$u_{B2} = 0 \mu\text{m} \cdot \text{m}^{-1}. \quad (\text{B.10})$$

### **Strain Gauge Adhesive Uncertainty**

The strain gauge adhesive uncertainty is set by the strain gauge producer. In accordance with the Document No. AL MZ 5-1 [61], it is

$$u_{B3} = 2.5 \mu\text{m} \cdot \text{m}^{-1}. \quad (\text{B.11})$$

### **Strain Gauge Resistance Uncertainty**

The strain gauge resistance uncertainty is set by the strain gauge producer. In accordance with the Document No. AL MZ 5-1 [61], it is

$$u_{BO} = \frac{0.35 \%}{3} \cdot 350 \Omega = 0.41 \Omega. \quad (\text{B.12})$$

### **Strain Gauge Factor Uncertainty**

The strain gauge factor uncertainty is set by the strain gauge producer. In accordance with the Document No. AL MZ 5-1 [61], it is

$$u_{BK} = \frac{1.0 \%}{1.73} \cdot 2.08 = 0.012. \quad (\text{B.13})$$

### **Strain Gauge Thermal Deformation Uncertainty**

The strain gauge used at the CWR strain measurements are produced with a self-compensating function to compensate for the linear part of the thermal deformation [61]. The strain gauge thermal deformation uncertainty is not related to the self-compensating function, but to a deviation from this function. Since the measurements are performed typically in the range of  $-10$  to  $45^\circ\text{C}$ , the deviation is negligible, thus

$$u_{B4} = 0 \mu\text{m} \cdot \text{m}^{-1}. \quad (\text{B.14})$$

### Strain Gauge Lateral Deformation Uncertainty

The strain gauge lateral deformation uncertainty is set by the strain gauge producer. In accordance with the Document No. AL MZ 5-1 [61], it can be neglected and set as

$$u_{B5} = 0 \mu m \cdot m^{-1}. \quad (B.15)$$

### B.2.2 Uncertainty of Strain Gauge – Data Acquisition System Cable

Only four-wire cables with a cable resistance change compensation are used for the CWR strain measurement. The uncertainty is therefore by several orders of magnitude lower than the actual measurement values [61], it can be therefore neglected and set as

$$u_{B6} = 0 \mu m \cdot m^{-1}. \quad (B.16)$$

### B.2.3 Data Acquisition System Uncertainty

The data acquisition system uncertainty in  $[mV \cdot V^{-1}]$  is calculated by equation [61]

$$u_{BD} = \frac{u_{BR}}{k} mV \cdot V^{-1}, \quad (B.17)$$

where the  $u_{BD}$  is the data acquisition system uncertainty in  $[mV \cdot V^{-1}]$ ,  $u_{BR}$  is the expanded uncertainty, and  $k$  is the coverage factor.

The values of  $u_{BR}$  and  $k$  are set in the calibration certificate of the data acquisition system. They can generally differ according to the data acquisition system used. For the data acquisition system used for the measurements performed for this dissertation, the value of  $u_{BR}$  is declared by the manufacturer as  $4.7 \cdot 10^{-4} mV \cdot V^{-1}$  and the value of  $k$  as 2. The uncertainty  $u_{BD}$  is then

$$u_{BD} = 0.235 mV \cdot V^{-1}. \quad (B.18)$$

Further recalculation into the data acquisition system uncertainty in  $[\mu m \cdot m^{-1}]$  is given by equation

$$u_{B7} = \sqrt{a + b}, \quad (B.19)$$

where  $a$  is

$$a = \left( \frac{1}{K_d} \cdot \left( 1 + \frac{4 \cdot U_M}{U_N - 2 \cdot U_M} \right)^{\frac{1}{K_d} - 1} \cdot \left( \frac{4 \cdot (U_N - 2 \cdot U_M) + 8 \cdot U_M^2}{U_N - 2 \cdot U_M} \right) \right)^2 \cdot u_{BD}^2 \quad (B.20)$$

and  $b$  is

$$b = \left( \left( 1 + \frac{4 \cdot U_M}{U_N - 2 \cdot U_M} \right)^{\frac{1}{K_d}} \cdot \ln \left( 1 + \frac{4 \cdot U_M}{U_N - 2 \cdot U_M} \right) \cdot \left( -\frac{1}{K_d^2} \right) \right)^2 \cdot u_{BK}^2, \quad (B.21)$$

and where  $K_d$  is the strain gauge k-factor,  $U_M$  is the maximum value of output voltage,  $U_N$  is the input voltage,  $u_{BD}$  is the data acquisition system uncertainty in  $[\text{mV}\cdot\text{V}^{-1}]$ , and  $u_{BK}$  is the strain gauge factor uncertainty.

The calculation process leading to the above shown equations in closer detail is presented in the Document No. AL MZ 5-1 [61], and therefore not elaborated here.

Upon the substitution of the particular values, the result is

$$u_{B7} = 5.56 \mu\text{m} \cdot \text{m}^{-1}. \quad (\text{B.22})$$

#### B.2.4 Uncertainty of Data Acquisition System – Personal Computer Cable

Only digital data are transferred by the data acquisition system – personal computer cable. The uncertainty is inadmissible and in the case of any data transfer collision, measurement is interrupted and shall be repeated [61]. Therefore,

$$u_{B8} = 0 \mu\text{m} \cdot \text{m}^{-1}. \quad (\text{B.23})$$

#### B.2.5 Uncertainty of PC Hardware

Only digital data are in the PC. Therefore,

$$u_{B9} = 0 \mu\text{m} \cdot \text{m}^{-1}. \quad (\text{B.24})$$

#### B.2.6 Uncertainty of PC Hardware

Only certified original software is used for data processing [61]. Therefore,

$$u_{B10} = 0 \mu\text{m} \cdot \text{m}^{-1}. \quad (\text{B.25})$$

#### B.2.7 Type B Total Evaluation of Uncertainty

The type B total evaluation of uncertainty is calculated as [61]

$$u_B = \sqrt{u_{B1}^2 + u_{B2}^2 + u_{B3}^2 + u_{B4}^2 + u_{B5}^2 + u_{B6}^2 + u_{B7}^2 + u_{B8}^2 + u_{B9}^2 + u_{B10}^2}. \quad (\text{B.26})$$

Upon the substitution, the result is

$$u_B = 6.36 \mu\text{m} \cdot \text{m}^{-1}. \quad (\text{B.27})$$

### B.3 Combined Evaluation of Uncertainty

The combined evaluation of uncertainty is calculated as [61]

$$u_y = \sqrt{u_A^2 + u_B^2}. \quad (\text{B.28})$$



## B.4 Expanded Evaluation of Uncertainty

The expanded evaluation of uncertainty is calculated as [61]

$$u = k \cdot u_y = 2 \cdot u_y, \quad (\text{B.29})$$

where  $k$  is the coverage factor, which corresponds the coverage of the measurement uncertainties of 95 %, considering the normal distribution.



## Appendix C

# CWR Strain Recordings

The full CWR strain recordings over time from the particular measuring spots in the Chotěvice and Bezprávi localities are presented in this appendix. Please note that the recordings include the apparent strain from the thermal loading.

The CWR strain recordings from both localities are presented in three subsections – the daily, weekly and monthly recordings. The presentation in this division respects the frequency at which the measurements were performed and ensures a better readability of the recorded data. For the daily recording, the data were obtained every day, for the weekly one every week, and for the monthly one every month.

In all the cases, the marking of the record is following: A.B.C, where A is the abbreviation of the locality (C – Chotěvice, D – Bezprávi), B is the number of the profile (the number is increasing in the direction of the increasing stationing), and C is the number of the measuring spot within the profile (from 1 in the very left-hand side to 4 in the very right-hand side). See the description in the annexed methodology for more details on the measuring spot markings.

## C.1 Chotěvice

### C.1.1 Daily Recordings

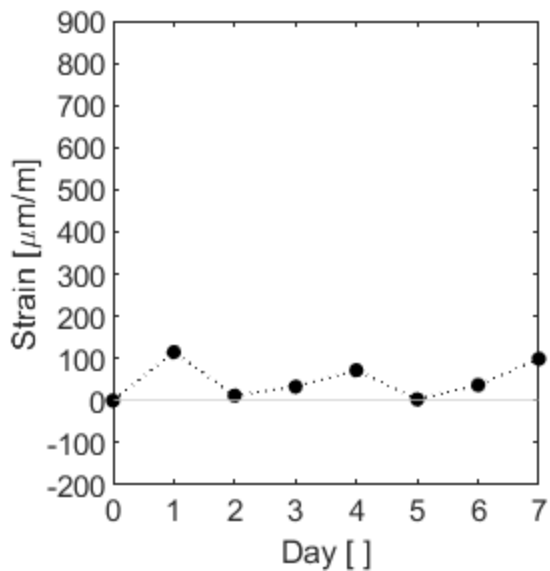


Figure C.1 – C.I.1

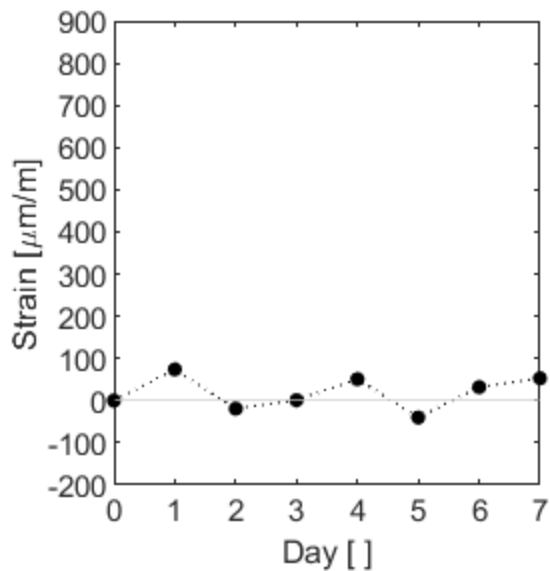


Figure C.2 – C.I.2

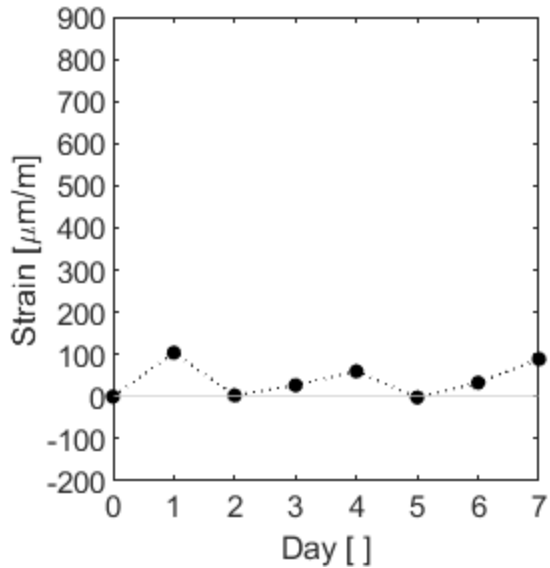


Figure C.3 – C.I.3

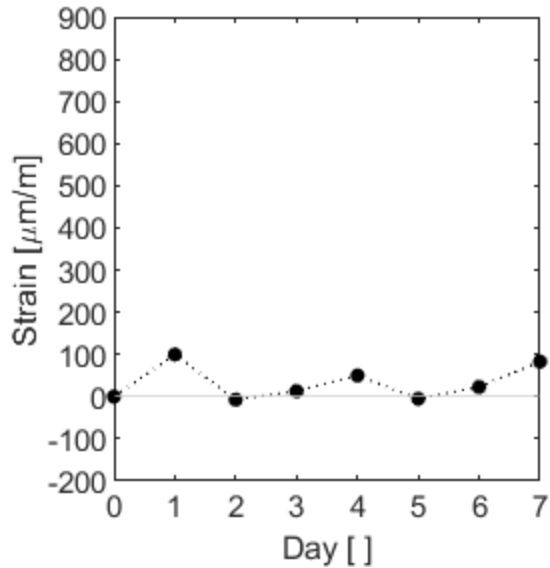


Figure C.4 – C.I.4

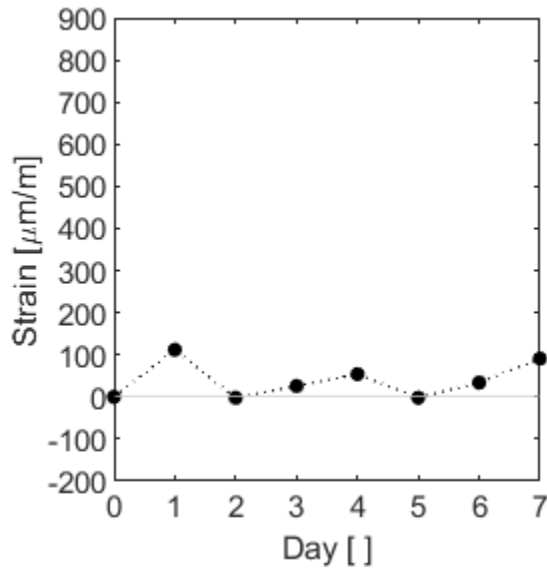


Figure C.5 – C.II.1

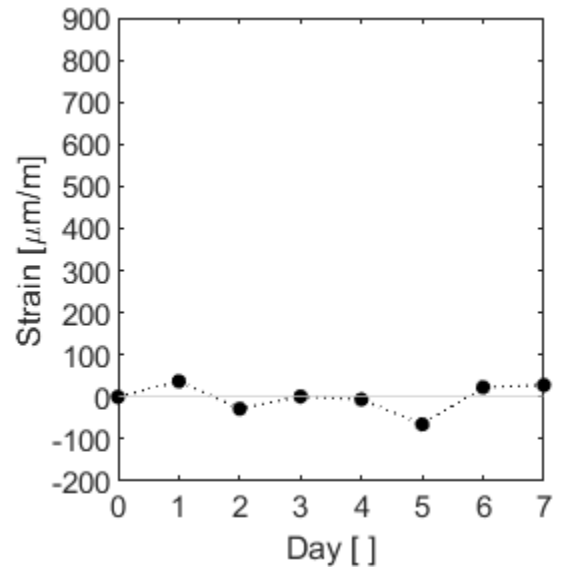


Figure C.6 – C.II.2

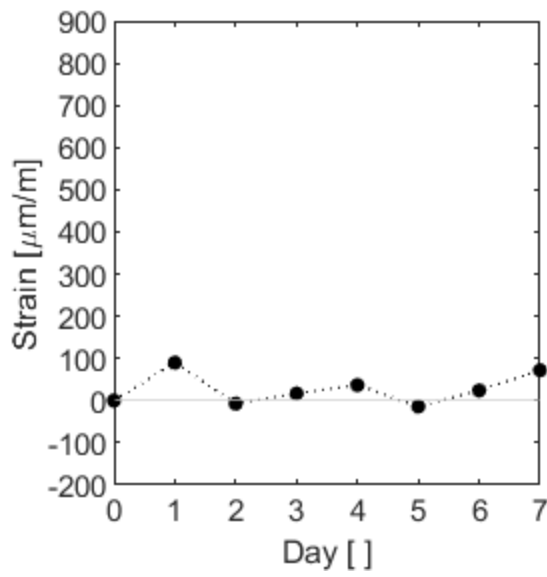


Figure C.7 – C.II.3

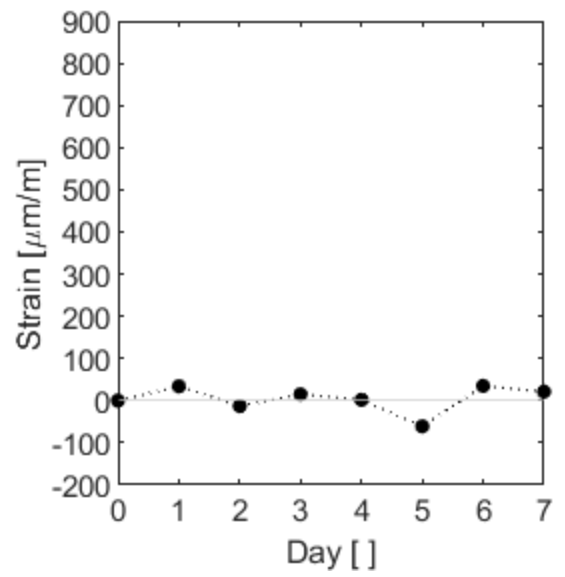


Figure C.8 – C.II.4

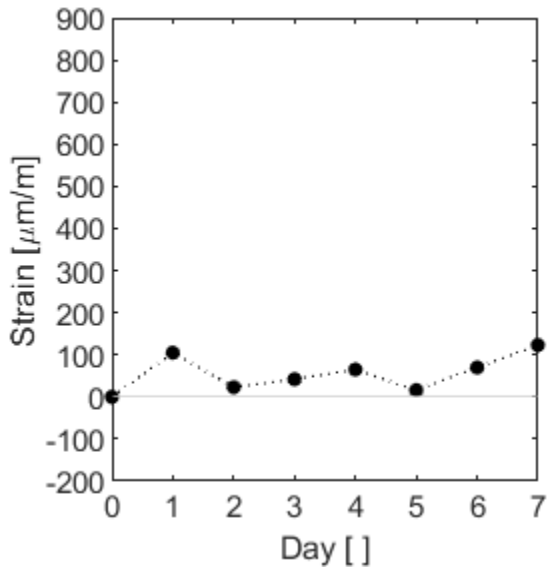


Figure C.9 – C.III.1

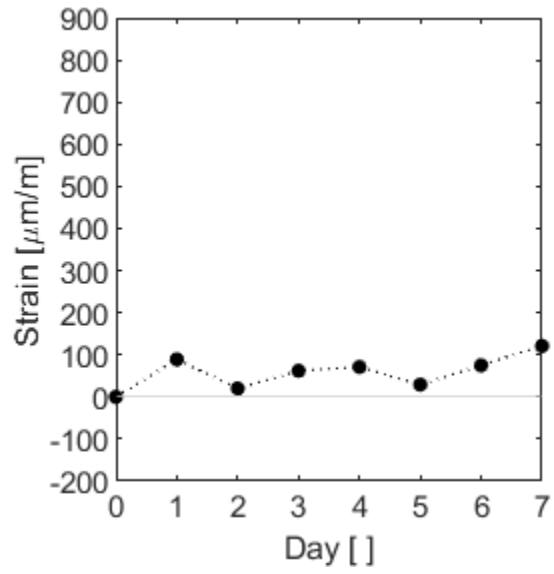


Figure C.10 – C.III.2

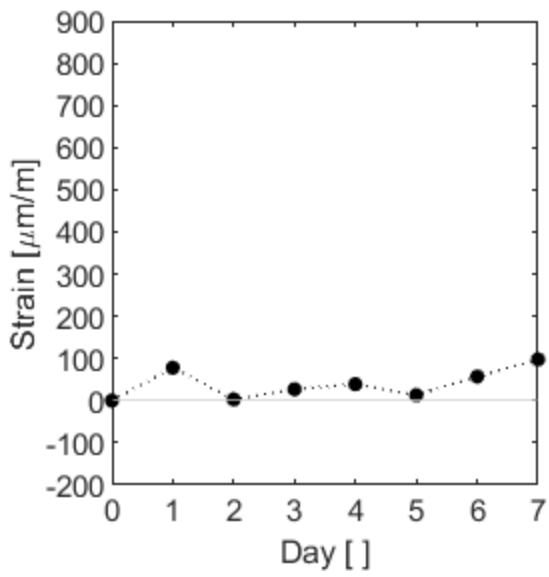


Figure C.11 – C.III.3

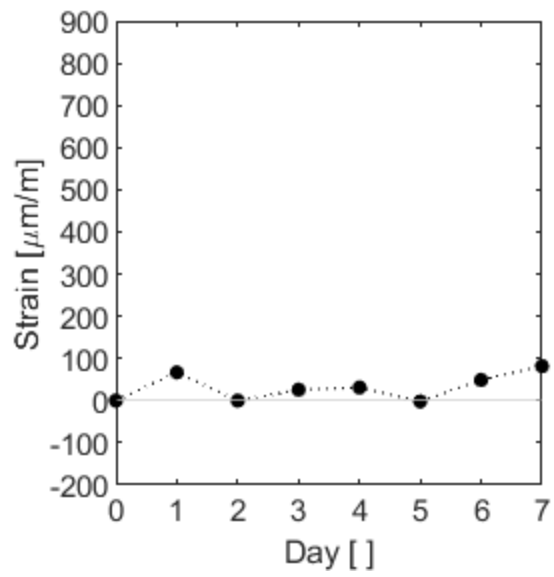


Figure C.12 – C.III.4

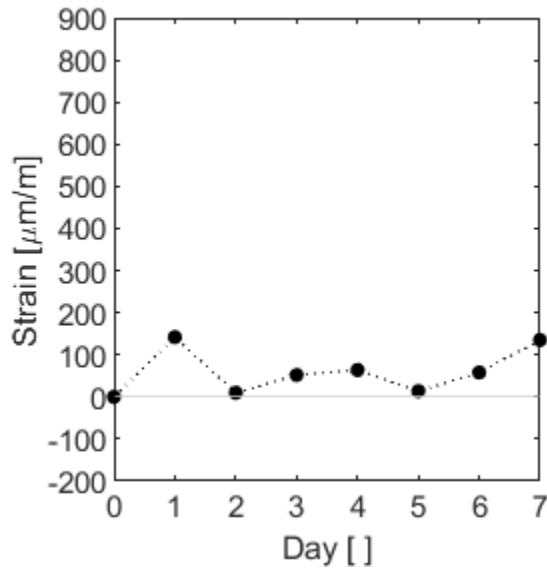


Figure C.13 – C.IV.1

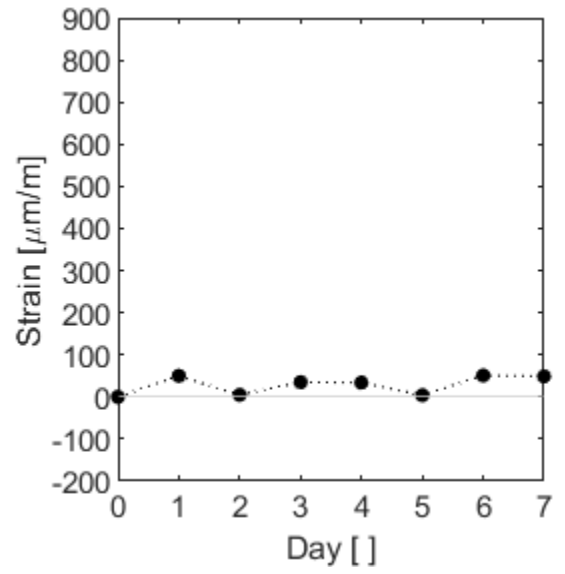


Figure C.14 – C.IV.2

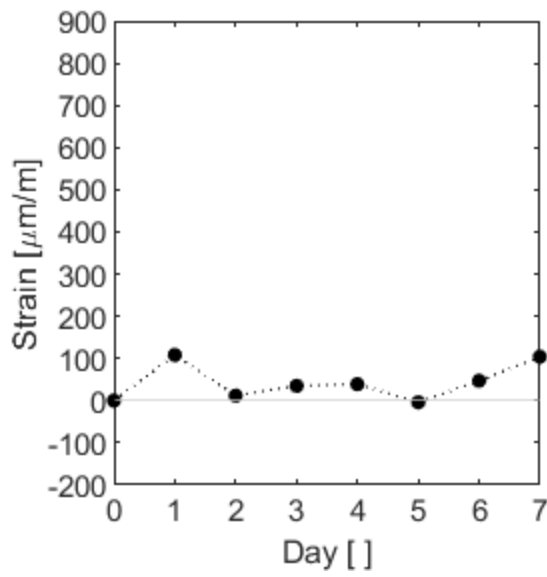


Figure C.15 – C.IV.3

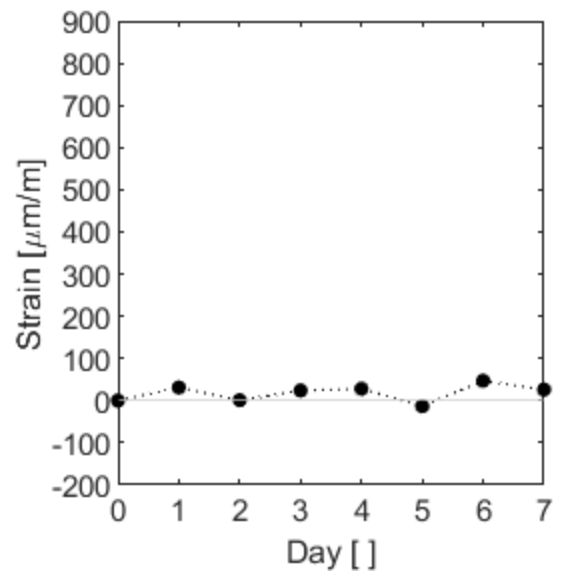


Figure C.16 – C.IV.4

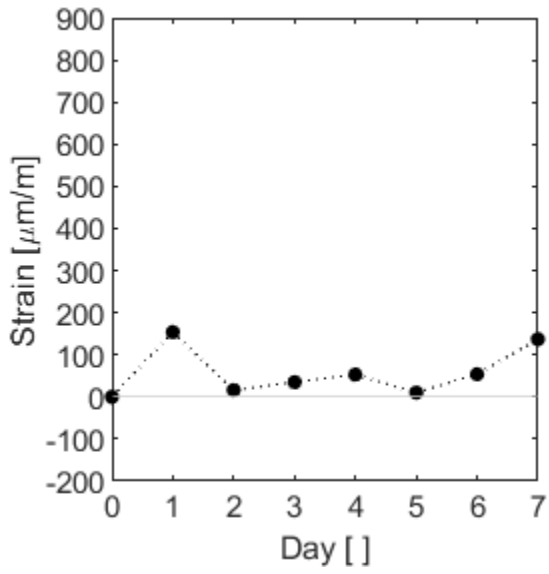


Figure C.17 – C.V.1

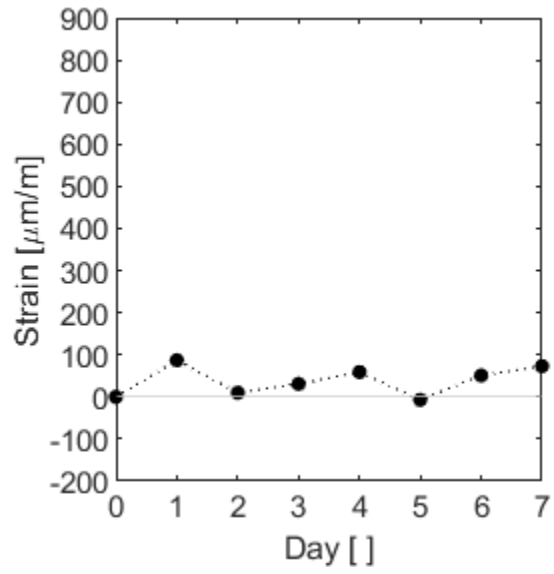


Figure C.18 – C.V.2

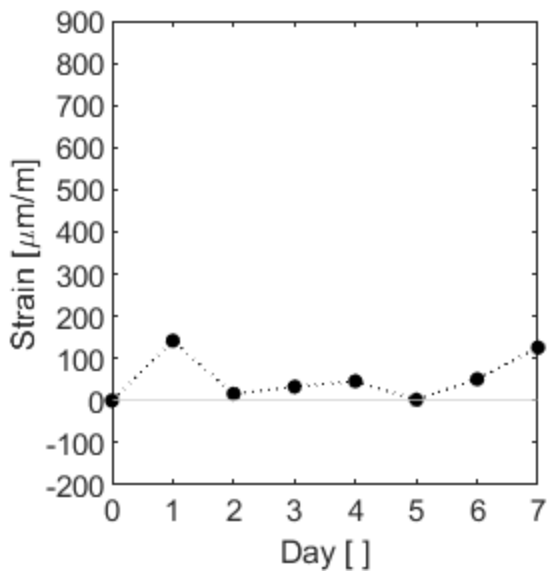


Figure C.19 – C.V.3

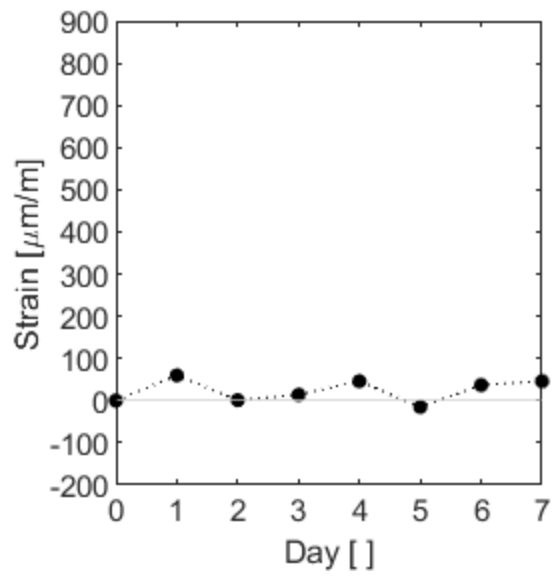


Figure C.20 – C.V.4



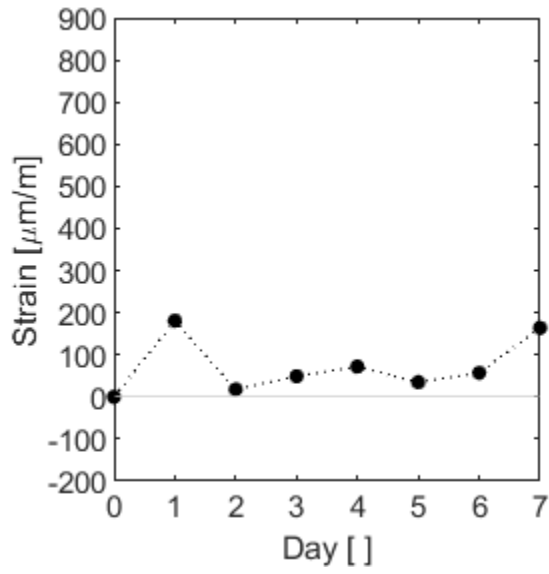


Figure C.21 – C.VI.1

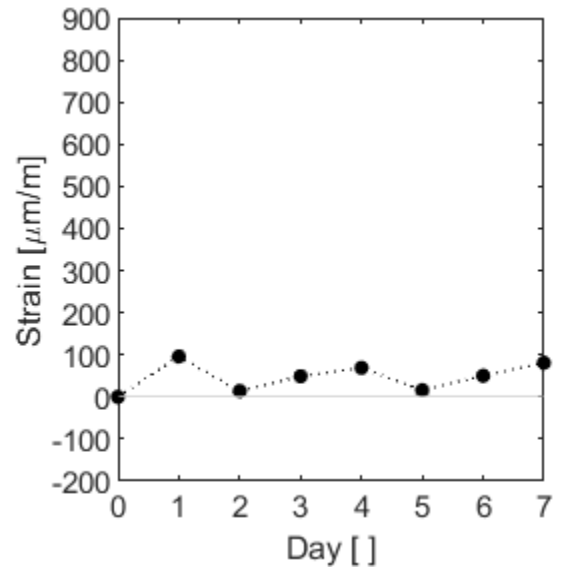


Figure C.22 – C.VI.2

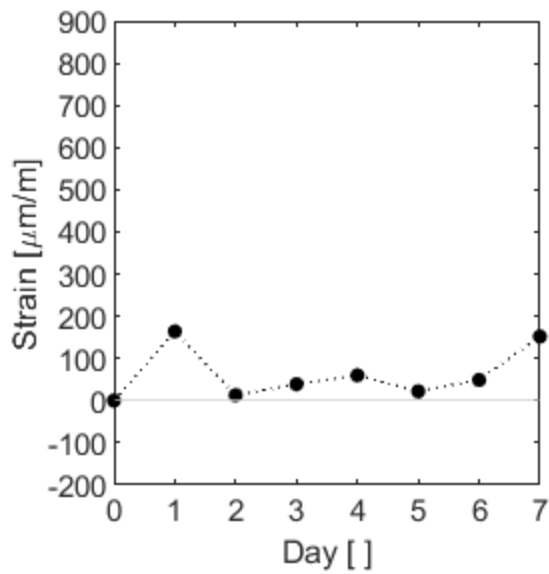


Figure C.23 – C.VI.3

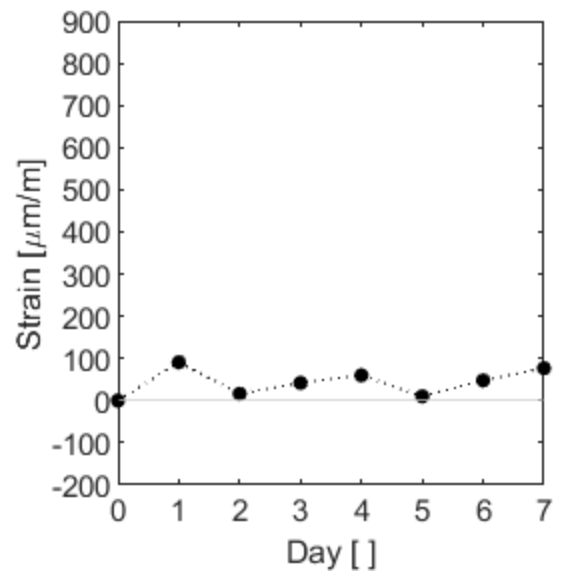


Figure C.24 – C.VI.4

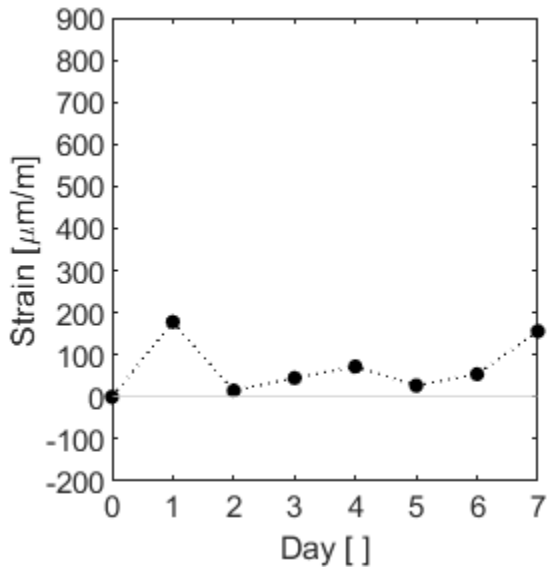


Figure C.25 – C.VII.1

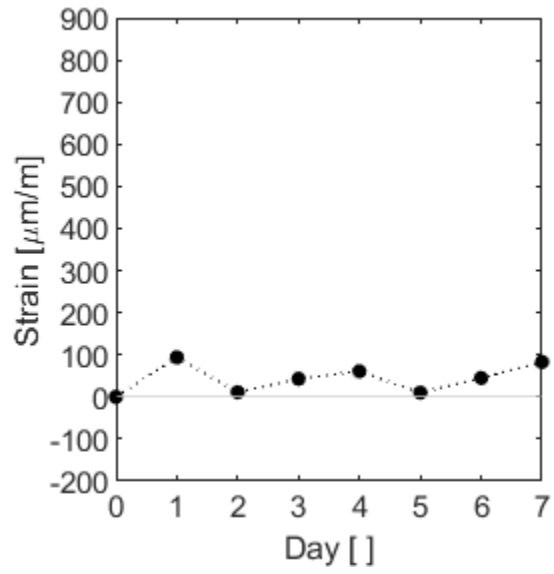


Figure C.26 – C.VII.2

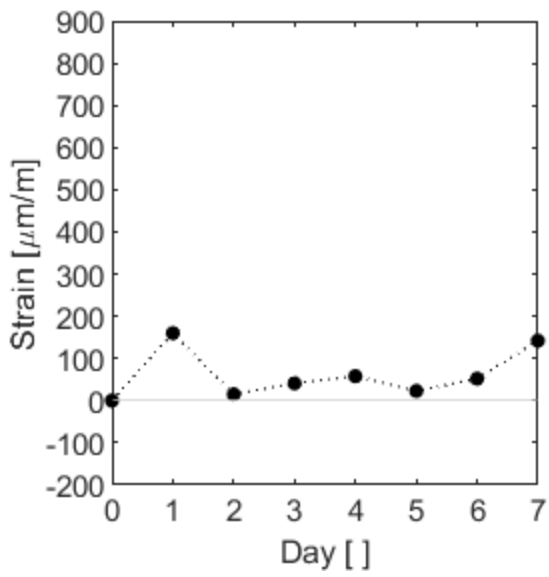


Figure C.27 – C.VII.3

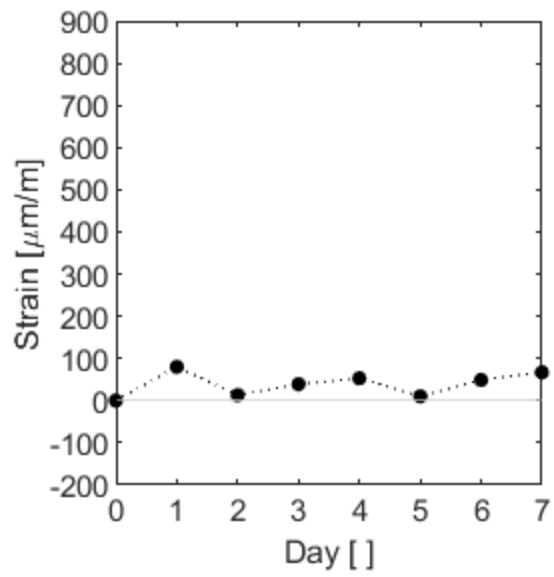


Figure C.28 – C.VII.4

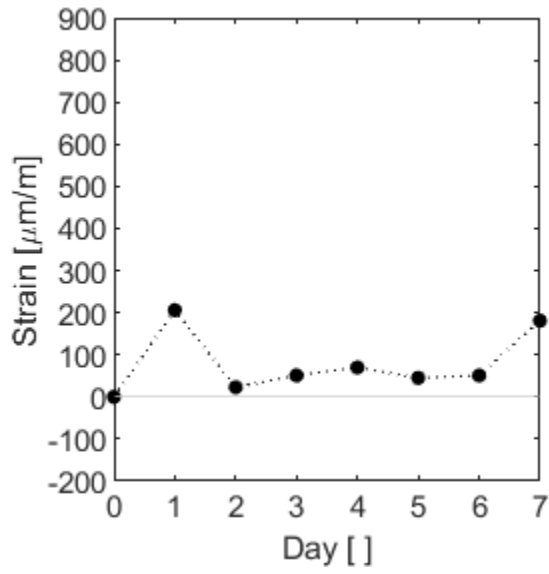


Figure C.29 – C.VIII.1

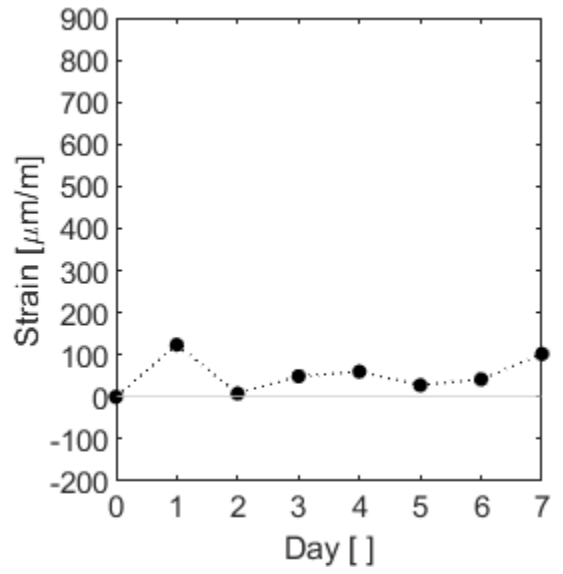


Figure C.30 – C.VIII.2

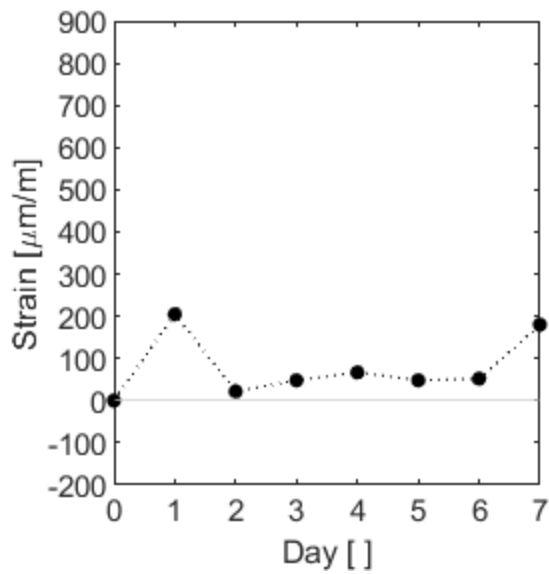


Figure C.31 – C.VIII.3

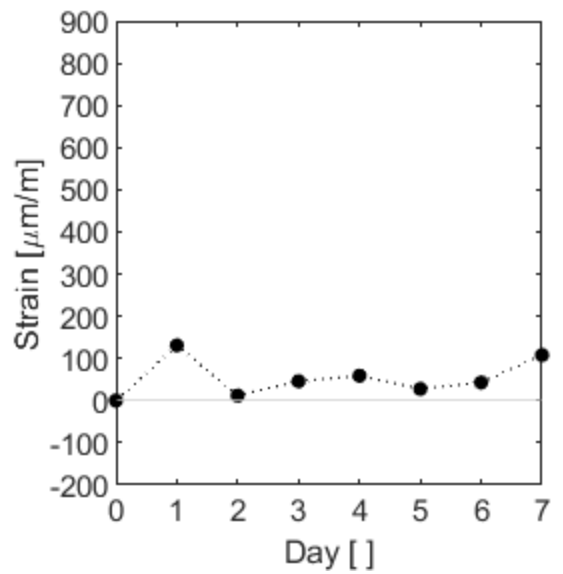


Figure C.32 – C.VIII.4

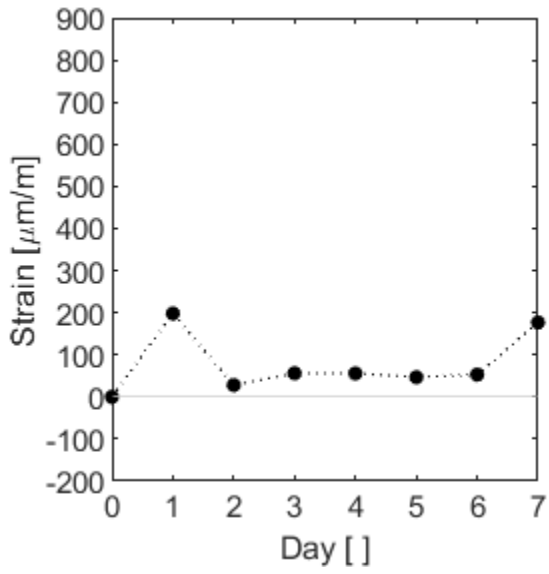


Figure C.33 – C.IX.1

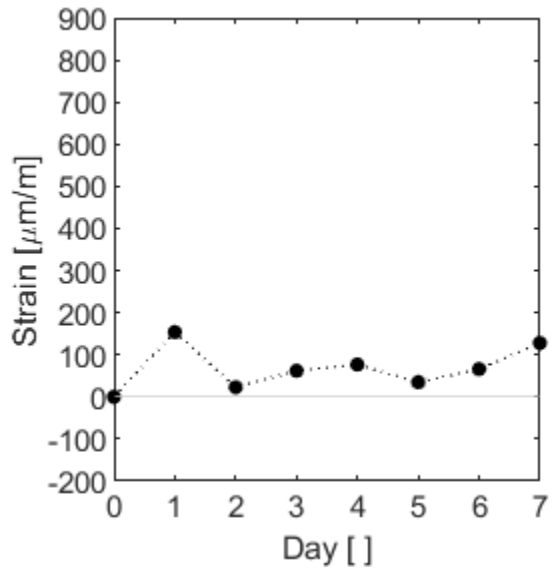


Figure C.34 – C.IX.2

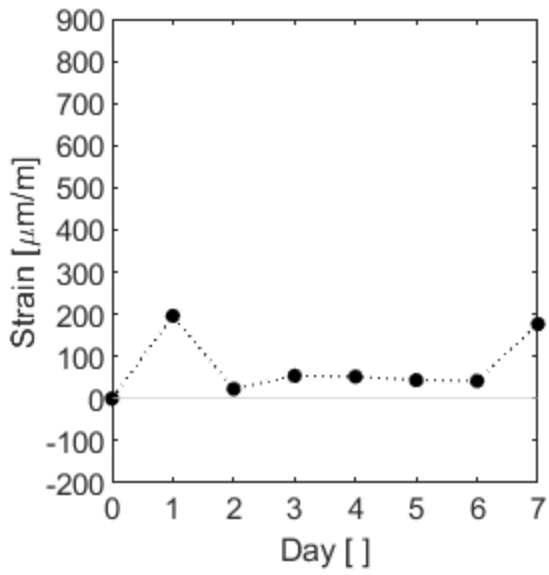


Figure C.35 – C.IX.3

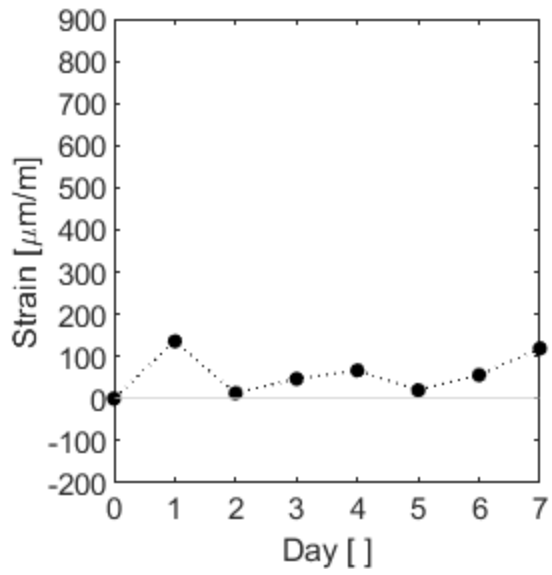


Figure C.36 – C.IX.4

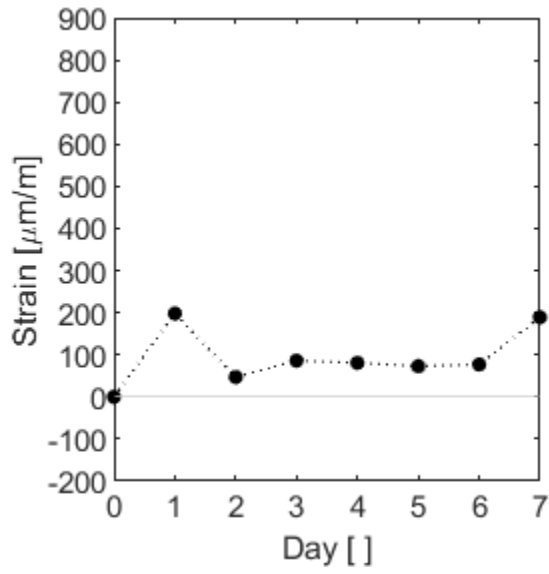


Figure C.37 – C.X.1

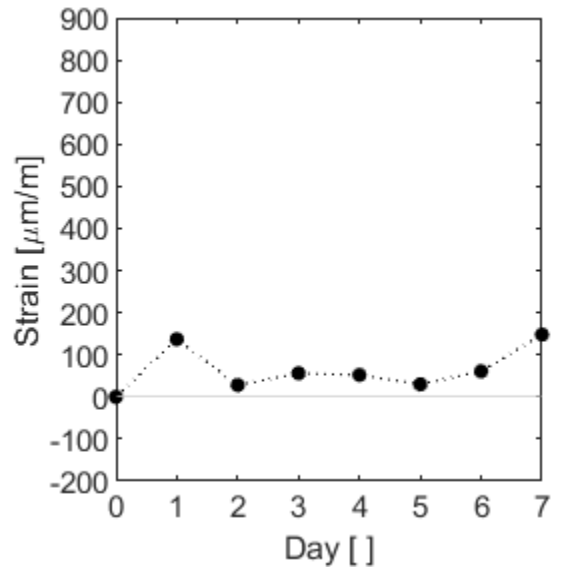


Figure C.38 – C.X.2

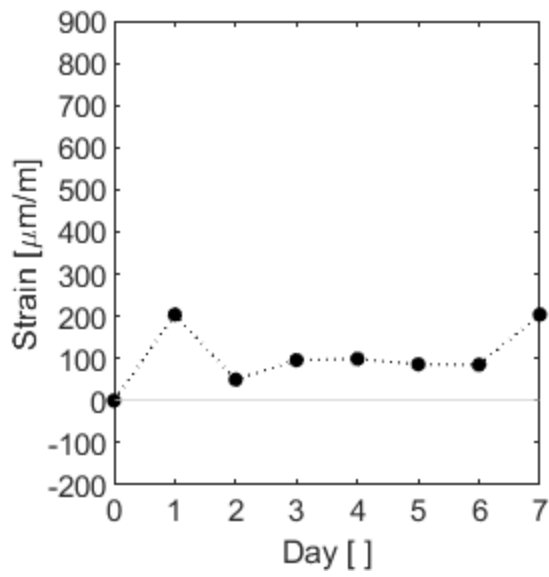


Figure C.39 – C.X.3

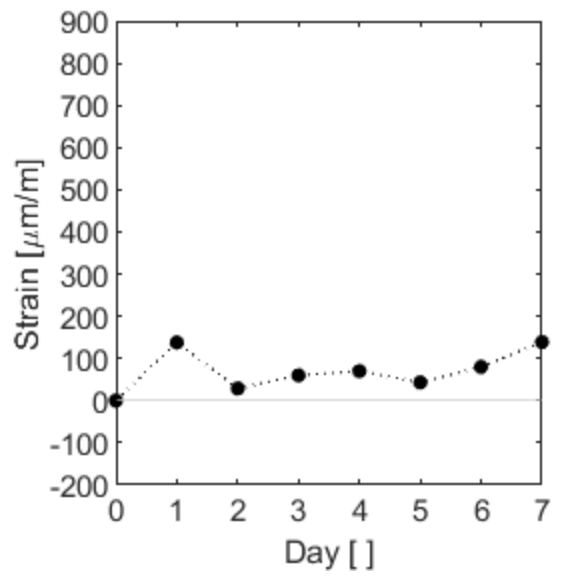


Figure C.40 – C.X.4

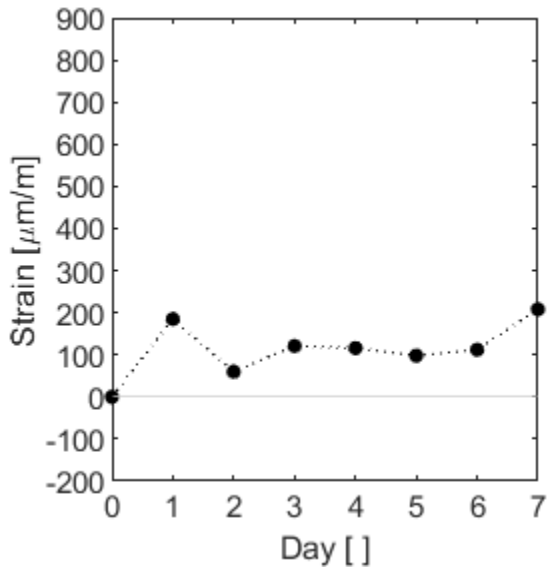


Figure C.41 – C.XI.1

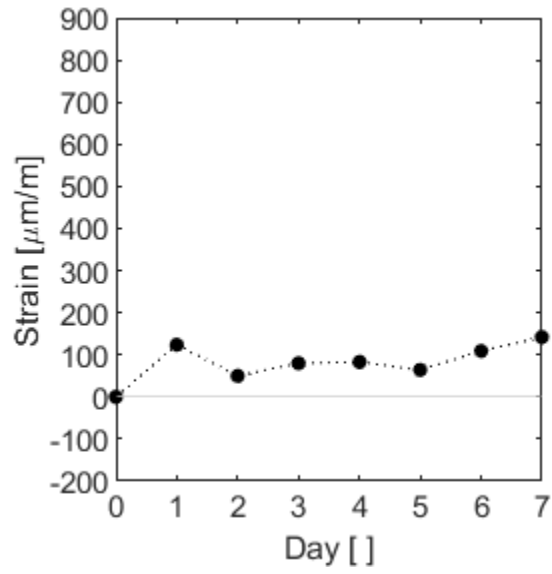


Figure C.42 – C.XI.2

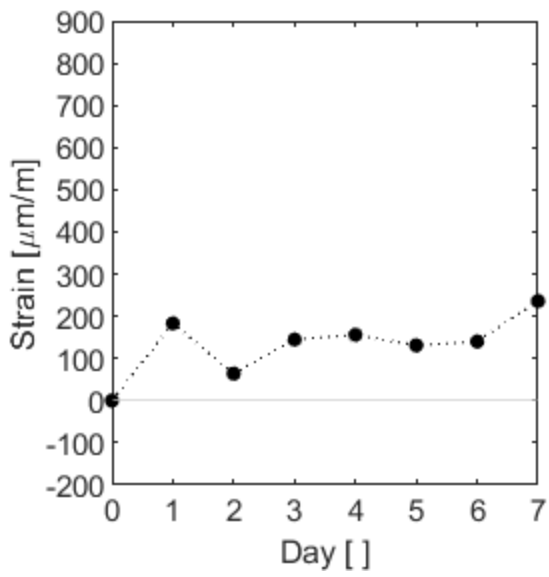


Figure C.43 – C.XI.3

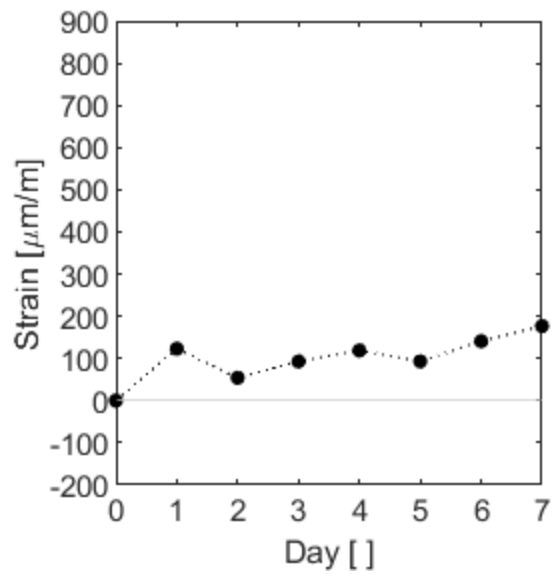


Figure C.44 – C.XI.4

### C.1.2 Weekly Recordings

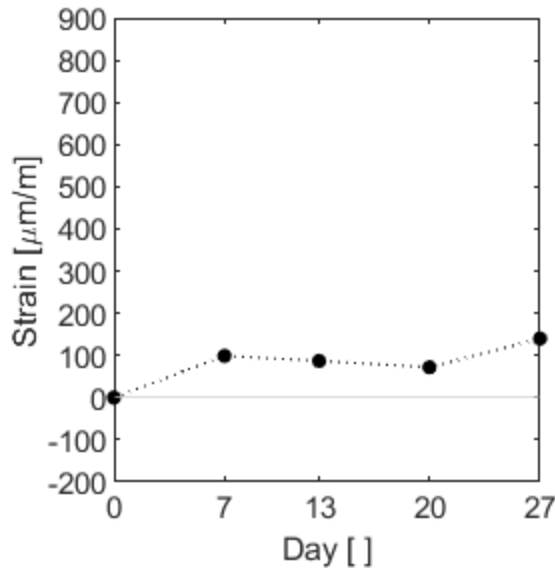


Figure C.45 – C.I.1

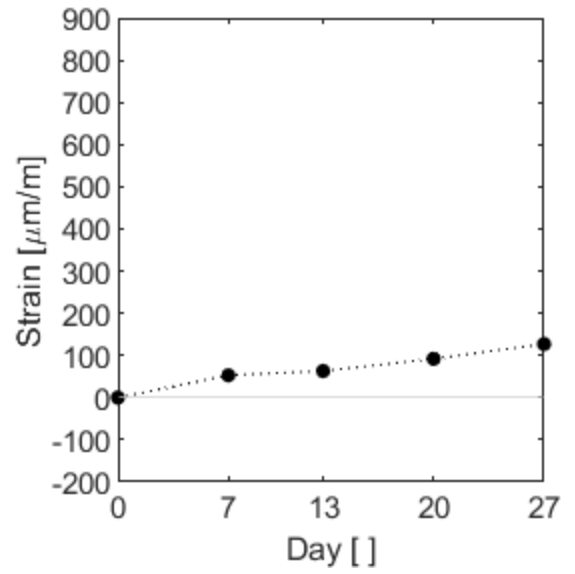


Figure C.46 – C.I.2

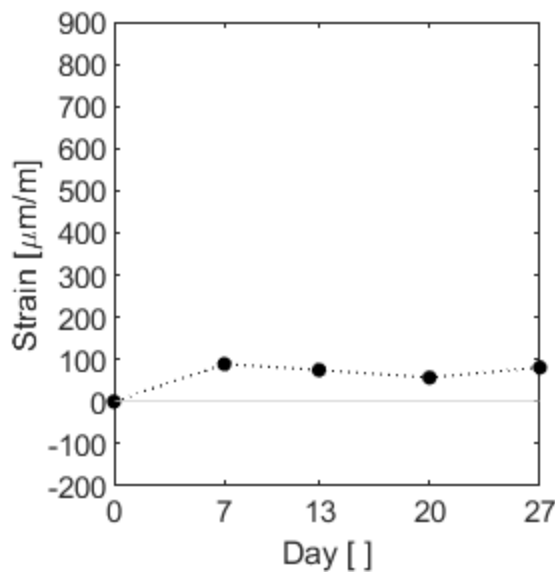


Figure C.47 – C.I.3

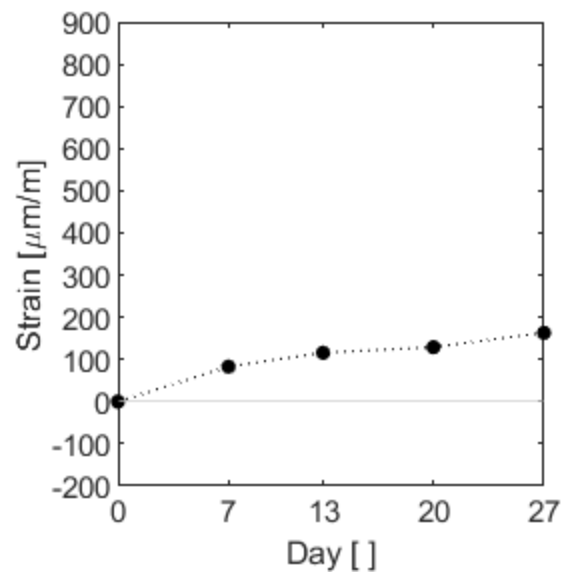


Figure C.48 – C.I.4

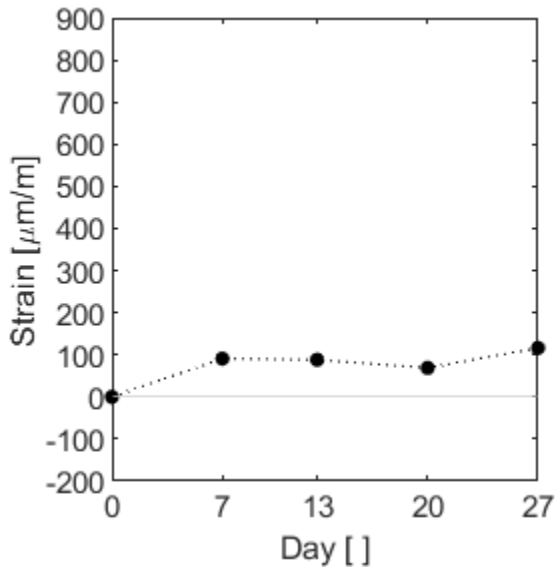


Figure C.49 – C.II.1

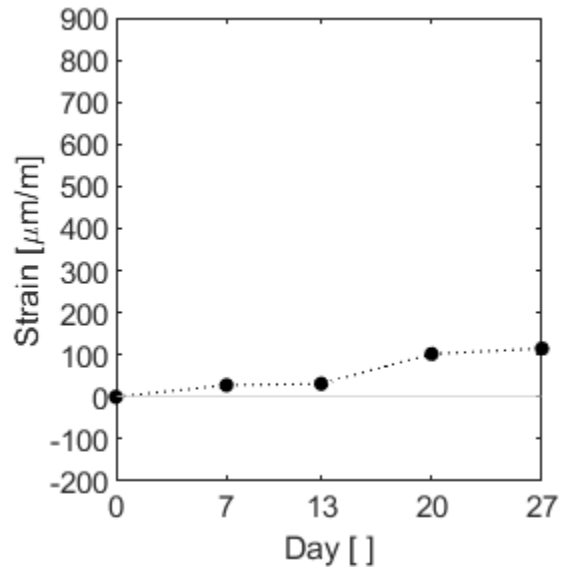


Figure C.50 – C.II.2

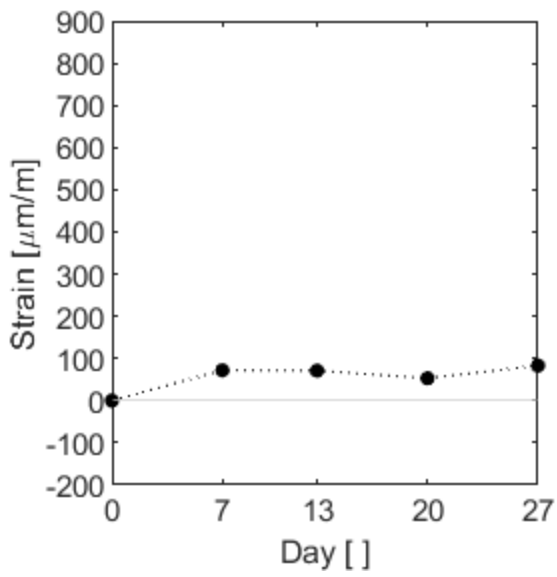


Figure C.51 – C.II.3

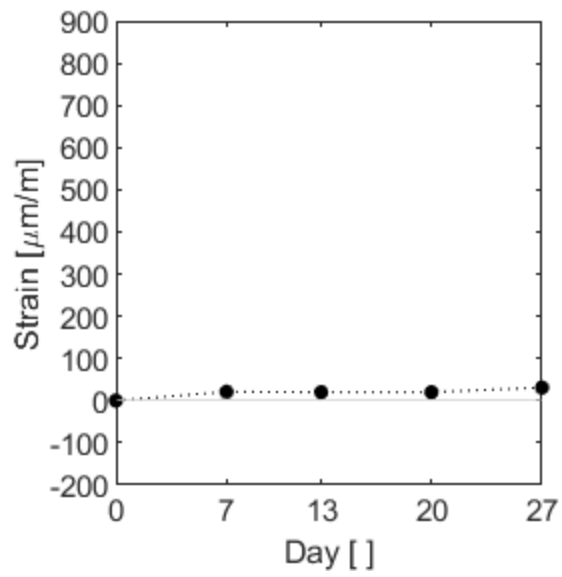


Figure C.52 – C.II.4



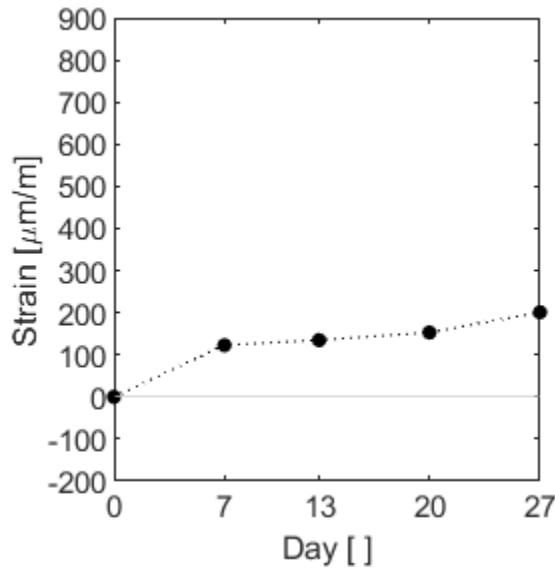


Figure C.53 – C.III.1

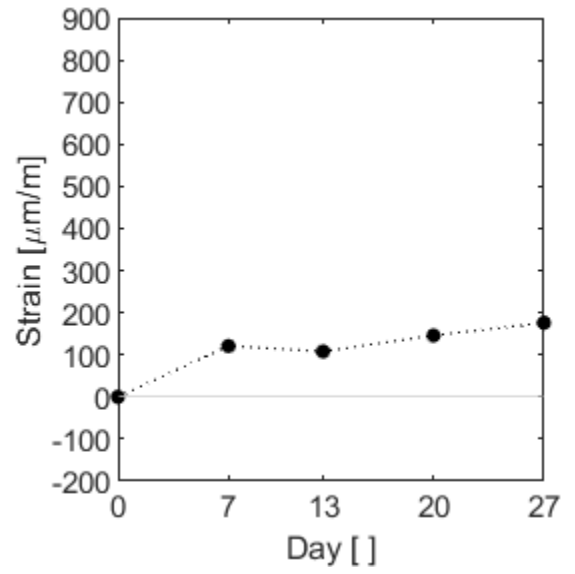


Figure C.54 – C.III.2

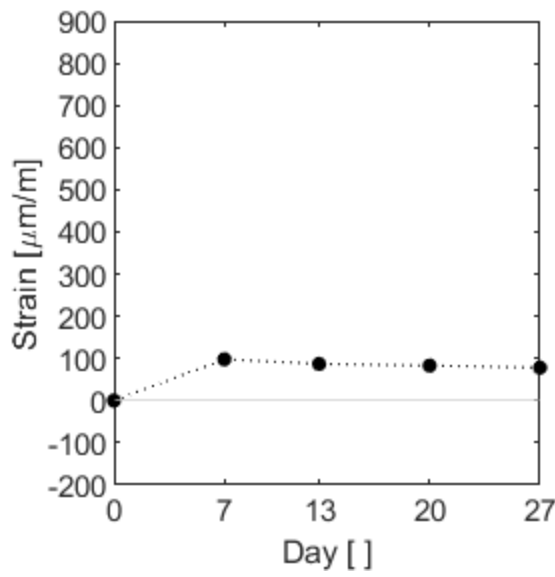


Figure C.55 – C.III.3

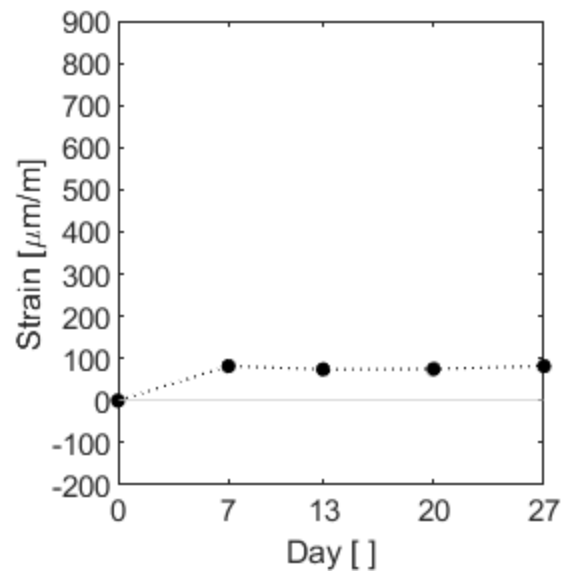


Figure C.56 – C.III.4

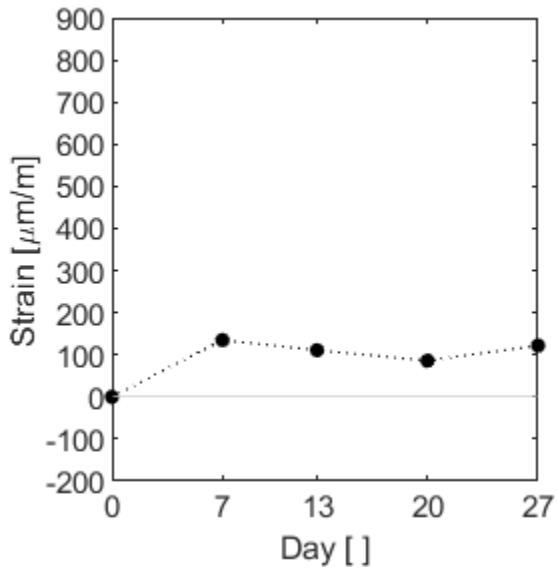


Figure C.57 – C.IV.1

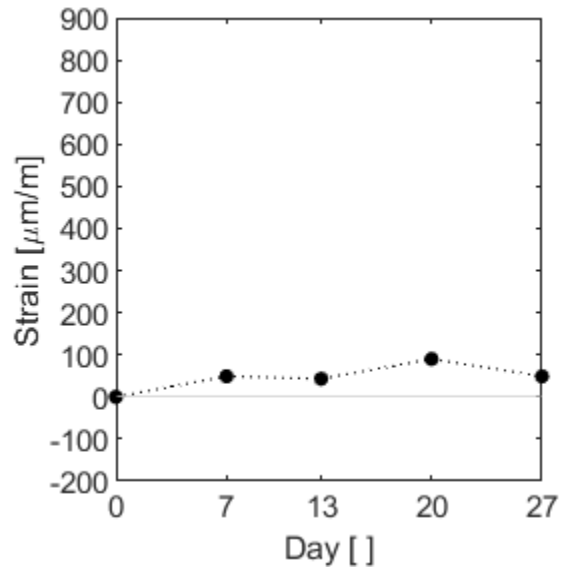


Figure C.58 – C.IV.2

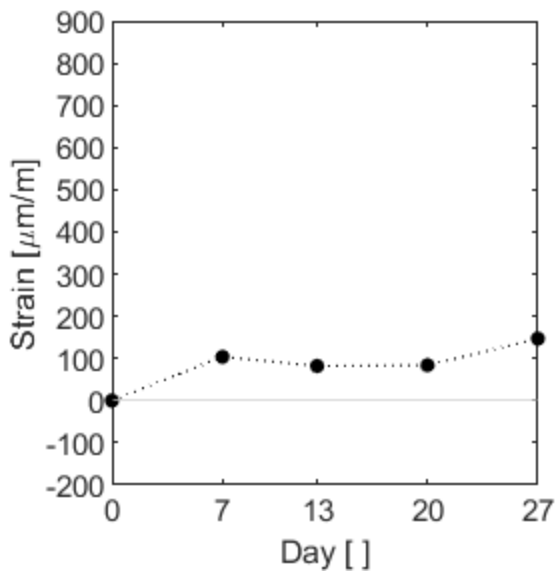


Figure C.59 – C.IV.3

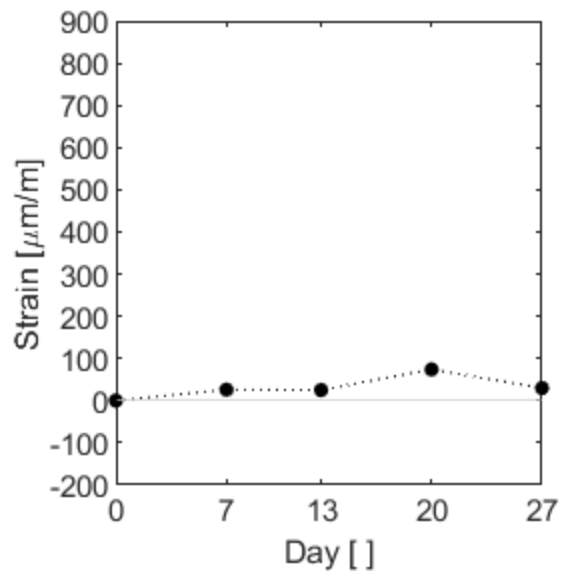


Figure C.60 – C.IV.4

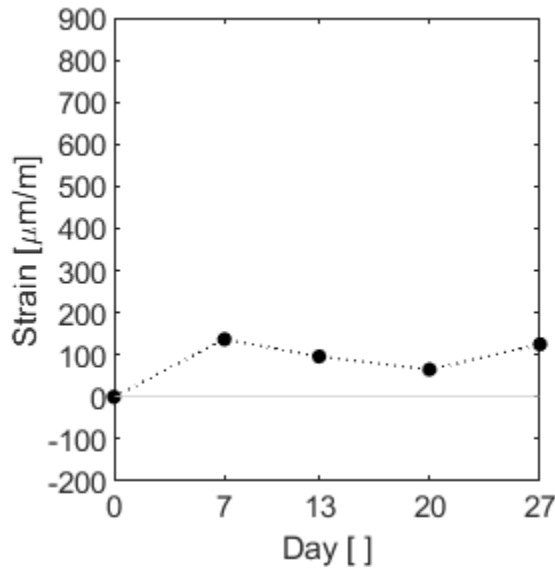


Figure C.61 – C.V.1

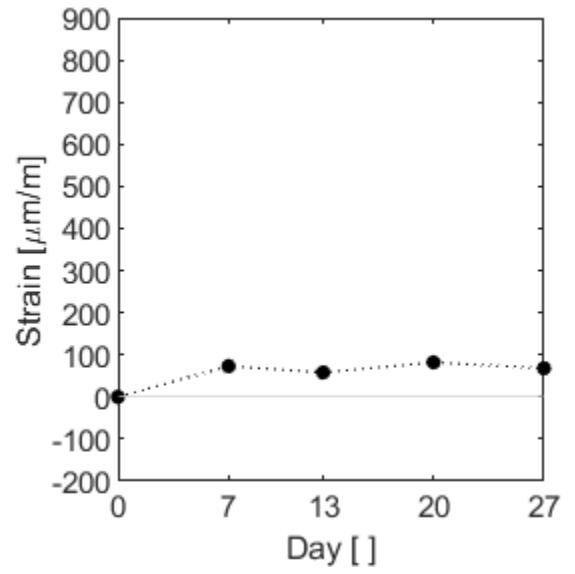


Figure C.62 – C.V.2

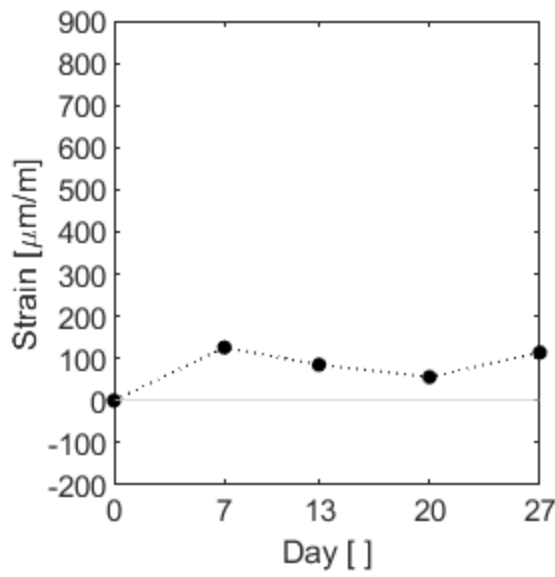


Figure C.63 – C.V.3

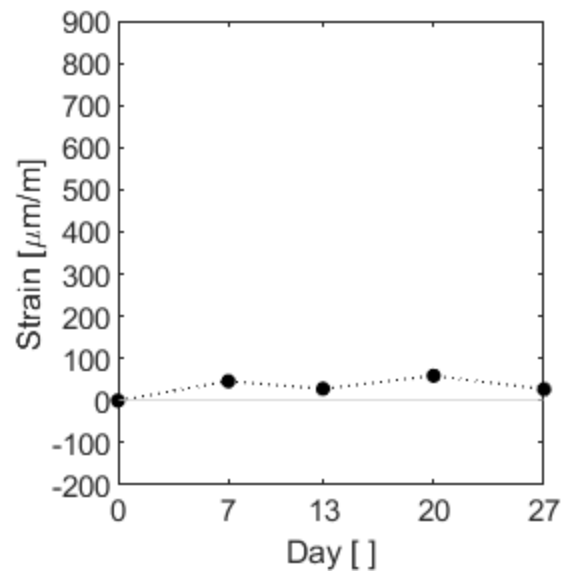


Figure C.64 – C.V.4

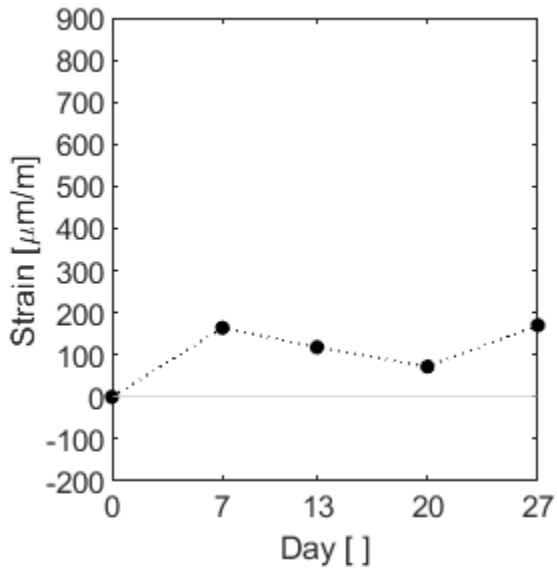


Figure C.65 – C.VI.1

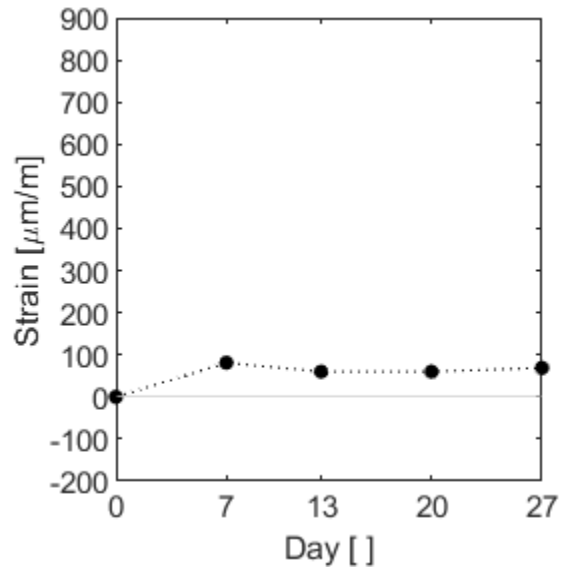


Figure C.66 – C.VI.2

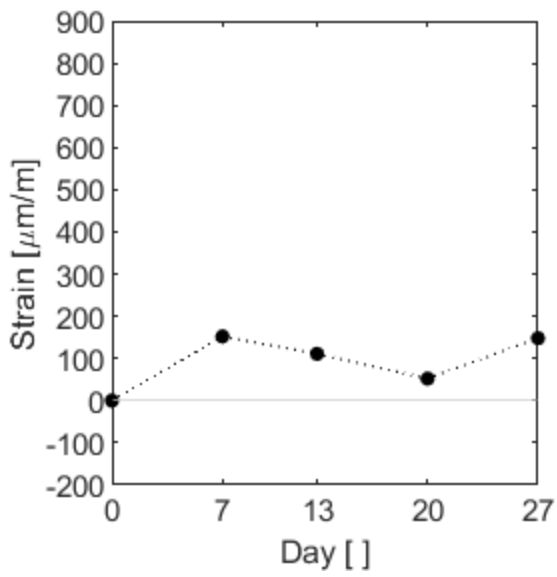


Figure C.67 – C.VI.3

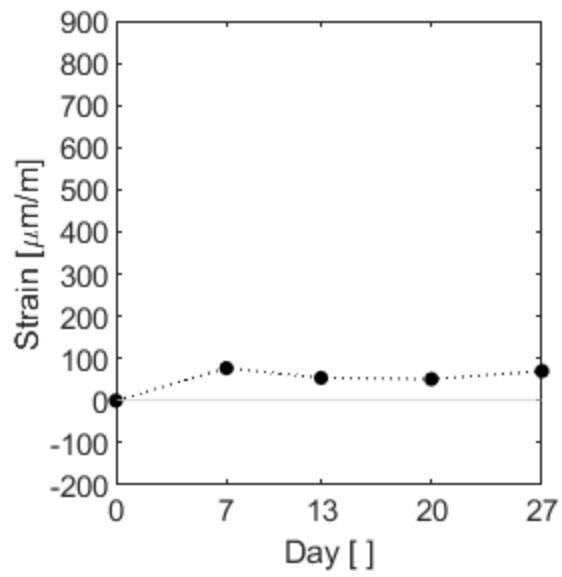


Figure C.68 – C.VI.4

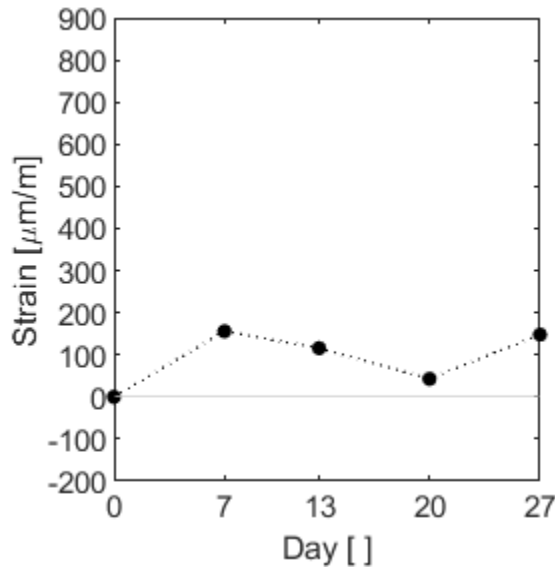


Figure C.69 – C.VII.1

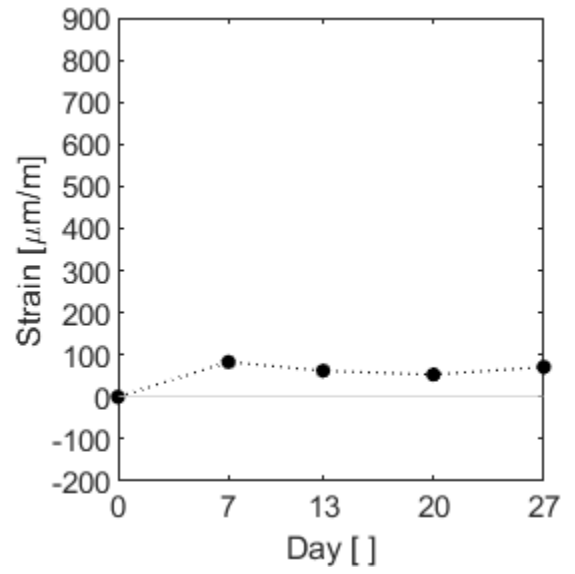


Figure C.70 – C.VII.2

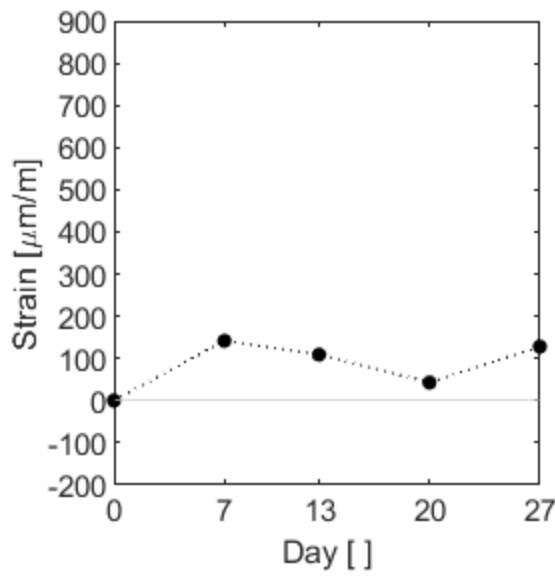


Figure C.71 – C.VII.3

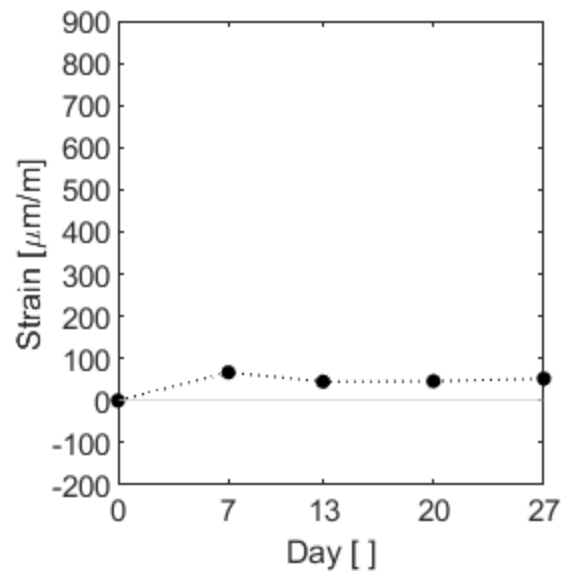


Figure C.72 – C.VII.4

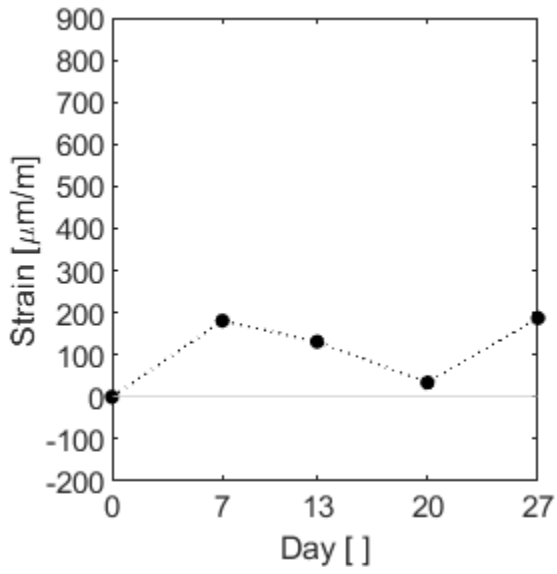


Figure C.73 – C.VIII.1

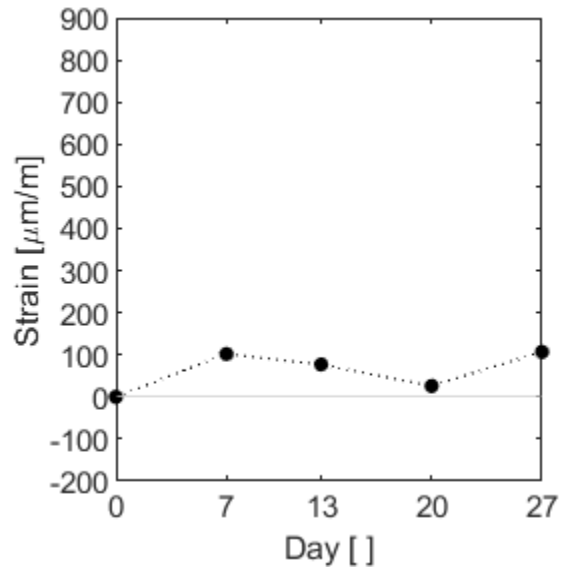


Figure C.74 – C.VIII.2

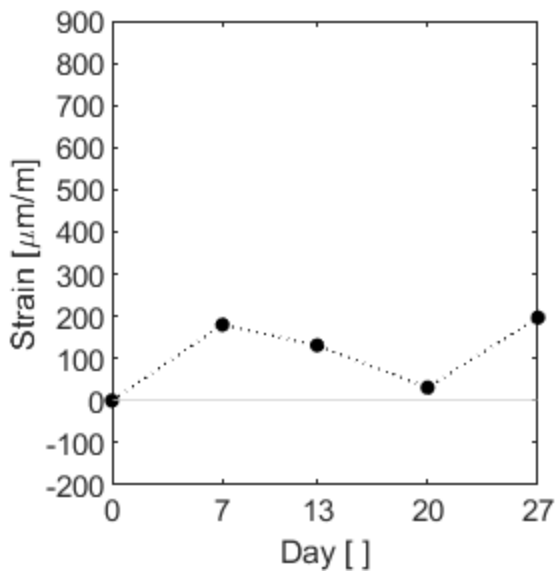


Figure C.75 – C.VIII.3

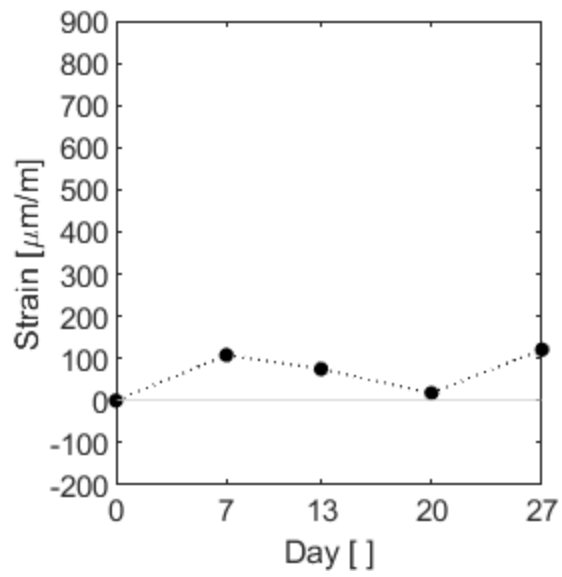


Figure C.76 – C.VIII.4

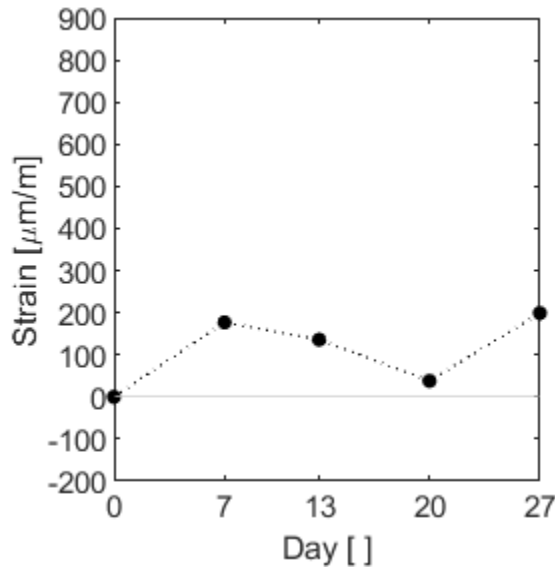


Figure C.77 – C.IX.1

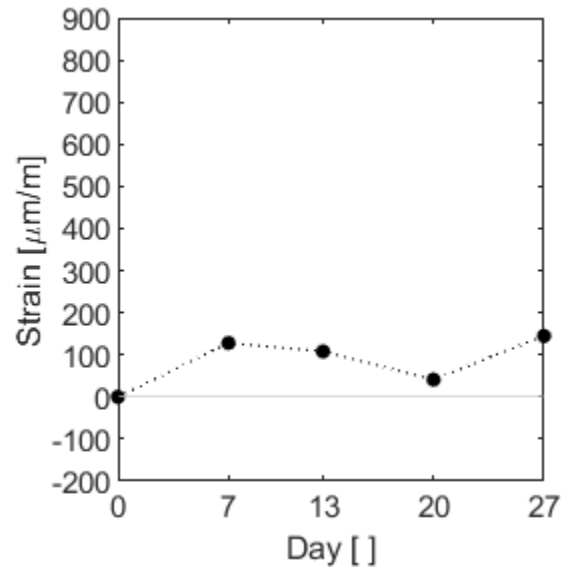


Figure C.78 – C.IX.2

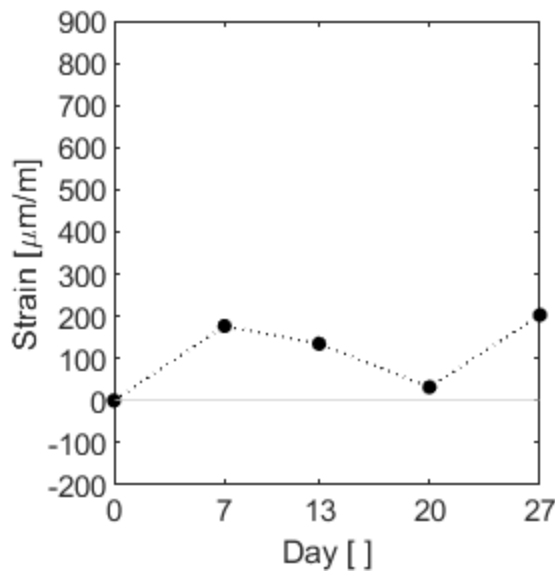


Figure C.79 – C.IX.3

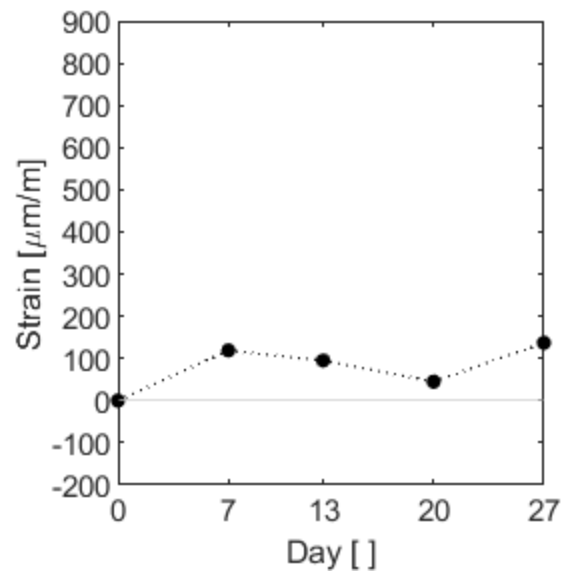


Figure C.80 – C.IX.4

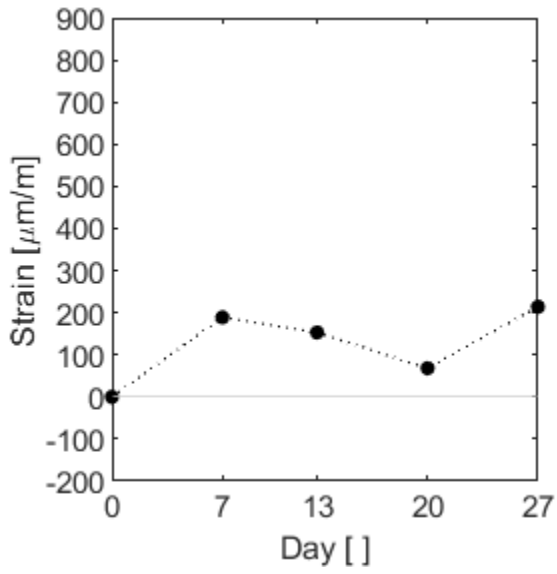


Figure C.81 – C.X.1

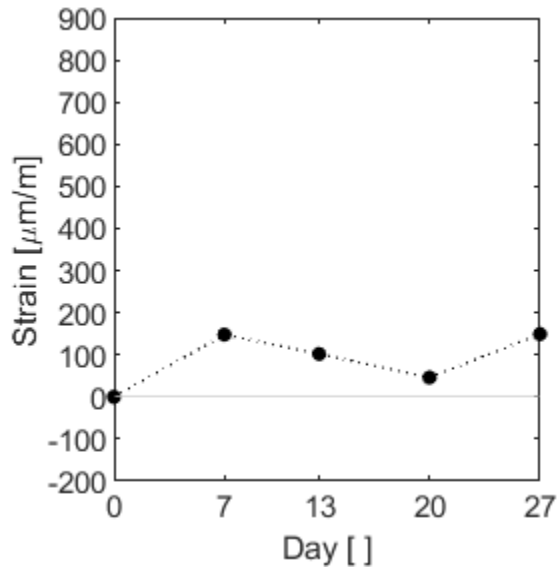


Figure C.82 – C.X.2

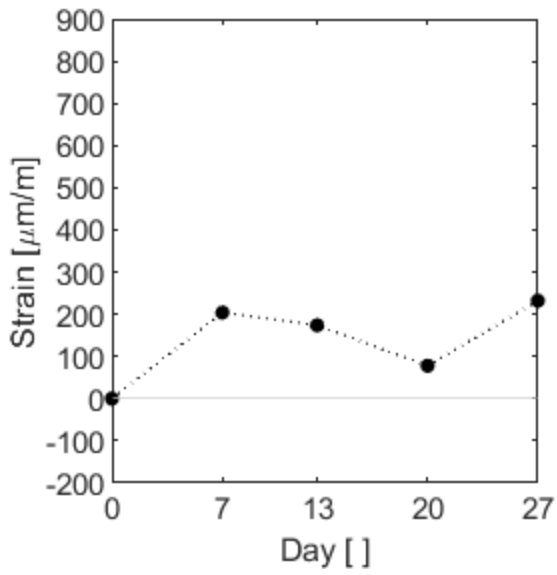


Figure C.83 – C.X.3

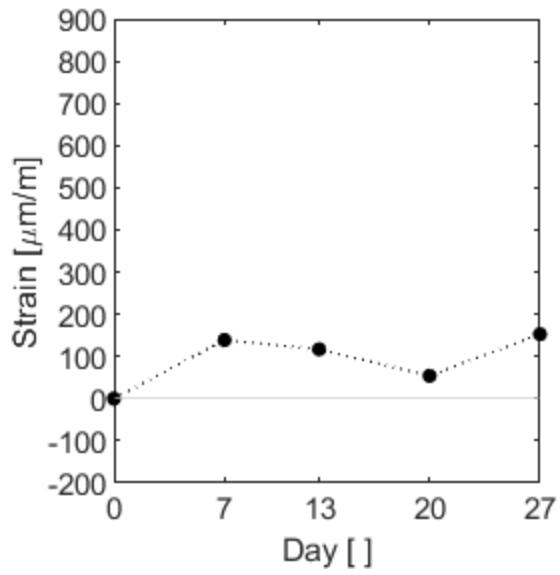


Figure C.84 – C.X.4



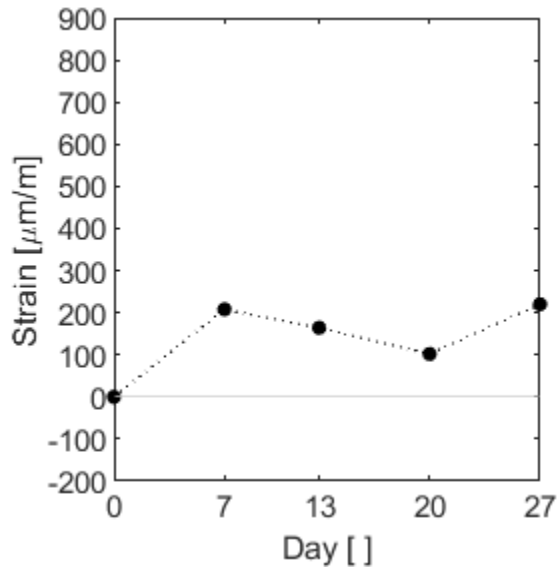


Figure C.85 – C.XI.1

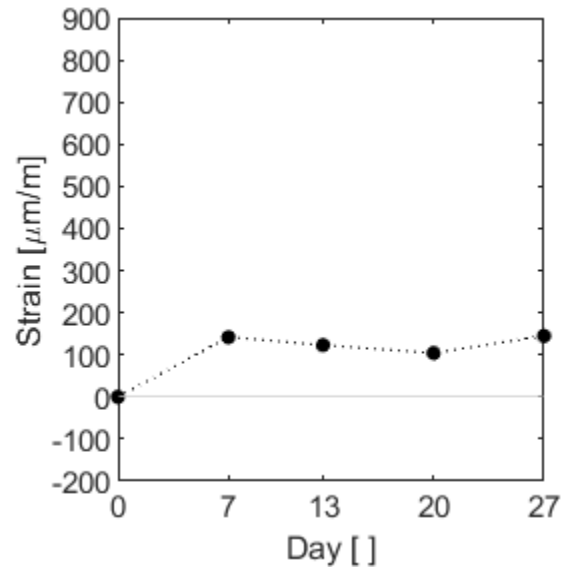


Figure C.86 – C.XI.2

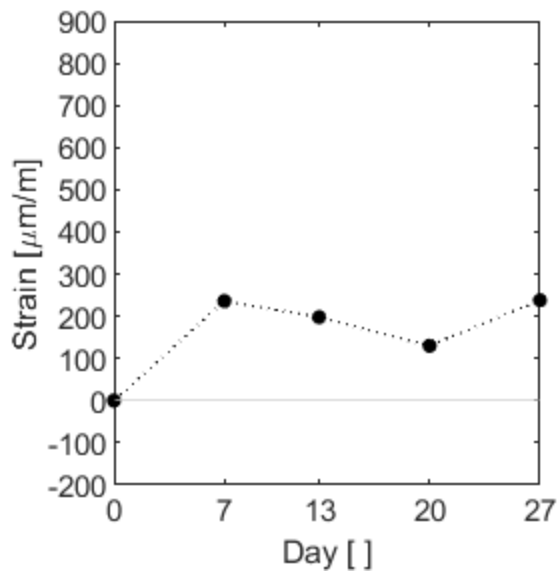


Figure C.87 – C.XI.3

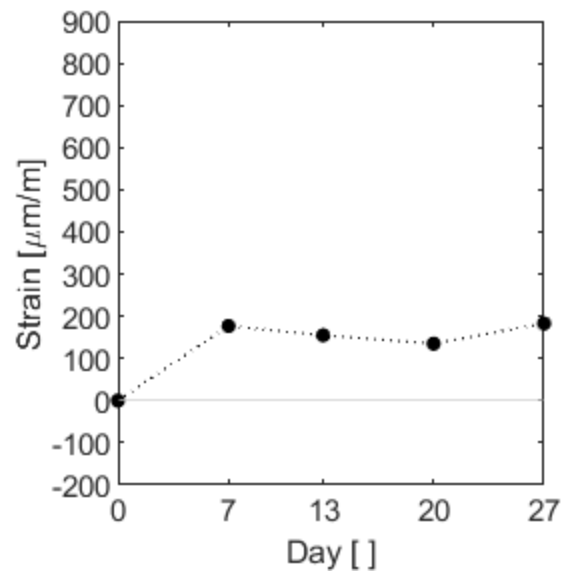


Figure C.88 – C.XI.4

C.1.3 Monthly Recordings

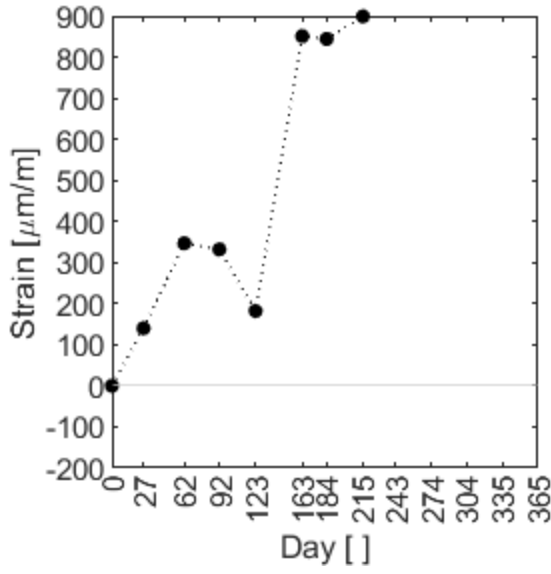


Figure C.89 – C.I.1

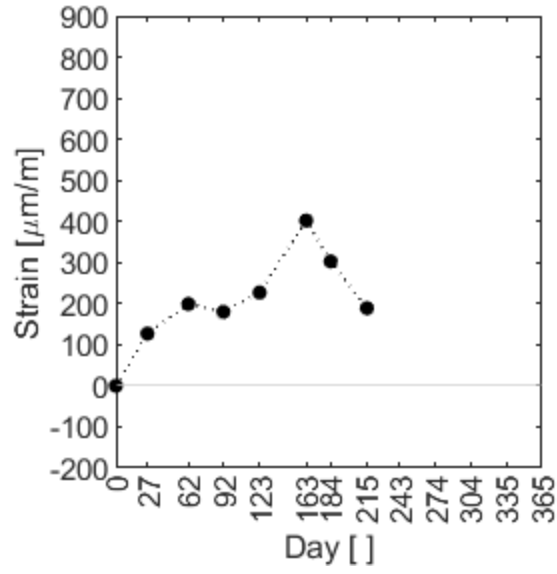


Figure C.90 – C.I.2

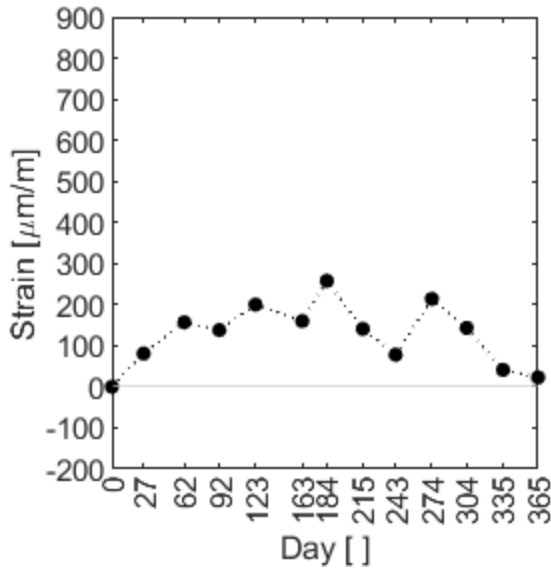


Figure C.91 – C.I.3

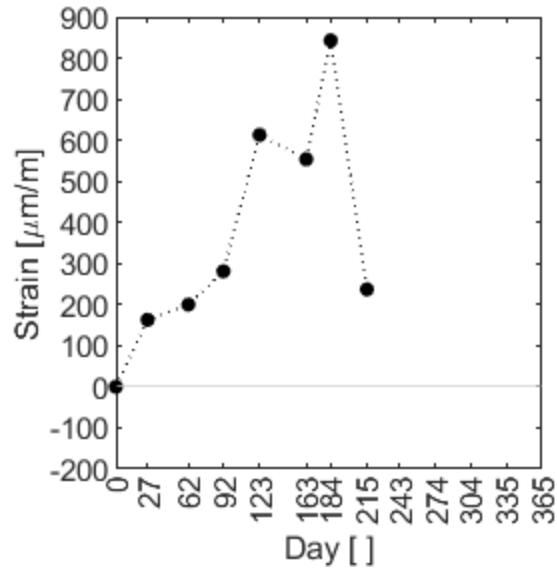


Figure C.92 – C.I.4

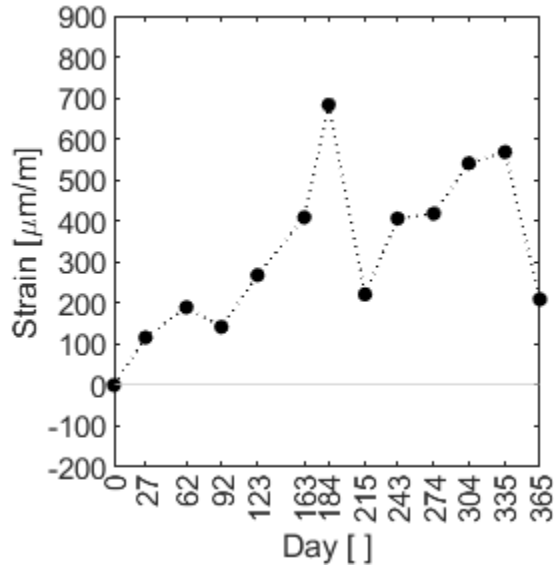


Figure C.93 – C.II.1

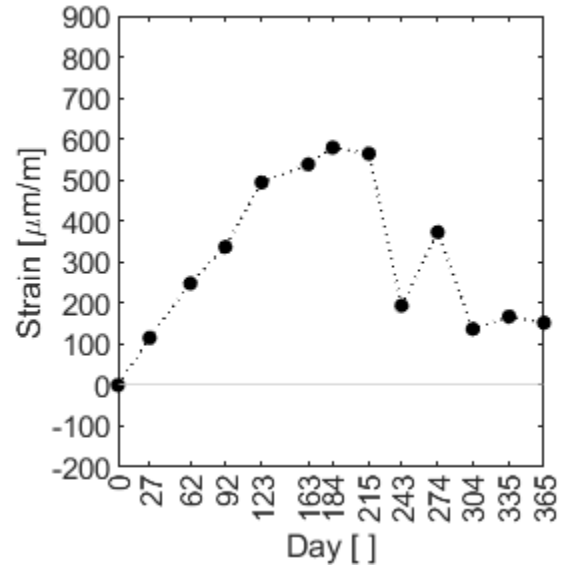


Figure C.94 – C.II.2

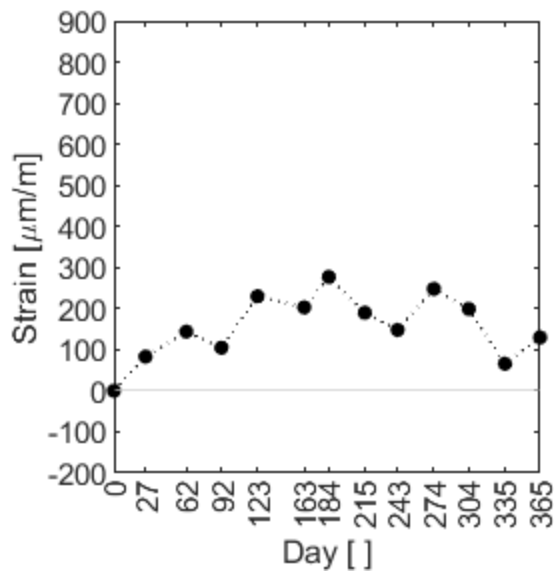


Figure C.95 – C.II.3

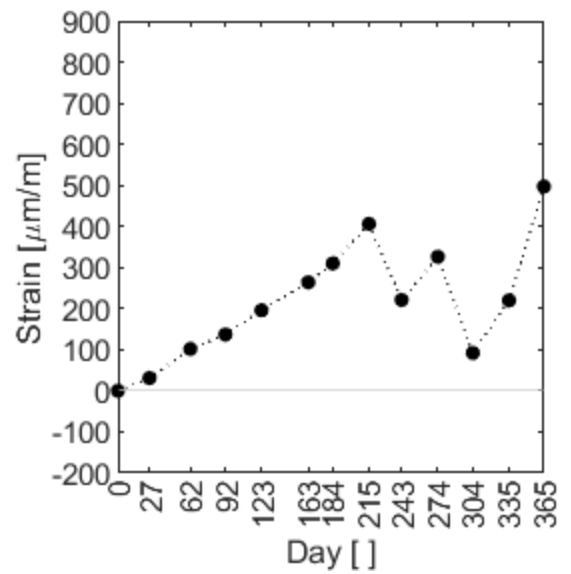


Figure C.96 – C.II.4

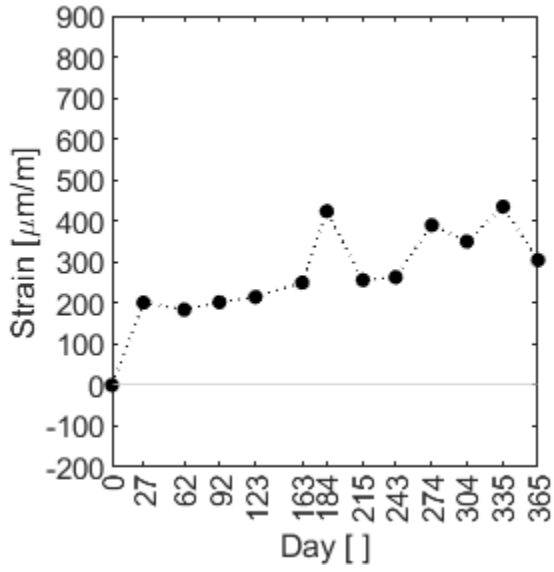


Figure C.97 – C.III.1

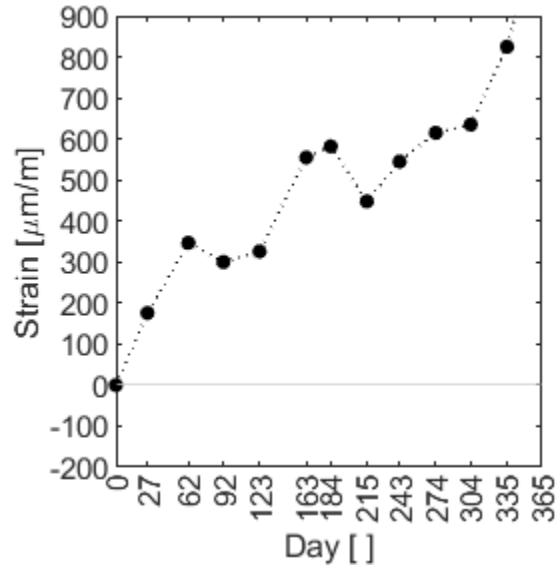


Figure C.98 – C.III.2

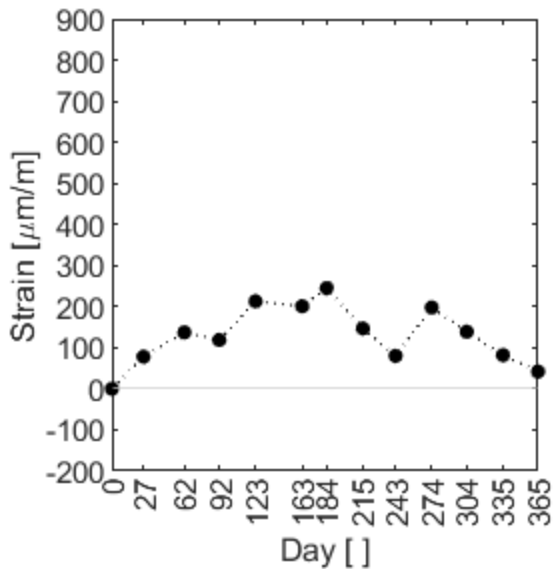


Figure C.99 – C.III.3

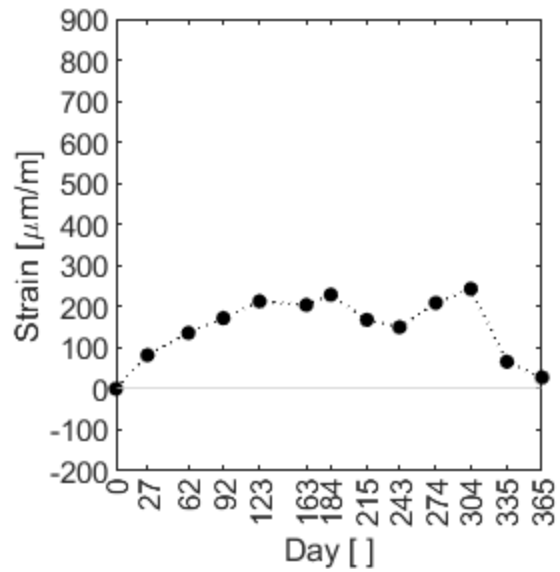


Figure C.100 – C.III.4

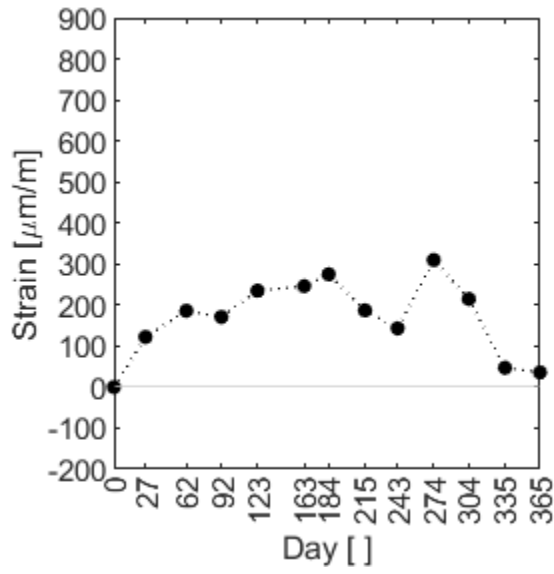


Figure C.101 – C.IV.1

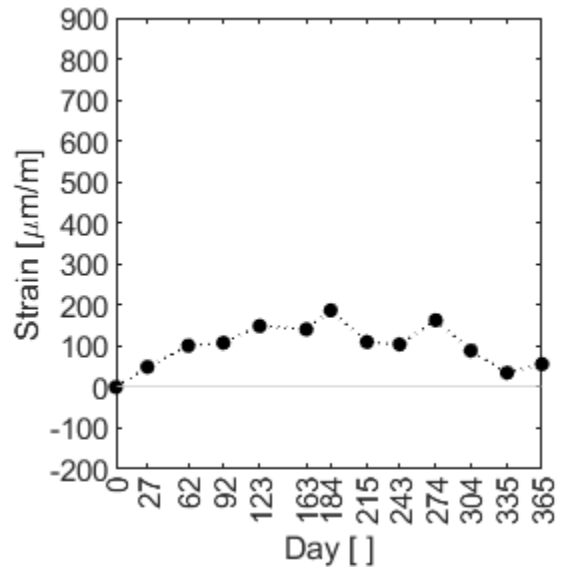


Figure C.102 – C.IV.2

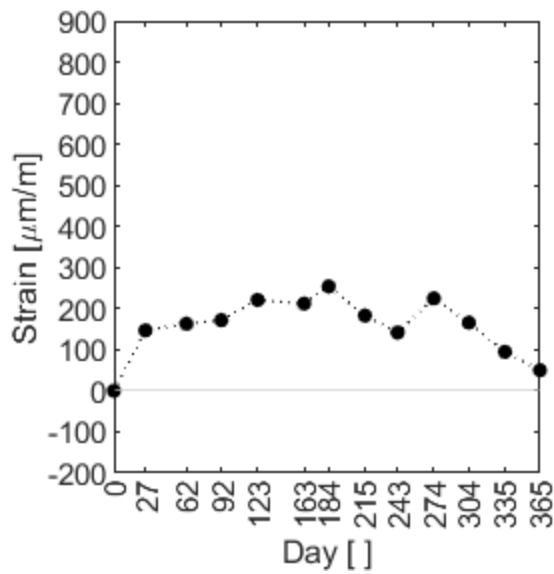


Figure C.103 – C.IV.3

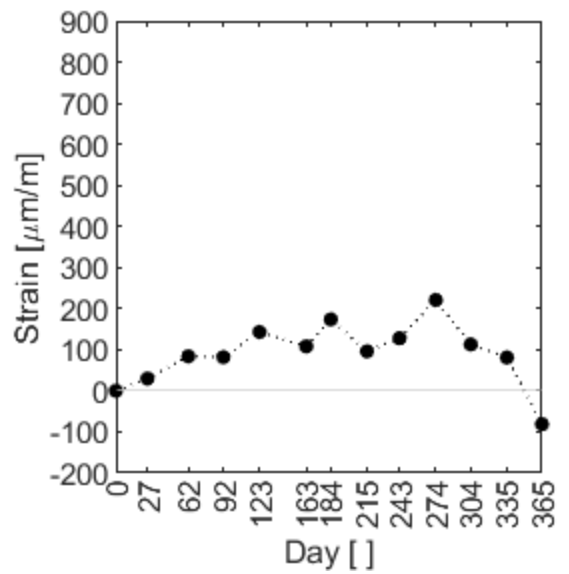


Figure C.104 – C.IV.4

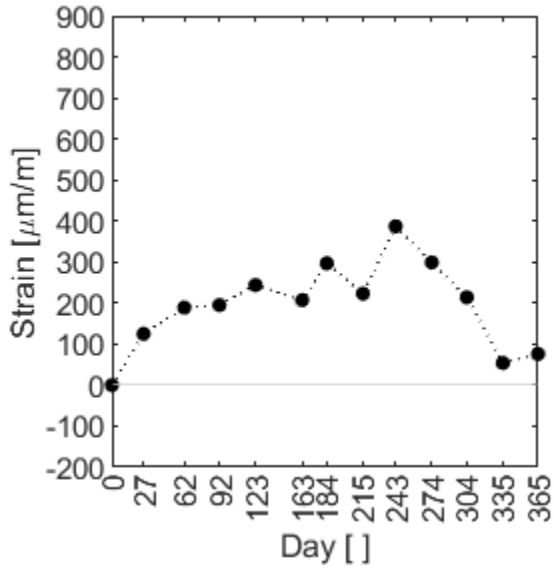


Figure C.105 – C.V.1

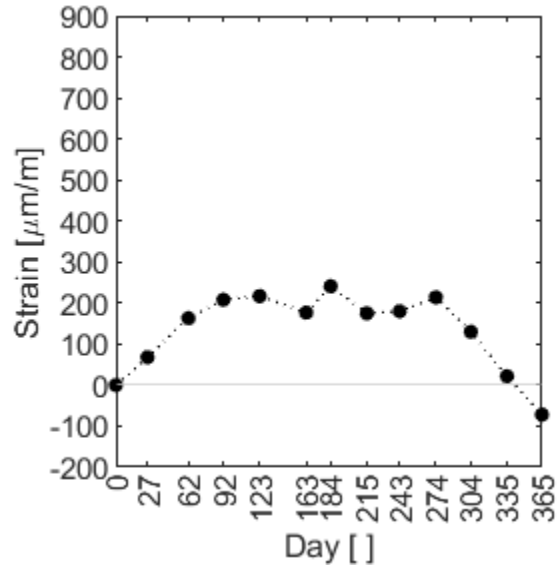


Figure C.106 – C.V.2

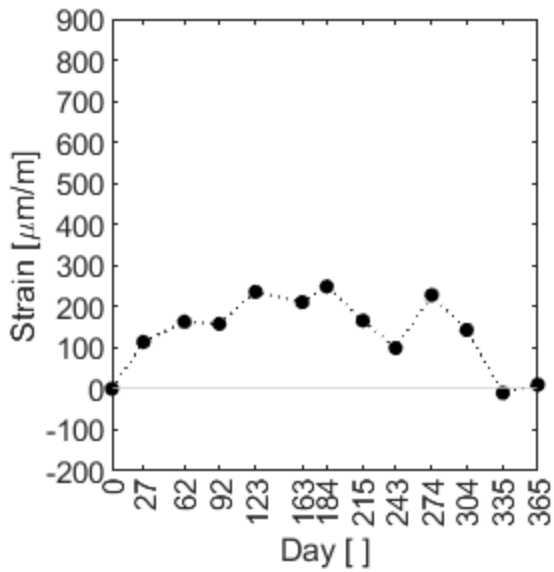


Figure C.107 – C.V.3

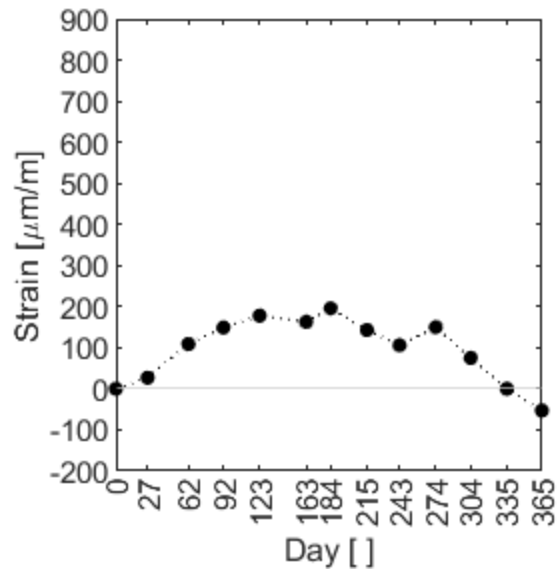


Figure C.108 – C.V.4

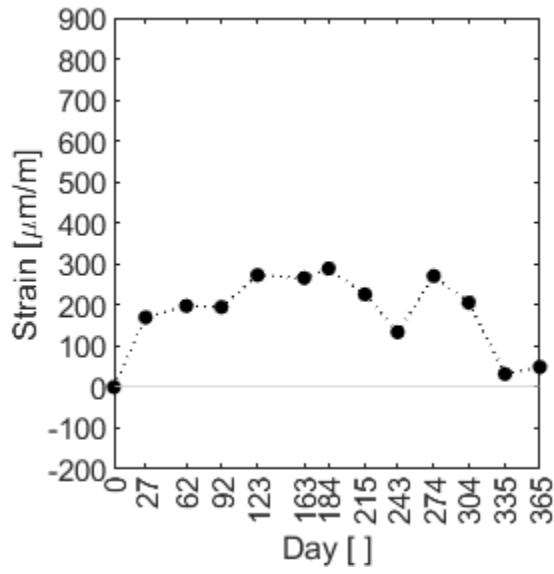


Figure C.109 – C.VI.1

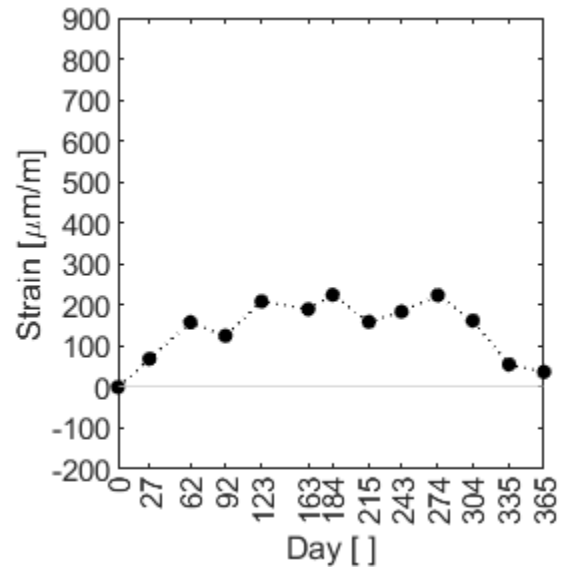


Figure C.110 – C.VI.2

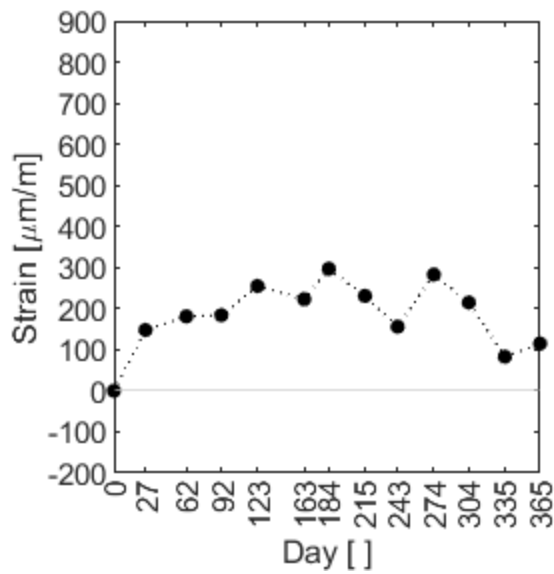


Figure C.111 – C.VI.3

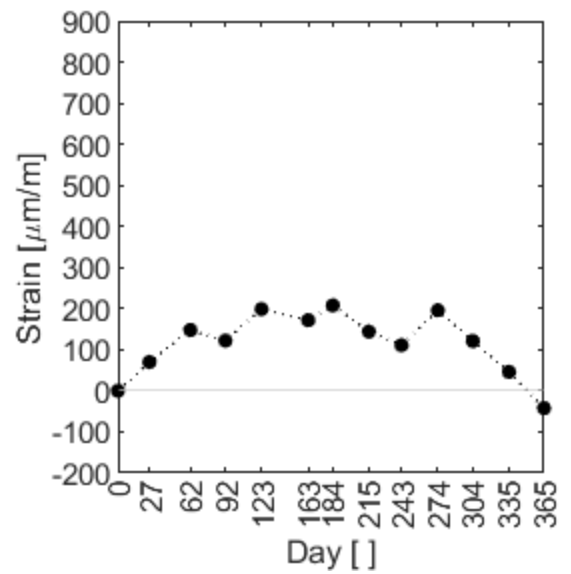


Figure C.112 – C.VI.4

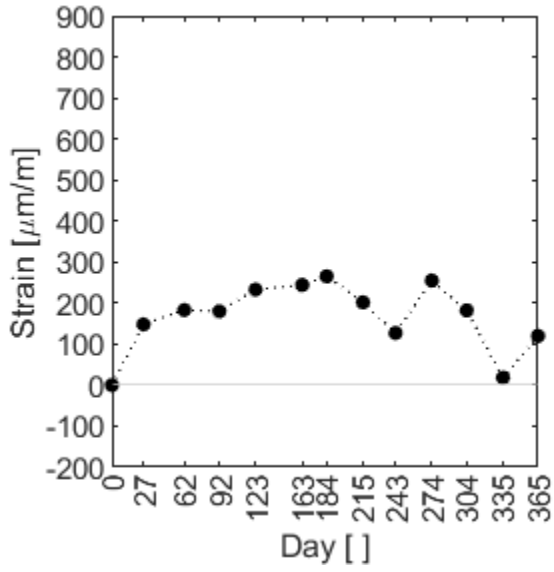


Figure C.113 – C.VII.1

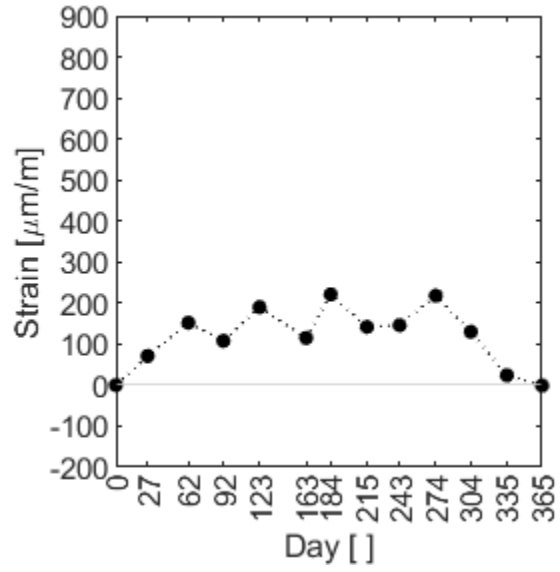


Figure C.114 – C.VII.2

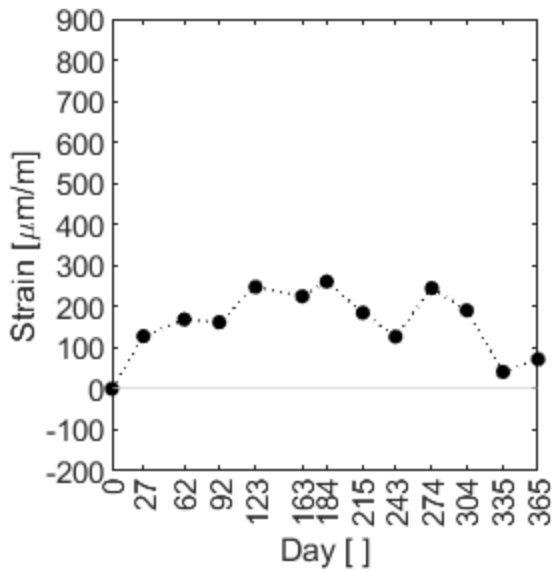


Figure C.115 – C.VII.3

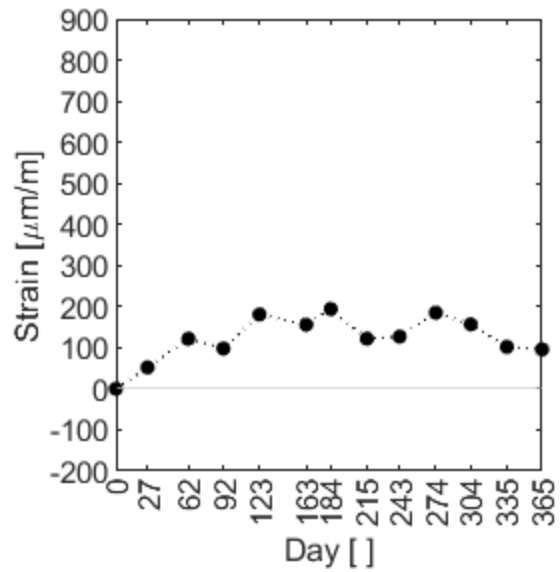


Figure C.116 – C.VII.4



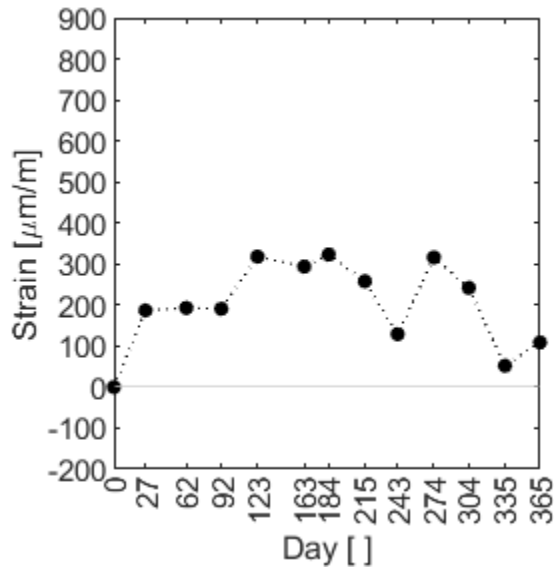


Figure C.117 – C.VIII.1

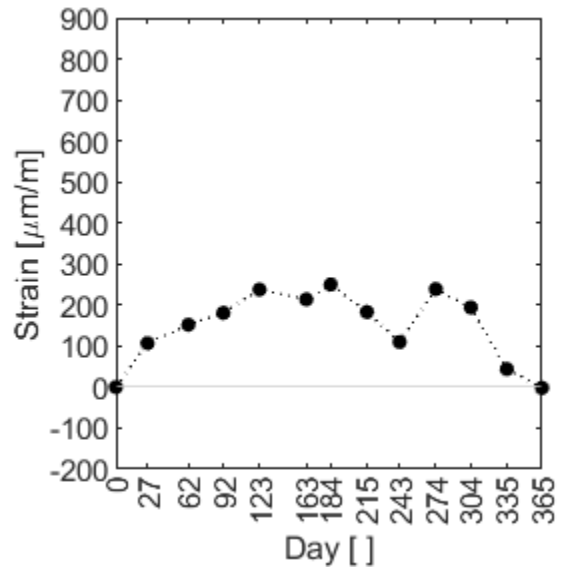


Figure C.118 – C.VIII.2

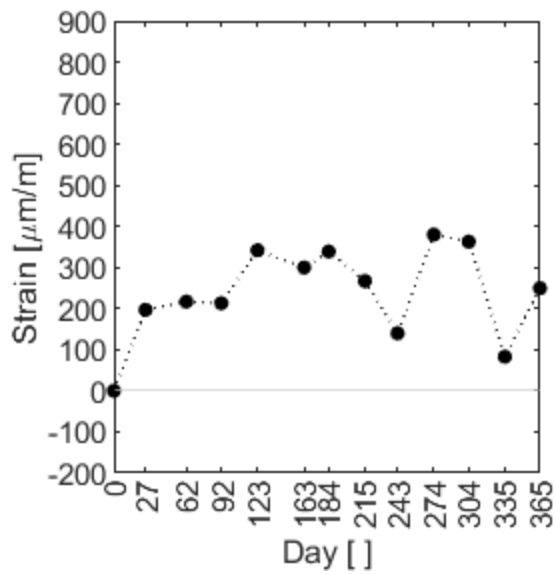


Figure C.119 – C.VIII.3

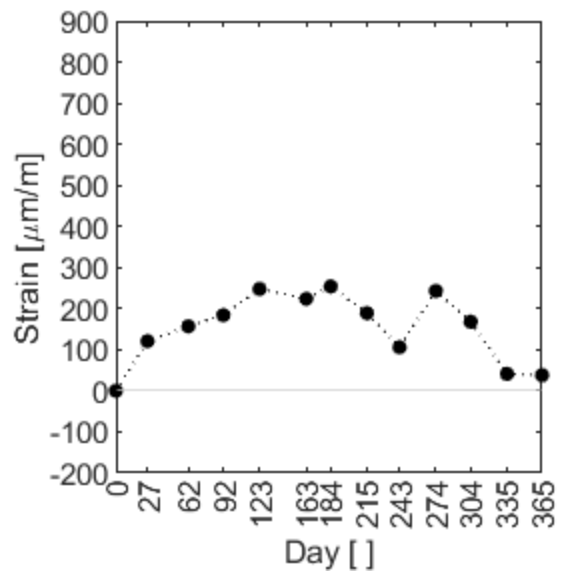


Figure C.120 – C.VIII.4

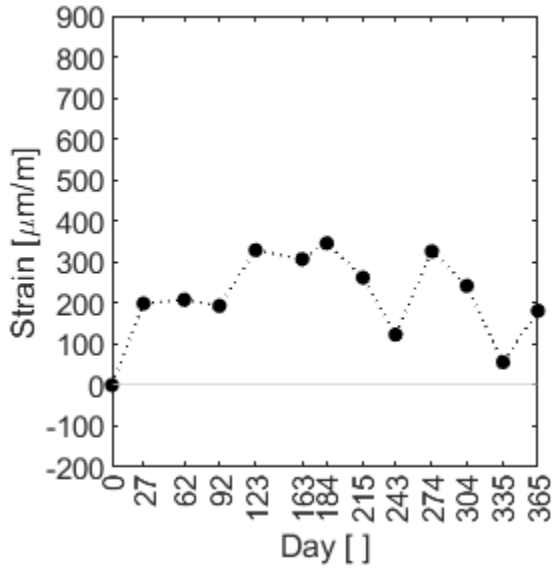


Figure C.121 – C.IX.1

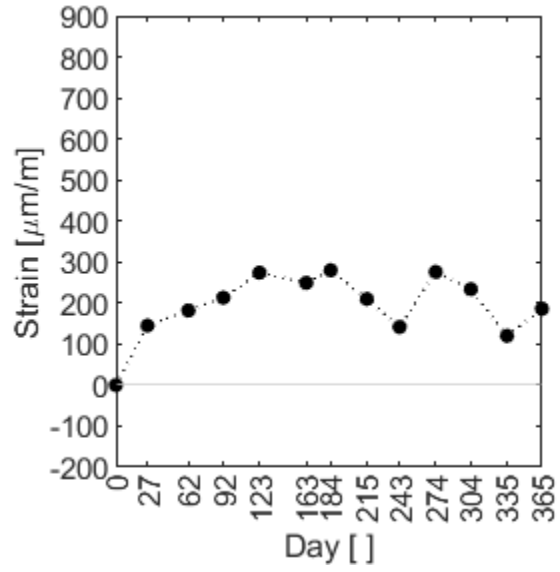


Figure C.122 – C.IX.2

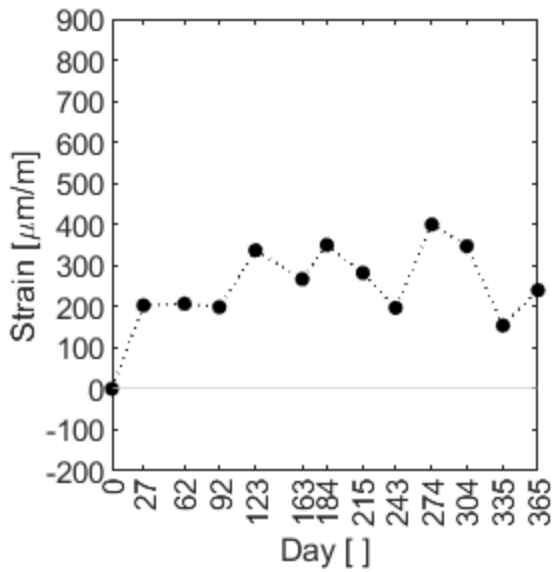


Figure C.123 – C.IX.3

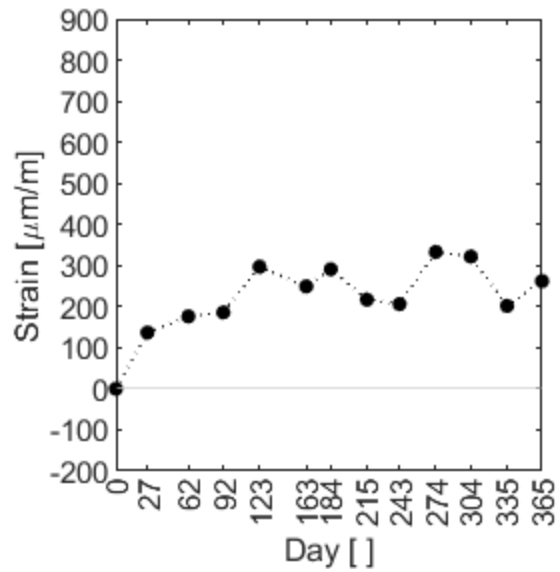


Figure C.124 – C.IX.4

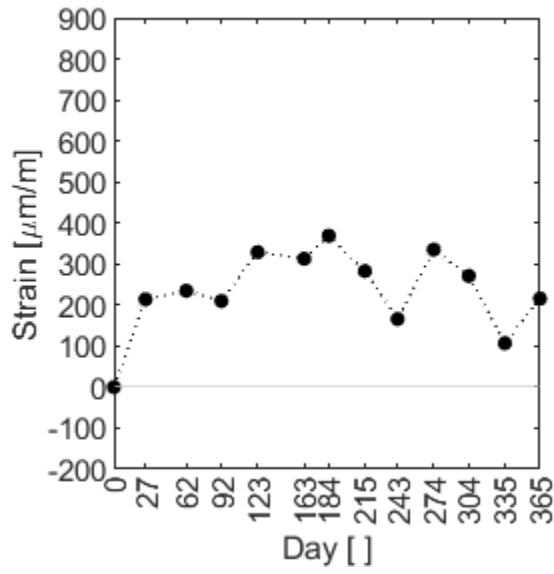


Figure C.125 – C.X.1

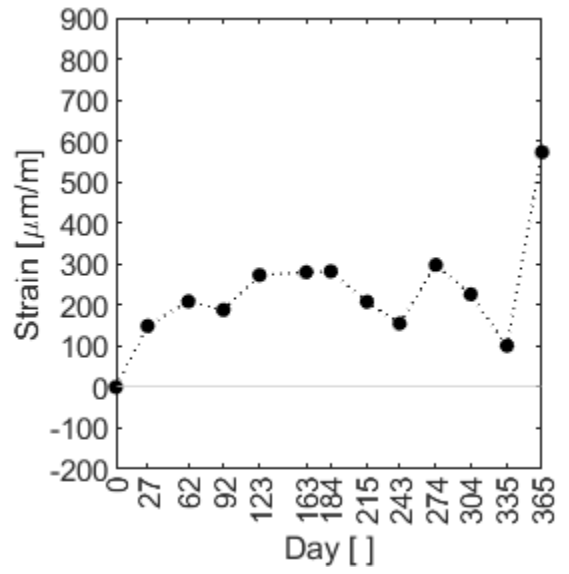


Figure C.126 – C.X.2

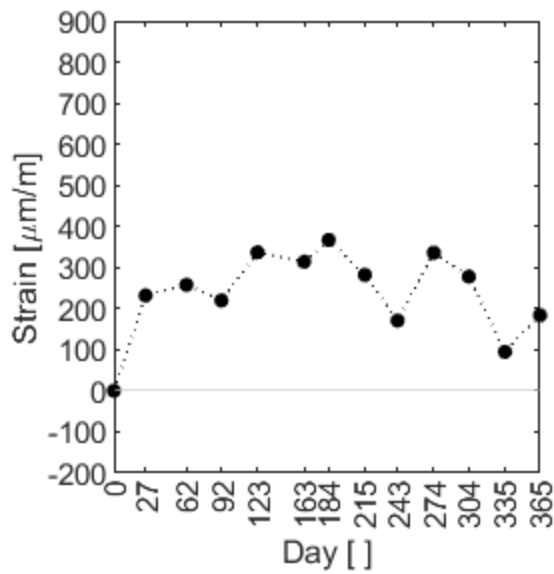


Figure C.127 – C.X.3

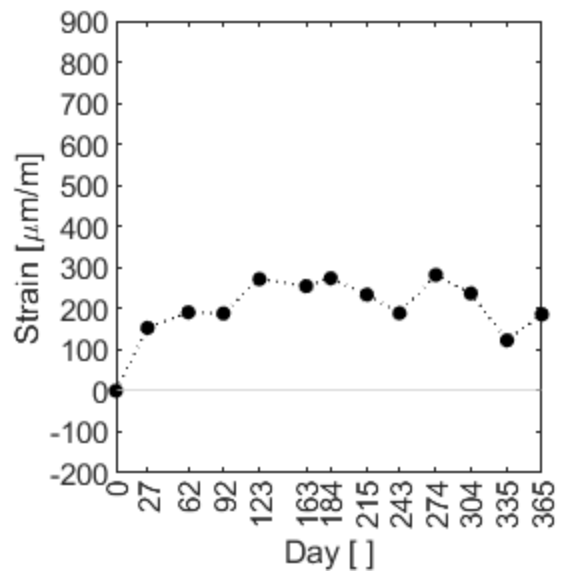


Figure C.128 – C.X.4

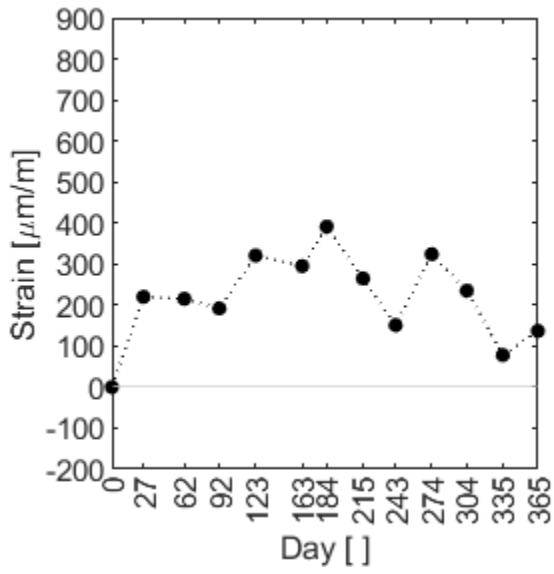


Figure C.129 – C.XI.1

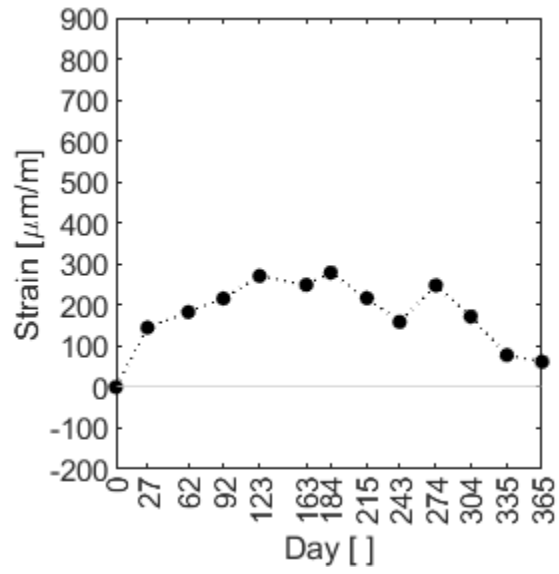


Figure C.130 – C.XI.2

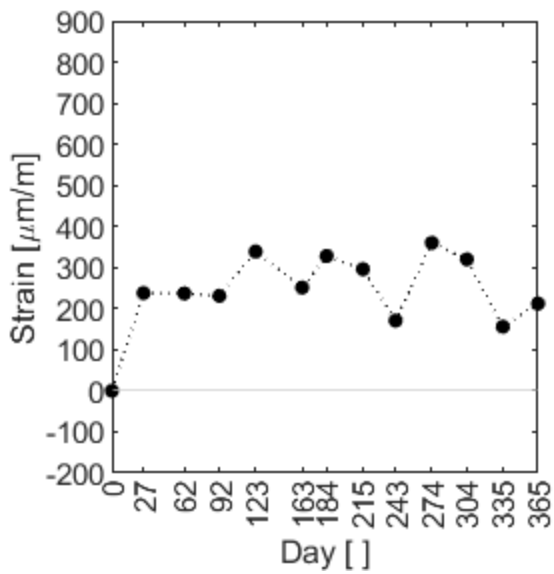


Figure C.131 – C.XI.3

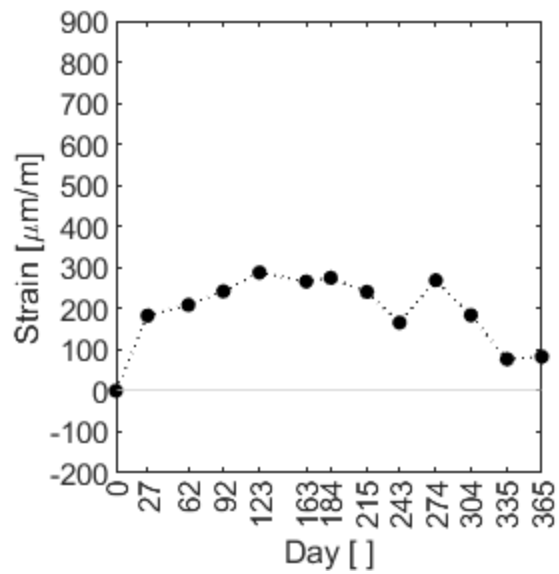


Figure C.132 – C.XI.4

## C.2 Bezprávi

### C.2.1 Daily Recordings

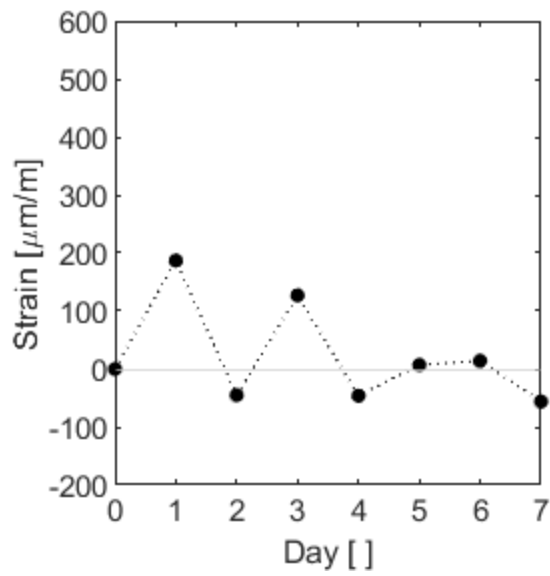


Figure C.133 – D.I.1

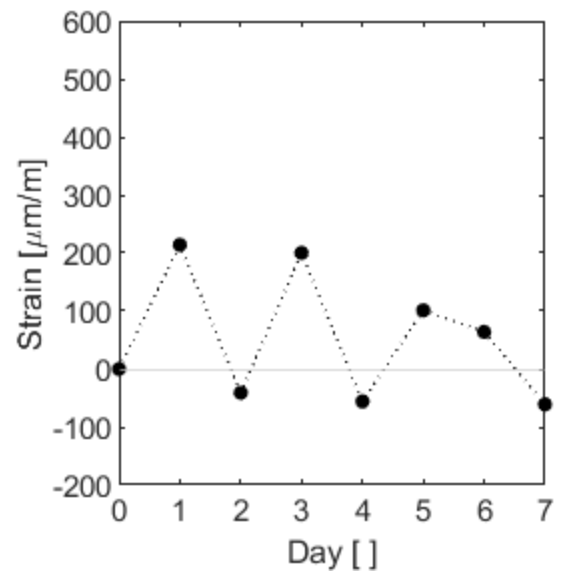


Figure C.134 – D.I.2

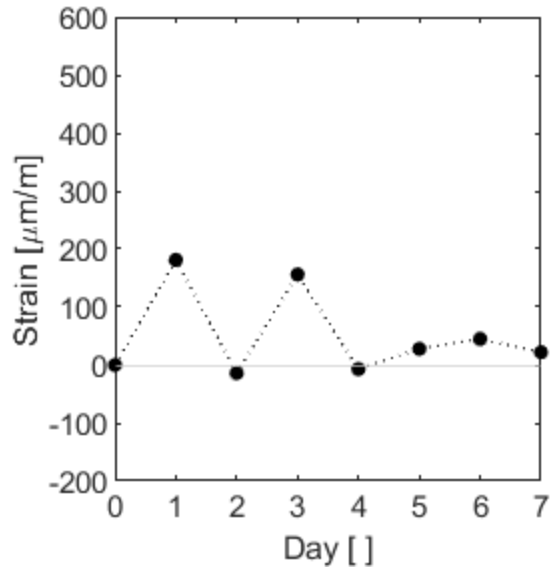


Figure C.135 – D.I.3

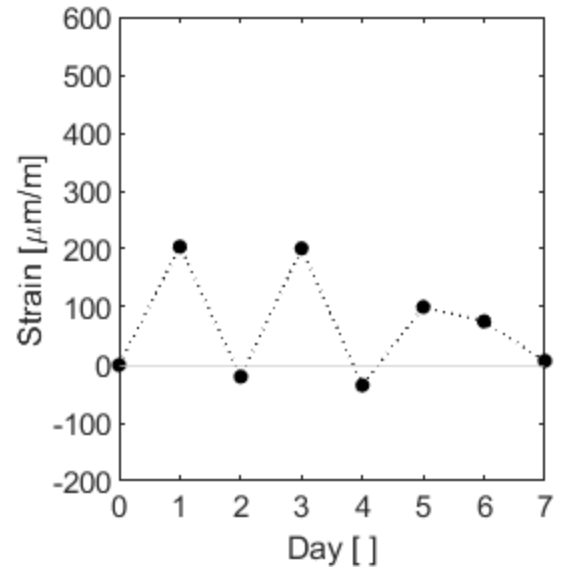


Figure C.136 – D.I.4

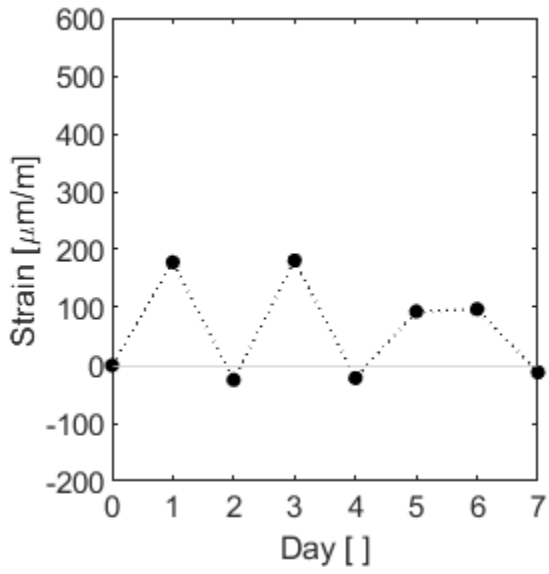


Figure C.137 – D.II.1

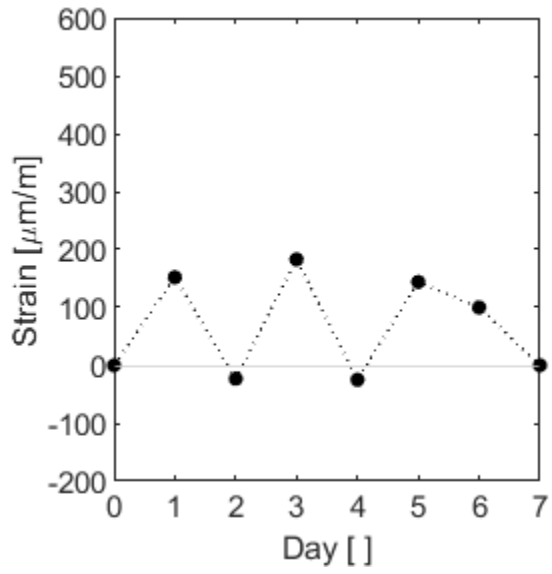


Figure C.138 – D.II.2

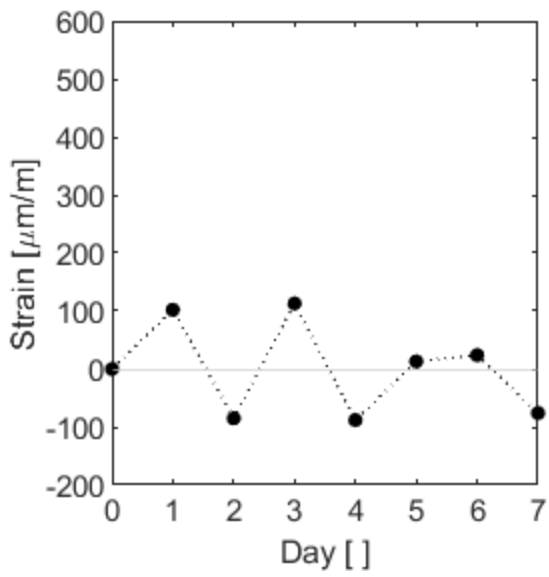


Figure C.139 – D.II.3

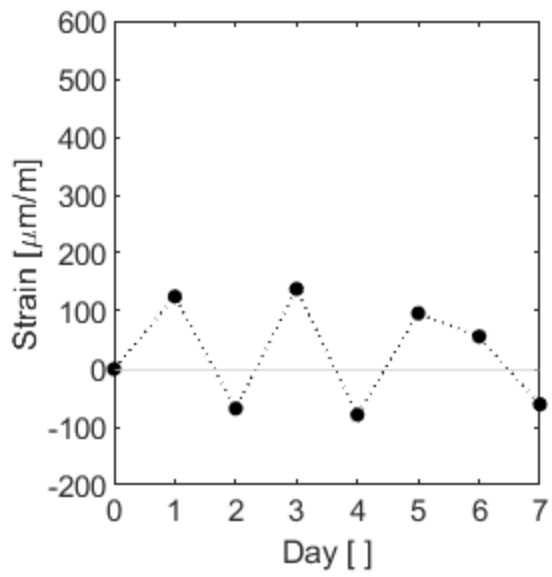


Figure C.140 – D.II.4

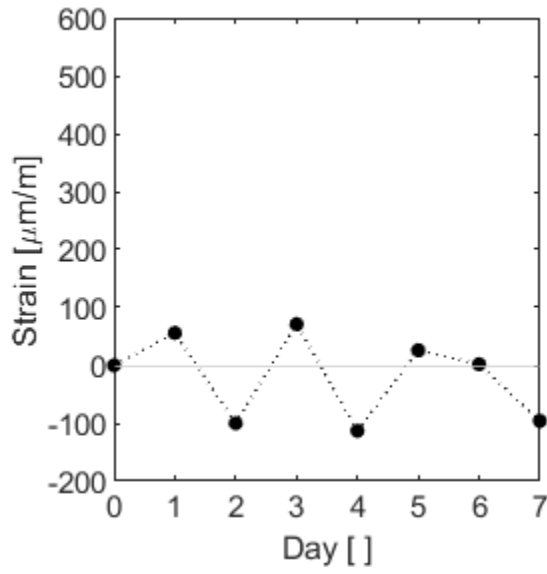


Figure C.141 – D.III.1

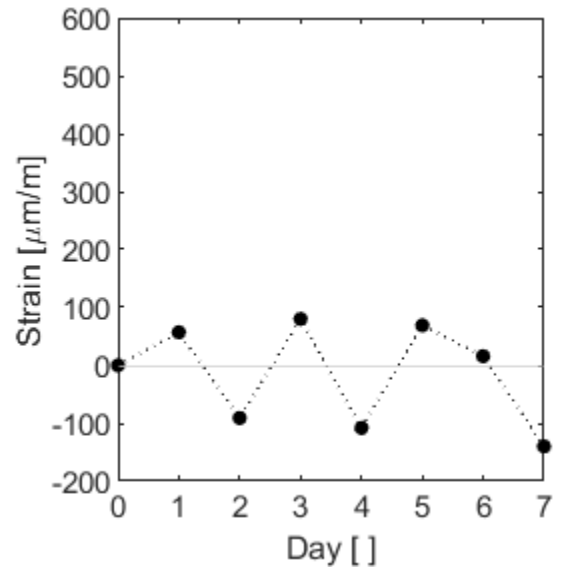


Figure C.142 – D.III.2

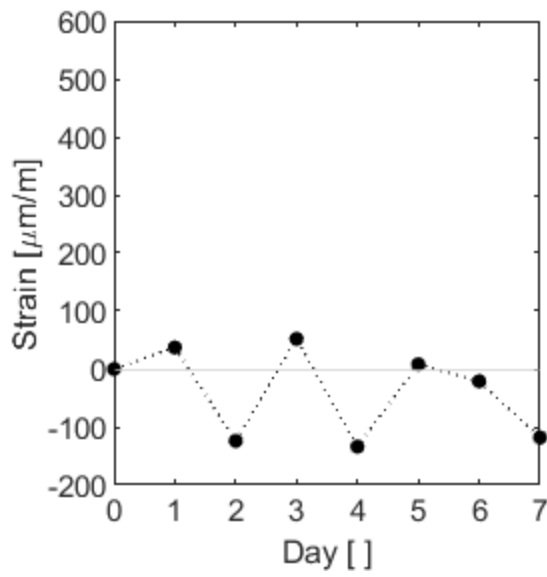


Figure C.143 – D.III.3

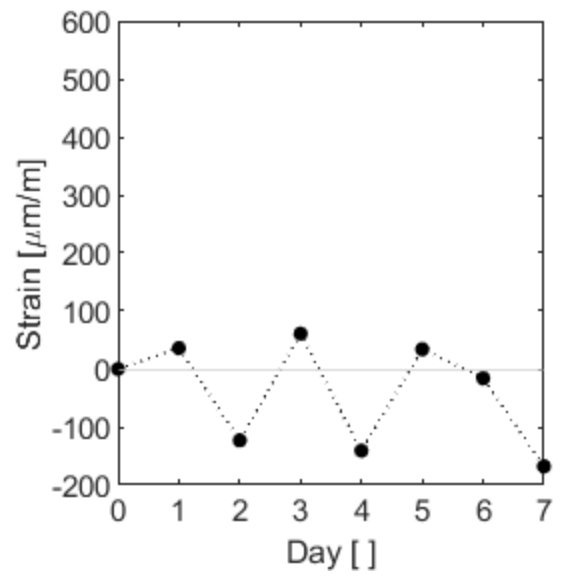


Figure C.144 – D.III.4

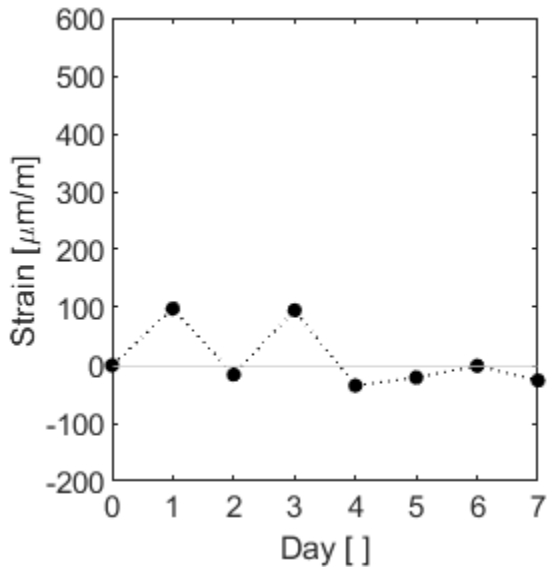


Figure C.145 – D.IV.1

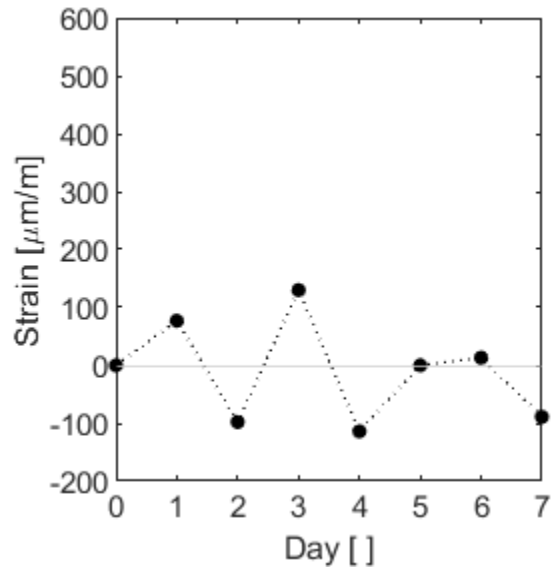


Figure C.146 – D.IV.2

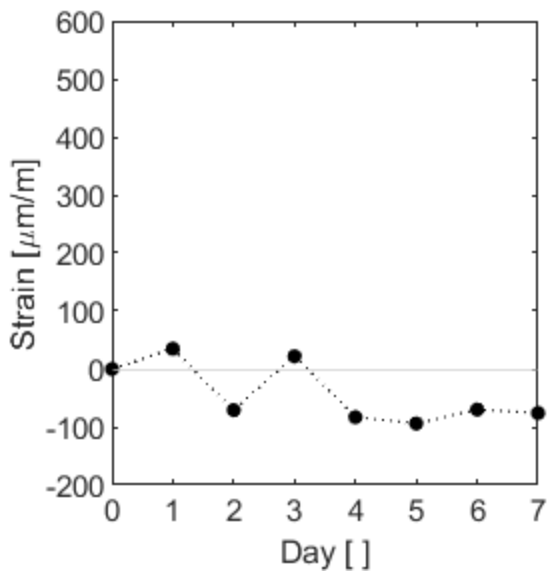


Figure C.147 – D.IV.3

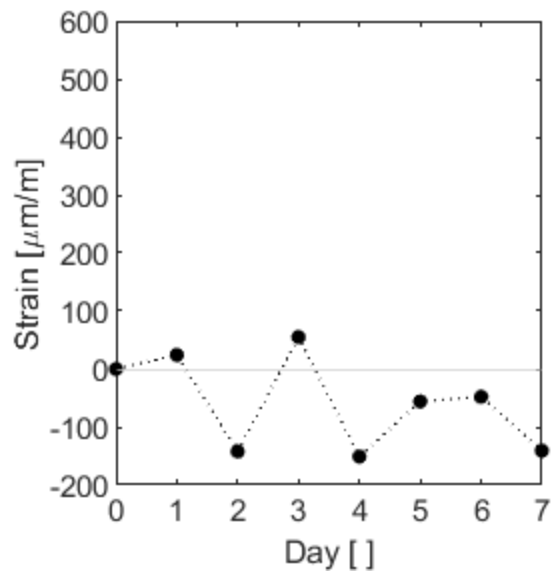


Figure C.148 – D.IV.4



## C.2.2 Weekly Recordings

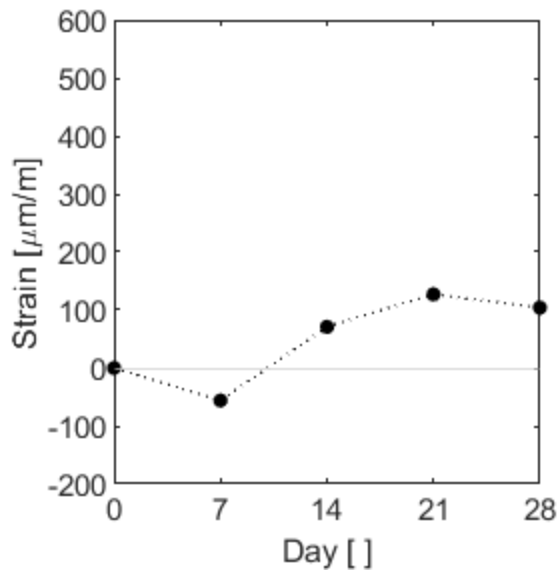


Figure C.149 – D.I.1

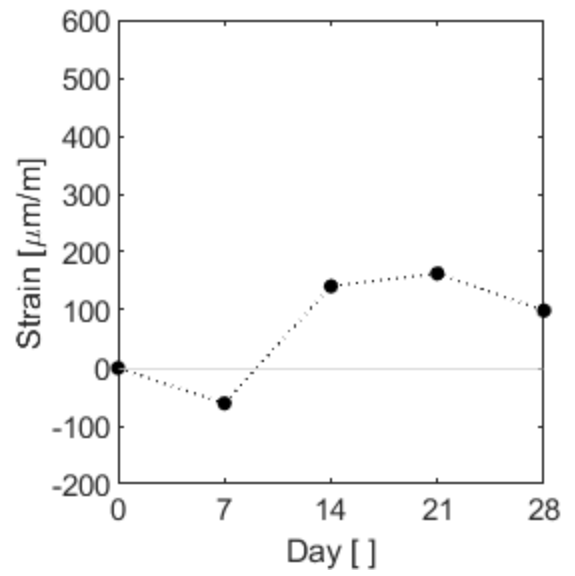


Figure C.150 – D.I.2

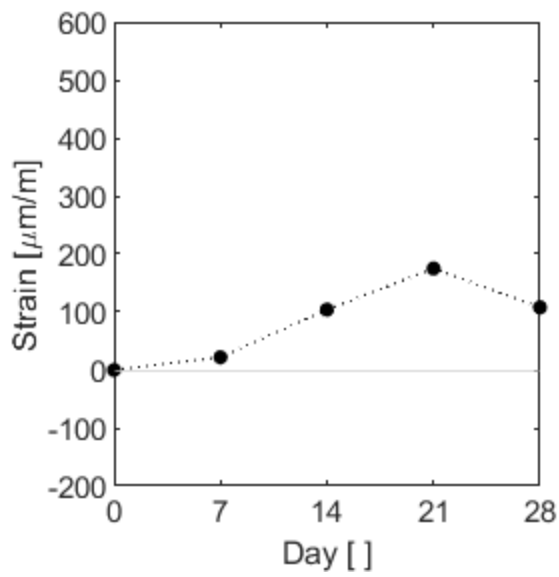


Figure C.151 – D.I.3

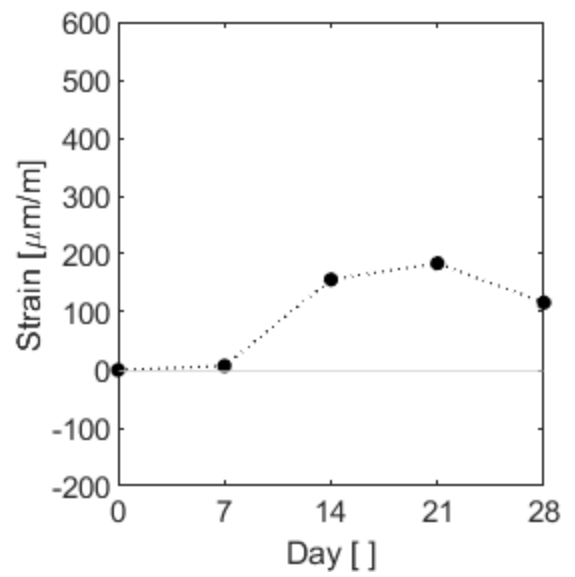


Figure C.152 – D.I.4

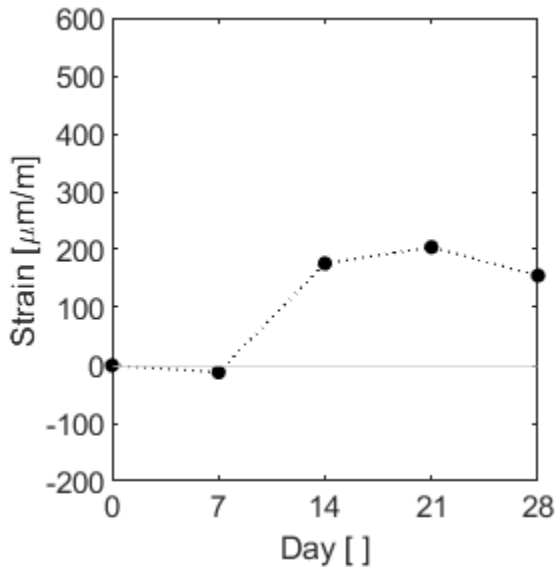


Figure C.153 – D.II.1

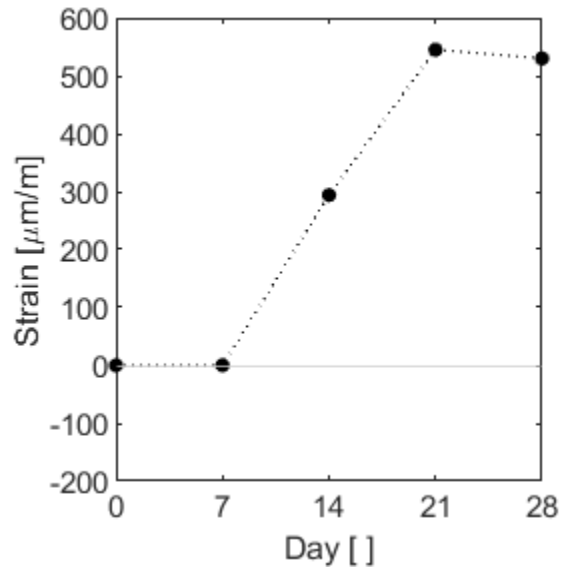


Figure C.154 – D.II.2

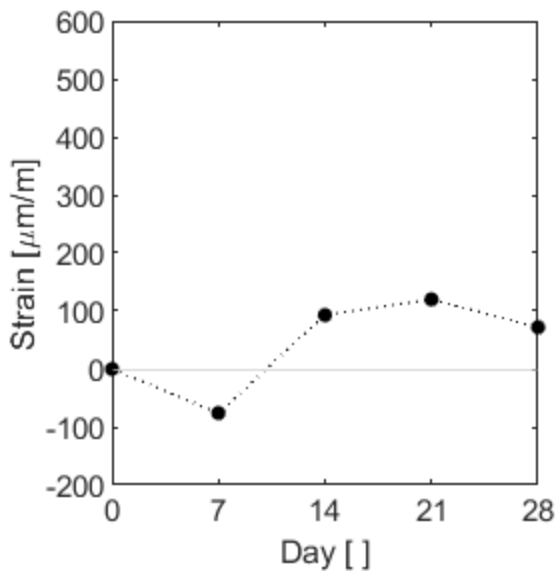


Figure C.155 – D.II.3

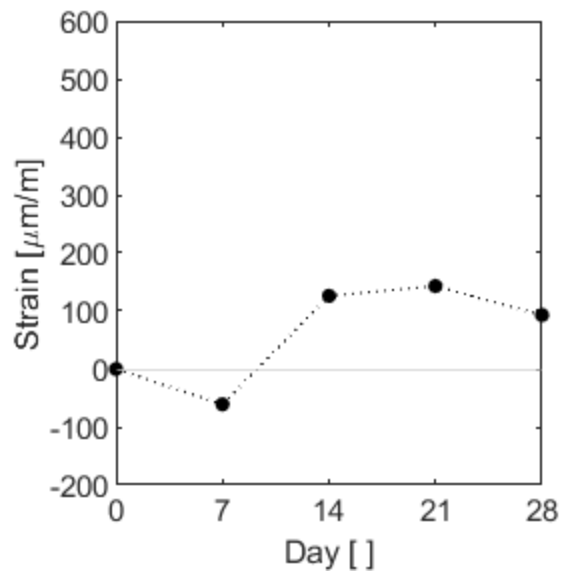


Figure C.156 – D.II.4

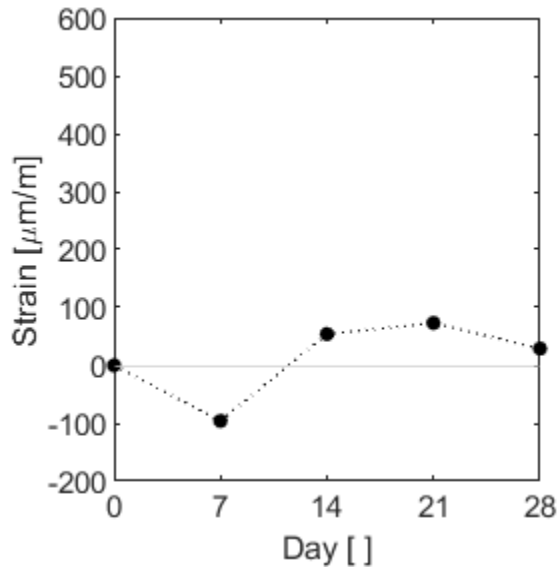


Figure C.157 – D.III.1

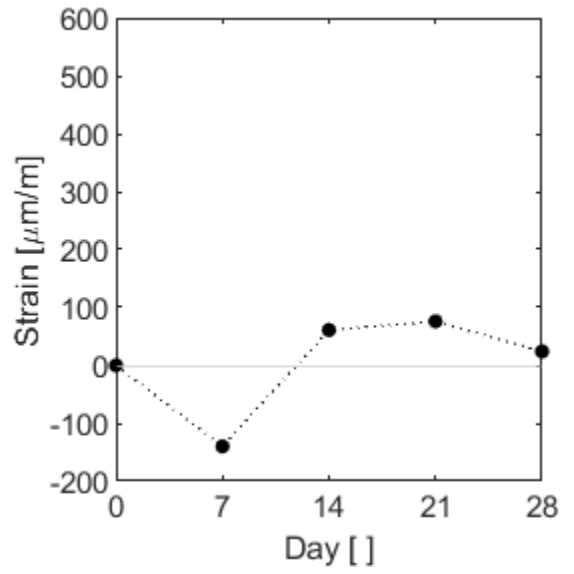


Figure C.158 – D.III.2

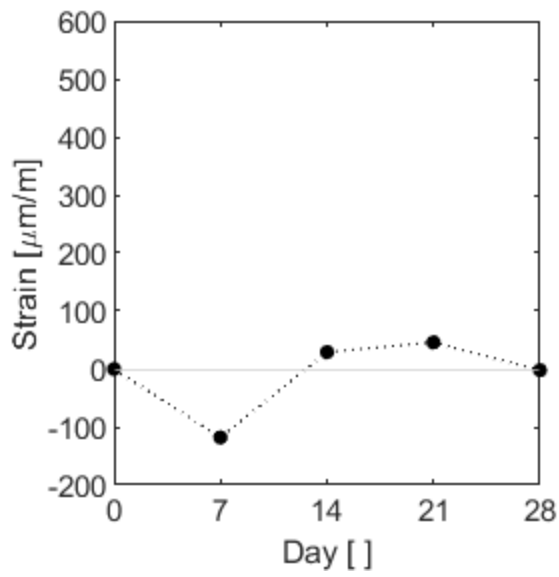


Figure C.159 – D.III.3

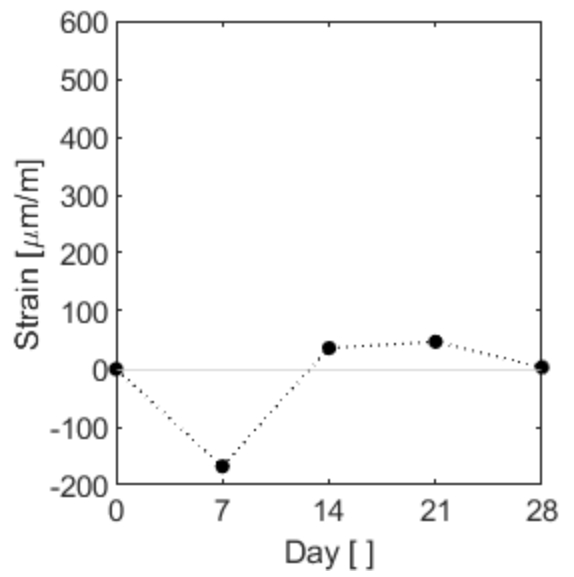


Figure C.160 – D.III.4

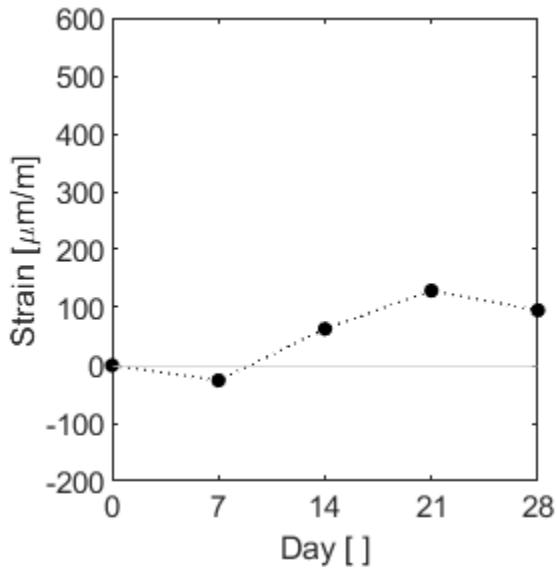


Figure C.161 – D.IV.1

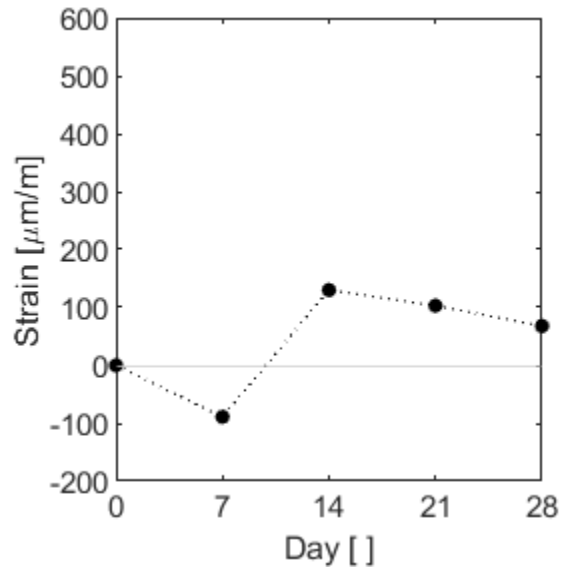


Figure C.162 – D.IV.2

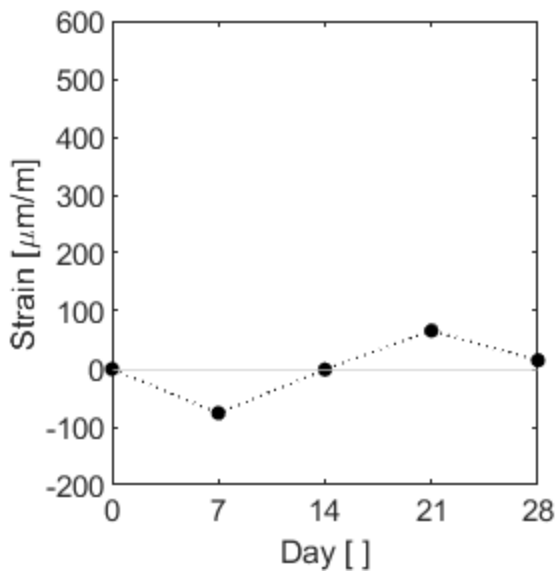


Figure C.163 – D.IV.3

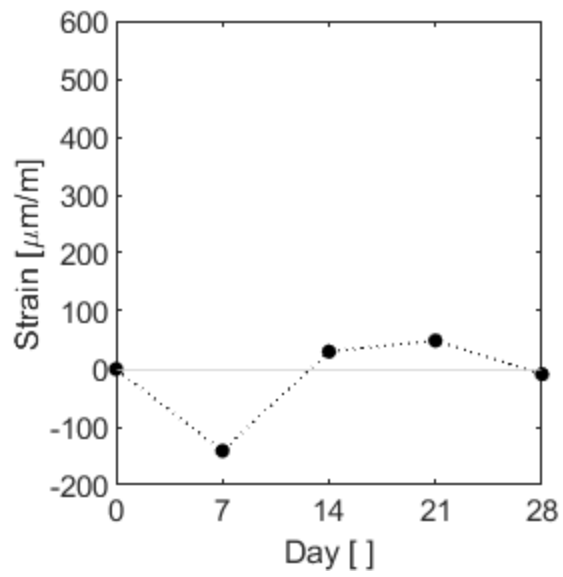


Figure C.164 – D.IV.4

### C.2.3 Monthly Recordings

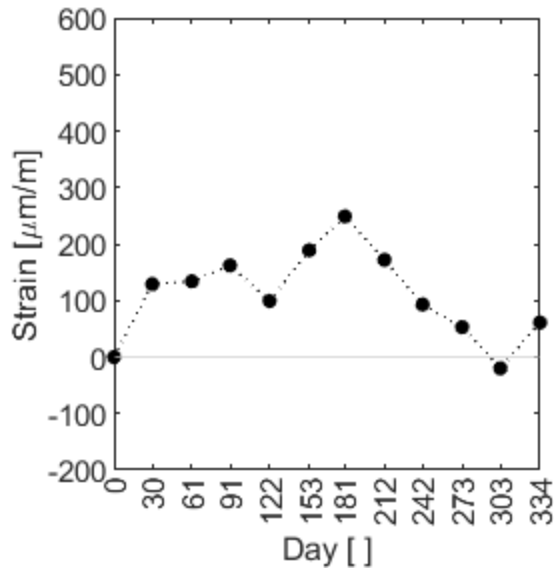


Figure C.165 – D.I.1

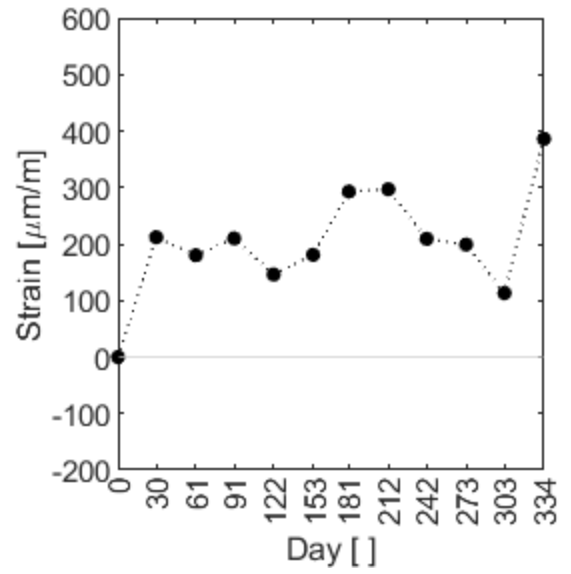


Figure C.166 – D.I.2

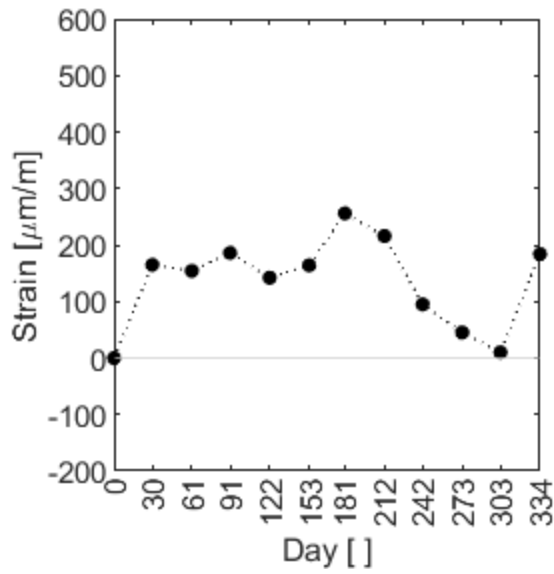


Figure C.167 – D.I.3

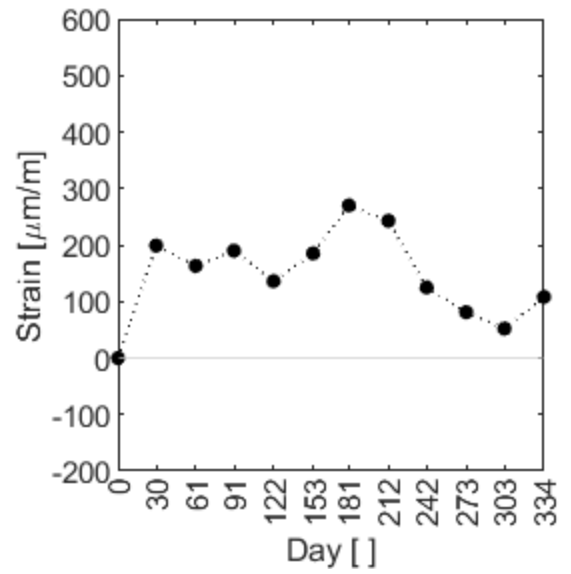


Figure C.168 – D.I.4

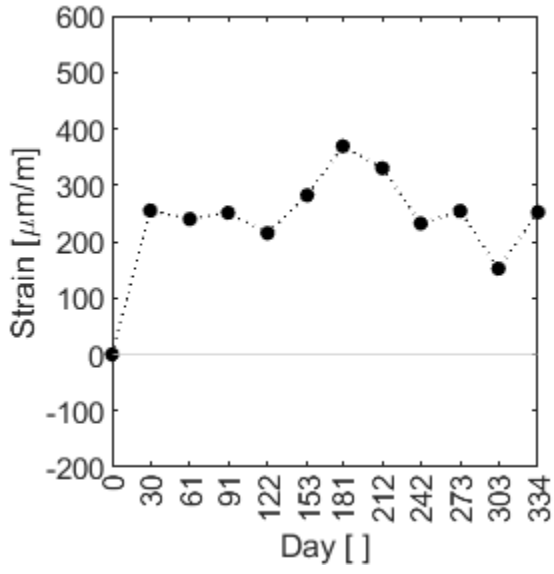


Figure C.169 – D.II.1

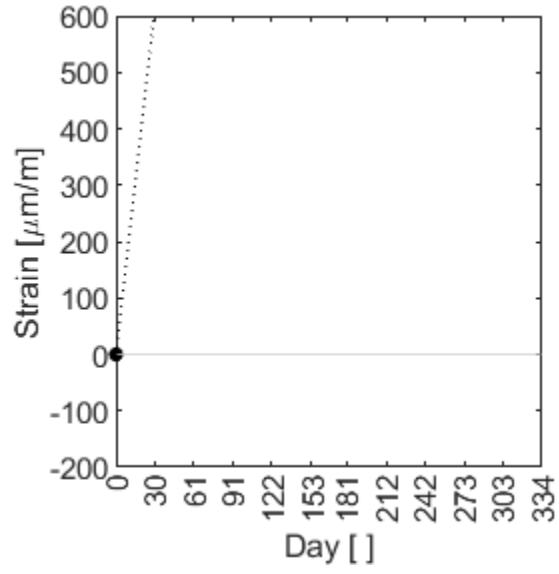


Figure C.170 – D.II.2

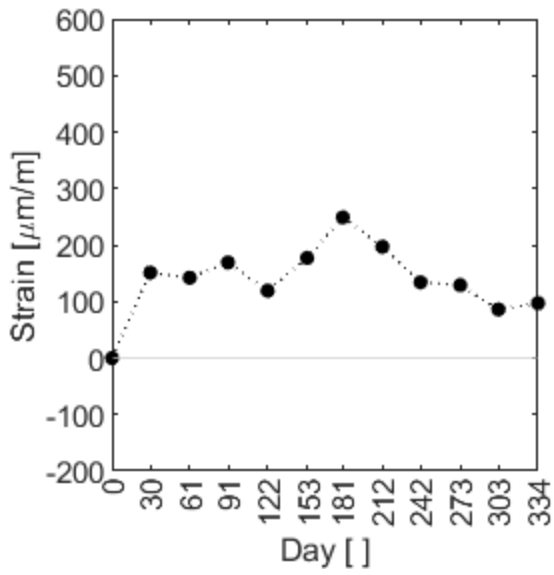


Figure C.171 – D.II.3

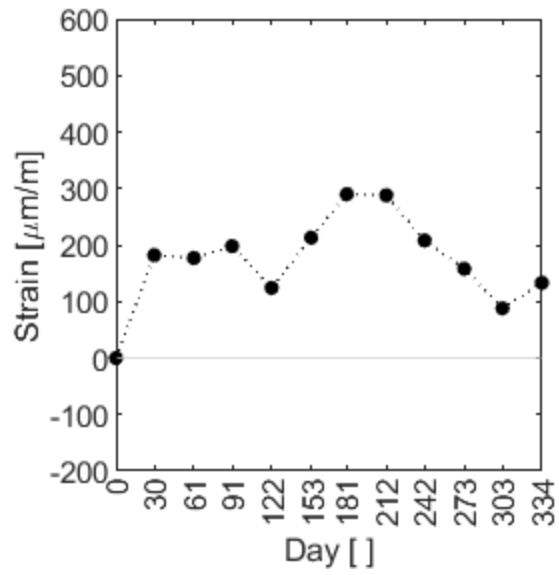


Figure C.172 – D.II.4

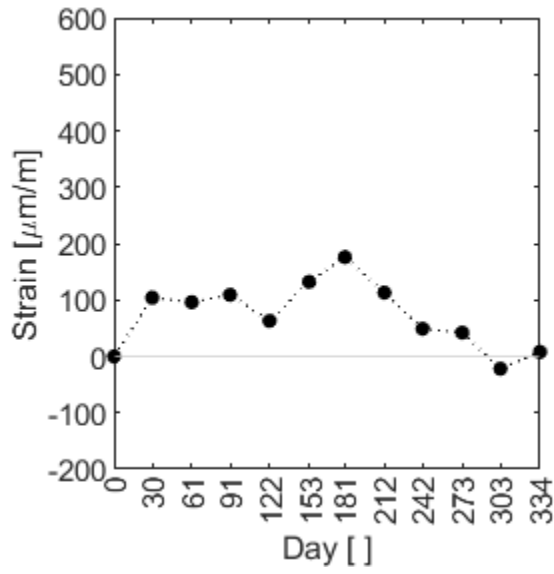


Figure C.173 – D.III.1

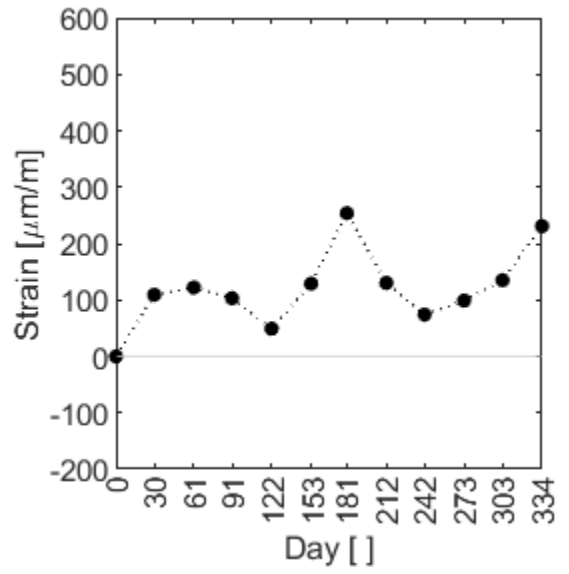


Figure C.174 – D.III.2

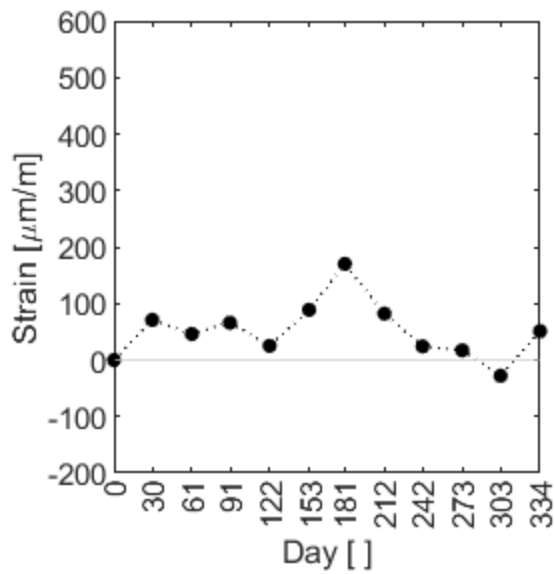


Figure C.175 – D.III.3

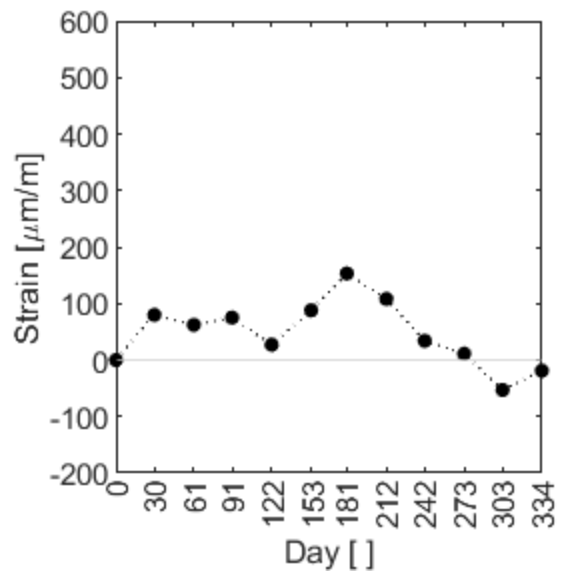


Figure C.176 – D.III.4

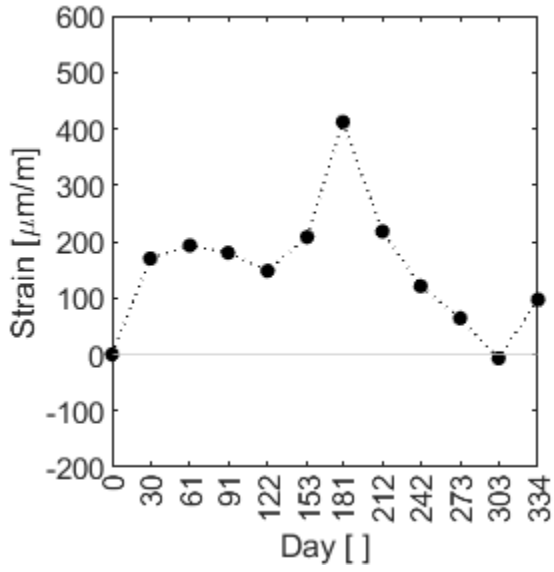


Figure C.177 – D.IV.1

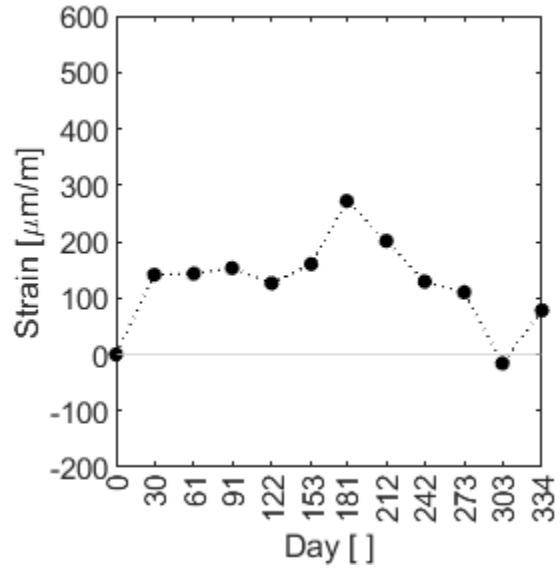


Figure C.178 – D.IV.2

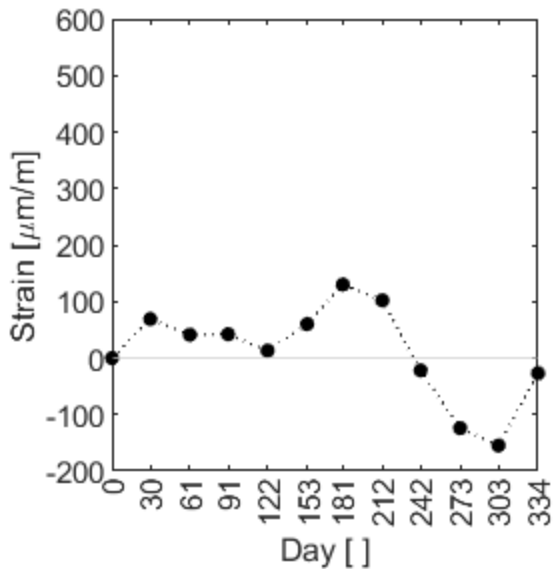


Figure C.179 – D.IV.3

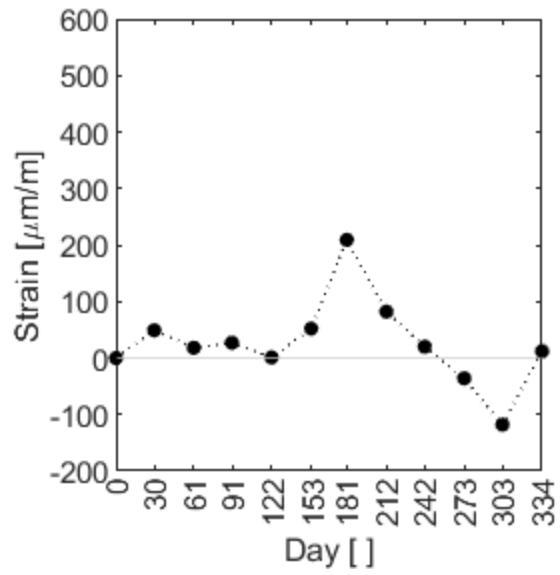


Figure C.180 – D.IV.4



## Appendix D

# Relation of Strain and Temperature

The relation of the measured strain in the CWR and the measured rail temperature from every measurement was calculated for each measuring spot from the data obtained within the period of the daily measurement frequency and from the complete monitoring period. The data is presented in this appendix. The marking of the record is the same like in the case of Appendix C.

In this appendix, the data from each monitoring period are presented next to each other for a better comparison of the trend line equation change based on the selected database. The daily measurement period database is presented in the left-hand side column and the complete monitoring period database is presented in the right-hand side column.

## D.1 Chotěvice

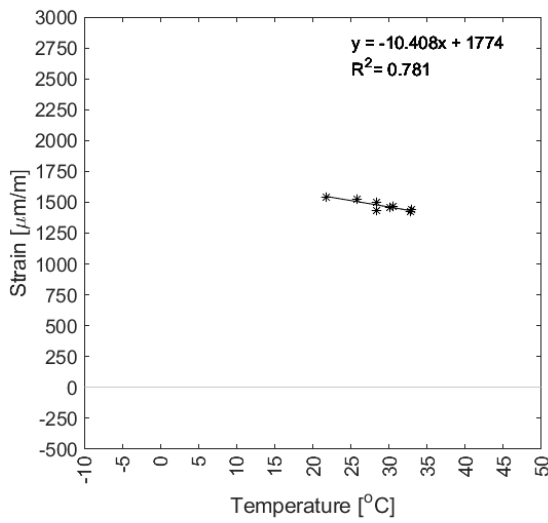


Figure D.1 – C.I.1 – Daily Measurement Period Database

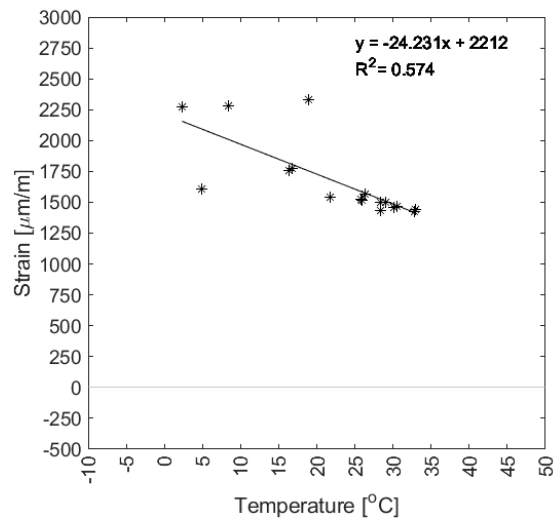


Figure D.2 – C.I.1 – Complete Monitoring Period Database

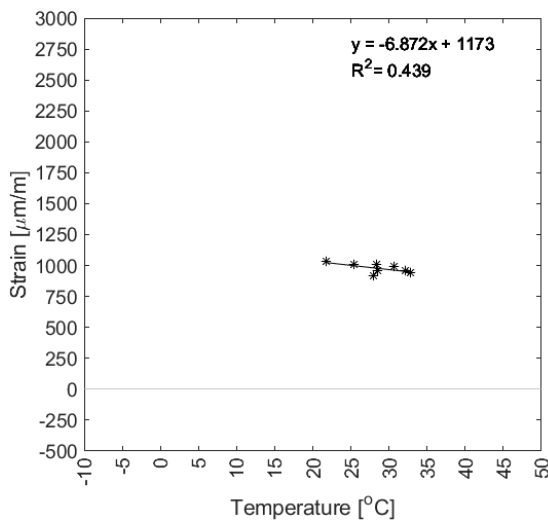


Figure D.3 – C.I.2 – Daily Measurement Period Database

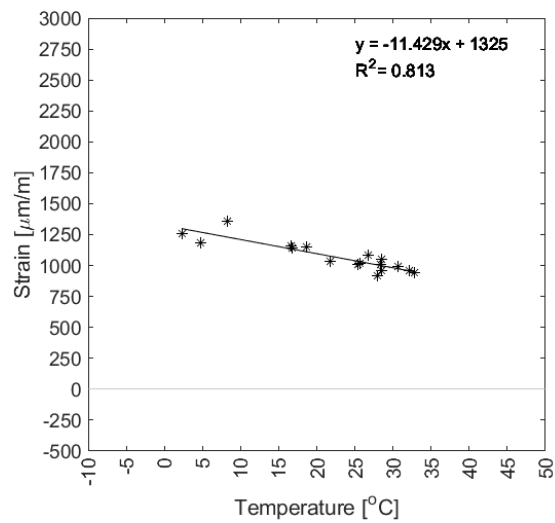
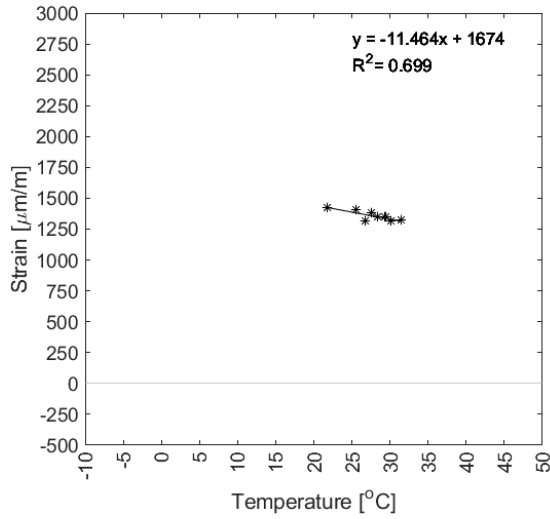
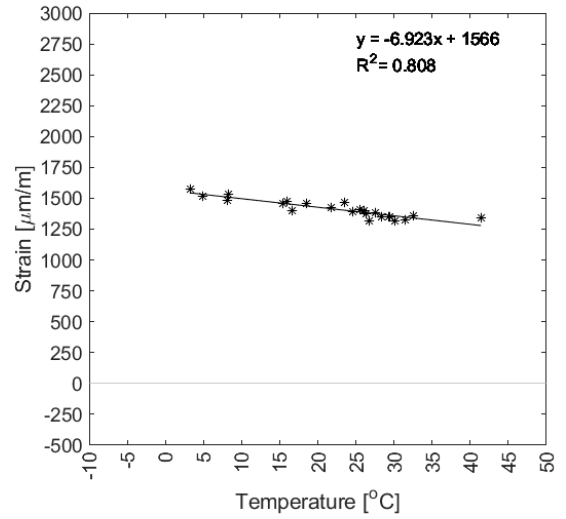


Figure D.4 – C.I.2 – Complete Monitoring Period Database



**Figure D.5** – C.I.3 – Daily Measurement Period Database



**Figure D.6** – C.I.3 – Complete Monitoring Period Database

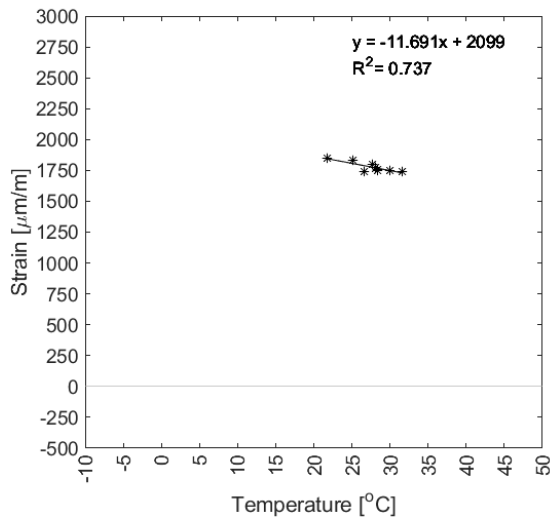


**Figure D.7** – C.I.4 – Daily Measurement Period Database

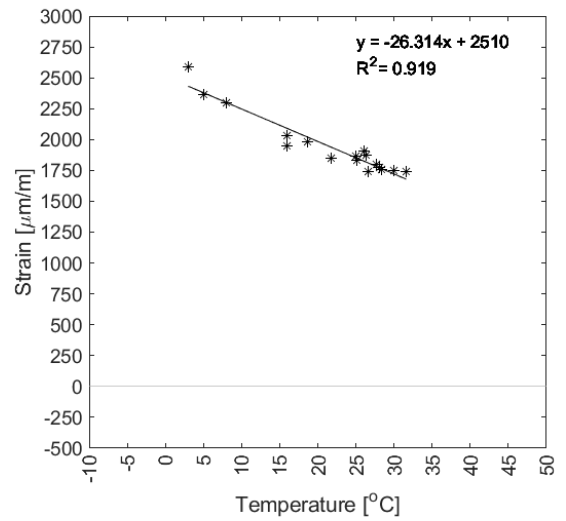


**Figure D.8** – C.I.4 – Complete Monitoring Period Database

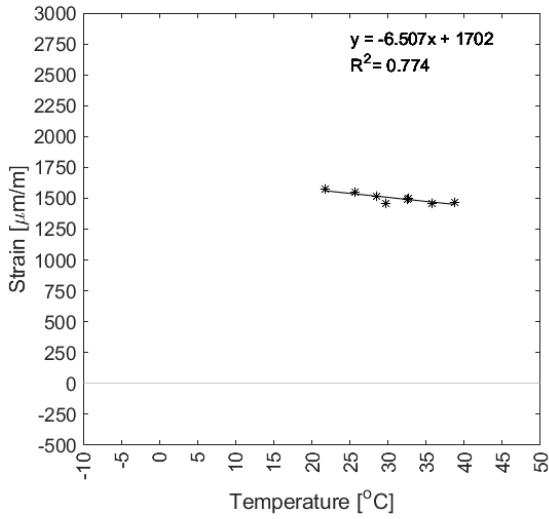


**Figure D.9** – C.II.1 – Daily Measurement Period Database

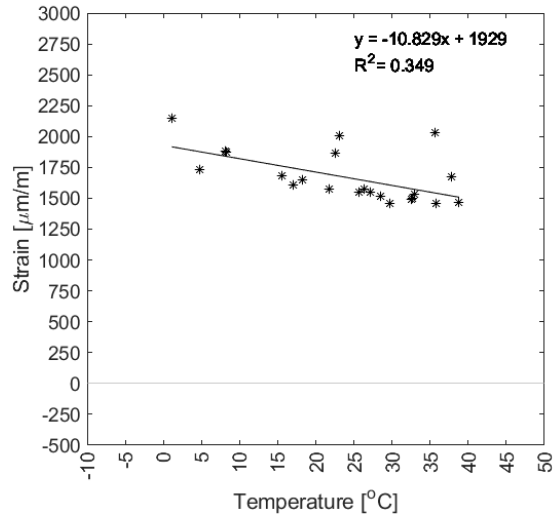


**Figure D.10** – C.II.1 – Complete Monitoring Period Database

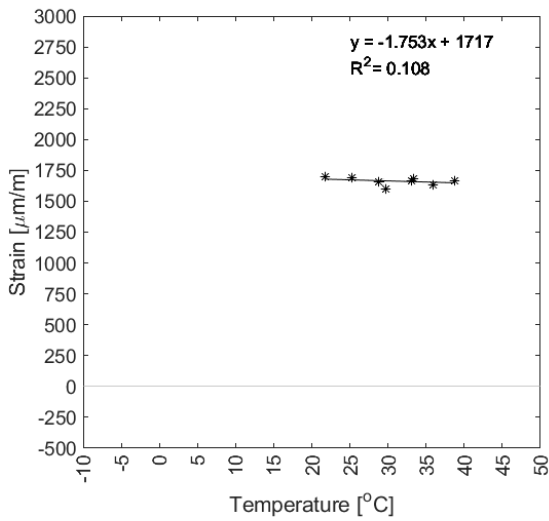


**Figure D.11** – C.II.2 – Daily Measurement Period Database

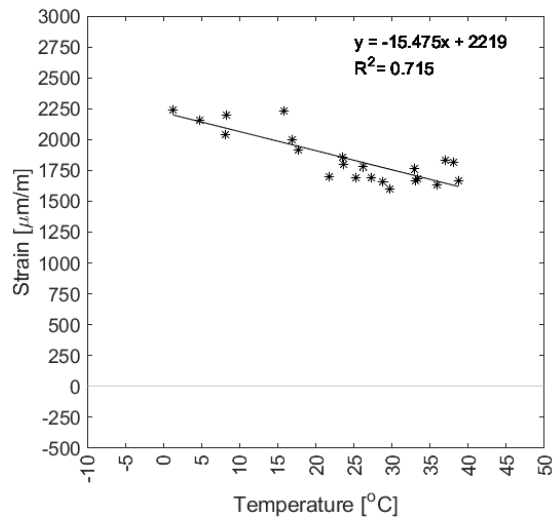


**Figure D.12** – C.II.2 – Complete Monitoring Period Database

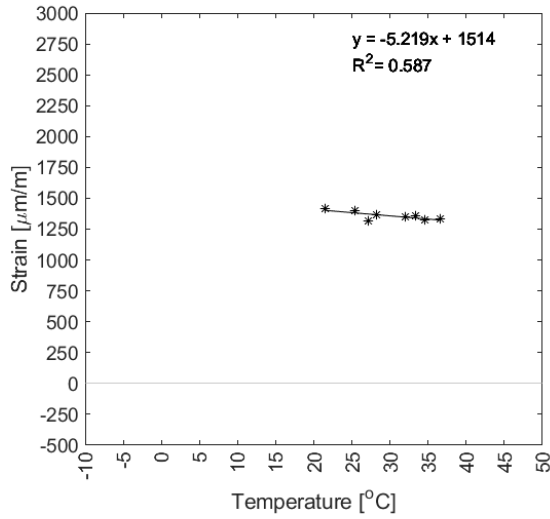


**Figure D.13** – C.II.3 – Daily Measurement Period Database

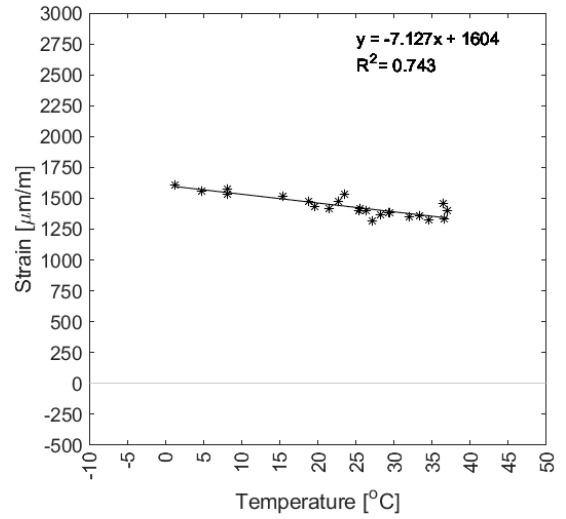


**Figure D.14** – C.II.3 – Complete Monitoring Period Database

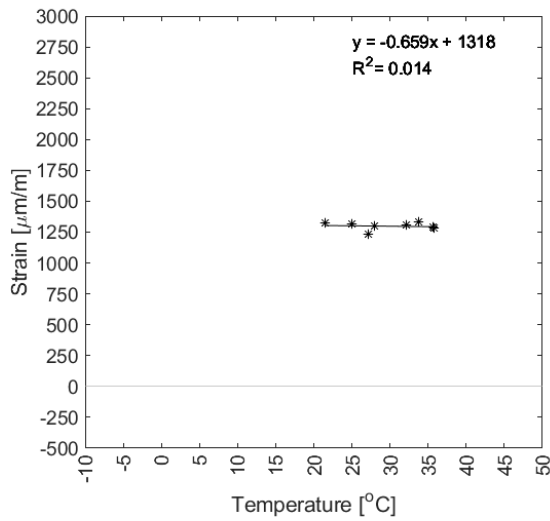


**Figure D.15** – C.II.4 – Daily Measurement Period Database

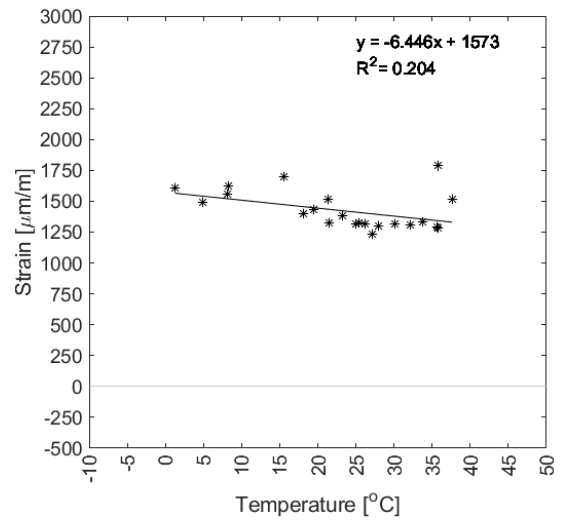


**Figure D.16** – C.II.4 – Complete Monitoring Period Database

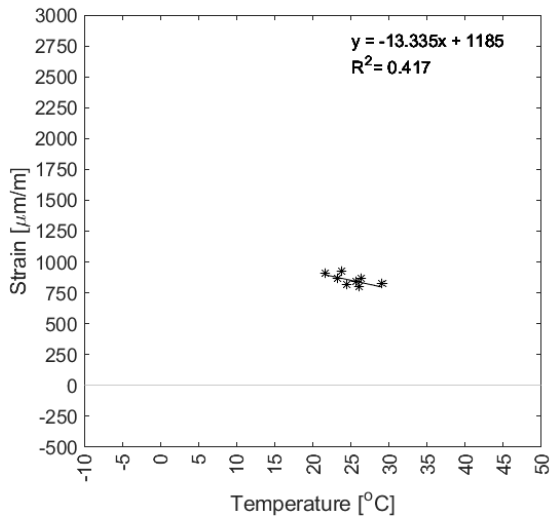


**Figure D.17** – C.III.1 – Daily Measurement Period Database

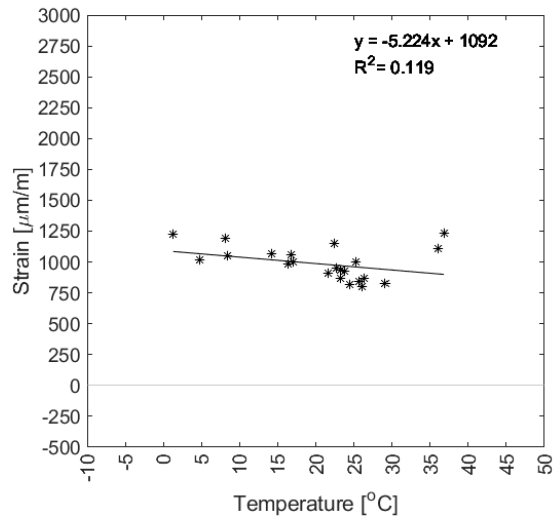


**Figure D.18** – C.III.1 – Complete Monitoring Period Database

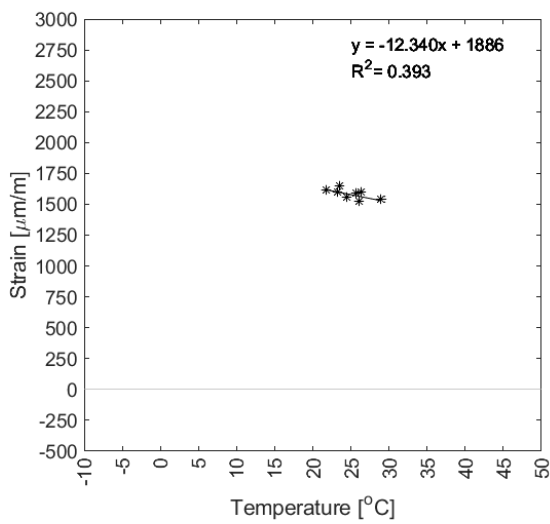


**Figure D.19** – C.III.2 – Daily Measurement Period Database

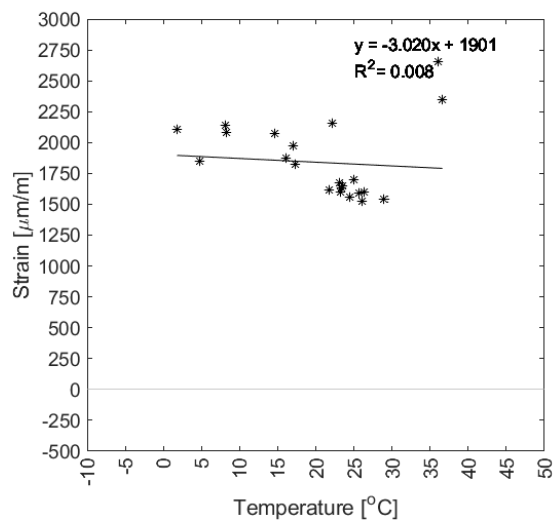


**Figure D.20** – C.III.2 – Complete Monitoring Period Database

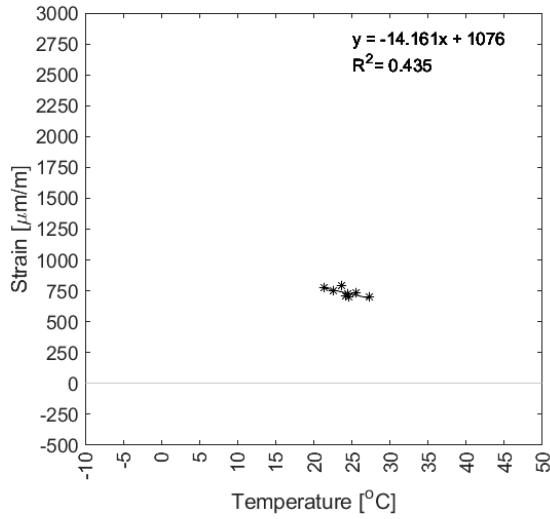


**Figure D.21** – C.III.3 – Daily Measurement Period Database

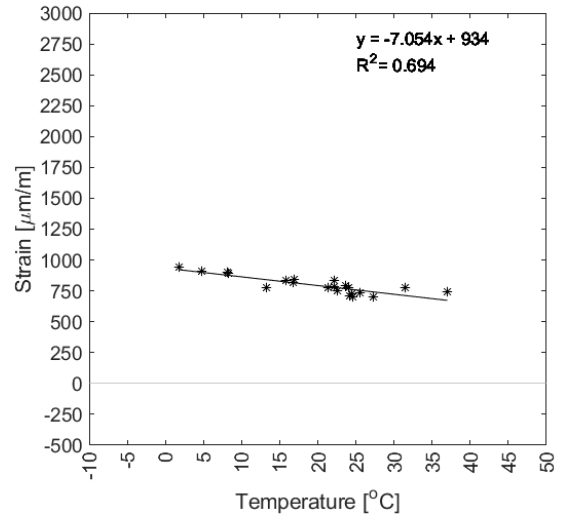


**Figure D.22** – C.III.3 – Complete Monitoring Period Database

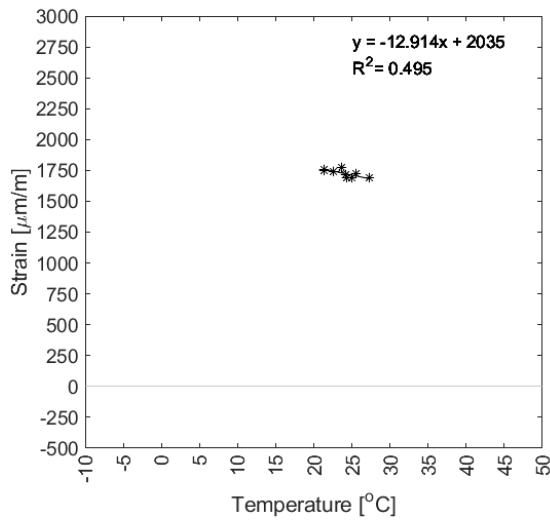


**Figure D.23** – C.III.4 – Daily Measurement Period Database

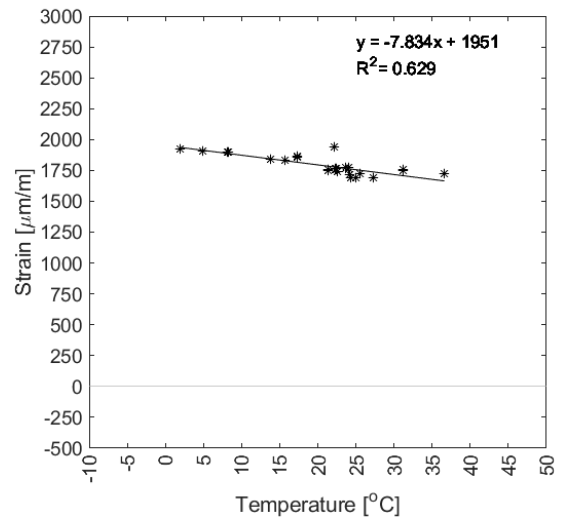


**Figure D.24** – C.III.4 – Complete Monitoring Period Database

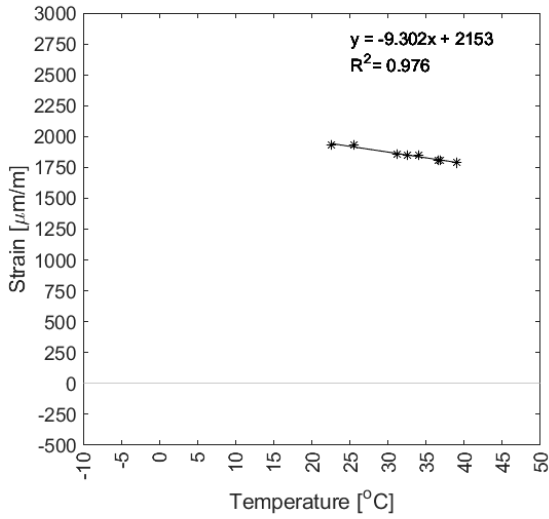


**Figure D.25** – C.IV.1 – Daily Measurement Period Database

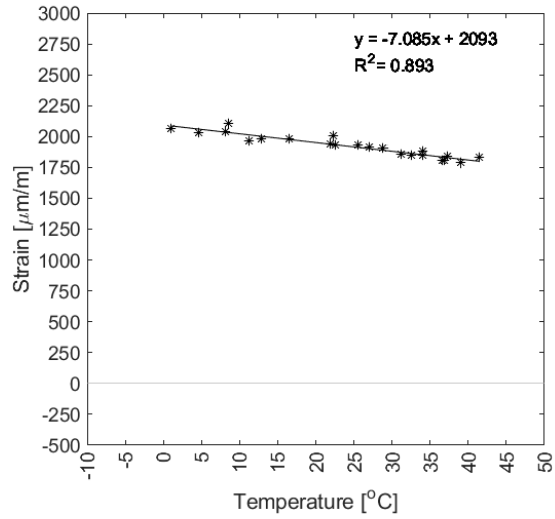


**Figure D.26** – C.IV.1 – Complete Monitoring Period Database

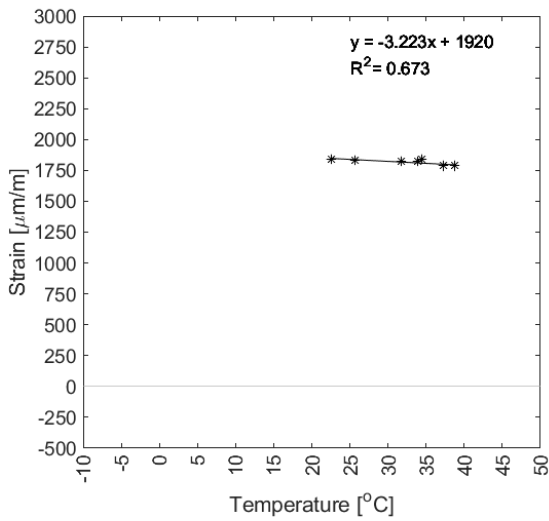


**Figure D.27** – C.IV.2 – Daily Measurement Period Database

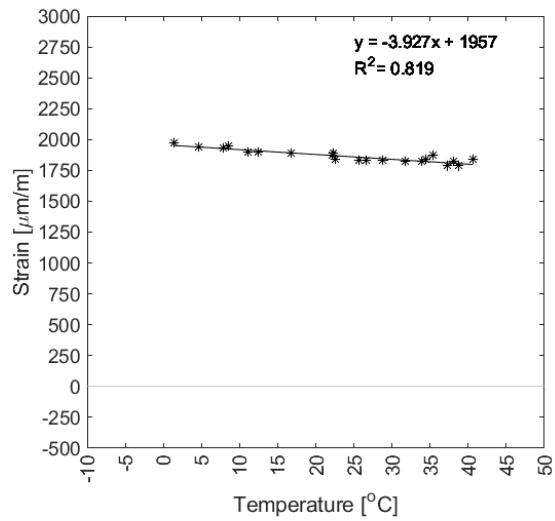


**Figure D.28** – C.IV.2 – Complete Monitoring Period Database



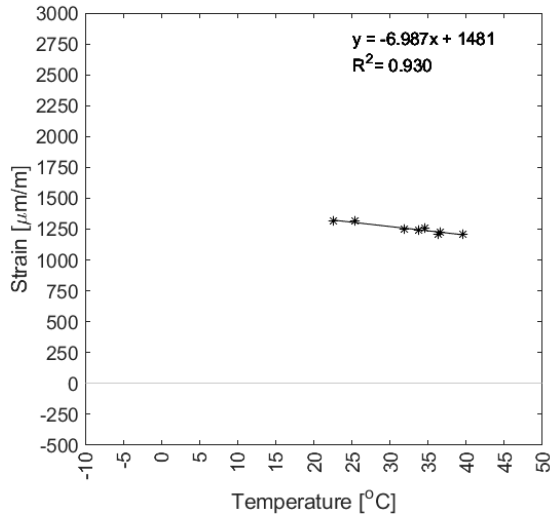


**Figure D.29** – C.IV.3 – Daily Measurement Period Database

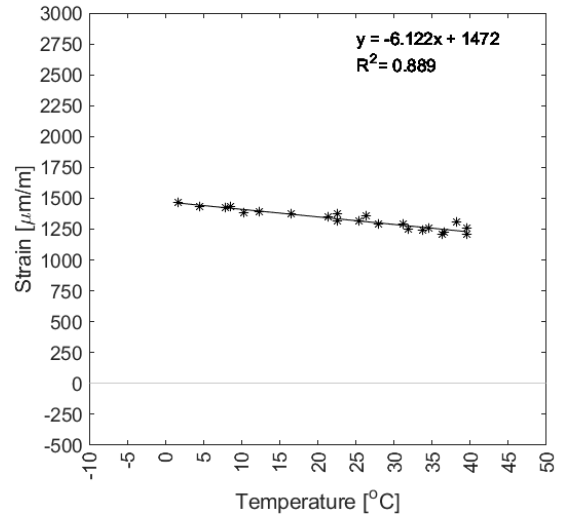


**Figure D.30** – C.IV.3 – Complete Monitoring Period Database

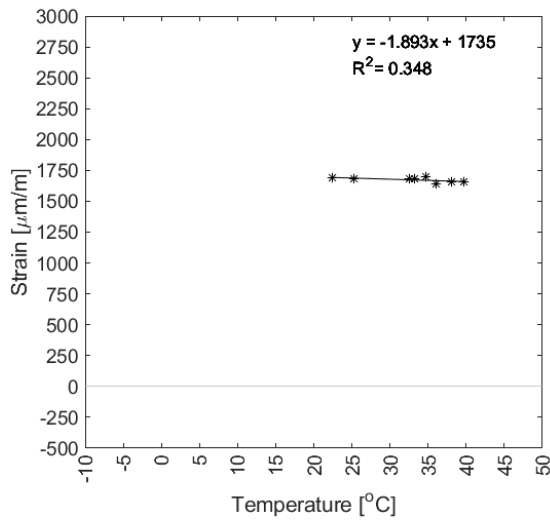


**Figure D.31** – C.IV.4 – Daily Measurement Period Database

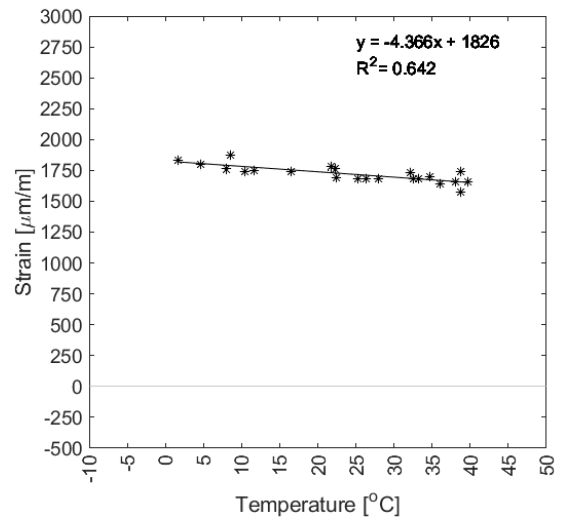


**Figure D.32** – C.IV.4 – Complete Monitoring Period Database

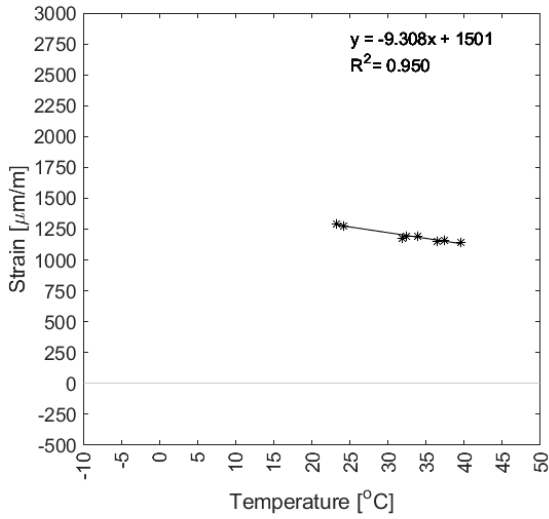


**Figure D.33** – C.V.1 – Daily Measurement Period Database

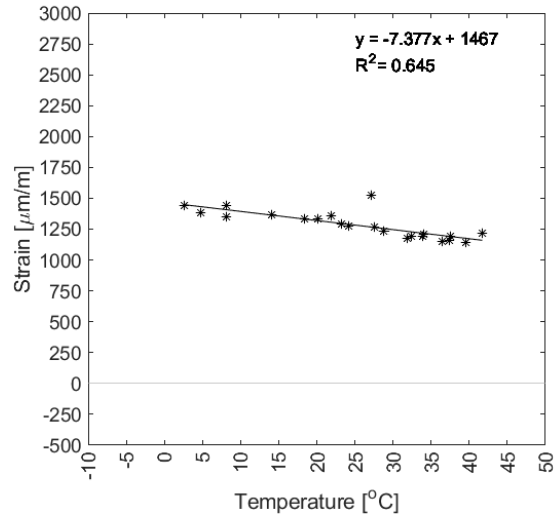


**Figure D.34** – C.V.1 – Complete Monitoring Period Database

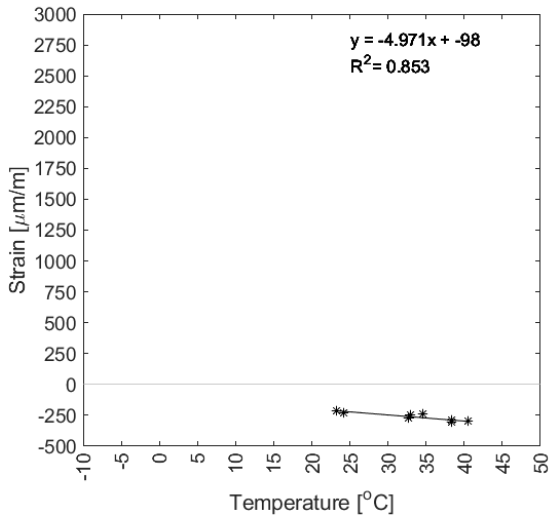


**Figure D.35** – C.V.2 – Daily Measurement Period Database

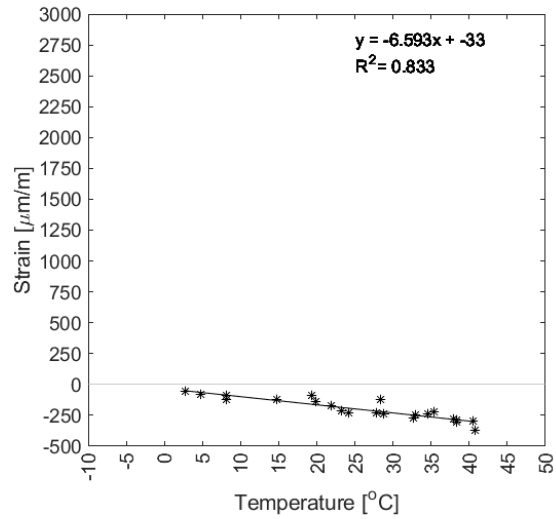


**Figure D.36** – C.V.2 – Complete Monitoring Period Database

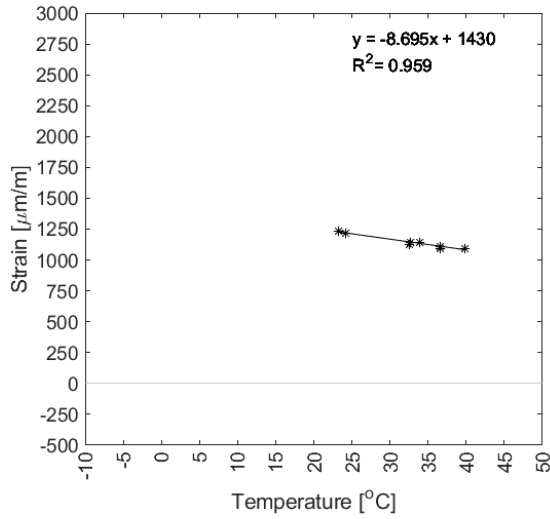


**Figure D.37** – C.V.3 – Daily Measurement Period Database

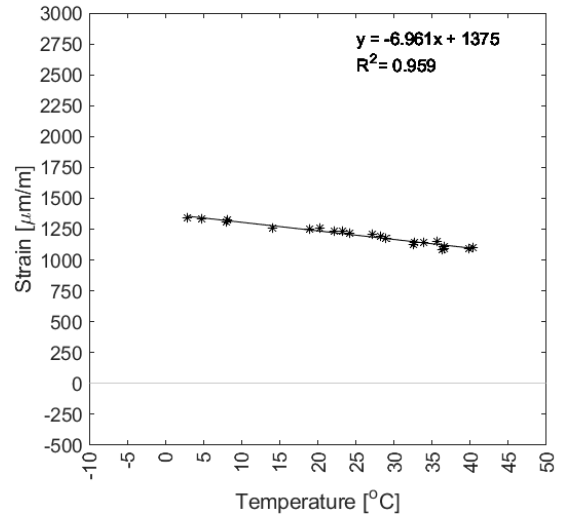


**Figure D.38** – C.V.3 – Complete Monitoring Period Database

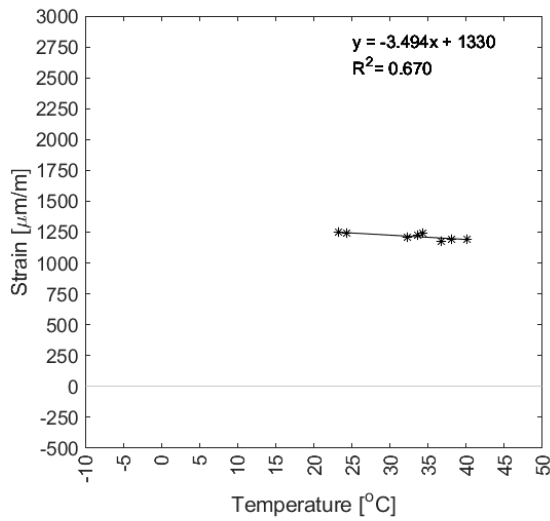


**Figure D.39** – C.V.4 – Daily Measurement Period Database

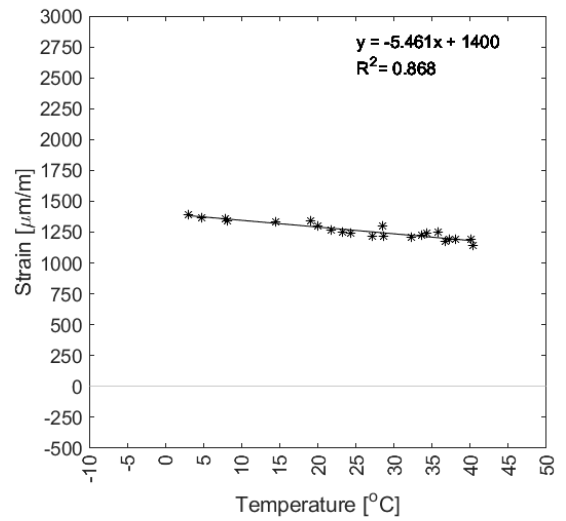


**Figure D.40** – C.V.4 – Complete Monitoring Period Database

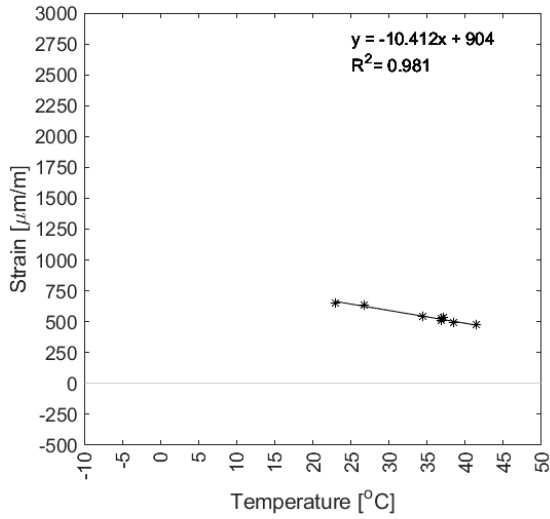


**Figure D.41** – C.VI.1 – Daily Measurement Period Database

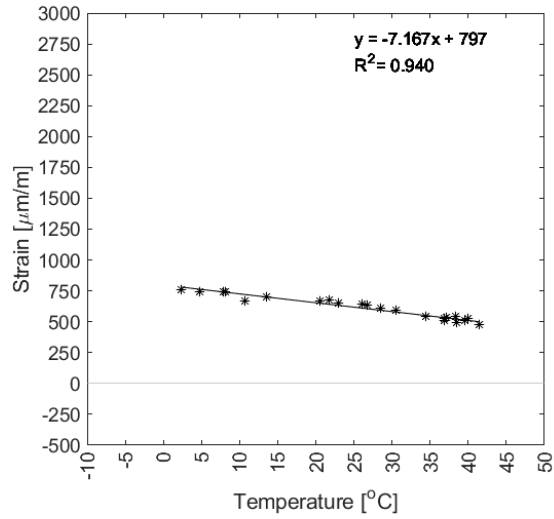


**Figure D.42** – C.VI.1 – Complete Monitoring Period Database

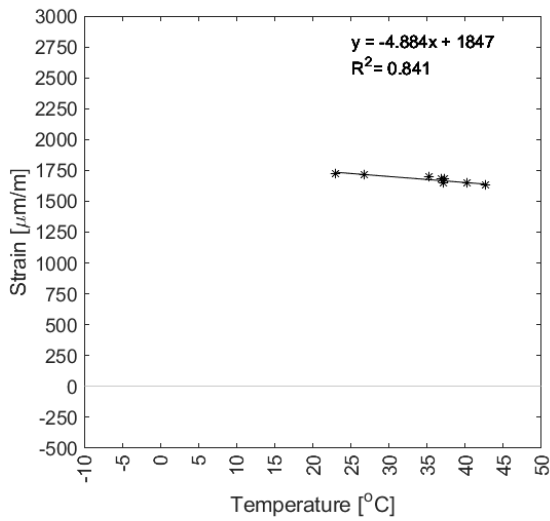


**Figure D.43** – C.VI.2 – Daily Measurement Period Database

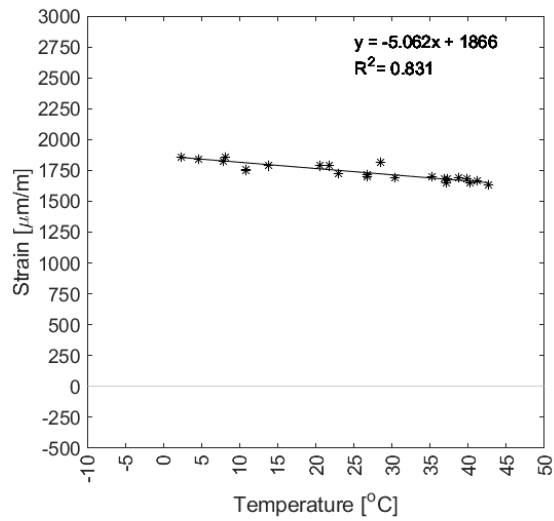


**Figure D.44** – C.VI.2 – Complete Monitoring Period Database

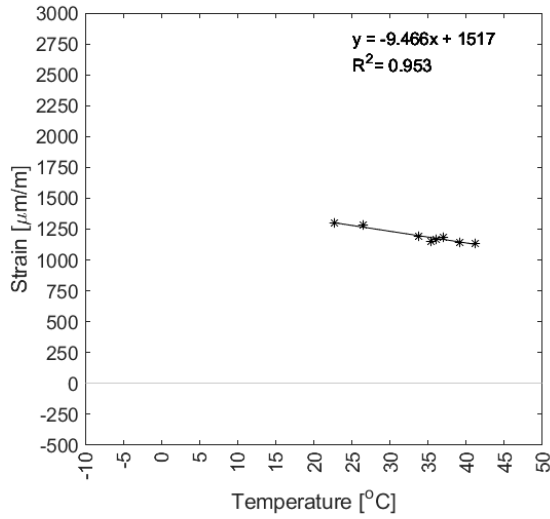


**Figure D.45** – C.VI.3 – Daily Measurement Period Database

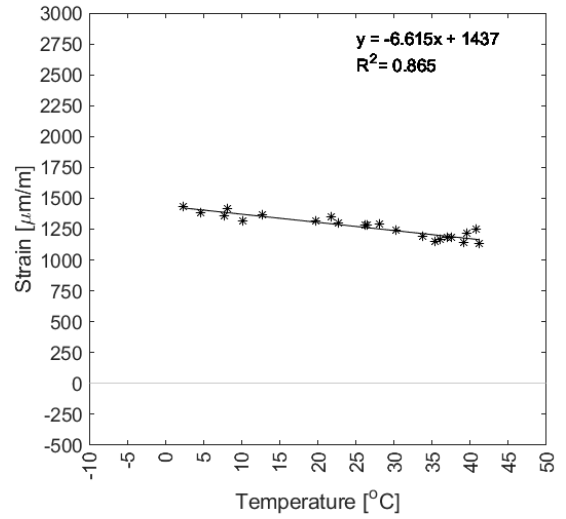


**Figure D.46** – C.VI.3 – Complete Monitoring Period Database

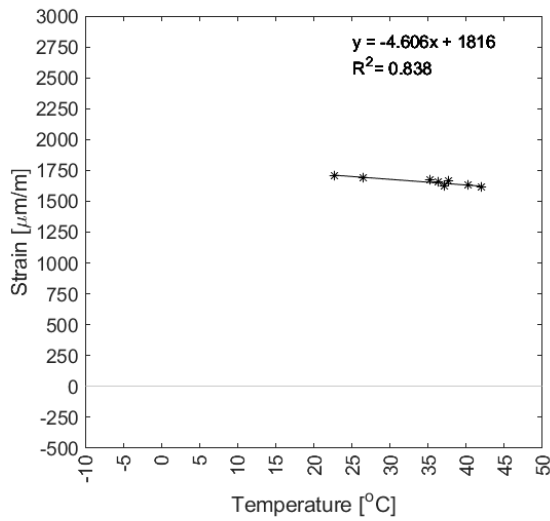


**Figure D.47** – C.VI.4 – Daily Measurement Period Database

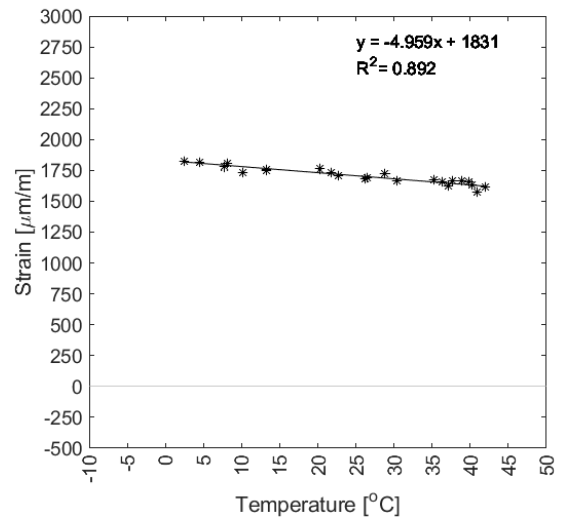


**Figure D.48** – C.VI.4 – Complete Monitoring Period Database

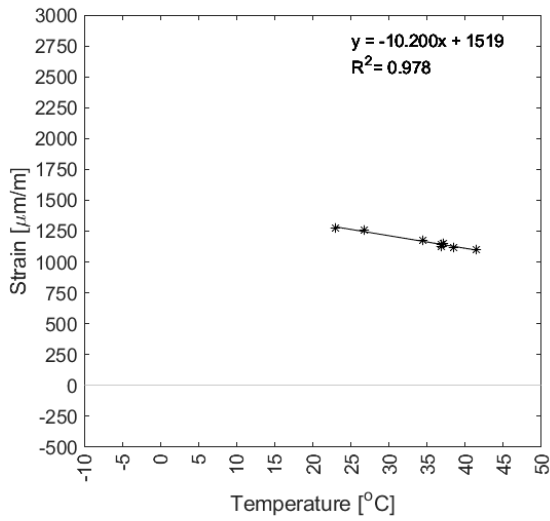


**Figure D.49** – C.VII.1 – Daily Measurement Period Database

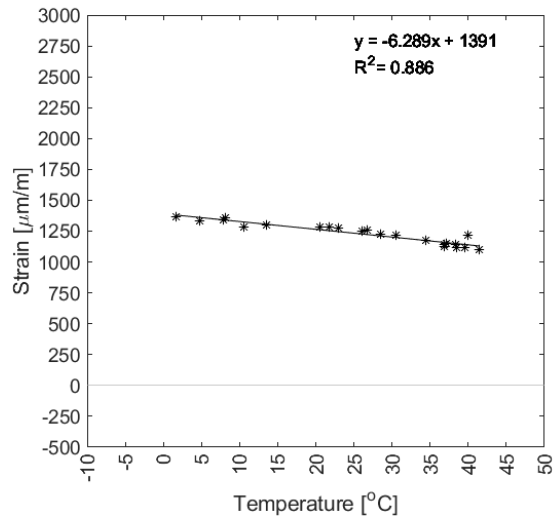


**Figure D.50** – C.VII.1 – Complete Monitoring Period Database

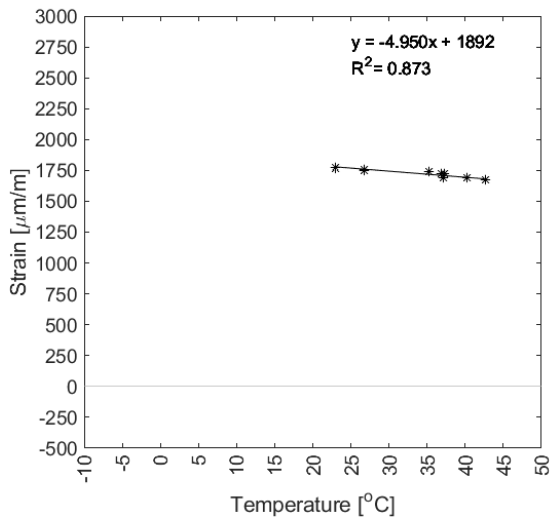


**Figure D.51** – C.VII.2 – Daily Measurement Period Database

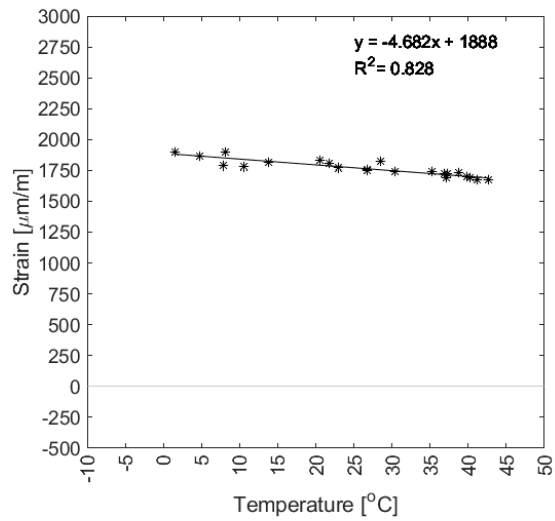


**Figure D.52** – C.VII.2 – Complete Monitoring Period Database

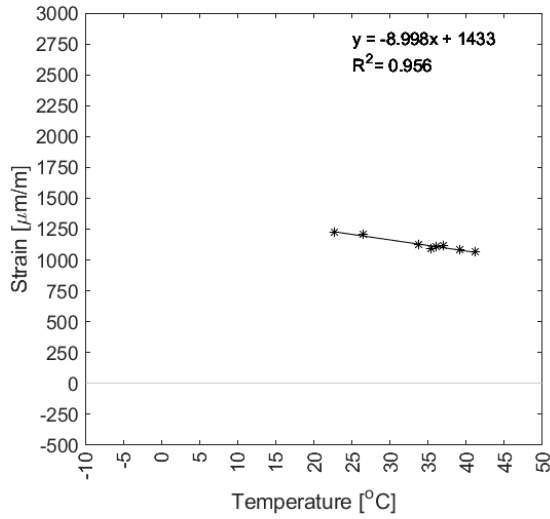


**Figure D.53** – C.VII.3 – Daily Measurement Period Database

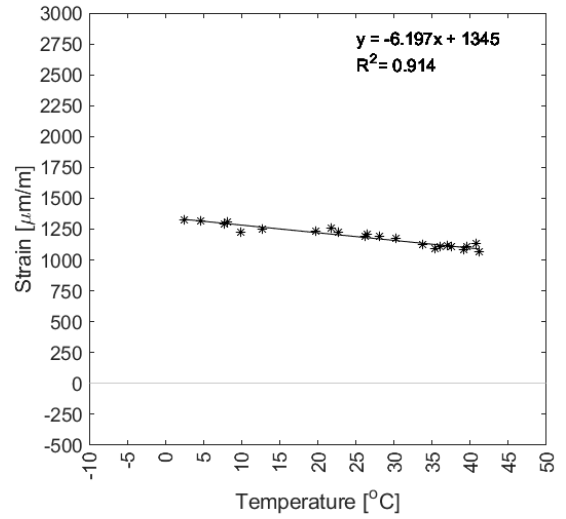


**Figure D.54** – C.VII.3 – Complete Monitoring Period Database

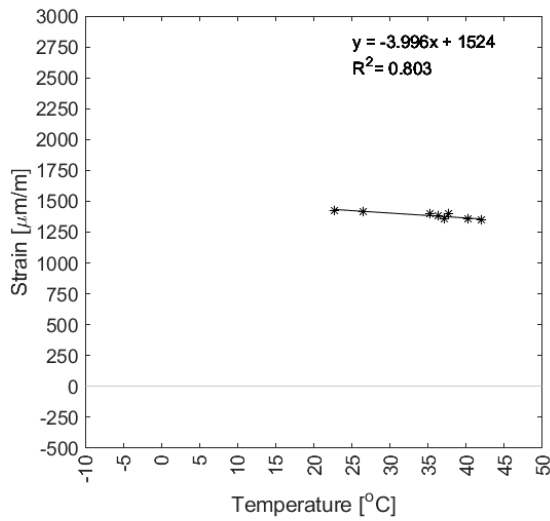


**Figure D.55** – C.VII.4 – Daily Measurement Period Database

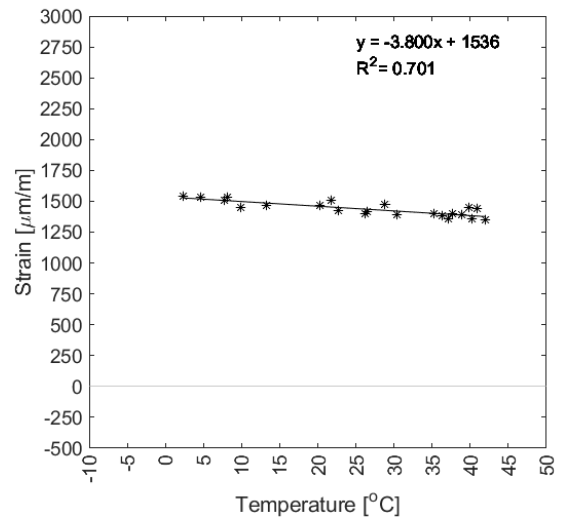


**Figure D.56** – C.VII.4 – Complete Monitoring Period Database

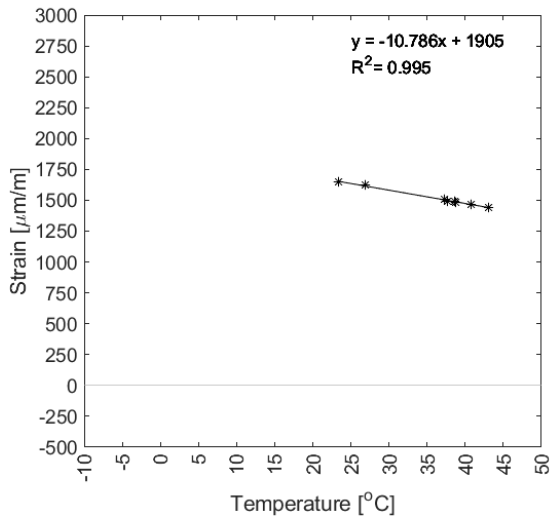


**Figure D.57** – C.VIII.1 – Daily Measurement Period Database

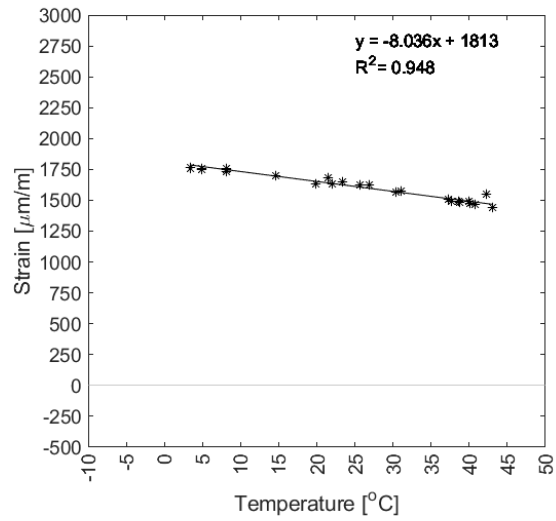


**Figure D.58** – C.VIII.1 – Complete Monitoring Period Database

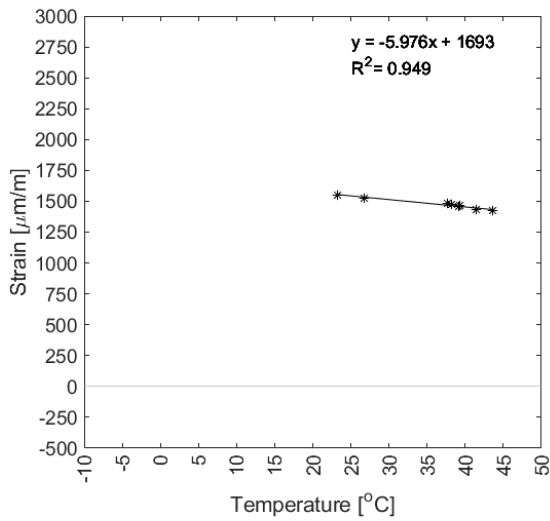


**Figure D.59** – C.VIII.2 – Daily Measurement Period Database

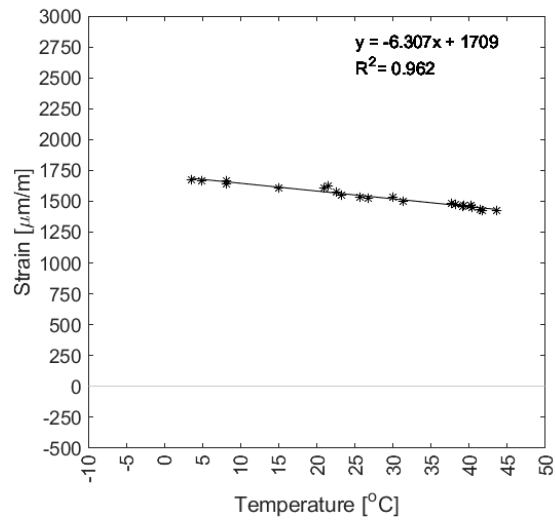


**Figure D.60** – C.VIII.2 – Complete Monitoring Period Database



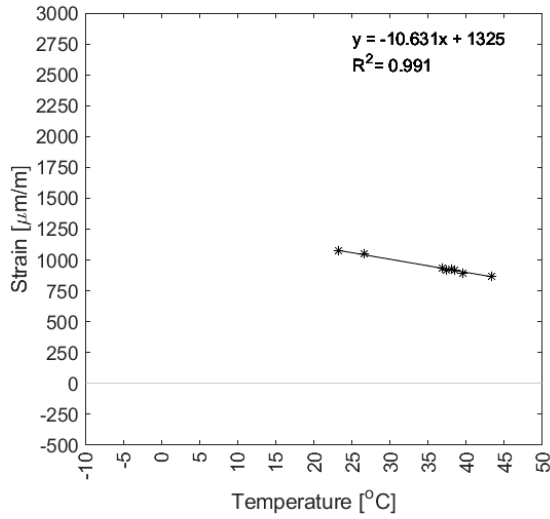


**Figure D.61** – C.VIII.3 – Daily Measurement Period Database

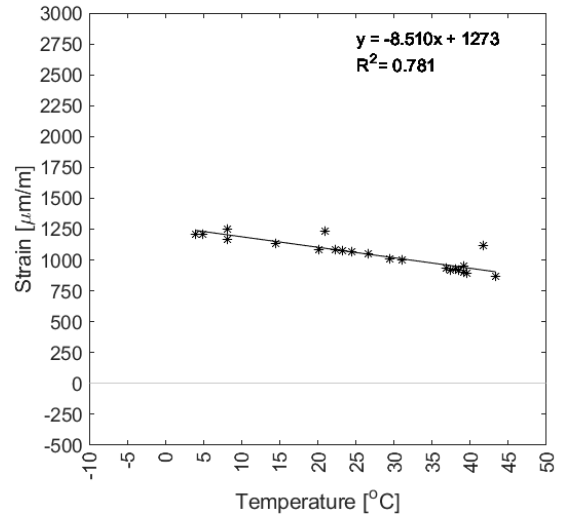


**Figure D.62** – C.VIII.3 – Complete Monitoring Period Database

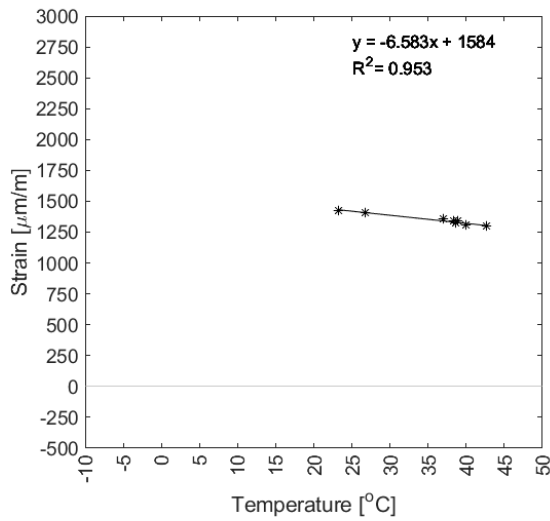


**Figure D.63** – C.VIII.4 – Daily Measurement Period Database

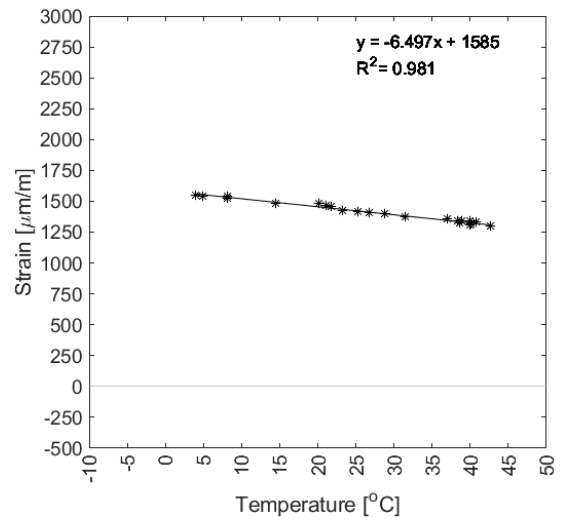


**Figure D.64** – C.VIII.4 – Complete Monitoring Period Database

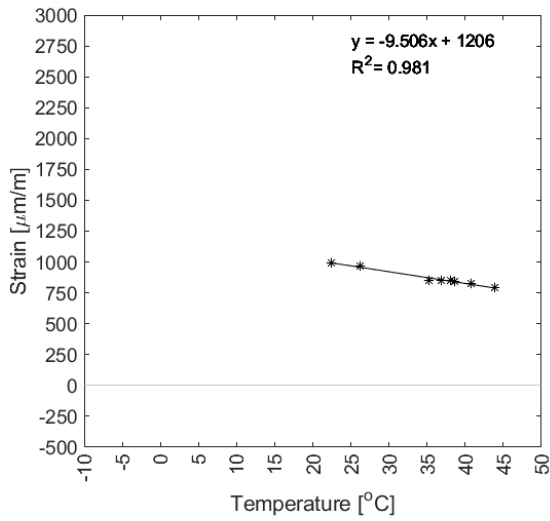


**Figure D.65** – C.IX.1 – Daily Measurement Period Database

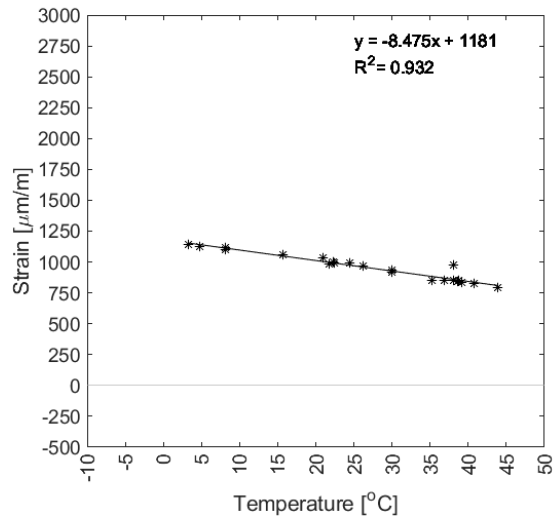


**Figure D.66** – C.IX.1 – Complete Monitoring Period Database

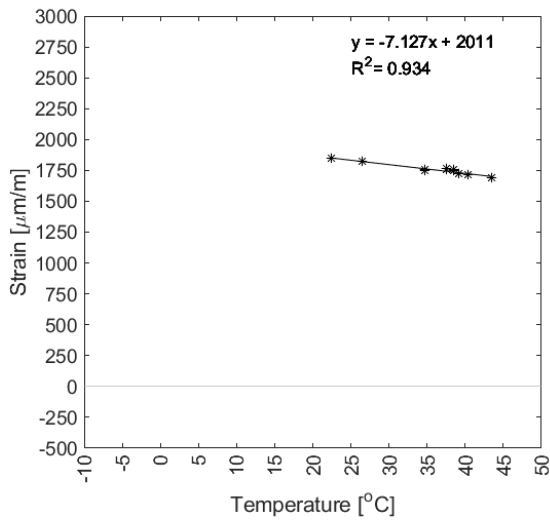


**Figure D.67** – C.IX.2 – Daily Measurement Period Database

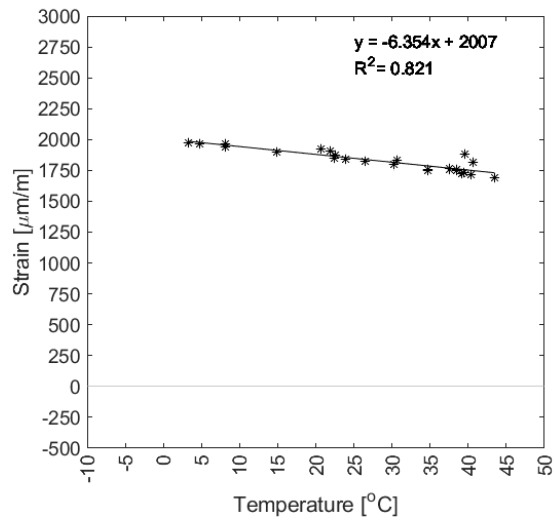


**Figure D.68** – C.IX.2 – Complete Monitoring Period Database

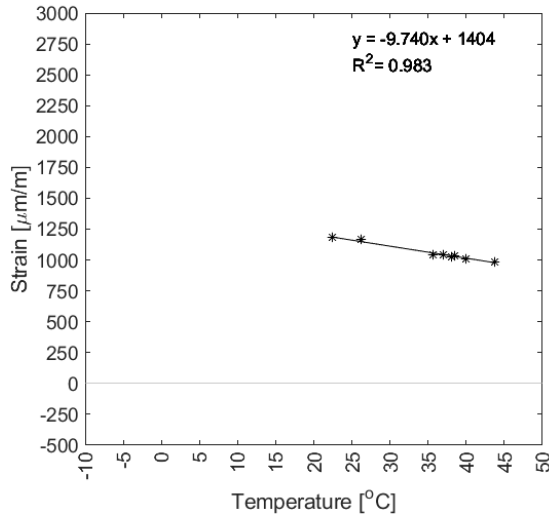


**Figure D.69** – C.IX.3 – Daily Measurement Period Database

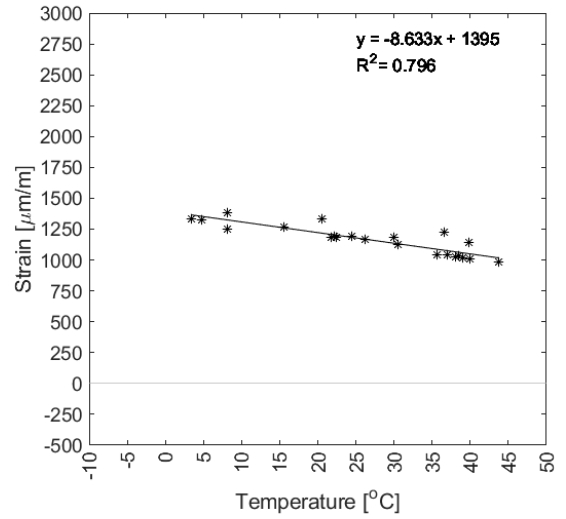


**Figure D.70** – C.IX.3 – Complete Monitoring Period Database

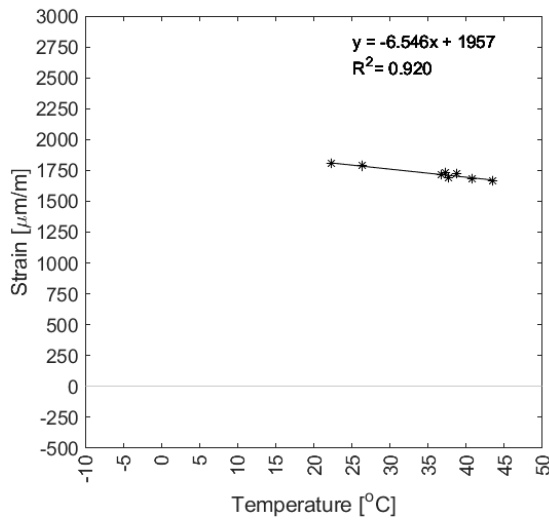


**Figure D.71** – C.IX.4 – Daily Measurement Period Database

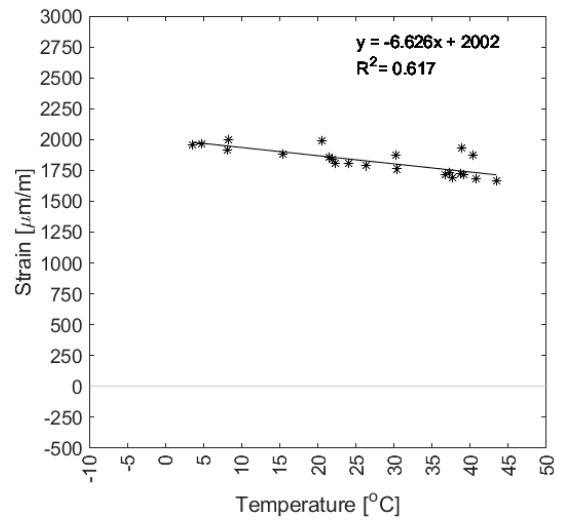


**Figure D.72** – C.IX.4 – Complete Monitoring Period Database

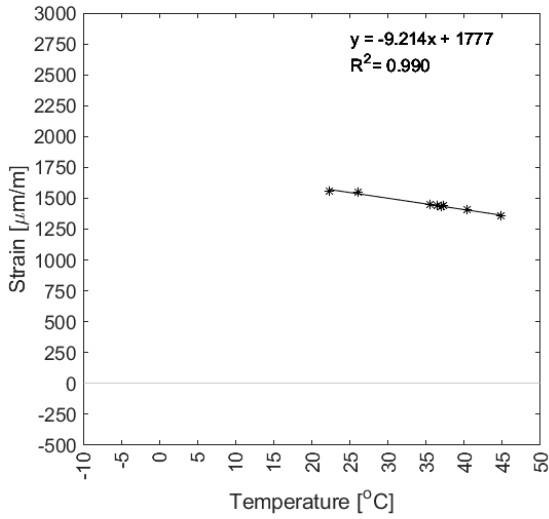


**Figure D.73** – C.X.1 – Daily Measurement Period Database

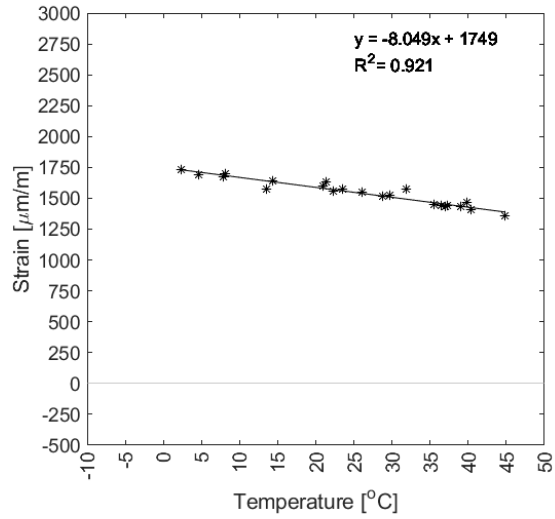


**Figure D.74** – C.X.1 – Complete Monitoring Period Database

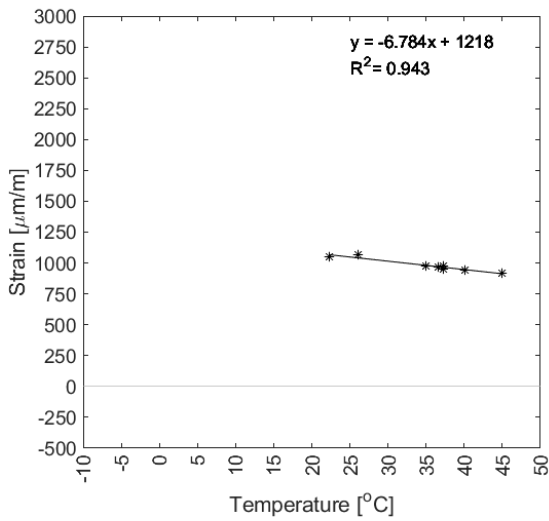


**Figure D.75** – C.X.2 – Daily Measurement Period Database

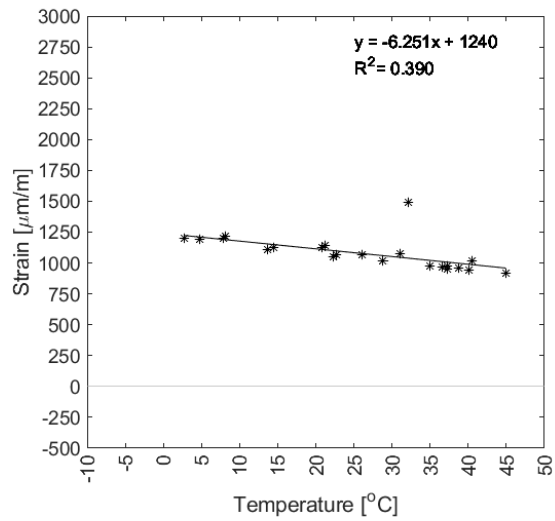


**Figure D.76** – C.X.2 – Complete Monitoring Period Database

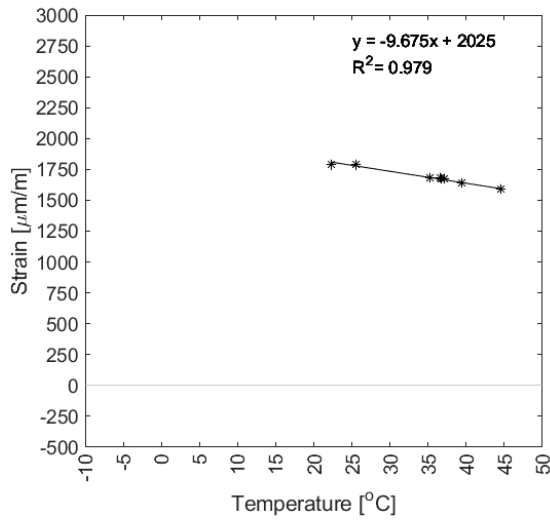


**Figure D.77** – C.X.3 – Daily Measurement Period Database

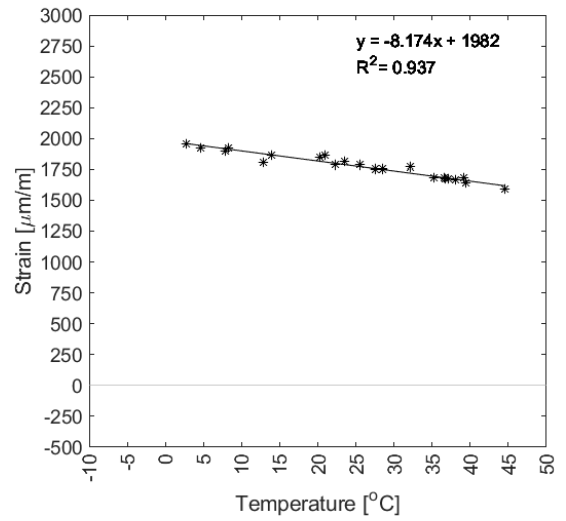


**Figure D.78** – C.X.3 – Complete Monitoring Period Database

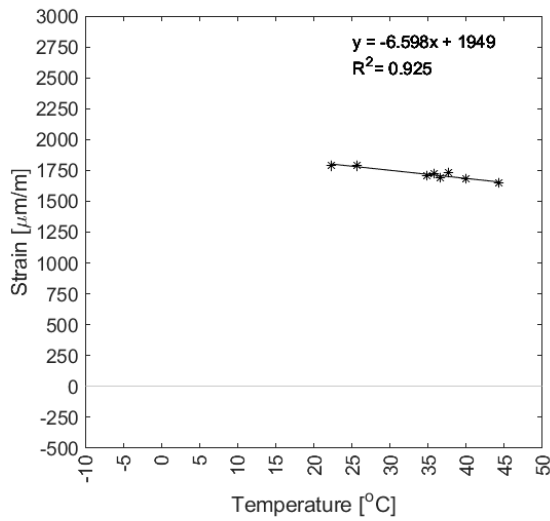


**Figure D.79** – C.X.4 – Daily Measurement Period Database

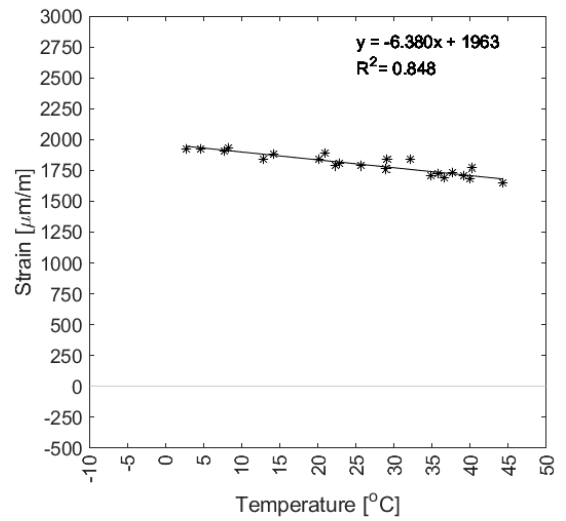


**Figure D.80** – C.X.4 – Complete Monitoring Period Database

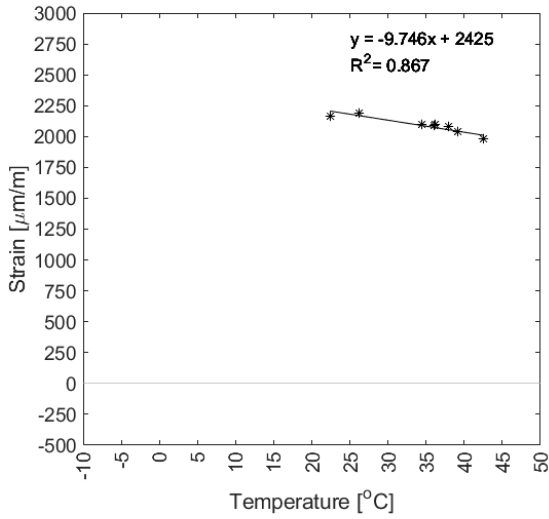


**Figure D.81** – C.XI.1 – Daily Measurement Period Database

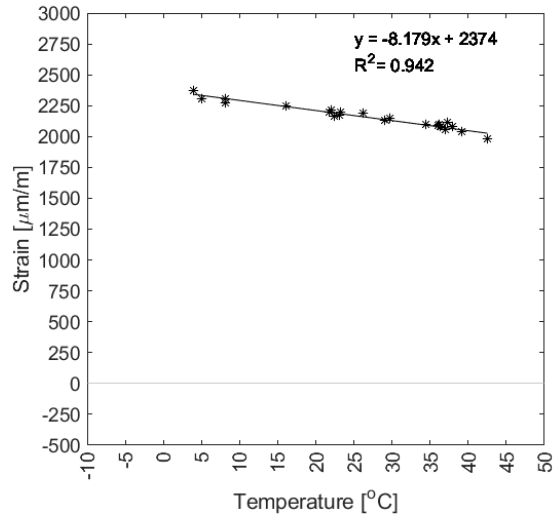


**Figure D.82** – C.XI.1 – Complete Monitoring Period Database

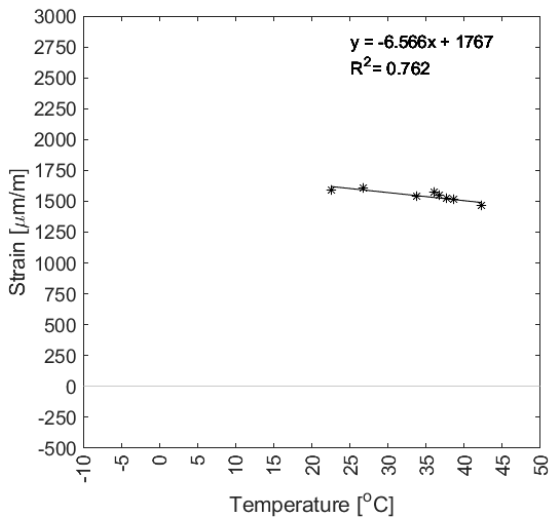


**Figure D.83** – C.XI.2 – Daily Measurement Period Database

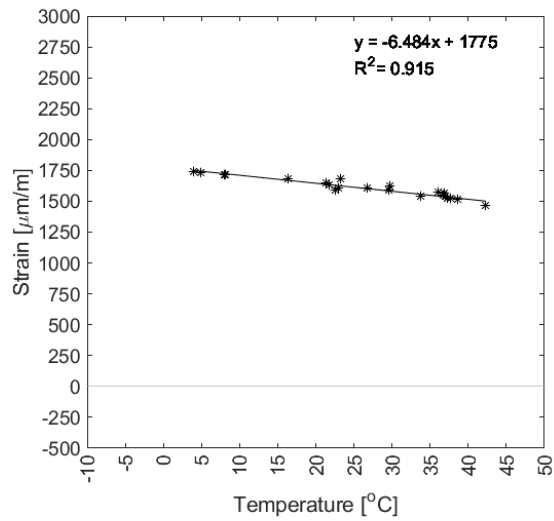


**Figure D.84** – C.XI.2 – Complete Monitoring Period Database

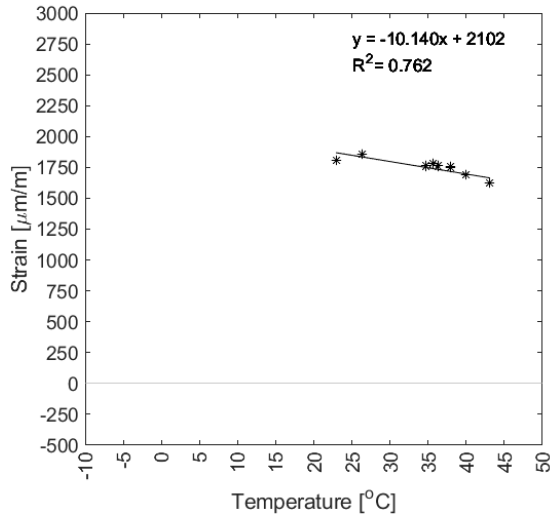


**Figure D.85** – C.XI.3 – Daily Measurement Period Database

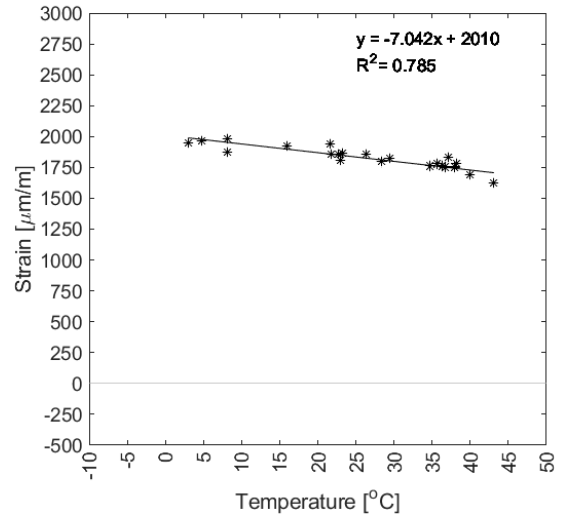


**Figure D.86** – C.XI.3 – Complete Monitoring Period Database

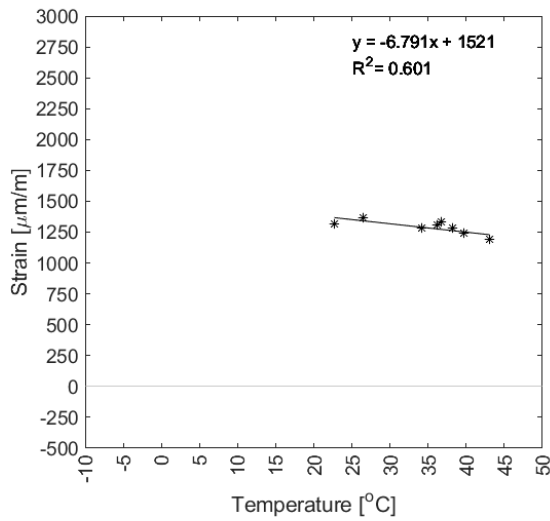


**Figure D.87** – C.XI.4 – Daily Measurement Period Database

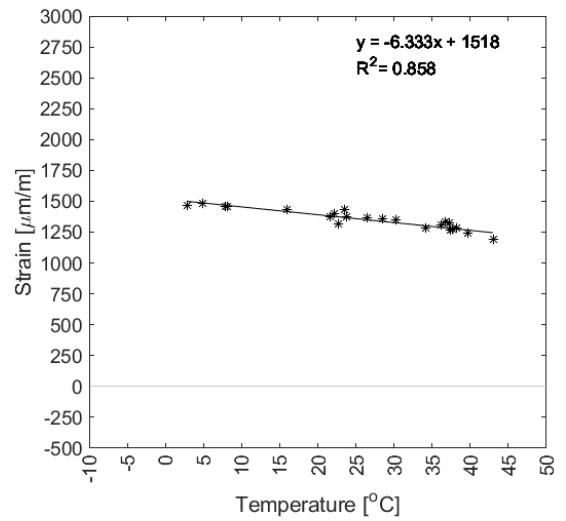


**Figure D.88** – C.XI.4 – Complete Monitoring Period Database

## D.2 Bezprávi

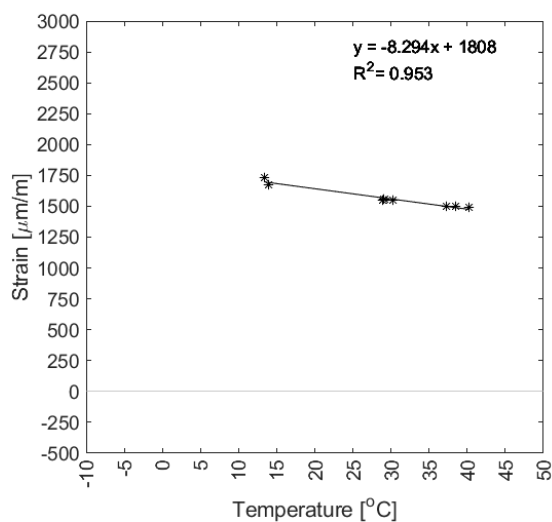


**Figure D.89** – D.I.1 – Daily Measurement Period Database

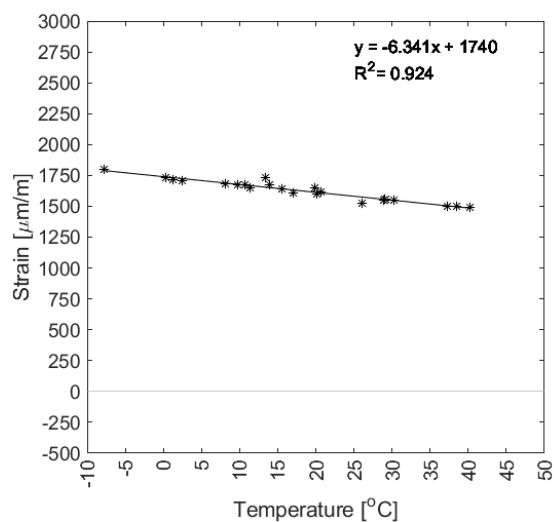


**Figure D.90** – D.I.1 – Complete Monitoring Period Database

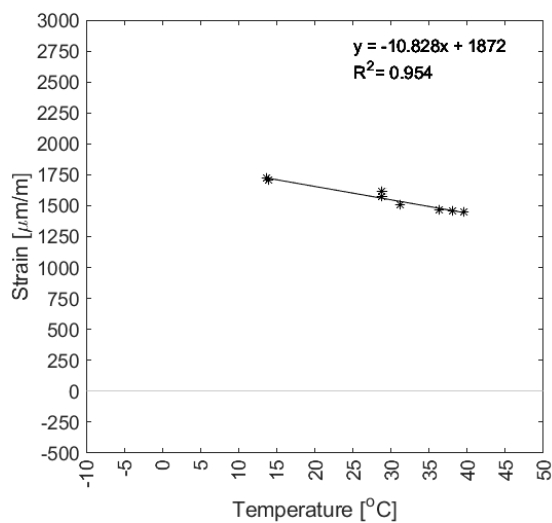


**Figure D.91** – D.I.2 – Daily Measurement Period Database

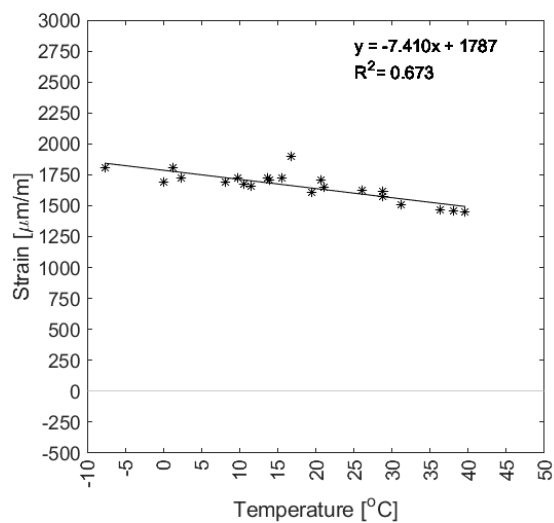


**Figure D.92** – D.I.2 – Complete Monitoring Period Database



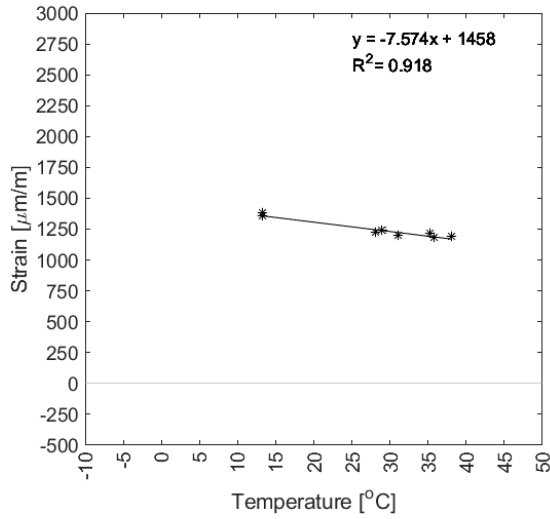


**Figure D.93** – D.I.3 – Daily Measurement Period Database

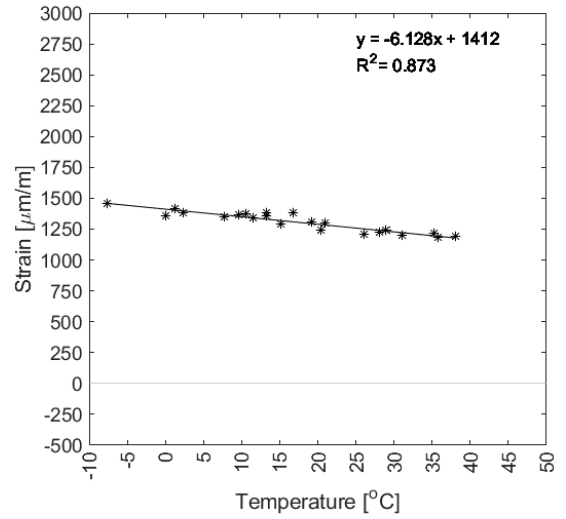


**Figure D.94** – D.I.3 – Complete Monitoring Period Database

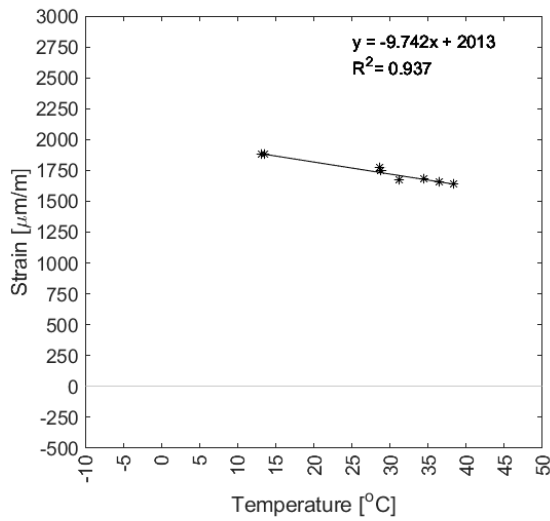


**Figure D.95** – D.I.4 – Daily Measurement Period Database

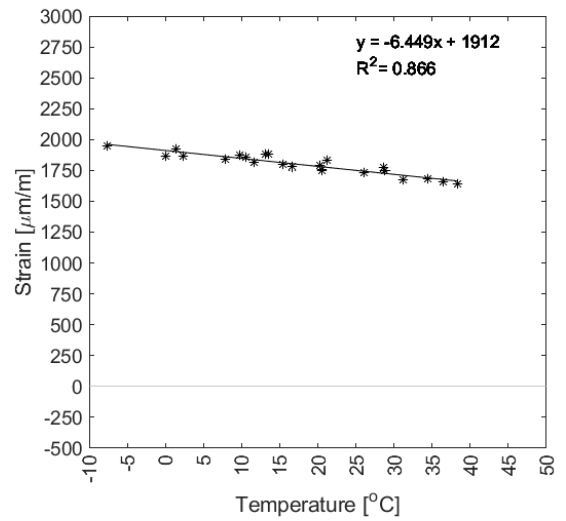


**Figure D.96** – D.I.4 – Complete Monitoring Period Database

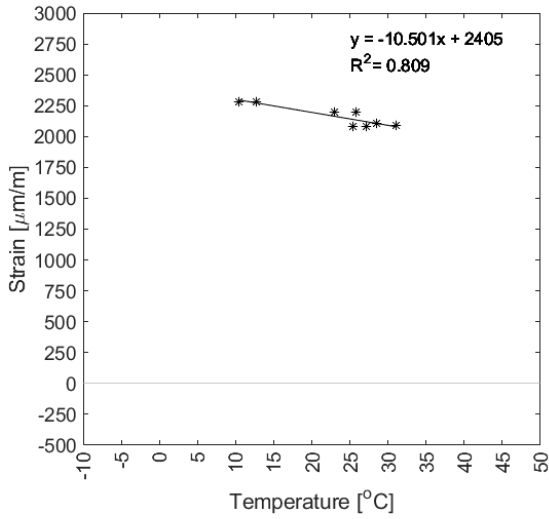


**Figure D.97** – D.II.1 – Daily Measurement Period Database

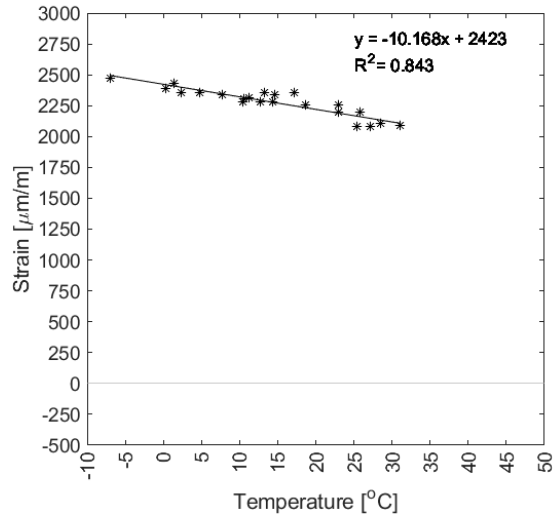


**Figure D.98** – D.II.1 – Complete Monitoring Period Database

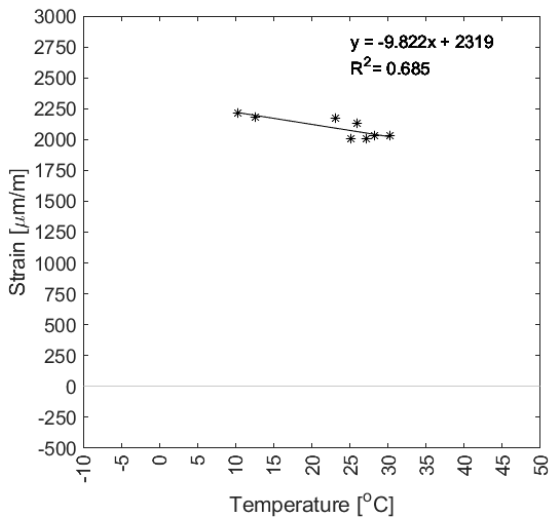


**Figure D.99** – D.II.2 – Daily Measurement Period Database

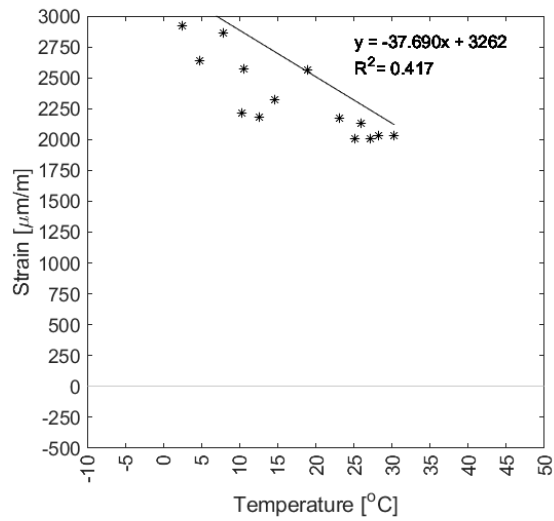


**Figure D.100** – D.II.2 – Complete Monitoring Period Database

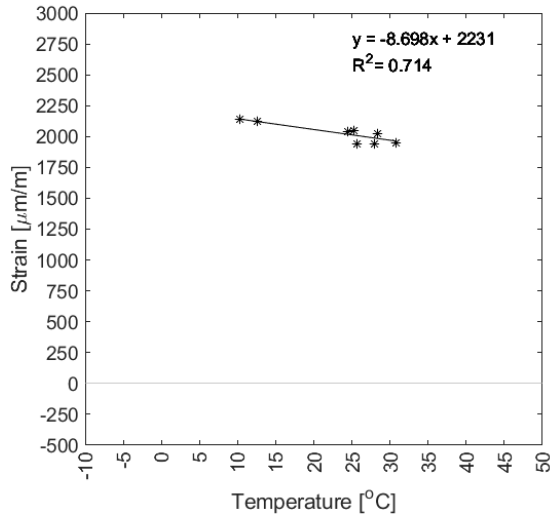


**Figure D.101** – D.II.3 – Daily Measurement Period Database

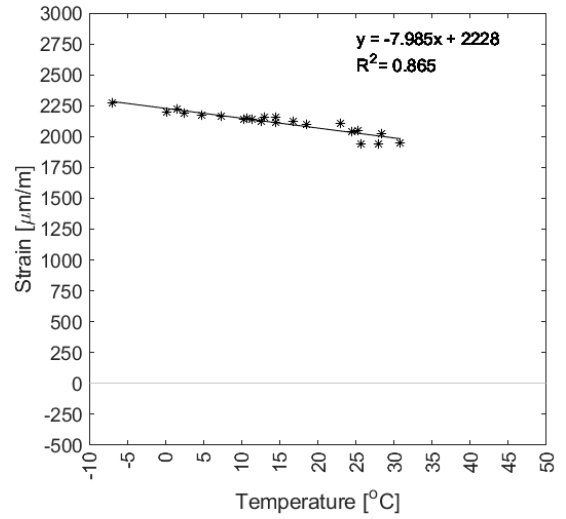


**Figure D.102** – D.II.3 – Complete Monitoring Period Database

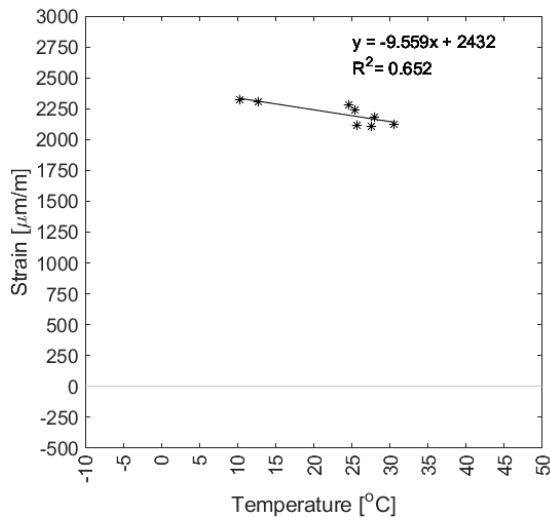


**Figure D.103** – D.II.4 – Daily Measurement Period Database

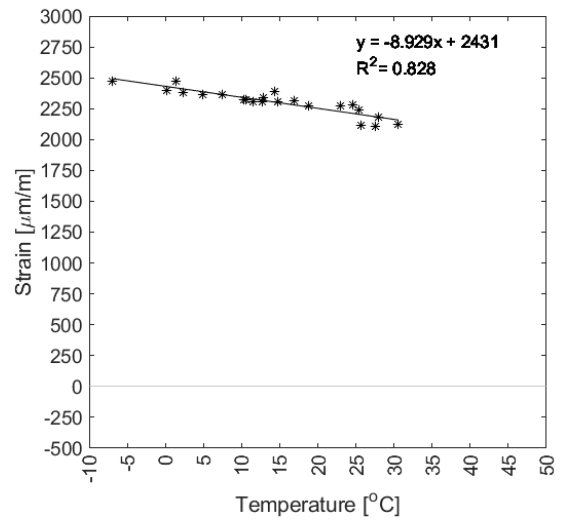


**Figure D.104** – D.II.4 – Complete Monitoring Period Database

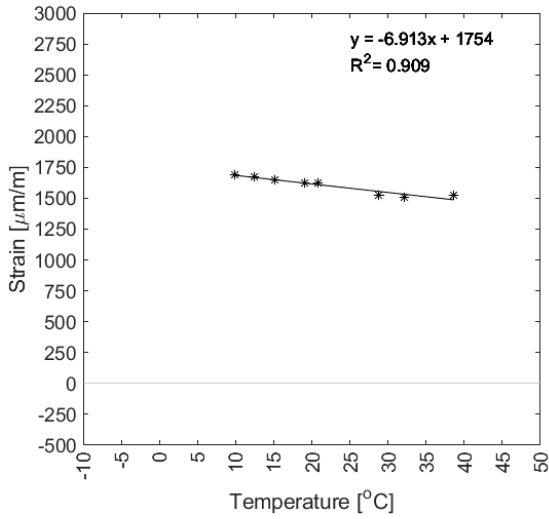


**Figure D.105** – D.III.1 – Daily Measurement Period Database

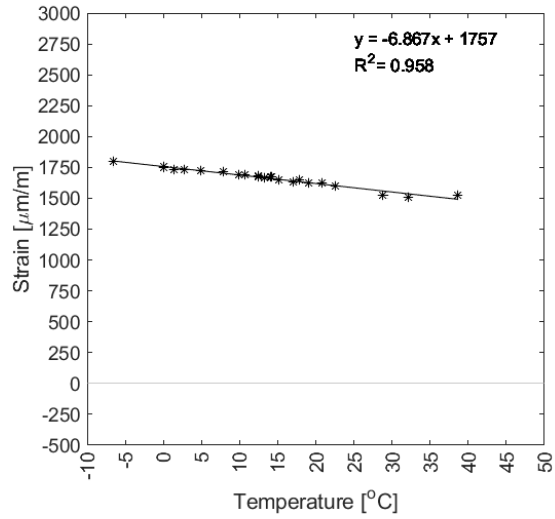


**Figure D.106** – D.III.1 – Complete Monitoring Period Database

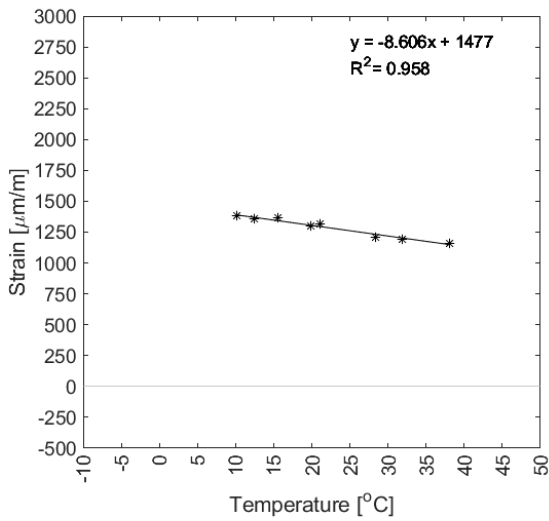


**Figure D.107** – D.III.2 – Daily Measurement Period Database

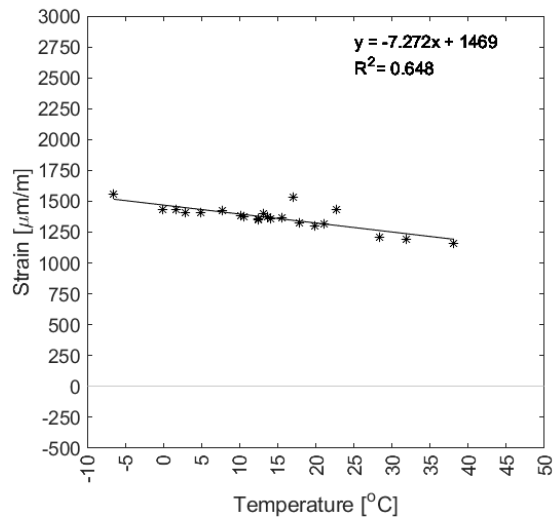


**Figure D.108** – D.III.2 – Complete Monitoring Period Database

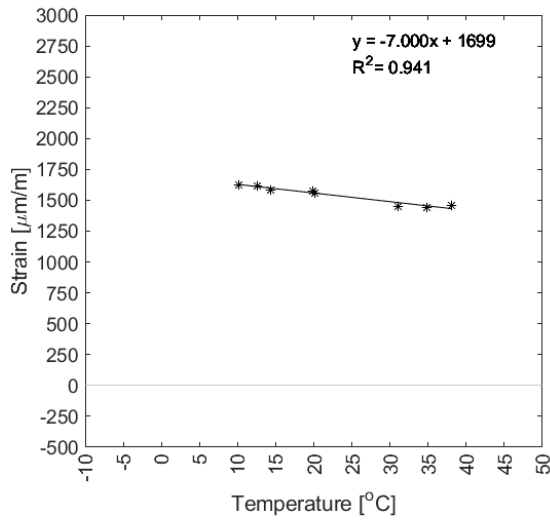


**Figure D.109** – D.III.3 – Daily Measurement Period Database

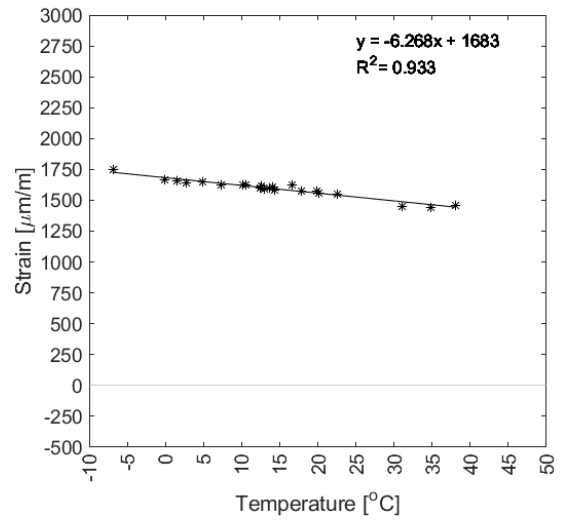


**Figure D.110** – D.III.3 – Complete Monitoring Period Database

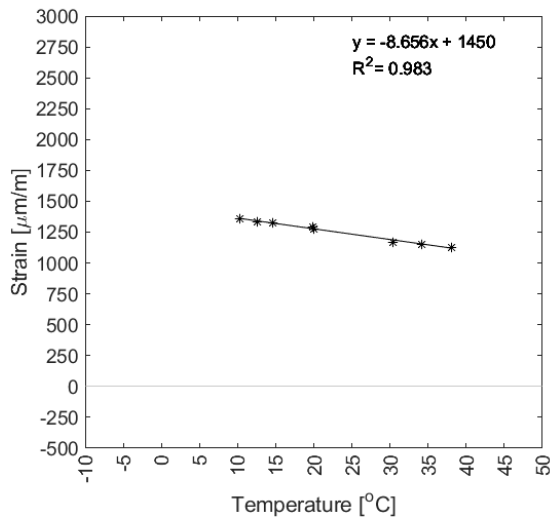


**Figure D.111** – D.III.4 – Daily Measurement Period Database

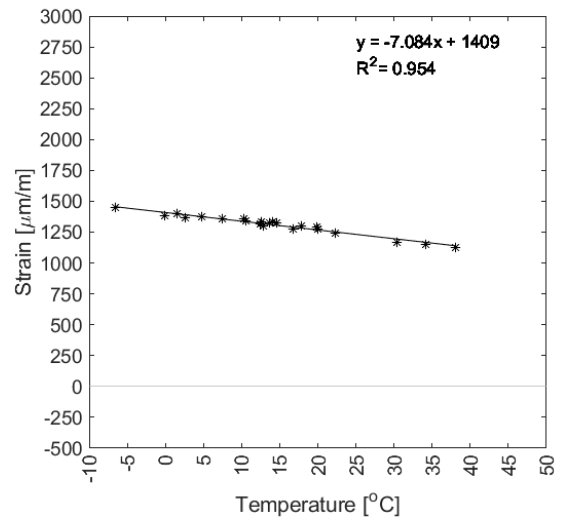


**Figure D.112** – D.III.4 – Complete Monitoring Period Database

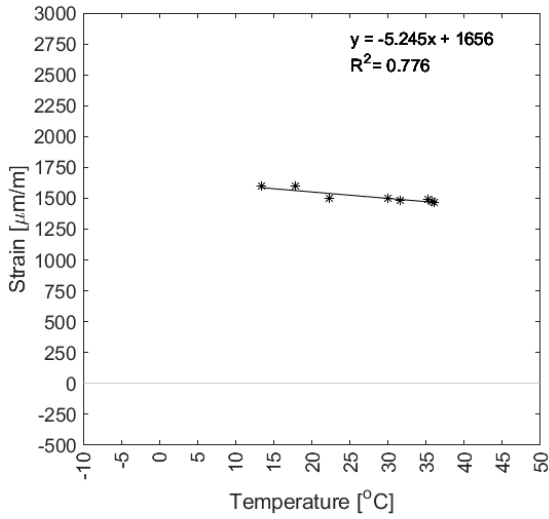


**Figure D.113** – D.IV.1 – Daily Measurement Period Database

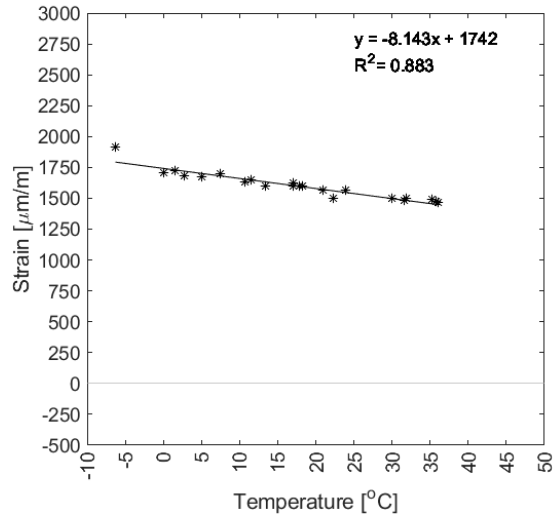


**Figure D.114** – D.IV.1 – Complete Monitoring Period Database

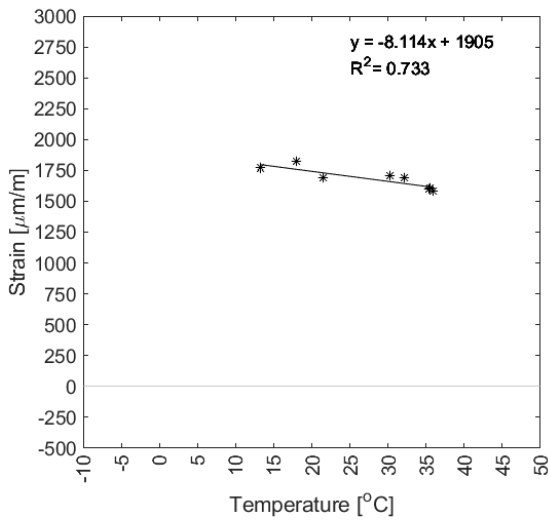


**Figure D.115** – D.IV.2 – Daily Measurement Period Database

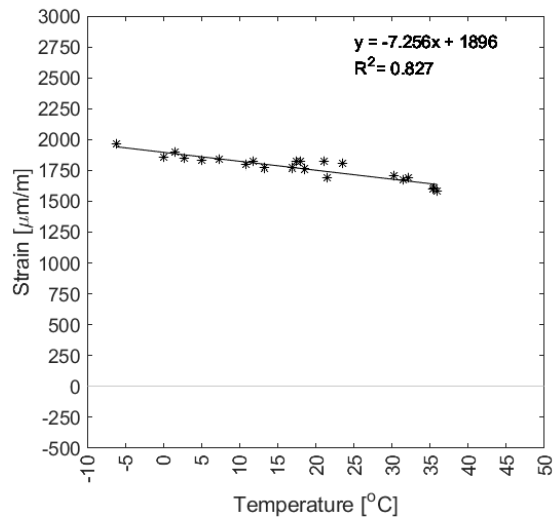


**Figure D.116** – D.IV.2 – Complete Monitoring Period Database

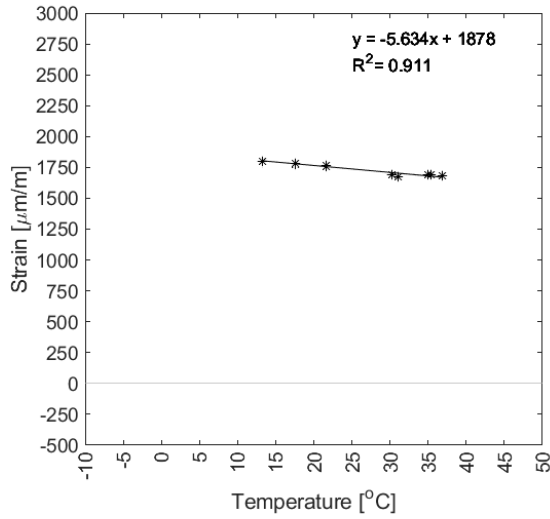


**Figure D.117** – D.IV.3 – Daily Measurement Period Database

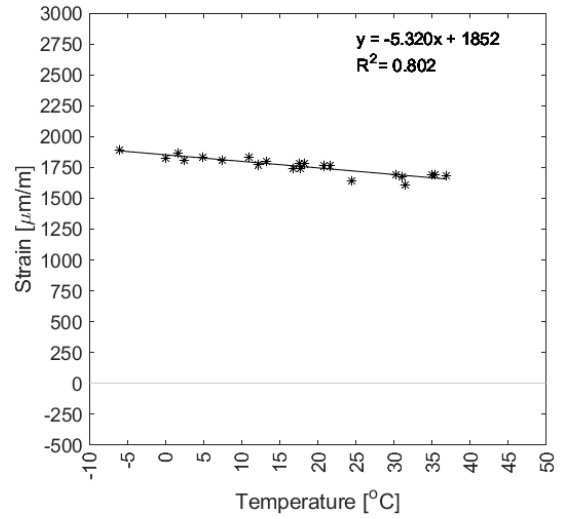


**Figure D.118** – D.IV.3 – Complete Monitoring Period Database

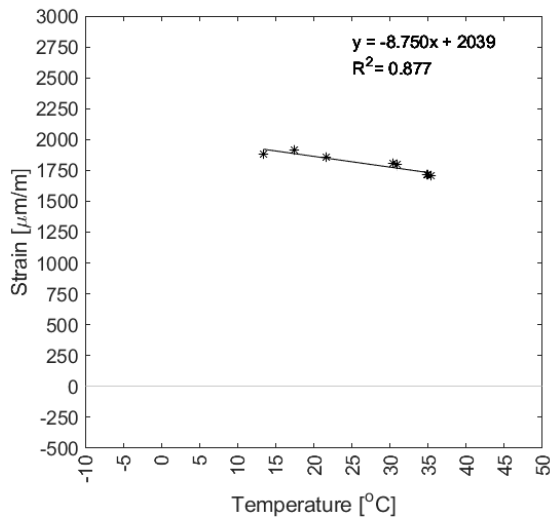


**Figure D.119** – D.IV.4 – Daily Measurement Period Database

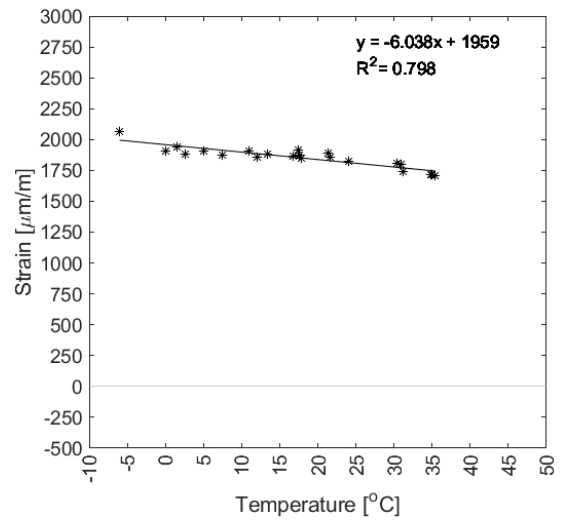


**Figure D.120** – D.IV.4 – Complete Monitoring Period Database





## Appendix E

# Development of Measured and Extrapolated Temperature Difference

The following graphs present the developments of the measured and extrapolated temperature at the particular measuring spots, and the difference between the two temperature values. The extrapolated temperature is calculated based on the description presented in Chapter 5. The graphs are compiled for every particular measuring spot in the Chotěvice and Bezprávi localities separately. The daily measurement period database is the basis of the extrapolated temperature calculation. The marking of the graphs is the same like in the case of Appendix C.

## E.1 Chotěvice

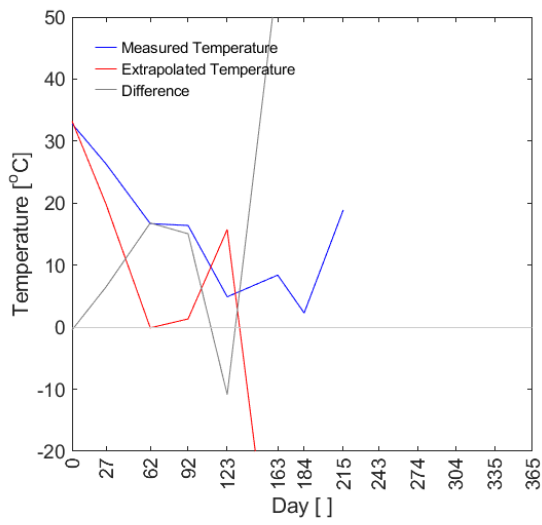


Figure E.1 – C.I.1

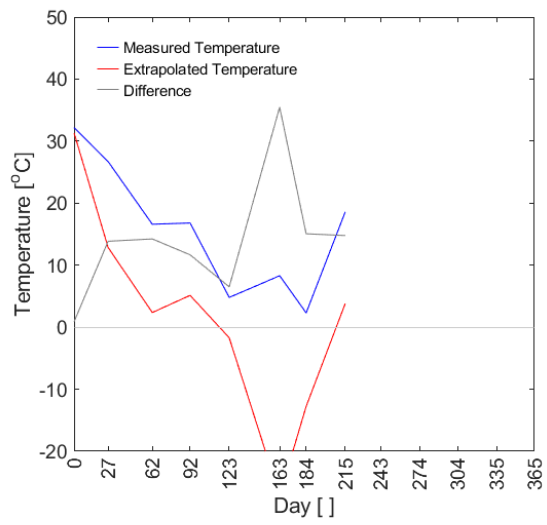


Figure E.2 – C.I.2

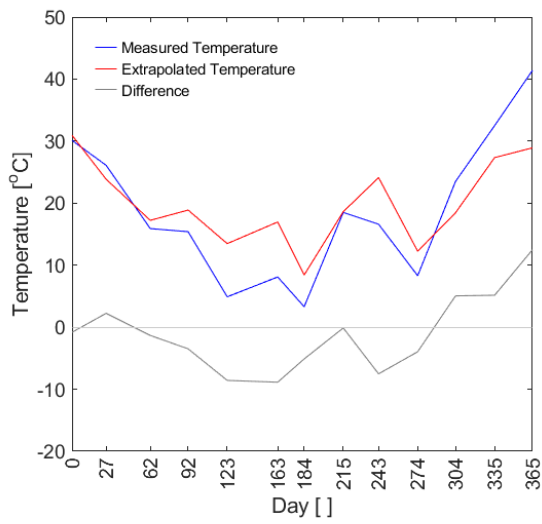


Figure E.3 – C.I.3

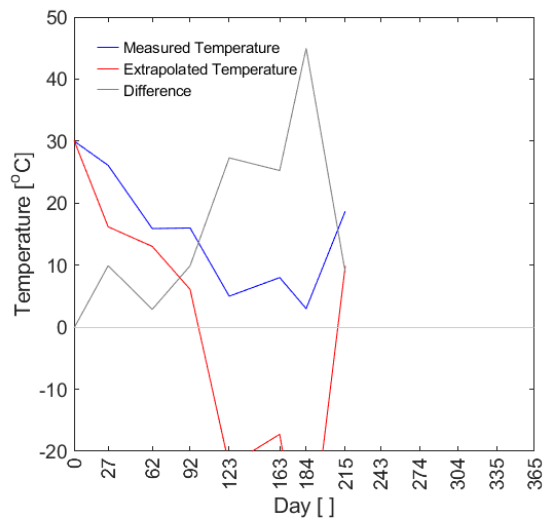
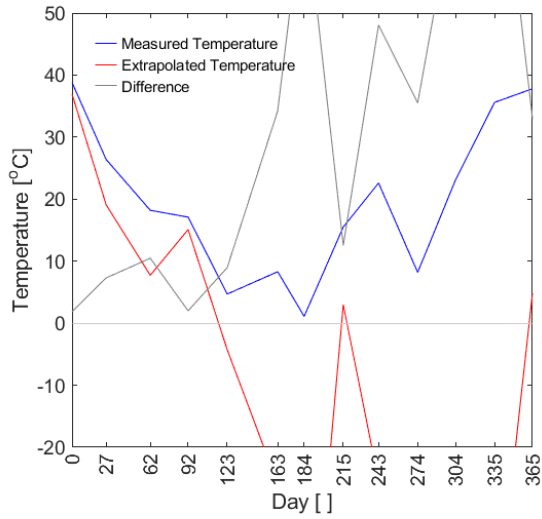
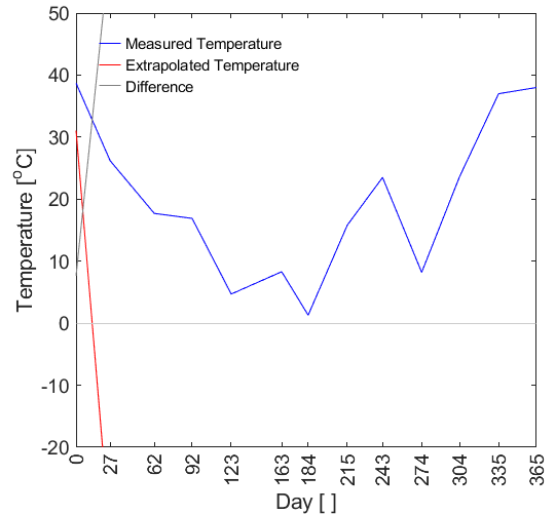


Figure E.4 – C.I.4



**Figure E.5 – C.II.1**



**Figure E.6 – C.II.2**

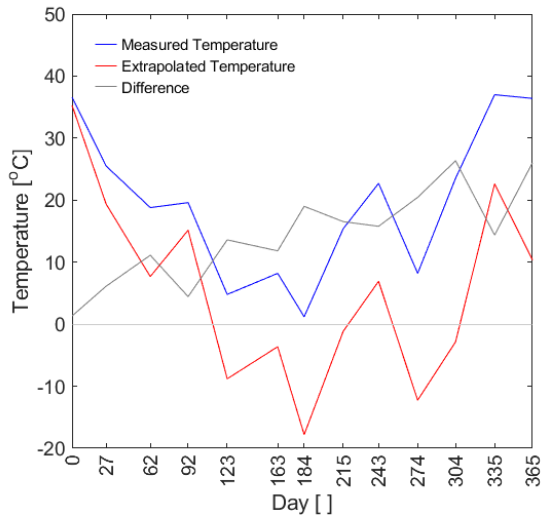


**Figure E.7 – C.II.3**

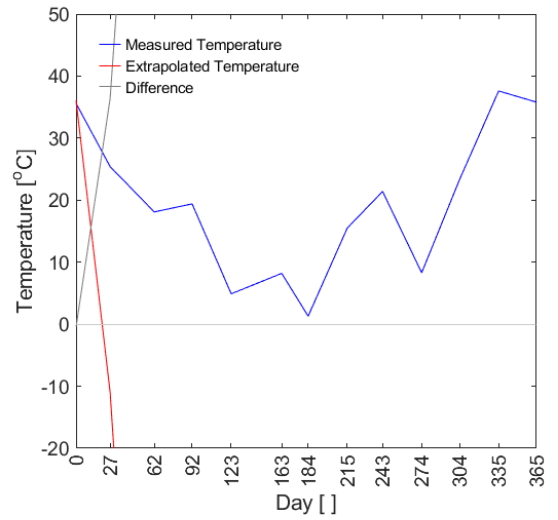


**Figure E.8 – C.II.4**

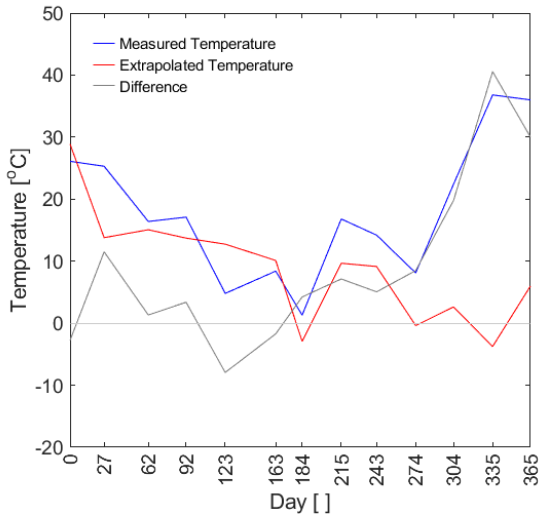


**Figure E.9 – C.III.1**

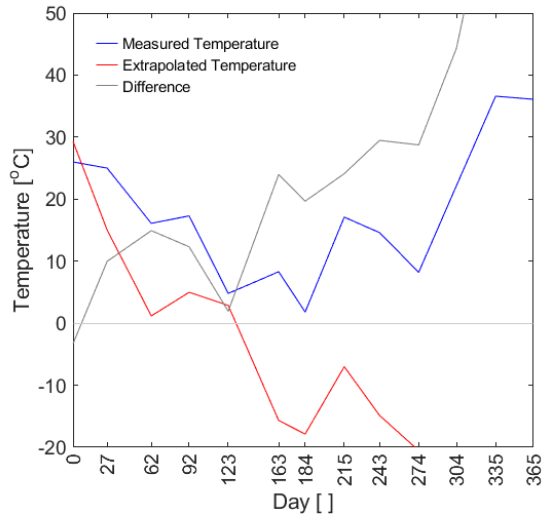


**Figure E.10 – C.III.2**

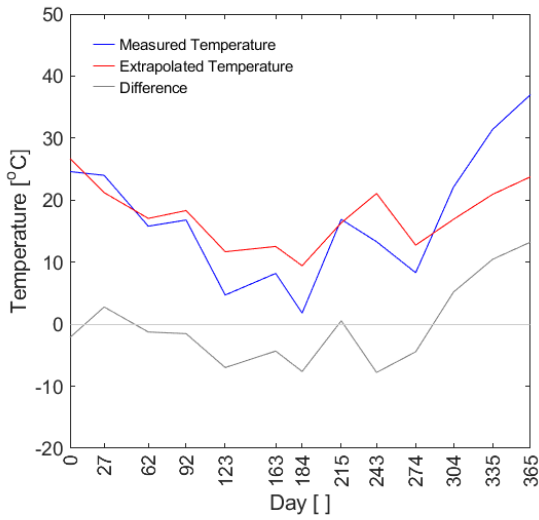


**Figure E.11 – C.III.3**

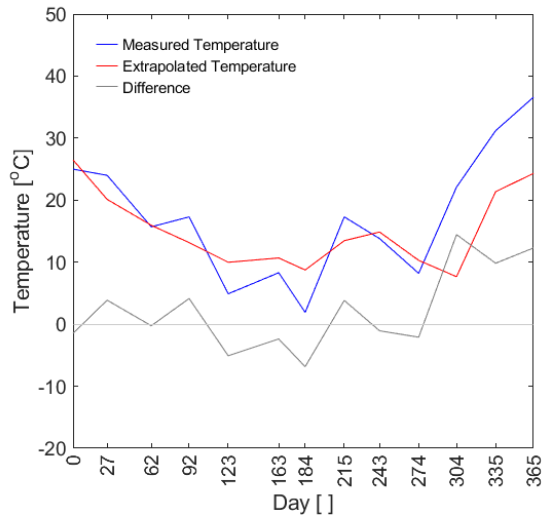


**Figure E.12 – C.III.4**

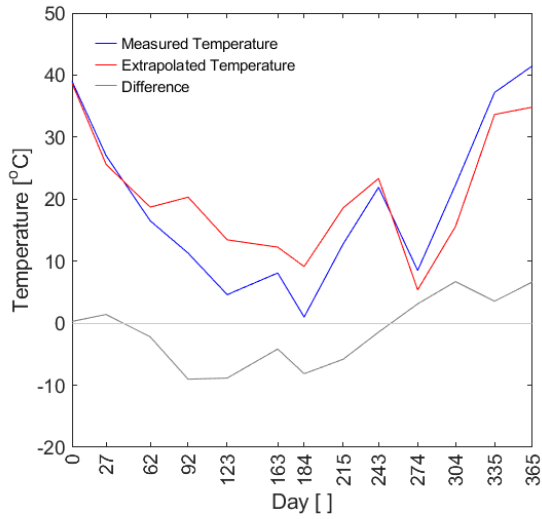


Figure E.13 – C.IV.1

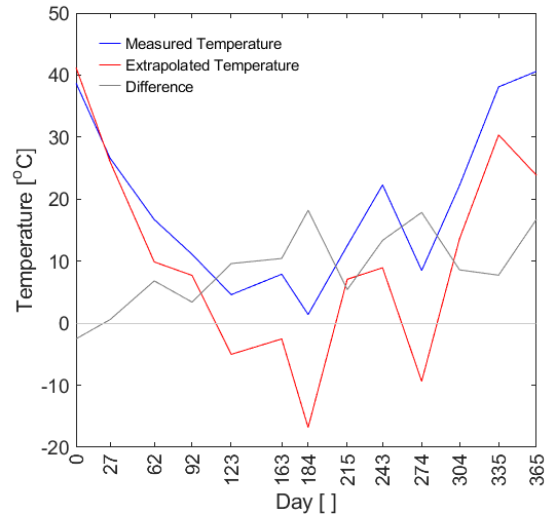


Figure E.14 – C.IV.2

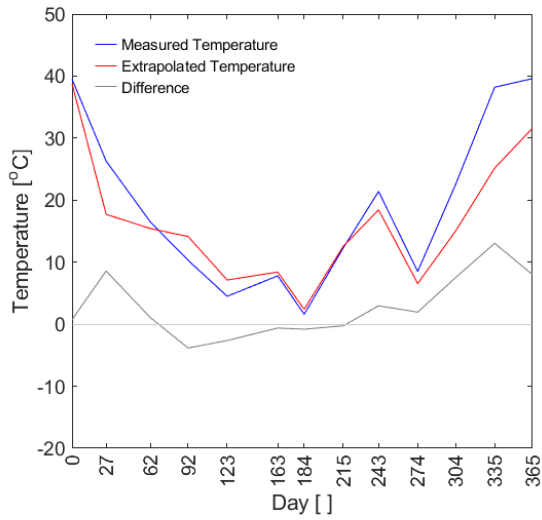


Figure E.15 – C.IV.3

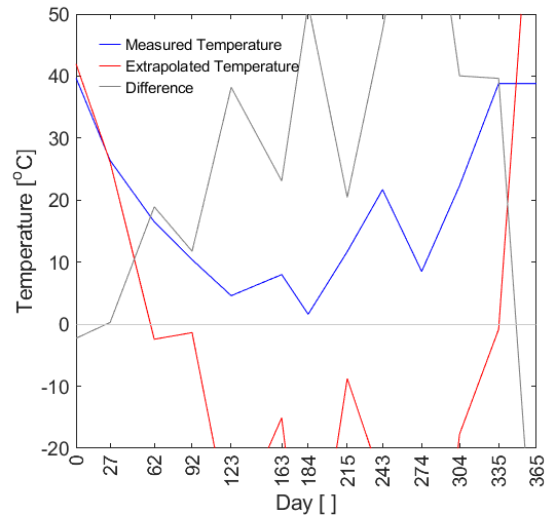
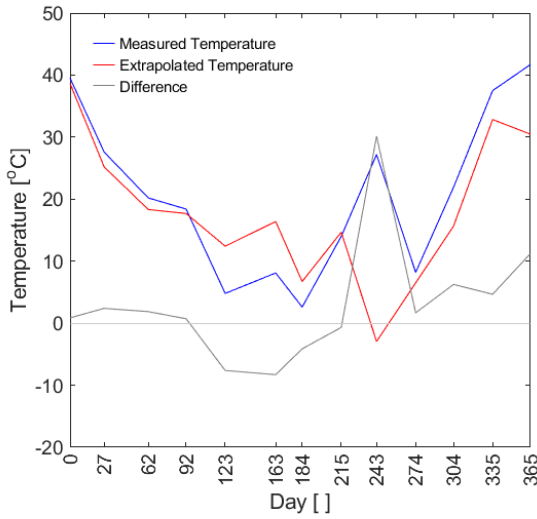
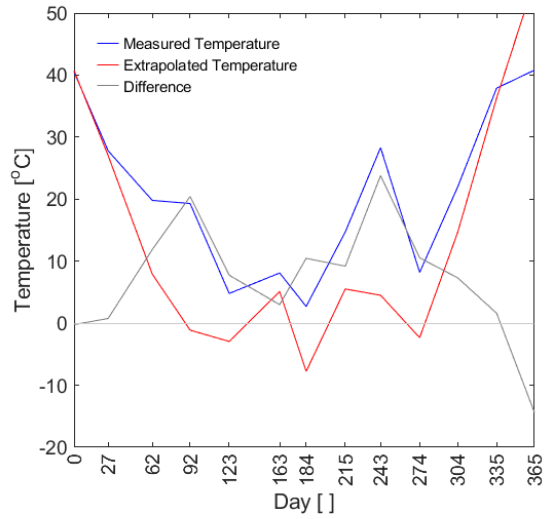


Figure E.16 – C.IV.4



**Figure E.17 – C.V.1**



**Figure E.18 – C.V.2**

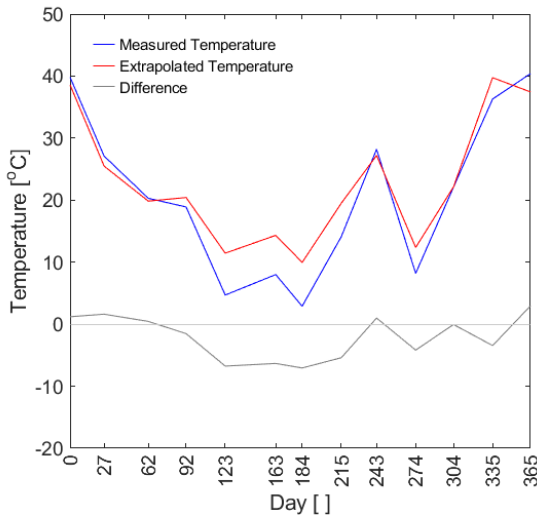


**Figure E.19 – C.V.3**

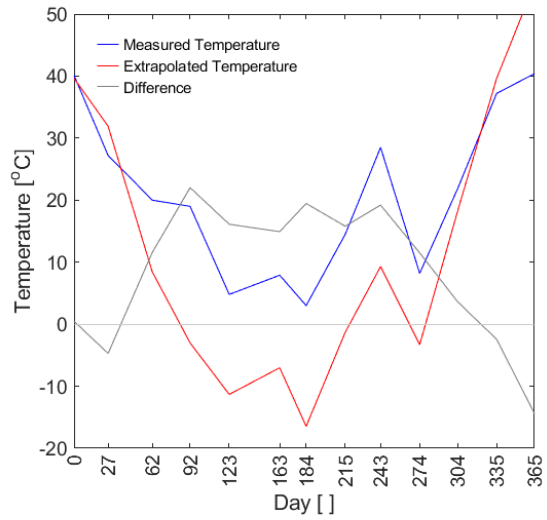


**Figure E.20 – C.V.4**

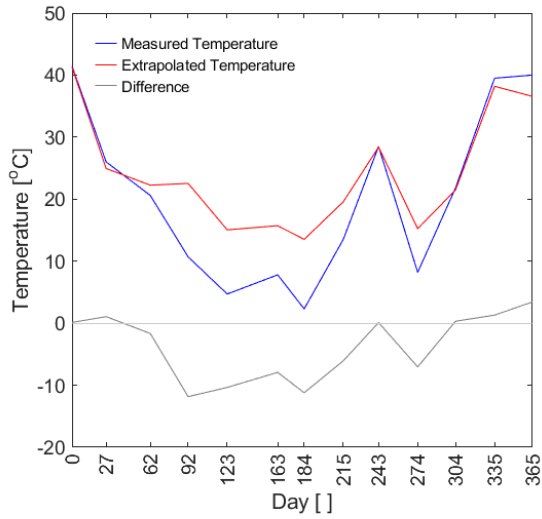


**Figure E.21 – C.VI.1**

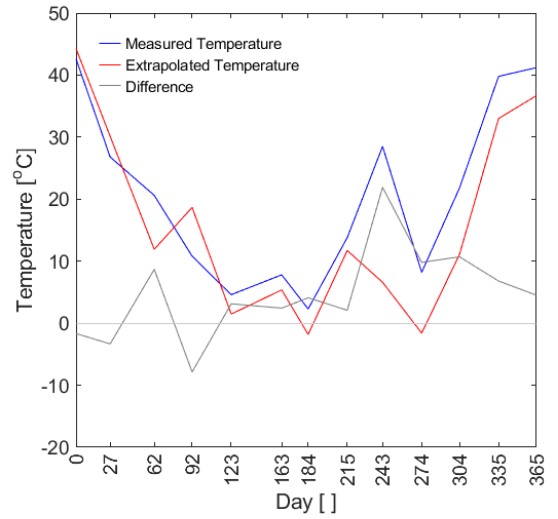


**Figure E.22 – C.VI.2**

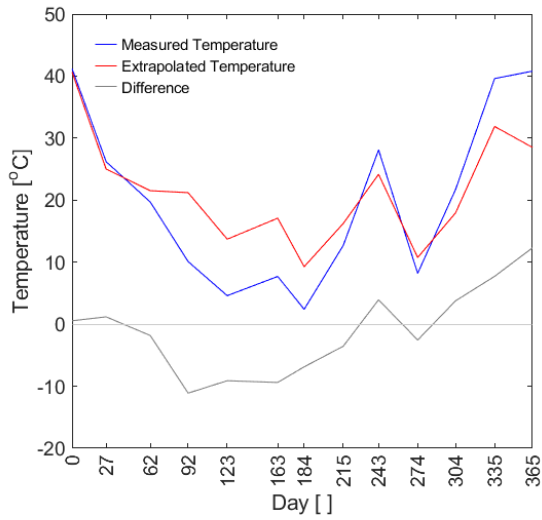


**Figure E.23 – C.VI.3**

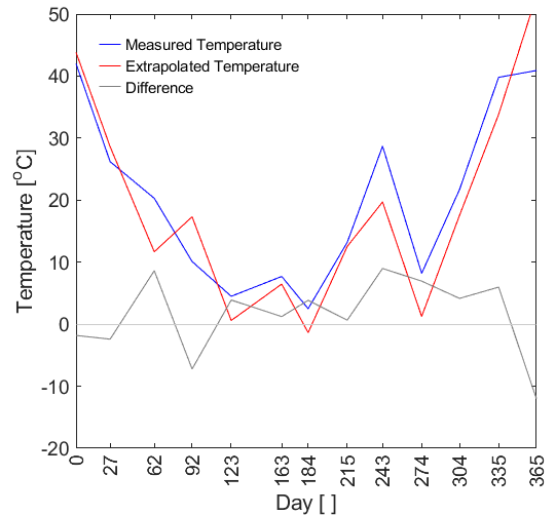


**Figure E.24 – C.VI.4**

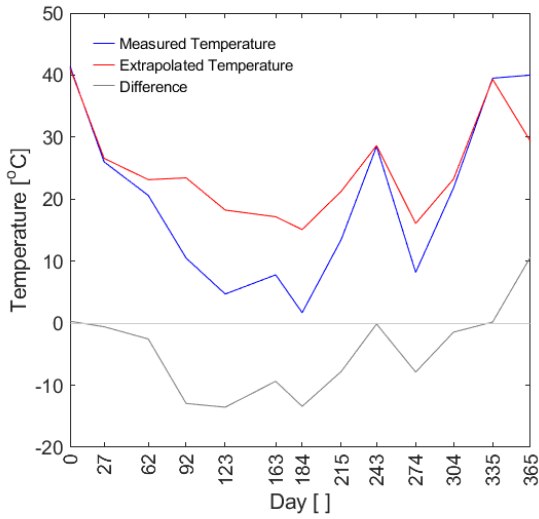


**Figure E.25 – C.VII.1**

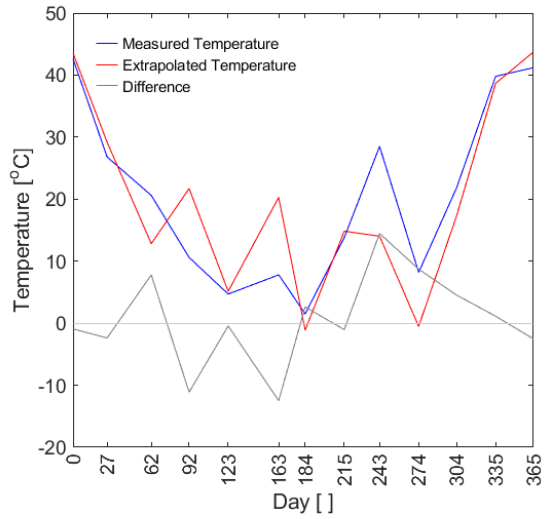


**Figure E.26 – C.VII.2**

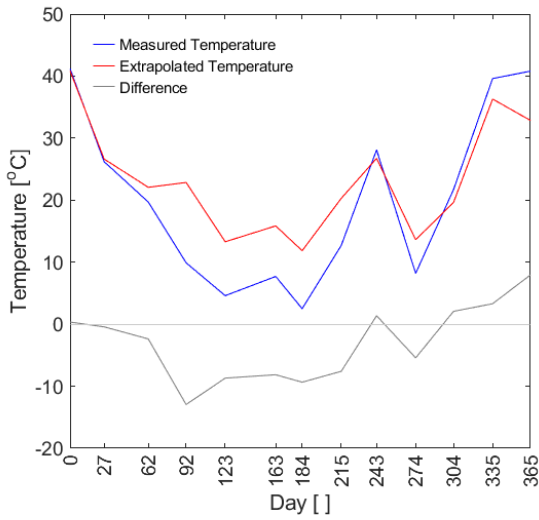


**Figure E.27 – C.VII.3**

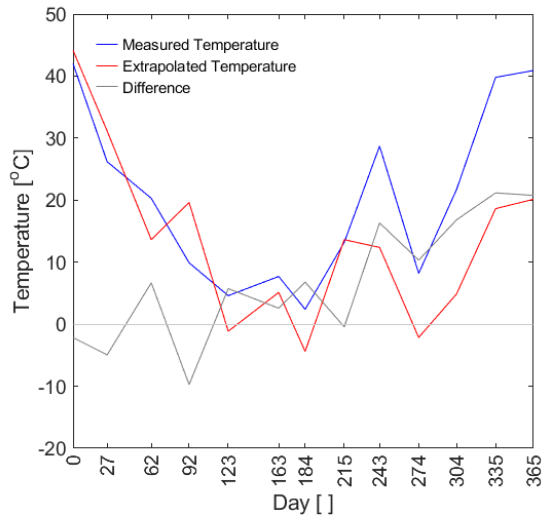


**Figure E.28 – C.VII.4**



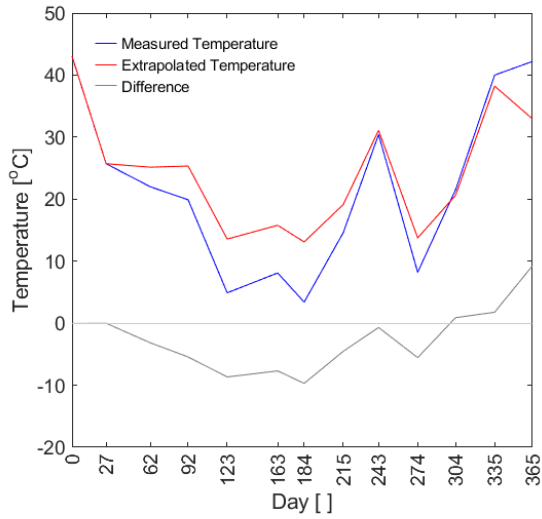


**Figure E.29 – C.VIII.1**

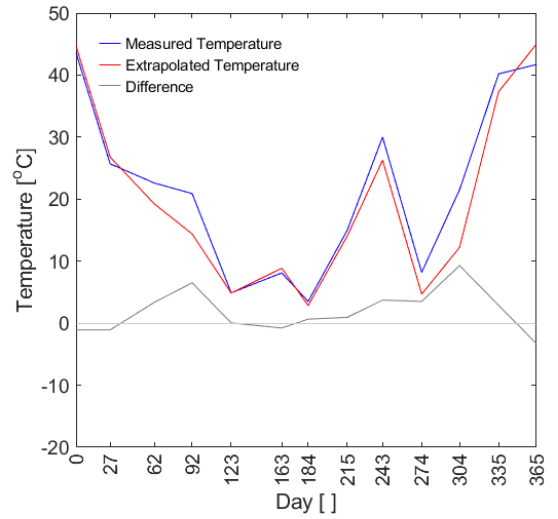


**Figure E.30 – C.VIII.2**

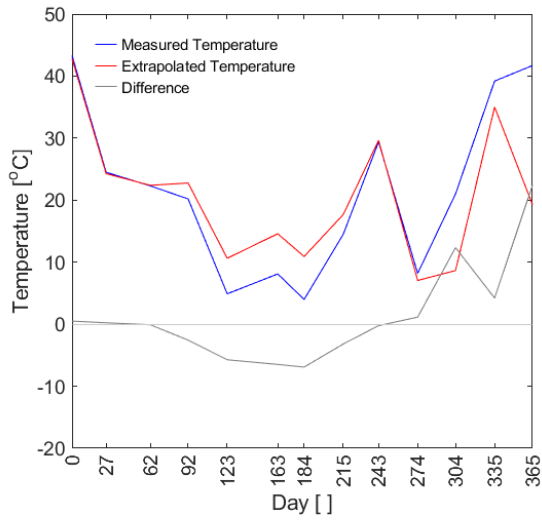


**Figure E.31 – C.VIII.3**

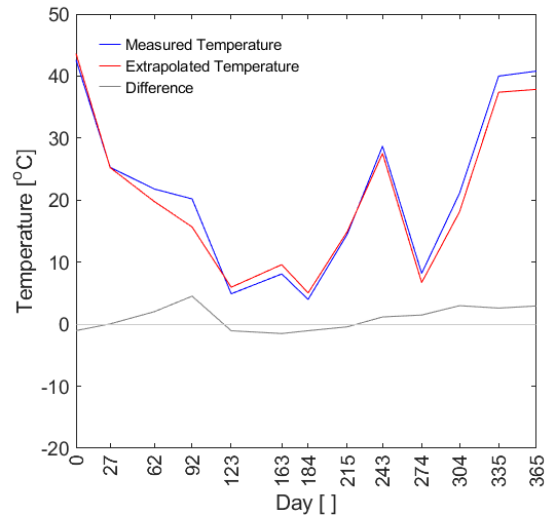


**Figure E.32 – C.VIII.4**

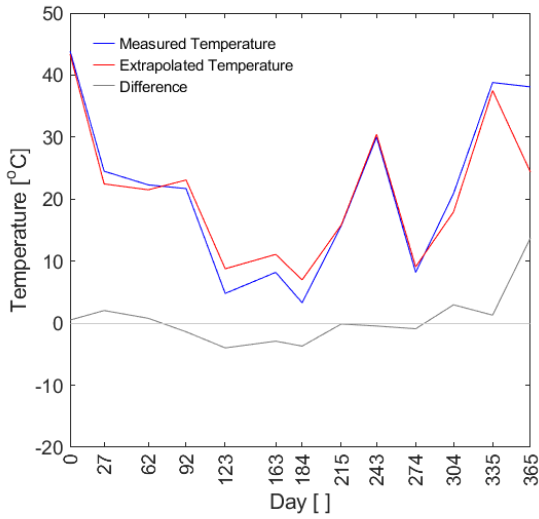


**Figure E.33 – C.IX.1**

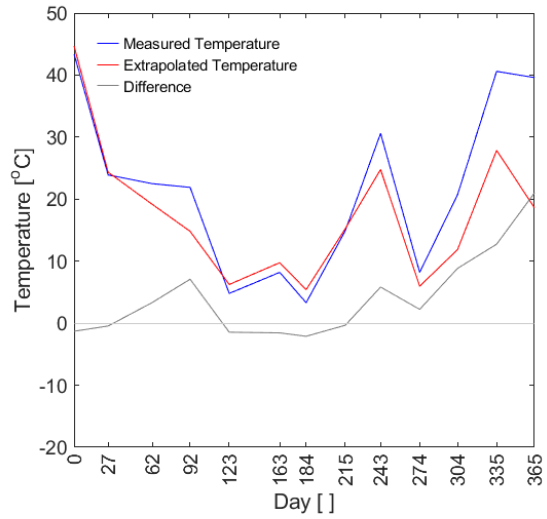


**Figure E.34 – C.IX.2**

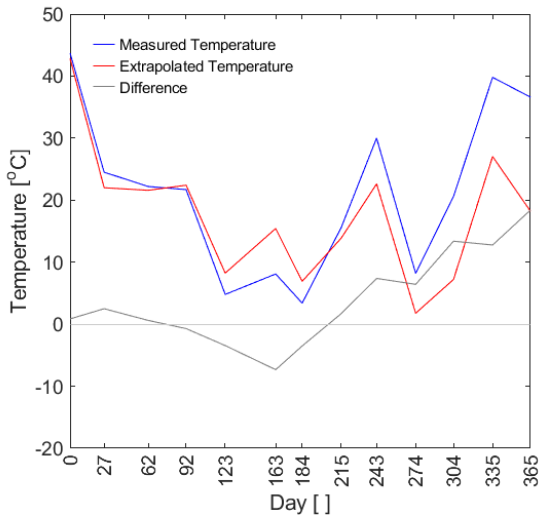


**Figure E.35 – C.IX.3**

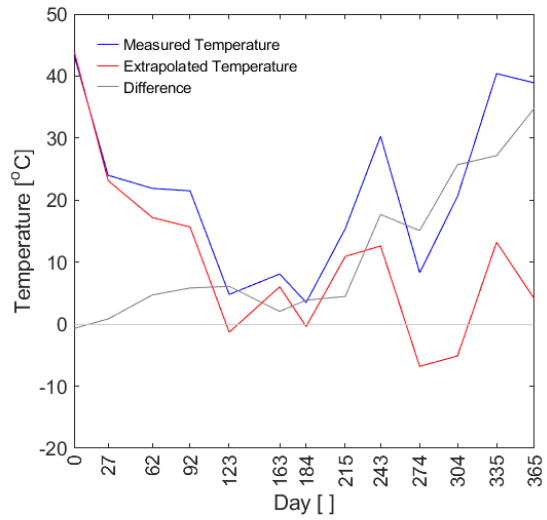


**Figure E.36 – C.IX.4**

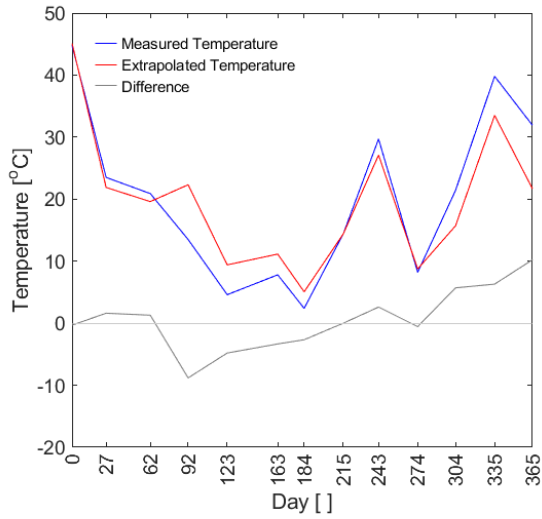


**Figure E.37 – C.X.1**

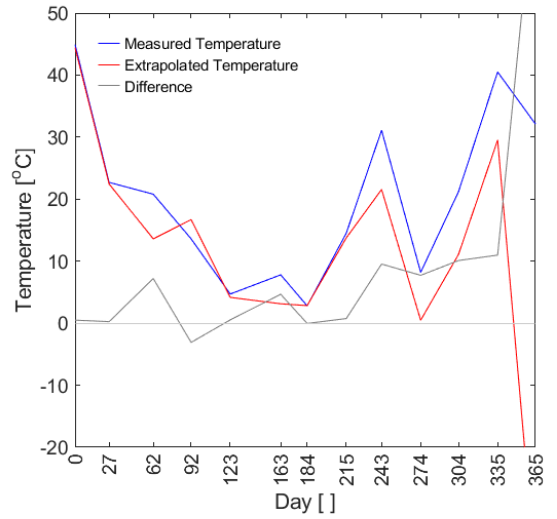


**Figure E.38 – C.X.2**

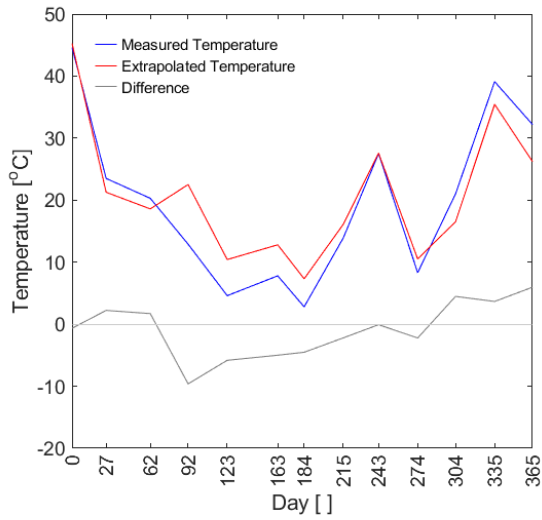


**Figure E.39 – C.X.3**

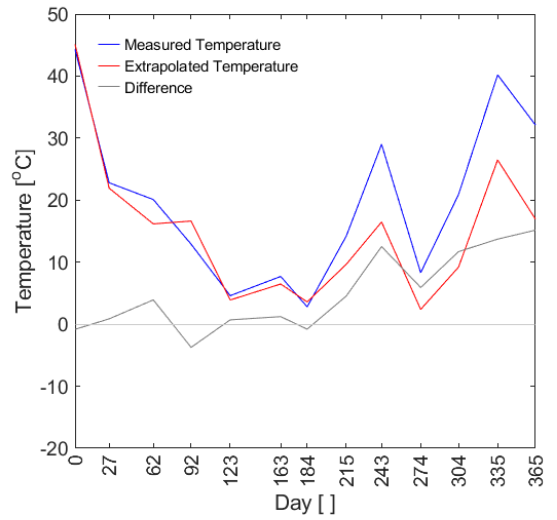


**Figure E.40 – C.X.4**

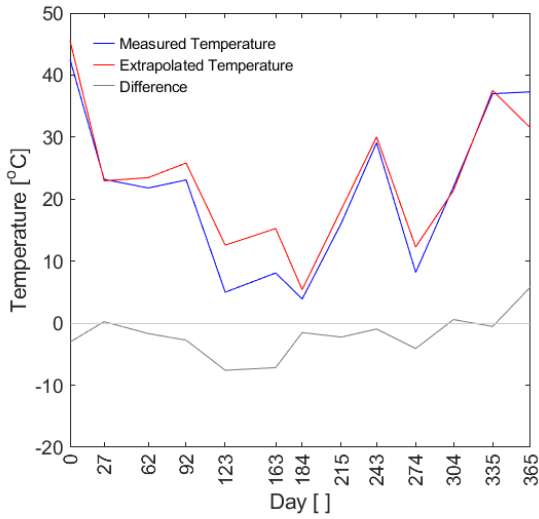


**Figure E.41 – C.XI.1**

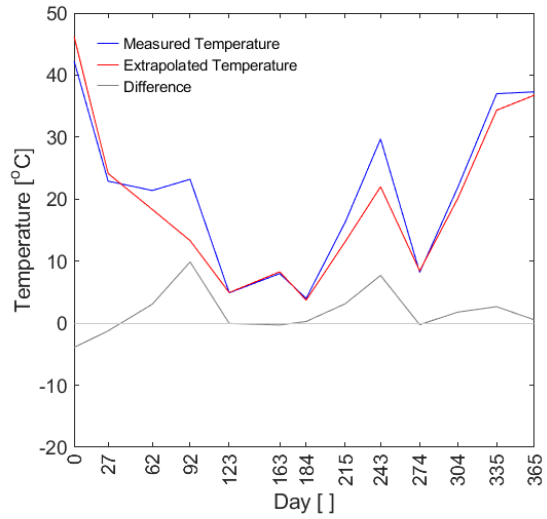


**Figure E.42 – C.XI.2**

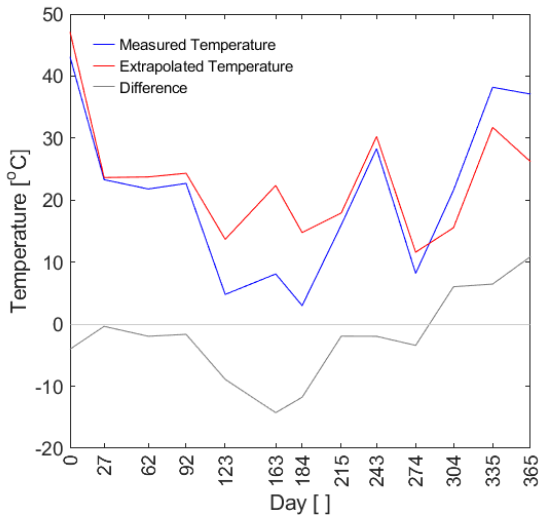


**Figure E.43 – C.XI.3**

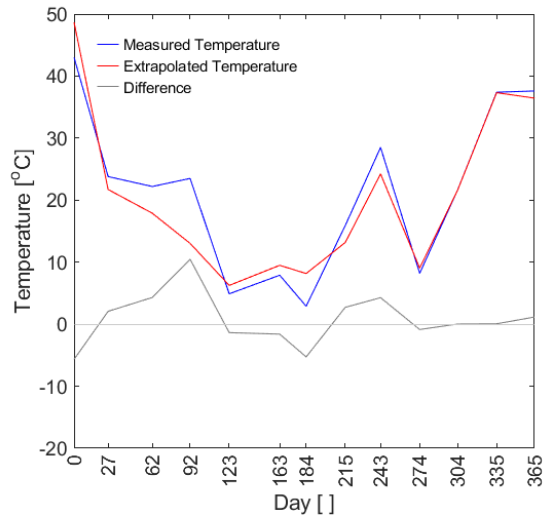


**Figure E.44 – C.XI.4**

## E.2 Bezprávi

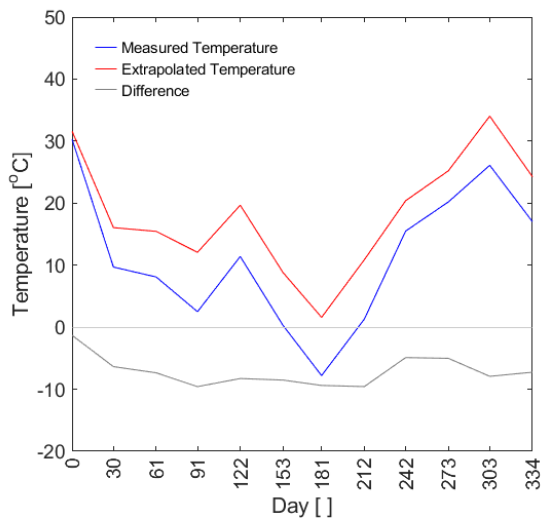


Figure E.45 – D.I.1

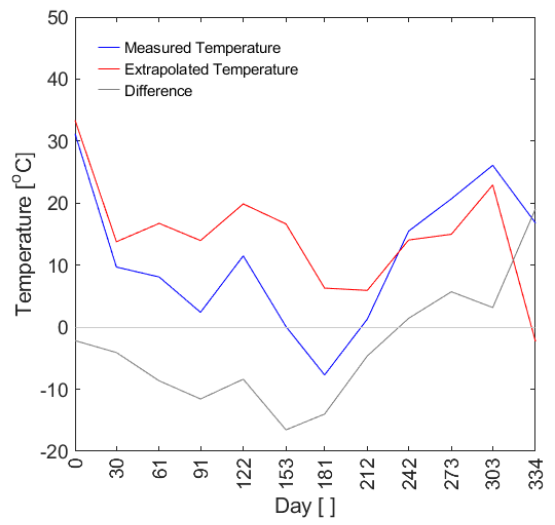


Figure E.46 – D.I.2

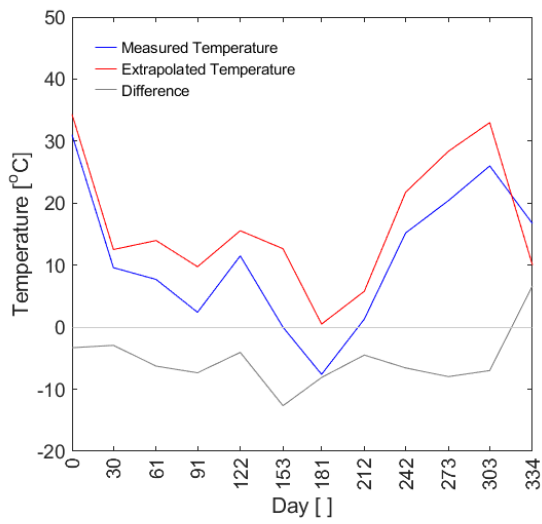


Figure E.47 – D.I.3

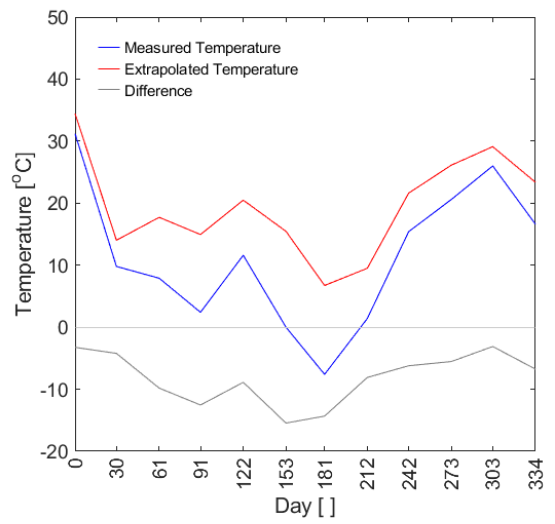
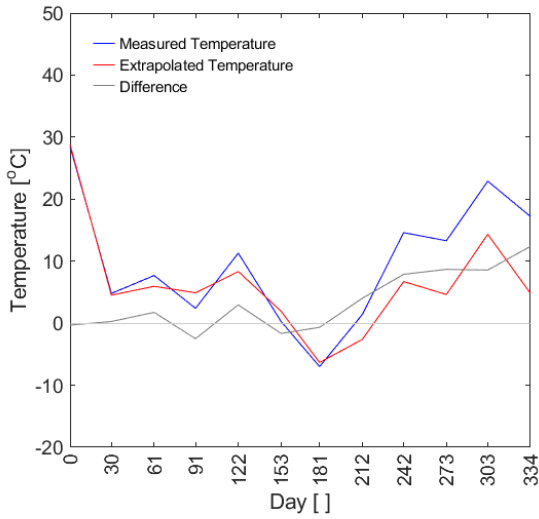
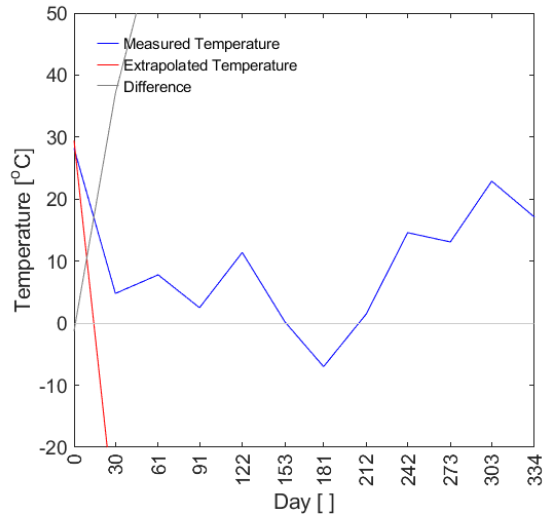


Figure E.48 – D.I.4



**Figure E.49 – D.II.1**



**Figure E.50 – D.II.2**

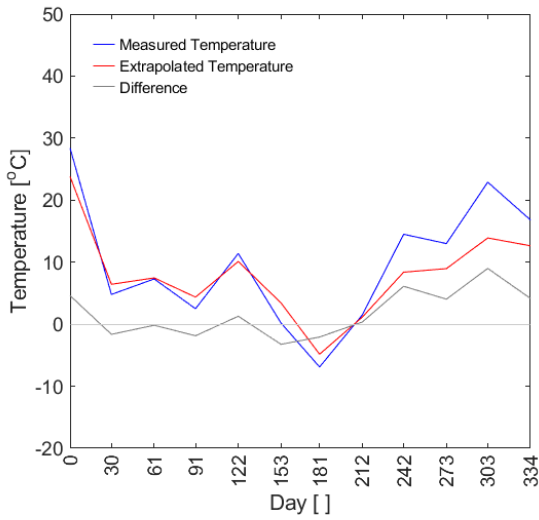


**Figure E.51 – D.II.3**

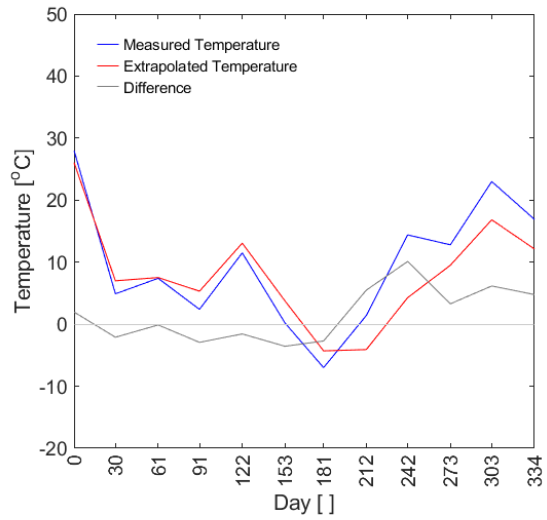


**Figure E.52 – D.II.4**

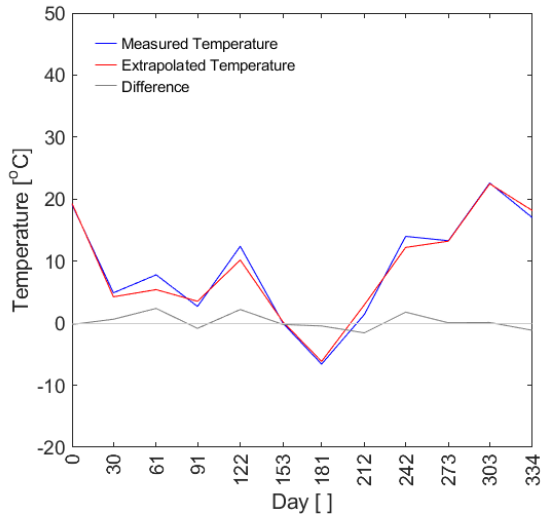


**Figure E.53 – D.III.1**

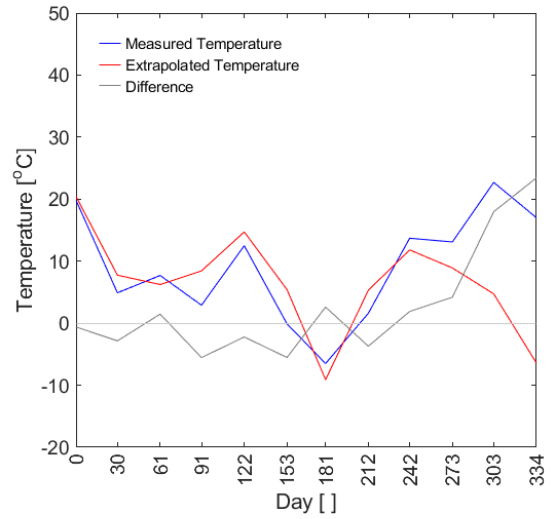


**Figure E.54 – D.III.2**

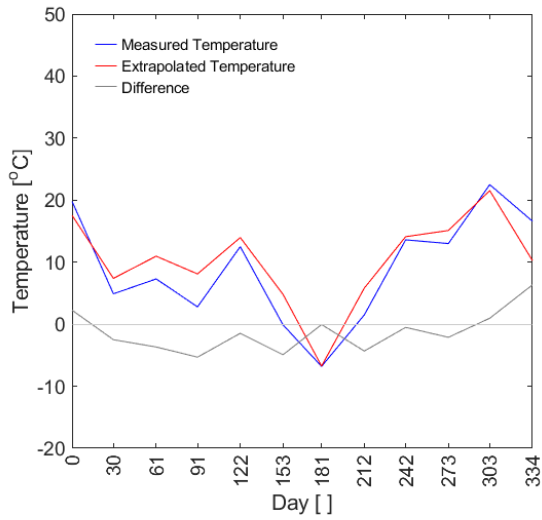


**Figure E.55 – D.III.3**

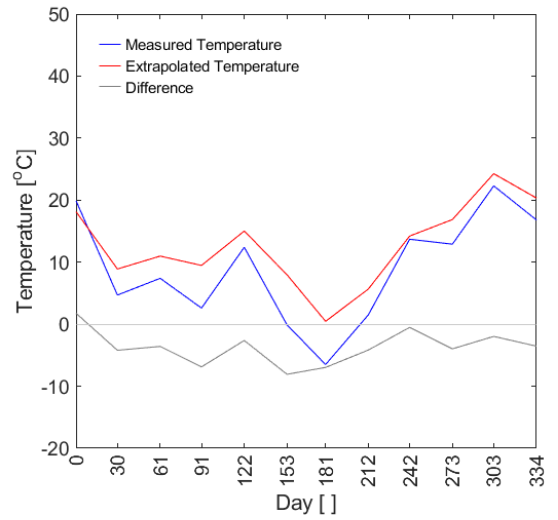


**Figure E.56 – D.III.4**

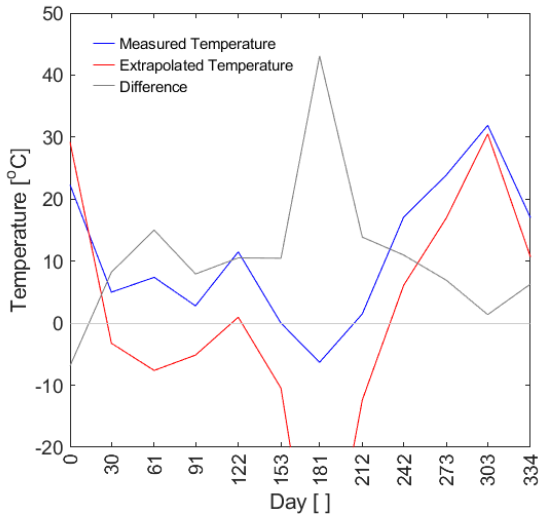


**Figure E.57 – D.IV.1**

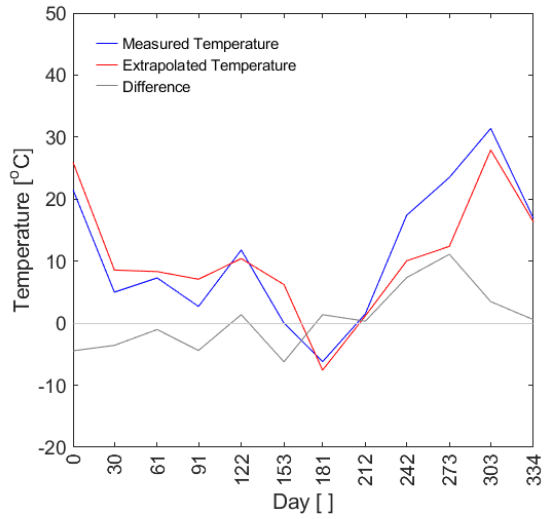


**Figure E.58 – D.IV.2**

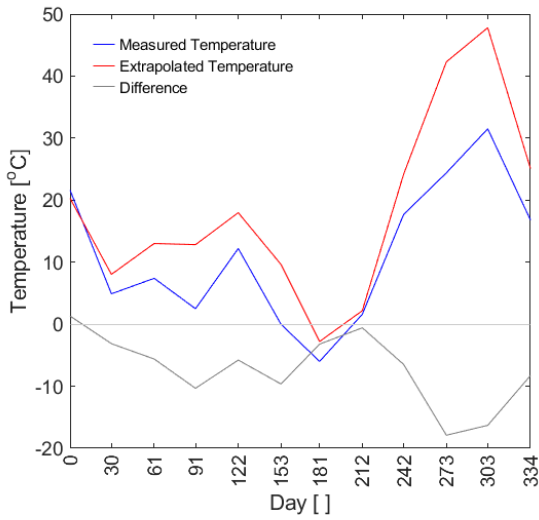


**Figure E.59 – D.IV.3**

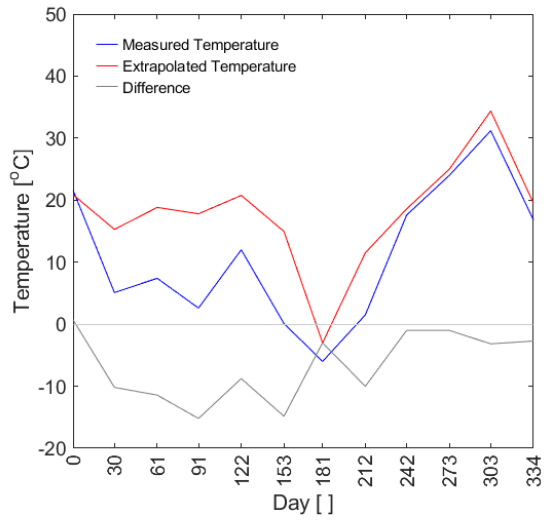


**Figure E.60 – D.IV.4**



## Appendix F

# Comparison of Temperature Differences per Cross-Sectional Profiles

The comparison of curves representing the difference development of the measured and extrapolated temperature from Appendix E is presented in the following graphs. Each comparison includes the difference curves from the measuring spots at one cross-sectional profile of track. The left and right annotation in the legend refer to the left-hand and right-hand side of the track in the direction of the increasing stationing. The marking of the graphs is the same like in the case of Appendix C.

## F.1 Chotěvice

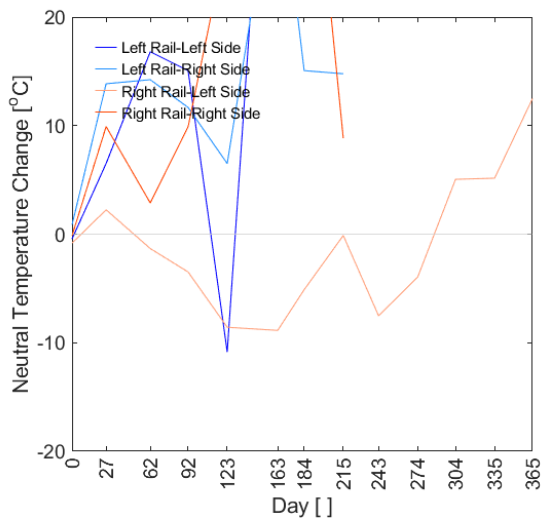


Figure F.1 – C.I

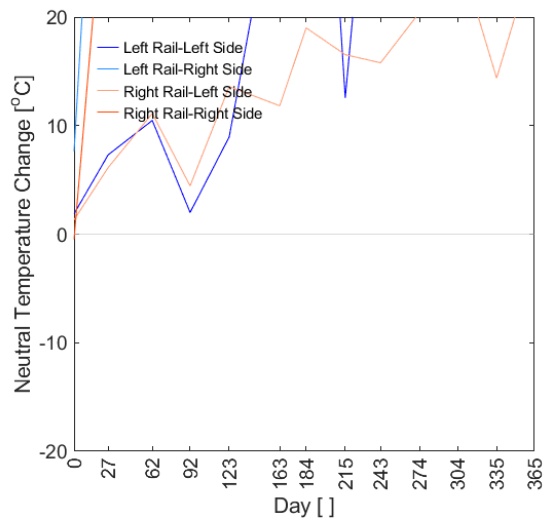


Figure F.2 – C.II

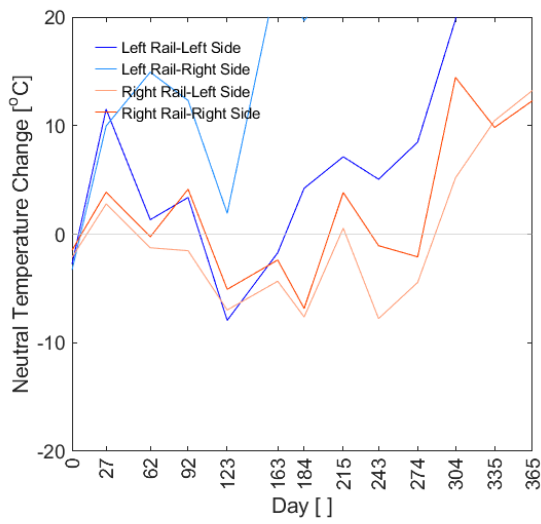


Figure F.3 – C.III

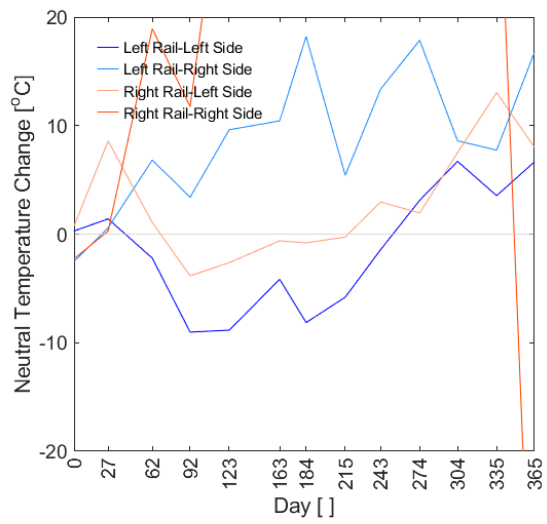
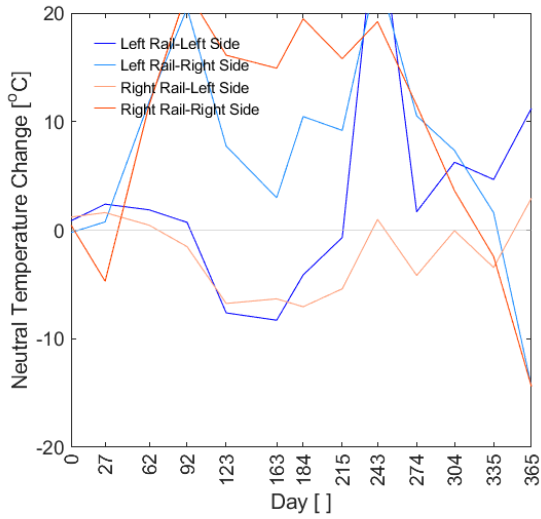
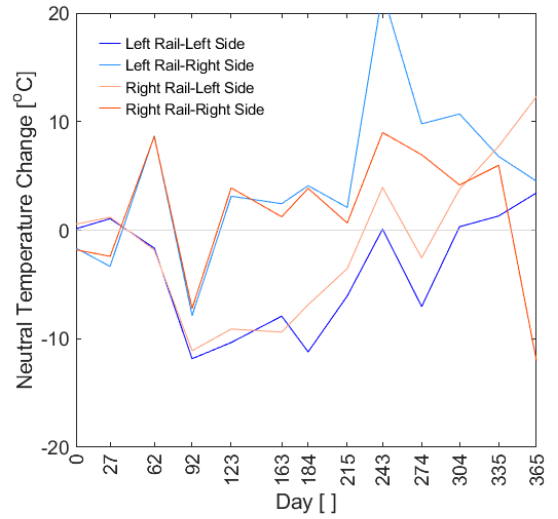


Figure F.4 – C.IV



**Figure F.5 – C.V**



**Figure F.6 – C.VI**

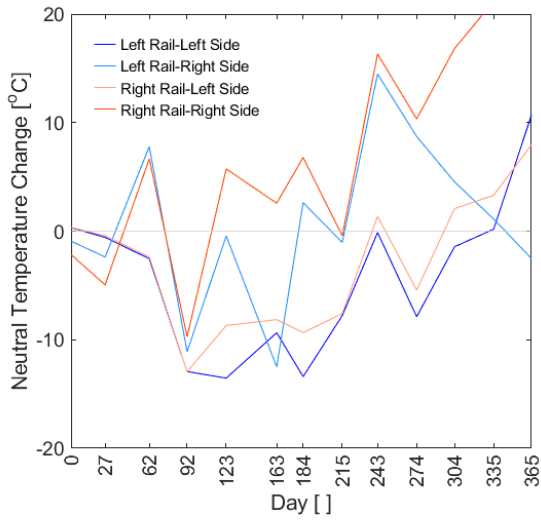


**Figure F.7 – C.VII**

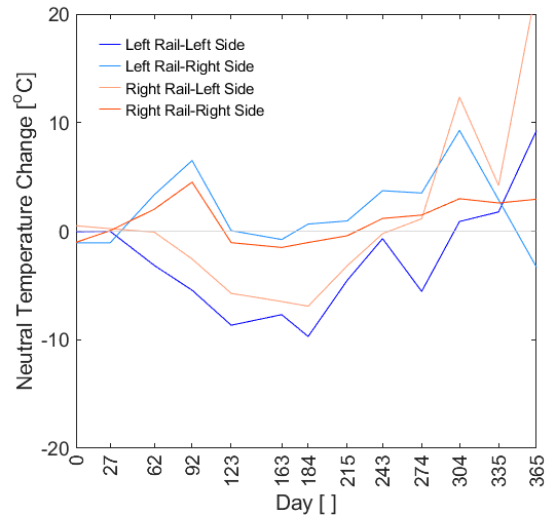


**Figure F.8 – C.VIII**

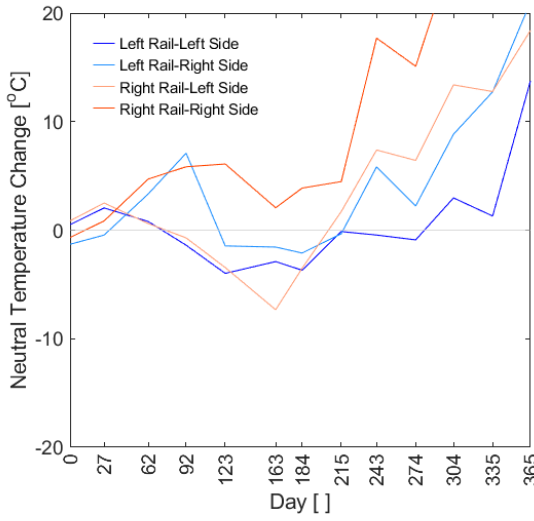


**Figure F.9 – C.IX**

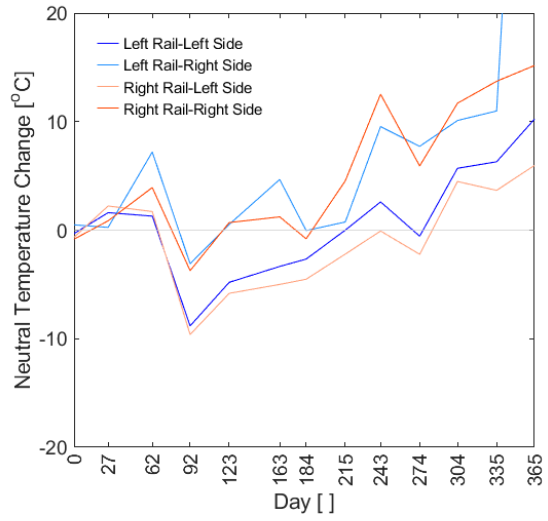


**Figure F.10 – C.X**

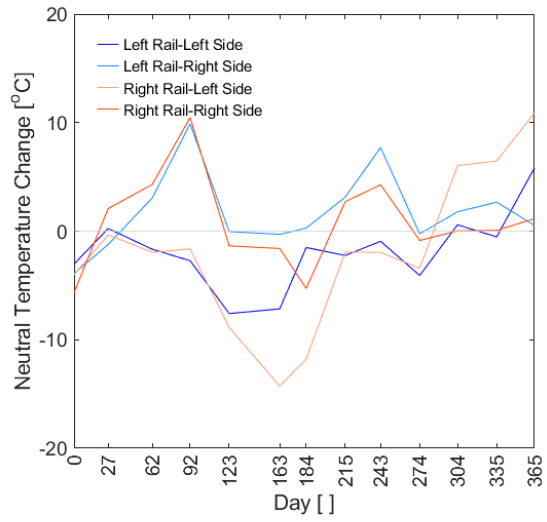


**Figure F.11 – C.XI**

## F.2 Bezprávi

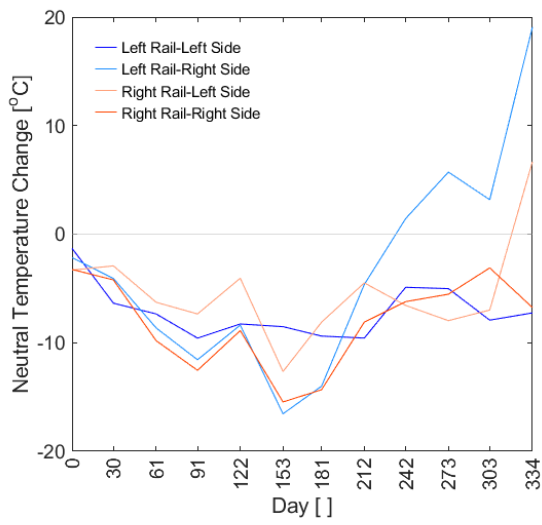


Figure F.12 – D.I

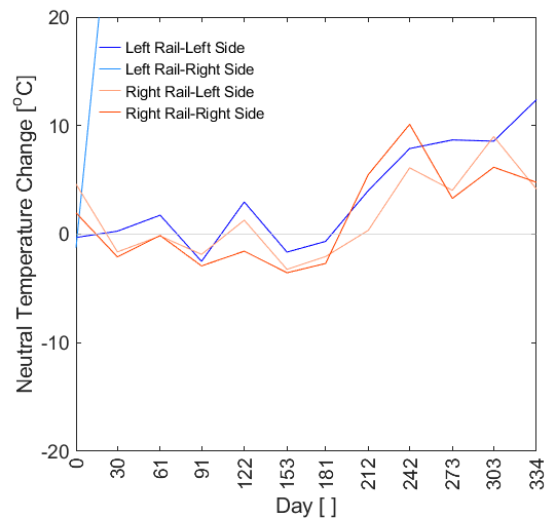


Figure F.13 – D.II

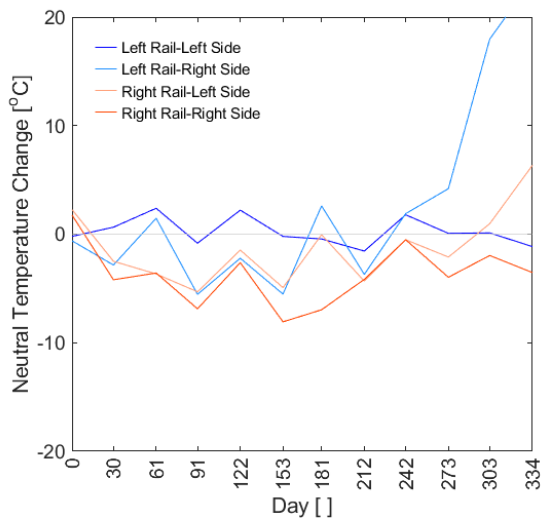


Figure F.14 – D.III

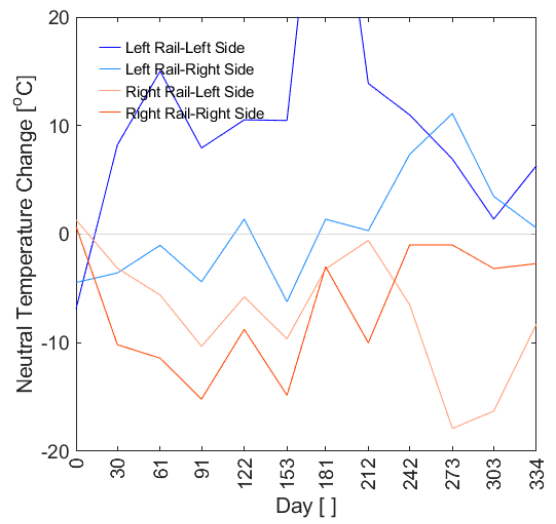


Figure F.15 – D.IV



## Appendix G

# Comparison of Standard and New Approach to the Thermal Stress Determination in CWR

The full scale versions of Figures 5.19 – 5.26 including the legends are presented in this appendix.

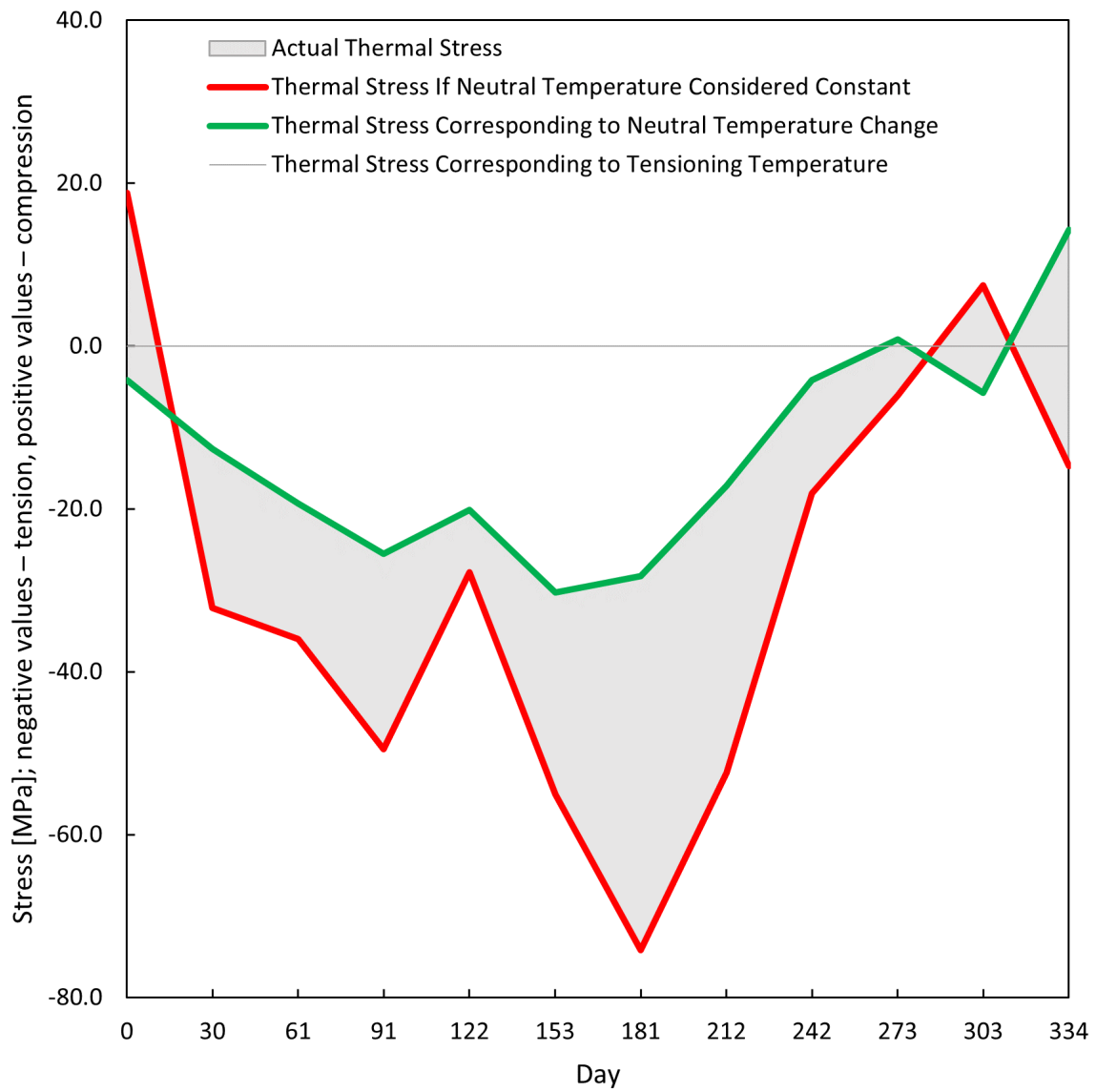


**Figure G.1** – D.I – Left Rail: Comparison of Standard and New Approach to the Thermal Stress Determination in CWR



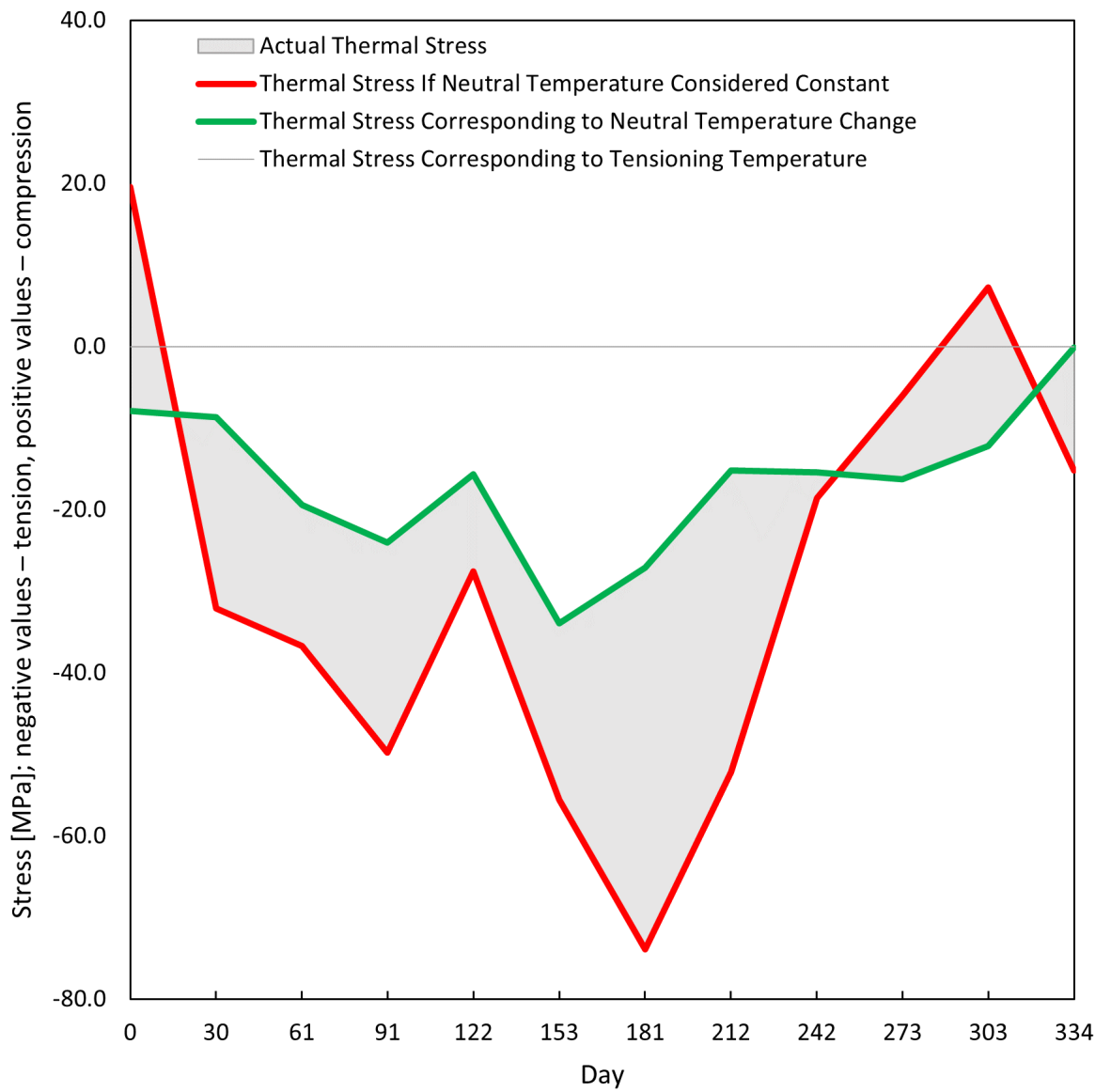


**Figure G.2** – D.I – Right Rail: Comparison of Standard and New Approach to the Thermal Stress Determination in CWR

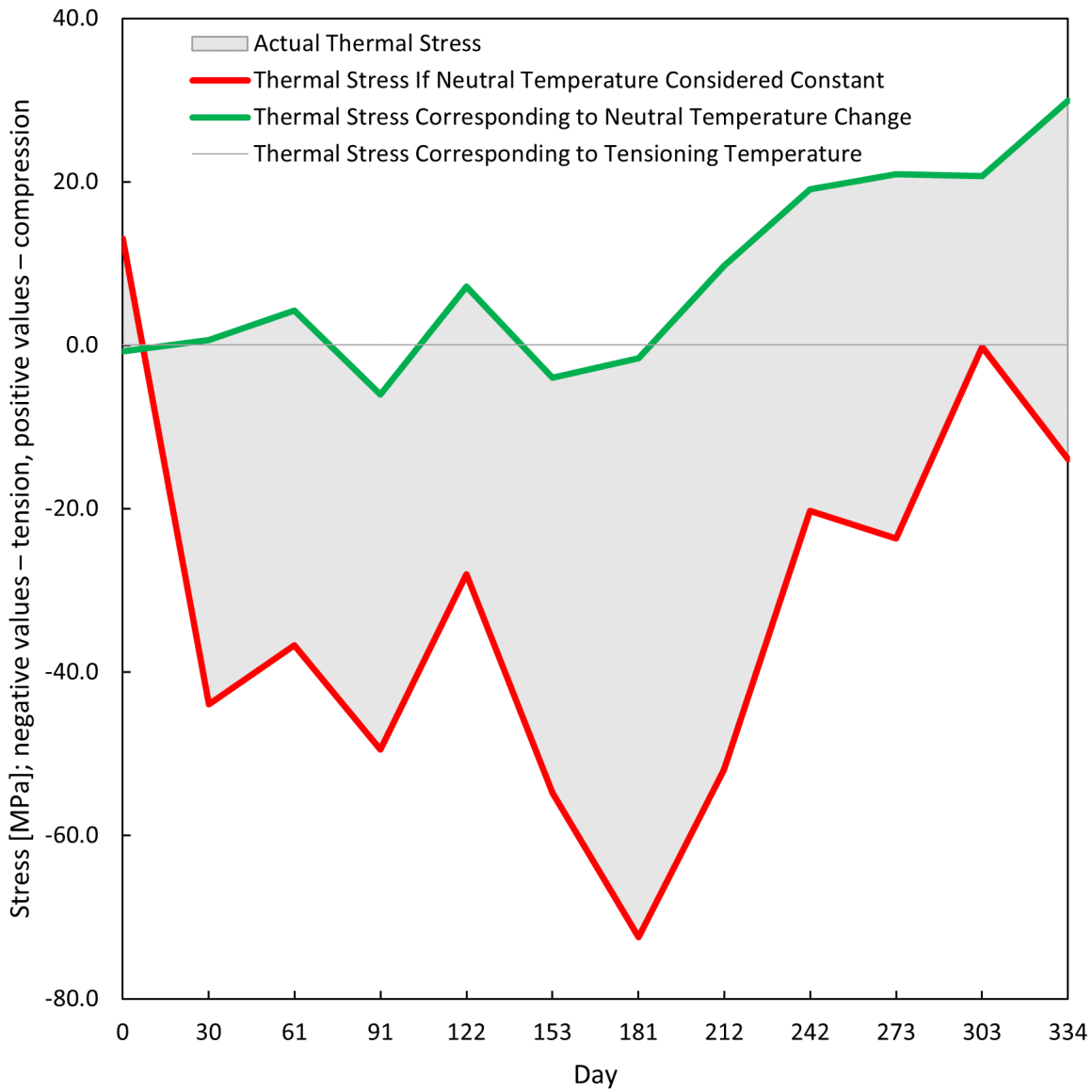


**Figure G.3 – D.II – Left Rail:** Comparison of Standard and New Approach to the Thermal Stress Determination in CWR

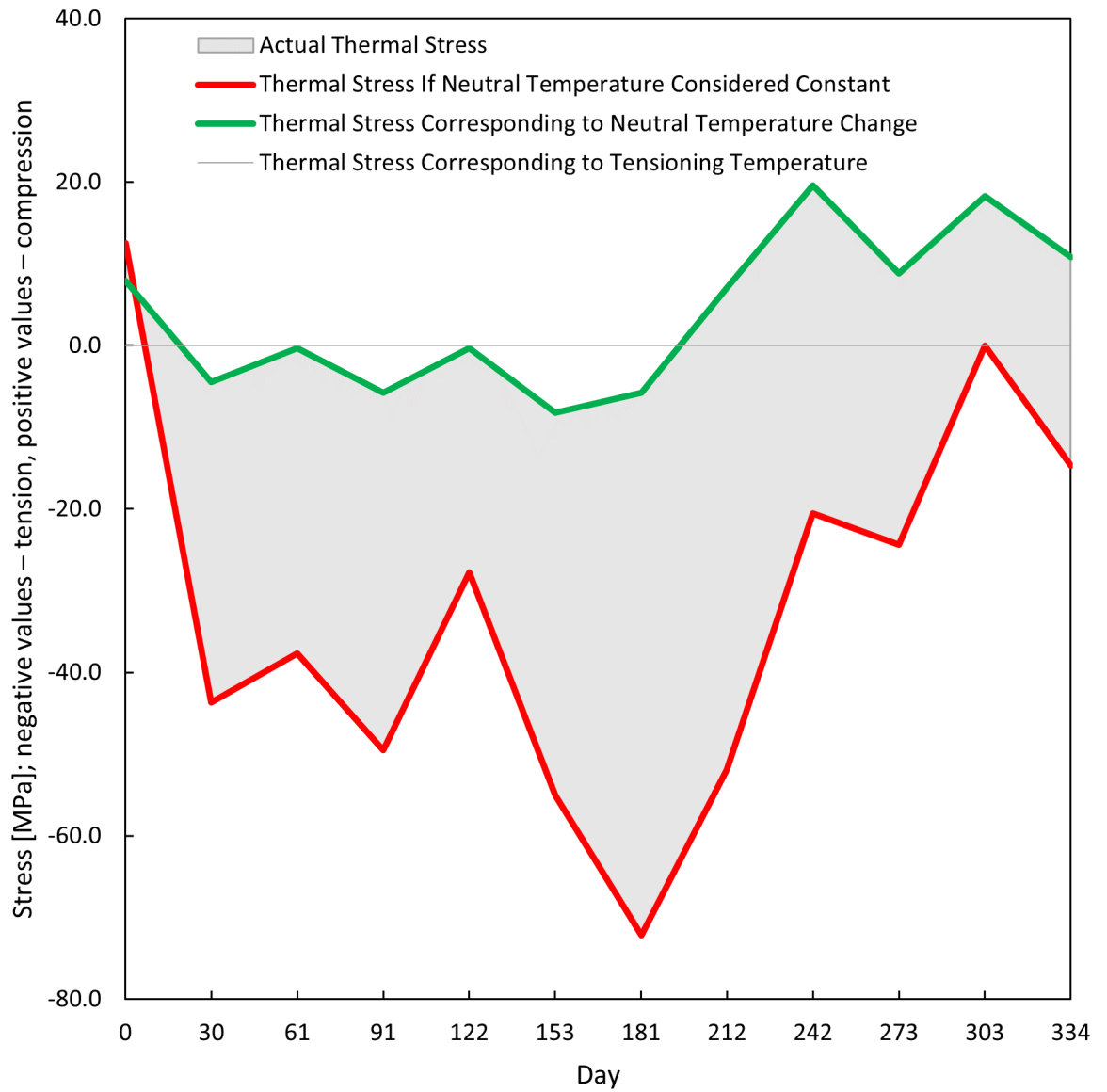


**Figure G.4 – D.II – Right Rail:** Comparison of Standard and New Approach to the Thermal Stress Determination in CWR

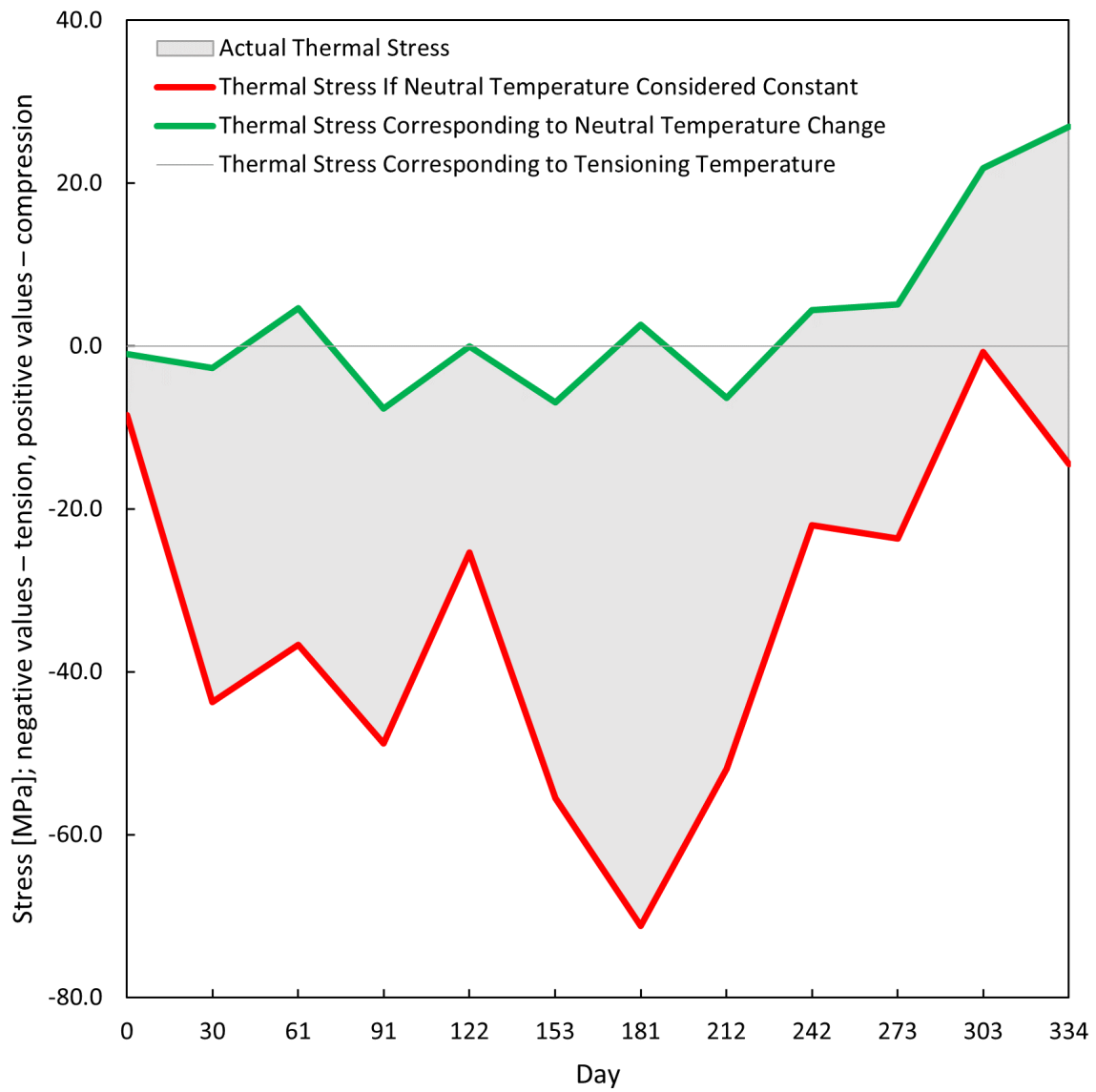


**Figure G.5 – D.III – Left Rail:** Comparison of Standard and New Approach to the Thermal Stress Determination in CWR

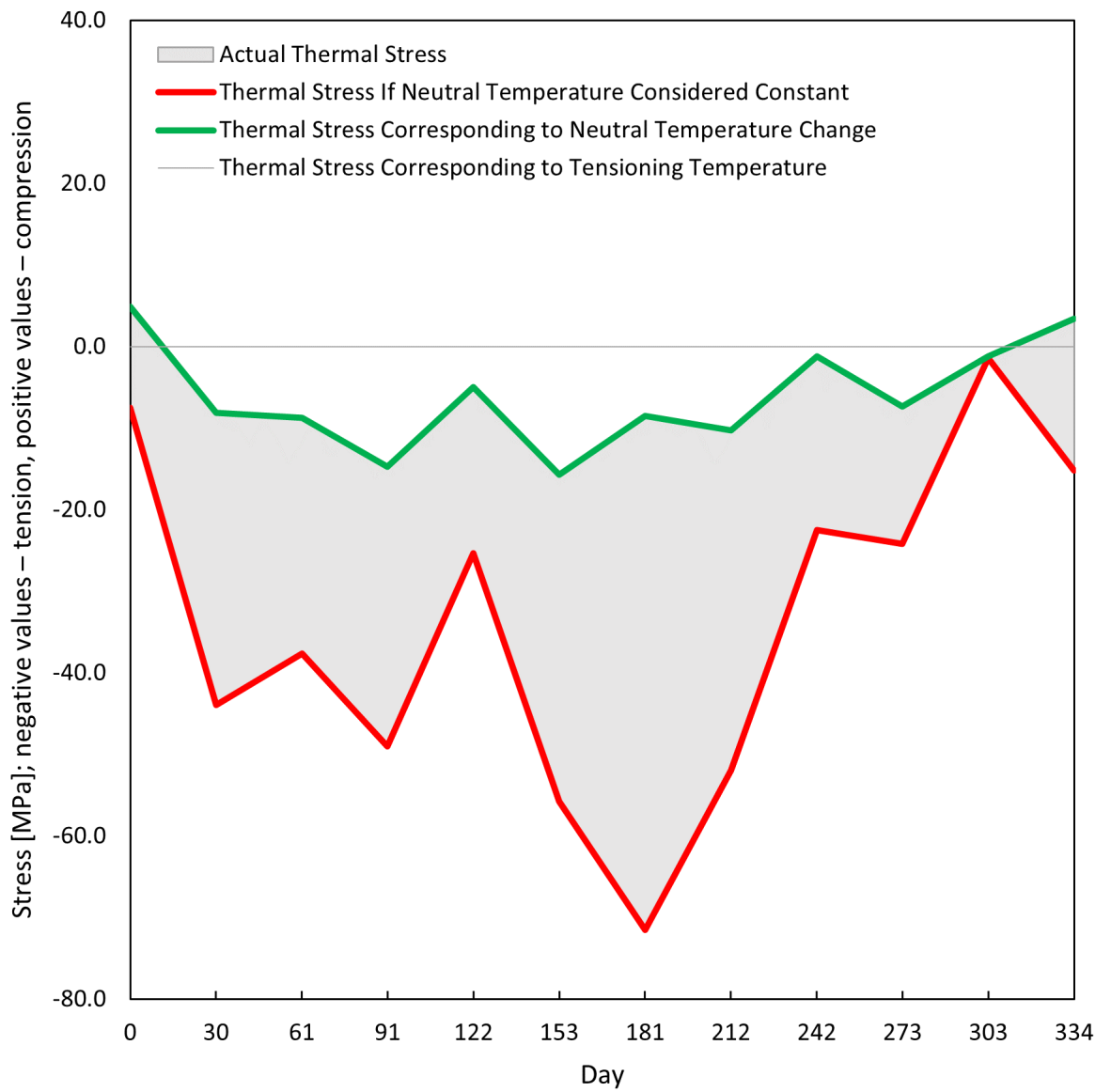


**Figure G.6 – D.III – Right Rail:** Comparison of Standard and New Approach to the Thermal Stress Determination in CWR

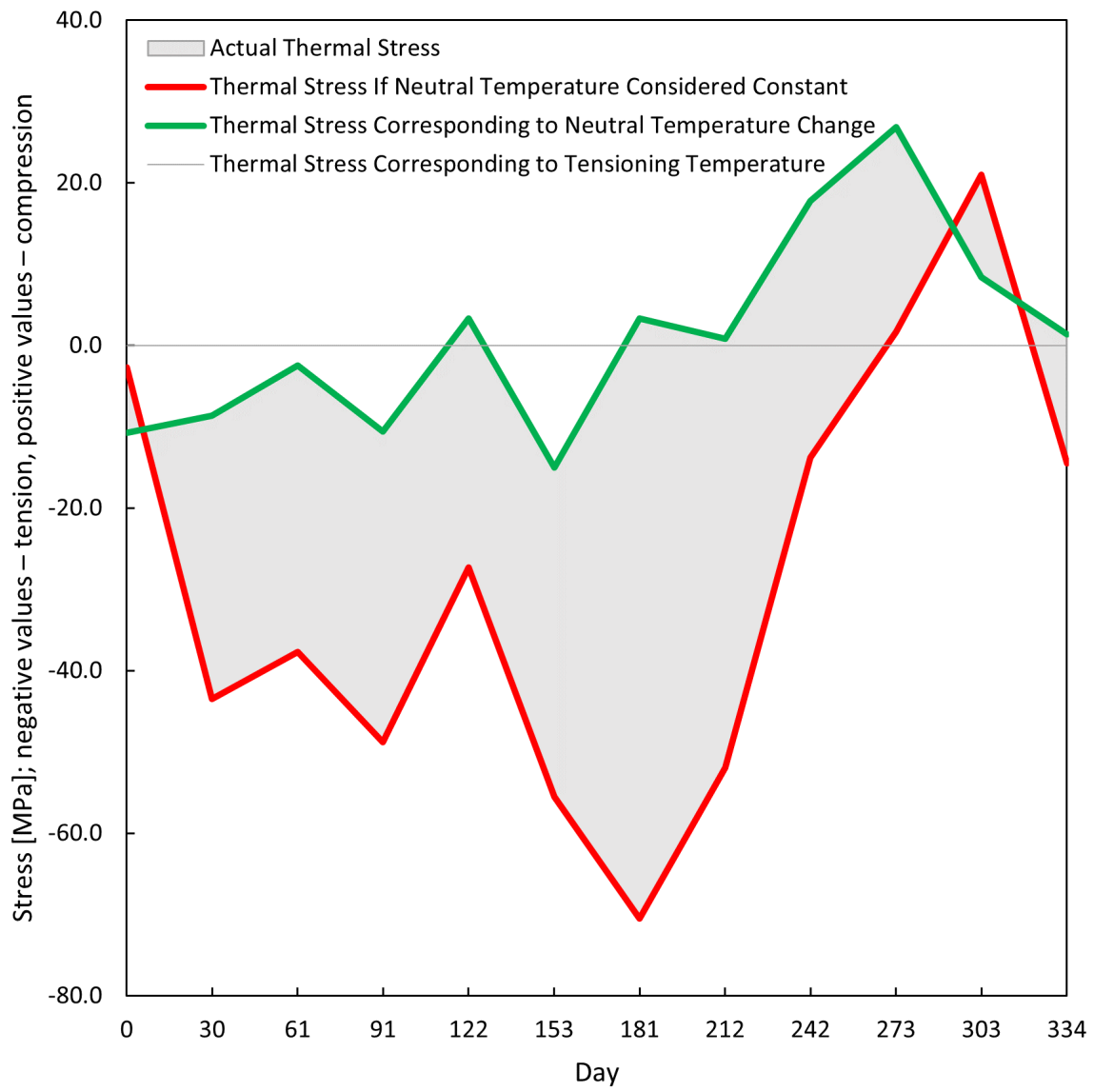


**Figure G.7 – D.IV – Left Rail:** Comparison of Standard and New Approach to the Thermal Stress Determination in CWR

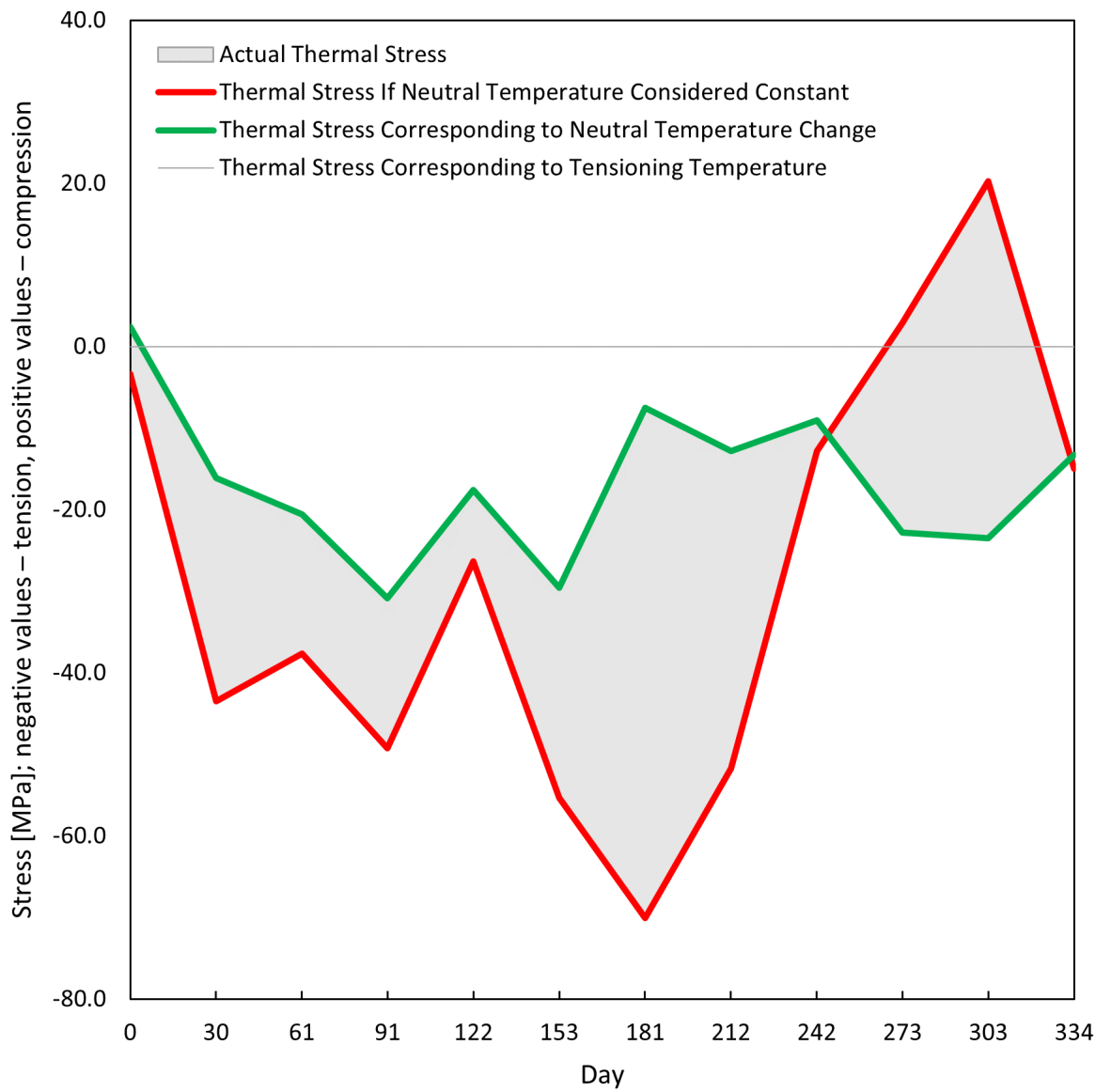


**Figure G.8 – D.IV – Right Rail: Comparison of Standard and New Approach to the Thermal Stress Determination in CWR**





# Annexes

The following documents are annexed to the dissertation:

- Methodology of Non-Destructive Determination of Mechanical Stress in Continuous Welded Rail *as an outcome No. TJ04000301-V1 of the research project No. TJ04000301 Non-Destructive Determination of Mechanical Stress in Continuous Welded Rail,*
- Scheme of Strain Gauge Installation in Bezprávi Locality *as an annex to the methodology,*
- Documentation of the Measuring Set for Diagnostics of Time-Based Development of Stress States in Continuous Welded Rail *as an outcome No. TJ04000301-V2 of the research project No. TJ04000301 Non-Destructive Determination of Mechanical Stress in Continuous Welded Rail and as an annex to the methodology,* and
- Certificate of Approval of the Methodology by the Ministry of Transport of the Czech Republic (in Czech only).



UNIVERSITY  
OF PARDUBICE  
FACULTY  
OF TRANSPORT  
ENGINEERING

# **Methodology of Non-Destructive Determination of Mechanical Stress in Continuous Welded Rail**

Authors: Petr Vnenk  
Özgür Yurdakul, Ph.D.  
Jiří Šlapák  
Vladimír Suchánek, Ph.D.  
Ondřej Sadílek, Ph.D.  
Filip Klejch  
Assoc. Prof. Bohumil Culek, Ph.D.  
Assoc. Prof. Ladislav Řoutil, Ph.D.

Released: 8<sup>th</sup> February 2022.

Development of this methodology is a direct outcome of research performed within the scope of investigation of the TACR TJ04000301 project *Non-Destructive Determination of Mechanical Stress in Continuous Welded Rail*.

# Contents

<b>Introduction</b>	<b>3</b>
<b>1 Goals</b>	<b>4</b>
<b>2 Terms and Acronyms</b>	<b>5</b>
2.1 Terms . . . . .	5
2.2 Acronyms . . . . .	6
<b>3 Used Instruments and Software</b>	<b>7</b>
<b>4 Methodology Description</b>	<b>9</b>
4.1 Test Fundamentals . . . . .	9
4.2 Test Procedure – Part I: Installation of Measuring Set Track Unit . . . . .	12
4.3 Test Procedure – Part II: Measurement . . . . .	14
4.4 Test Output . . . . .	15
4.5 Test Evaluation . . . . .	16
4.6 Recommendations . . . . .	18
<b>5 Novelty of Procedures</b>	<b>21</b>
<b>6 Methodology Applicability Description</b>	<b>22</b>
<b>7 Economic Aspects</b>	<b>23</b>
7.1 Measurement Costs . . . . .	23
7.2 Possible Economic Assets . . . . .	24
<b>8 References</b>	<b>25</b>
<b>9 Annexes</b>	<b>26</b>
9.1 Complete List of Items for Installation and Measurements Used by the Authors .	26
9.2 Example of Methodology Application – Bezprávi Locality . . . . .	29
9.3 Other Annexes . . . . .	31

## Introduction

This methodology describes a procedure for a non-destructive determination of an instant value of normal mechanical stress in continuous welded rail (CWR).

In addition, it focuses on determining the development of longitudinal deformation of continuous welded rail in time and on the rail neutral temperature changes. Further significant factors influencing the mechanical stress in rail are the residual stress and the stress from railway operations. State-of-art literature provides determination of these stresses [1, 2, 3, 4, 5], but their description exceeds the scope of this methodology.

The methodology brings benefits to science and practice. Although the methodology meets the criteria set for the desired way of the CWR stress determination by Kish and Samavedam in 1987 [6] only partially, it allows scientific and academic institutions' research teams and railway infrastructure R&D managers focusing on the continuous welded rail to benefit from the valuable information on CWR behaviour. [7, 8]

A precise determination of the mechanical stress value in CWR is essential for a correct and timely adoption of measures preventing failures of the continuous welded rail, mostly rail breaks and track buckling. The methodology's assets lie in its non-destructive character, relatively simple installation of a measuring set track unit, high precision of strain gauges and fast measurement, which may be carried out even on heavy haul railway lines without the need for a track closure.

Implementation of this methodology enables obtaining data on longitudinal rail deformation. The rail deformation development can be observed both in the long and short term.

The long-term observation may rest in the determination of a level or a period of consolidation of a newly constructed permanent way. The short-term observation may serve to control the level of rail stressing or the equality of its elongation at the time of welding.

The rail neutral temperature is a temperature at which there is zero thermal load stress in the CWR. [7] It is one of the important factors influencing the current value of the normal mechanical stress in the CWR.

The methodology was developed within the scope of investigation of the TACR TJ04000301 project *Non-Destructive Determination of Mechanical Stress in Continuous Welded Rail*. The research team consisted of the following departments of the Faculty of Transport Engineering of the University of Pardubice: Educational and Research Centre in Transport, Department of Transport Structures, Department of Transport Means and Diagnostics, and Department of Electrical and Electronic Engineering and Signalling in Transport.

## 1 Goals

- 1.1 This methodology contains a procedure to determine the instant value of normal mechanical stress in CWR by a non-destructive way using strain gauges and a measuring set. It focuses mostly on values of deformation and neutral temperature in CWR.
- 1.2 Functioning sample No. TJ04000301-V2 *Measuring Set for Diagnostics of Time-Based Development of Stress States in Continuous Welded Rail*, which is an outcome of investigation of the TACR TJ04000301 project *Non-Destructive Determination of Mechanical Stress in Continuous Welded Rail* is utilised for determination of the instant value of mechanical stress in CWR, CWR deformation, and neutral temperature according to this methodology. Documentation of this functioning sample is provided in the annex to this methodology.

## 2 Terms and Acronyms

### 2.1 Terms

*in alphabetical order:*

breathing end	– section at the beginning and the end of a CWR where rail dilation occurs due to rail temperature changes [8]
continuous welded rail (CWR)	– rail of length of 150 m and more [8]
corridor line	– main railway line which concentrates a significant amount of traffic performance in a network
data acquisition system	– hardware that serves to charge sensors, collect and process recorded signal
measuring set	– functioning sample with identification code TJ04000301-V2, which is an outcome of investigation of the TACR TJ04000301 project <i>Non-Destructive Determination of Mechanical Stress in Continuous Welded Rail</i>
measuring spot	– place on rail where deformation monitoring is performed using a measuring set
monitored section	– railway line section where measurement according to this methodology is performed
rail foot	– bottom flange of rail, which resides on supports and which is tightened by fasteners
rail neutral axis	– rail axis which defines zero mechanical stress level under bending load from a vertical force
rail neutral temperature	– rail temperature at which rails are stress-free from rail temperature change [8]
rail web	– central, narrow part of rail
sleeper spacing	– axial distance of two adjacent sleepers in traditional track structure
stationing	– railway line distance marking from a specified datum
strain gauge quarter bridge	– electrical circuit for measuring of small changes of resistance using one strain gauge sensor only
strain gauge	– passive electrotechnical component utilised for deformation measurement
stress-controlled rail weld	– weld with imperative stress management for CWR construction
stress-free rail weld	– weld for connection of rails into a longer rail as a preparation for a CWR construction [8]
surface emissivity	– ratio of the energy radiated from a material's surface to that radiated from a blackbody at the same temperature
tonnes carried	– total weight of rolling stock and freight that were transported through a particular railway line section

## 2.2 Acronyms

*in alphabetical order:*

$\alpha$	–	coefficient of linear thermal expansion for steel
CZ	–	Czech Republic
CZK	–	Czech koruna
$E$	–	Young's modulus
$\varepsilon$	–	relative linear deformation of rail
$h$	–	length of installation of the measuring set track unit in hours
$l$	–	original length of rail, or its part
$\Delta l$	–	change of original length of rail, or its part
LED	–	light-emitting diode
$n$	–	number of workers installing the measuring set track unit
$\sigma$	–	mechanical stress induced by thermal load on rail
$t$	–	instant value of rail temperature
$t_0$	–	initial (tensioning, i.e. neutral at the time of welding) value of rail temperature
$t_1$	–	instant value of rail neutral temperature
USA	–	United States of America
USD	–	United States dollar
$x$	–	number of installed measuring set track units

### 3 Used Instruments and Software

**3.1** Following instruments and aids are needed for installation of measuring set track unit (the complete equipment used by the authors is listed in the annex to this methodology):

- strain gauges
- covering foil with kneading compound
- cleaning agent with cleaning pads
- sandcloth of grit size 180
- sandpaper of grit size 400
- gauge of rail neutral axis
- thin permanent markers, oil markers can be applied
- steel ruler
- cable ties
- cable tie holders
- contact adhesive
- polypropylene tubes HTEM DN 40 of 150 mm length
- end caps to polypropylene tubes HTEM DN 40
- polyurethane foam cube of 5 cm length edge
- polyurethane lacquer
- strain gauge adhesive
- connecting cable D-Sub 15 pin male/RJ11 female
- recording sheet for measurement results
- digital data acquisition system
- computer with software for collection of strain gauge measured data
- 12 V maintenance-free battery
- surface thermometer



**3.2** Following instruments and aids are needed for performing measurements (the complete equipment used by the authors is listed in the annex to this methodology):

- connecting cable D-Sub 15 pin male/RJ11 female
- recording sheet for measurement results
- digital data acquisition system
- computer with software for collection of strain gauge measured data
- digital radios
- reflective vests
- 12 V maintenance-free battery
- surface thermometer

## 4 Methodology Description

### 4.1 Test Fundamentals

4.1.1 Test procedure according to this methodology is combined out of two basic parts

- installation of measuring set track unit and
- performing measurement at installed measuring spots.

Procedures of installation and measurement are described separately in the following chapters.

4.1.2 Measuring spots have to be determined within the scope of each monitored section. Selection of number and position of measuring spots is given by an intent where the information of values and development of normal mechanical stress in rail shall be gained. It is advisable to select more measuring spots in each monitored section. This helps to identify strain gauges which may fail to provide correct data and is practical for mutual comparison of deformation development of several near rail sections. It is advisable to establish four measuring spots in each monitored track in each selected stationing. One measuring spot shall always be positioned on each side of each rail. Using this procedure, maximum volume of information on rail deformation in the selected track stationing shall be gained.

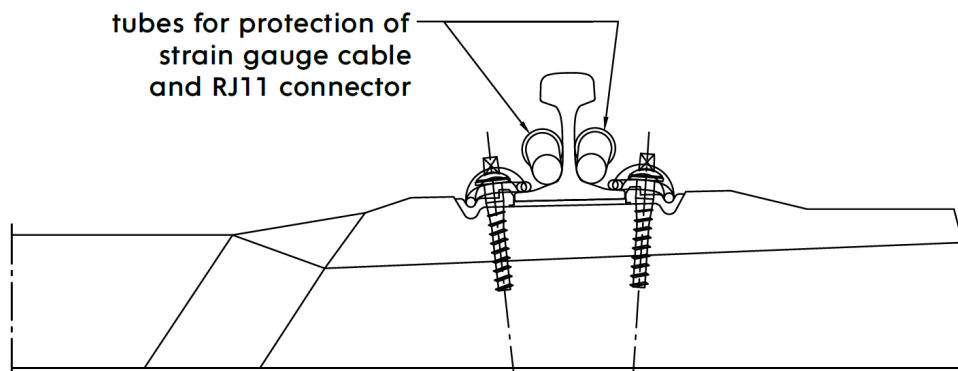


**Figure 1** – Cross section of rail with double-sided position of measuring spots.

4.1.3 Length of monitored section and number of involved measuring spots are parameters, which shall be chosen. Selection of the spots yields to the rule that the higher density of points in a certain length of monitored section is, the more accurately the course of axial deformation of rail in monitored section can be determined.

4.1.4 A new measuring set track unit has to be installed into each measuring spot.

4.1.5 It is necessary to install measuring set track unit on rails before construction of CWR for non-destructive determination of instant value of normal mechanical stress in CWR and its development in time. Installation on rails can be performed both before and after stress-free rail welding, but always before stress-controlled rail welding. Rail can be fastened to sleepers in the time of installation. State when the rail is already placed in a track is desirable, as rail web surface for installation of measuring set track unit can be set in a better way.

**4.1.6** After the installation, it is necessary to measure the instant value of strain gauge deformation at freely laid rail, i. e. rail which is supported by rollers and not fastened. It is advisable to perform this zero axial stress measurement at least twice. The best time to perform this measurement is just before stress-controlled rail welding, or just before rail stressing (if applied) that precedes the stress-controlled rail welding.

**4.1.7** It is advisable to measure the instant rail temperature (see Figure 2) and make a cloudiness record at every measurement, including the initial one, described in the preceding point. The best spot for temperature measurement is on the rail web as close to the installed strain gauge as possible. The best way to measure the temperature is to use a surface thermometer, which provides an accurate value regardless the instant state of rail surface emissivity. It is sufficient to determine the cloudiness in meteorological tenths by estimation. The list of necessary and recommended measurements is provided in the Table 1.

**Table 1** – List of Necessary and Recommended Measurements.

Necessary		Recommended
Monitored Section	• Date	<ul style="list-style-type: none"> <li>• Cloudiness</li> <li>• Air Temperature</li> <li>• Precipitation Intensity</li> <li>• Air Velocity</li> <li>• Track Structure Humidity</li> </ul>
	<ul style="list-style-type: none"> <li>• Strain Gauge Deformation [<math>\mu\text{m}/\text{m}</math>]</li> <li>• Rail Temperature</li> <li>• Time</li> </ul>	<ul style="list-style-type: none"> <li>• Strain Gauge Technical State</li> </ul>



**Figure 2** – Temperature Measurement by Surface Thermometer with Parallel Connection of Track and Mobile Unit of Measuring Set (in the Background).

- 4.1.8** If rail stressing was applied before stress-controlled rail welding, the measured values can be used for verification of applied strain gauges functionality, and, if measuring set track unit was installed in multiple measuring spots along the stressed rails, unevenness of rail stressing can be determined out of the measured data.
- 4.1.9** Recommended time schedule of measurements is presented in the Table 2. It is advisable to perform a measurement on the day preceding the start of track operation, on the day of the start of track operation and on one day after the start of track operation, especially in the case of heavy haul railway tracks.

**Table 2** – Recommended Schedule of Measurements.

Measurement Number	Date
1	on released rails on sliding pads, or rollers, before stress-controlled rail welding
2	on released rails on sliding pads, or rollers, before stress-controlled rail welding (again)
3	immediately after stress-controlled rail welding, or after fastening of stressed rail
4	immediately after stress-controlled rail welding, or after fastening of stressed rail (again)
5	$D + 1$ ( $D$ denotes day of stress-controlled rail welding)
6	$D + 2$
7	$D + 3$
8	$D + 4$
9	$D + 5$
10	$D + 6$
11	$D + 7$
12	$D + 14$
13	$D + 21$
14	$D + 28$
15	$D + 2M$ ( $M$ denotes month)
16	$D + 3M$
17	$D + 4M$
18	$D + 5M$
19	$D + 6M$
20	$D + 7M$
21	$D + 8M$
22	$D + 9M$
23	$D + 10M$
24	$D + 11M$
25	$D + 12M$

## 4.2 Test Procedure – Part I: Installation of Measuring Set Track Unit

**4.2.1** Procedure of measuring set track unit installation at one measuring spot is described in this chapter. The procedure shall repeat for installation in more measuring spots.

**4.2.2** It is advisable to perform the installation in higher number of persons. For a rough estimation of time required for installation, under good weather conditions, if workers are dexterous, and if installation is not limited by works in the affected section, an experience-based formula can be defined as

$$h = \frac{x}{n}, \quad (1)$$

where  $h$  is the number of installation hours,  $x$  is number of installed measuring set track units and  $n$  is number of workers. The time required for installation of determined number of strain gauges needs to be prolonged under unfavourable weather conditions, especially rain, or if it is the first installation of the group of workers, or if the installation works need to be suspended due to space clearing for other works in the track.

**4.2.3** Rail surface shall be cleaned from rust in an area of  $3 \times 3$  cm at a neutral axis level in a position determined for a measuring spot. At first, coarse rust shall be cleaned by a drill with a coarse steel ending brush. Afterwards, manual cleaning by a sandcloth of grit size 180 shall be applied. Finally, rail surface shall be cleaned by sandpaper of grit size 400.

**4.2.4** Areas on rail web of  $3 \times 3$  cm dimensions for attachment of cable tie holders for cable protecting and strain gauge connector tube shall be cleaned in the same way approximately (a) 10 and (b) 20 cm from the measuring point. Upper edge of area (a) is under the rail neutral axis in such a way that its lower edge is on the level of the rail web to rail foot transition rounding. Area (b) is by its centre placed to the rail neutral axis.

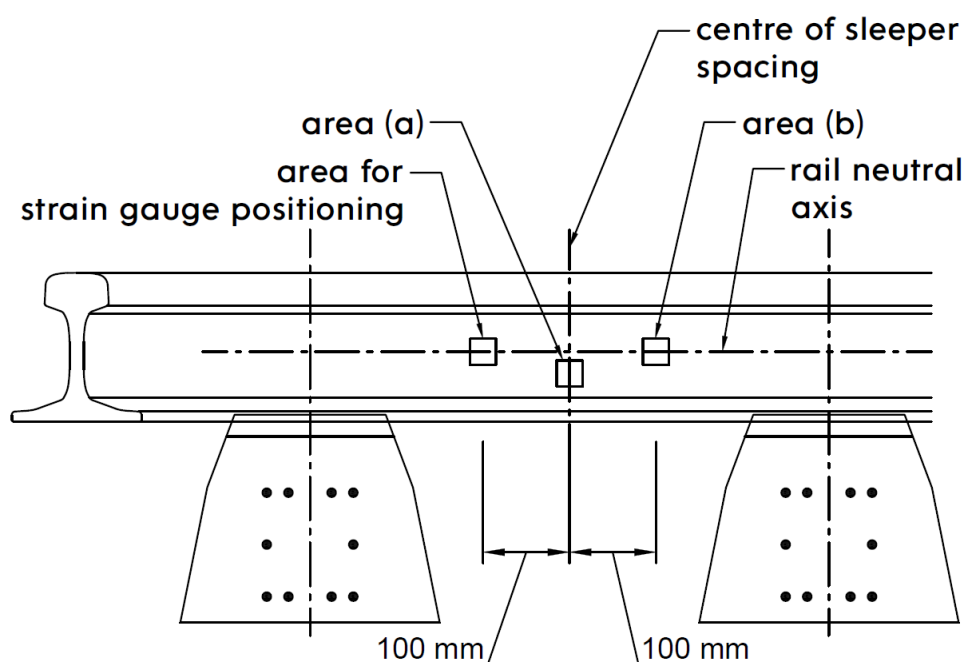


**Figure 3** – Scheme of Cleaning Areas Distribution on Rail Web.

- 4.2.5** It is necessary to heed the complete removal of rust from rail. Thicker layer of material than necessary shall not be removed from rail web surface. At the area intended for strain gauge installation, it is necessary to ensure as high measure of evenness as possible after the rust removal. Material level removed due to the rust affection shall be as even as possible and ground surface shall be as smooth as possible, without grooves caused by uneven intensity of grinding.
- 4.2.6** Smooth and ground surface after rust removal shall be degreased by freon-free cleaning agent with cleaning pads.
- 4.2.7** Neutral axis level shall be marked by a permanent marker of a thin nib in the area cleaned for strain gauge installation. It shall be marked by two horizontal marks interrupted by a space for a strain gauges.
- 4.2.8** Strain gauge shall be glued using a strain gauge adhesive into the space between marks of the rail neutral axis. Strain gauge installation shall be done according to the user instruction.



**Figure 4** – Glued Strain Gauge (with Teflon Cover) with Marked Horizontal Lines.

- 4.2.9** Adhesive pad shall be removed from cable tie holders to keep the plastic part of the holder only. Cable tie holder surface after the adhesive pad removal and degreased areas (a) and (b) of the rail web shall be covered by a contact adhesive and after a period set in user instructions, cable tie holders shall be glued by pressure to the areas (a) and (b) of the rail web..
- 4.2.10** After the cable tie holders safely hold glued to the rail web, a polypropylene tube HTEM DH 40 of 150 mm length ended by an end cap from one side shall be connected to them using cable ties. The tube shall be attached in such orientation that the fill end is on the side of the (b) area.
- 4.2.11** Redundant part of the tied cable tie shall be cut off by pincers. The cable tie on the tube shall be covered by a contact adhesive as a precaution.
- 4.2.12** A layer of polyurethane lacquer shall be painted on the strain gauge with dried adhesive. The lacquer shall get dry according to its user instruction.

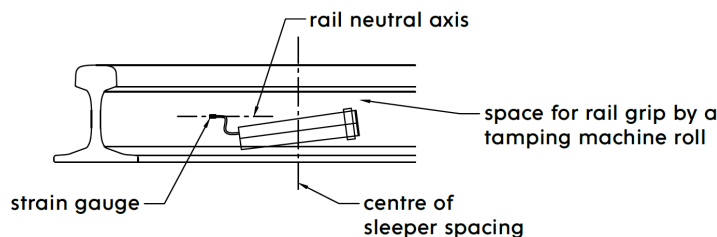


**Figure 5** – Scheme of Strain Gauge and Protective Tube Position on a Rail.

- 4.2.13** The strain gauge shall be covered by a snippet of covering foil with kneading compound. The snippet shall be of 3×3 cm size and shall be pressed to the rail web.
- 4.2.14** Strain gauge cable with the RJ11 connector shall be inserted into the protective tube.
- 4.2.15** The free end of the protective tube shall be filled by a polyurethane foam cube of 5 cm length edge.

### 4.3 Test Procedure – Part II: Measurement

- 4.3.1** Procedure of longitudinal rail deformation in one measuring spot is described in this chapter. The procedure shall repeat for measurement in more measuring spots.
- 4.3.2** Before the measurement commencement, it is necessary to connect a data acquisition system to a 12 V maintenance-free battery and connect to a computer. If the data acquisition system requires warm up period according to the user instruction, it shall be kept. Software for data collection shall be run in the computer. Signal show as a strain gauge quarter bridge deformation in  $\mu\text{m}/\text{m}$  units shall be set in the particular data channel. Further settings shall be set according to the data collection software user instruction. A connecting cable with an RJ11 female connector shall be connected to the data acquisition system. With the described procedure, mobile unit of the *Measuring set for diagnostics of time-based development of stress states in continuous welded rail* shall be ready.
- 4.3.3** Following the above described procedure, polyurethane foam cube shall be removed from the protective tube, and male and female RJ11 connectors shall be connected. This shall provide a connection of the track and mobile units of the measuring set.
- 4.3.4** After reading and recording of the measured value in the data collection software, measuring set mobile and track unit shall be disconnected. Track unit cable shall be inserted back into the protective tube at rail. The tube shall be filled by the polyurethane foam cube again. The measuring set mobile unit can be transferred to the next measuring spot without the need to turn the unit off if there are multiple measuring spots in the locality.
- 4.3.5** If there are two readings performed at any measurement after the stress-controlled rail welding, the measured values in both readings performed minutes after each other shall be practically the same – acceptable difference is in the order of magnitude of single digits of  $\mu\text{m}/\text{m}$ .
- 4.3.6** **Warning:** Measurement must be performed on rails separately to exclude their conductive connection if performed on both rail of a track.

#### 4.4 Test Output

4.4.1 Minimum scope of test output corresponds to the list of necessary measurements presented in the Table 1 and therefore contains:

- date,
- strain gauge deformation [ $\mu\text{m}/\text{m}$ ],
- rail temperature [ $^{\circ}\text{C}$ ] and
- time.

4.4.2 Gaining the longitudinal rail deformation of CWR is the first goal of the methodology. The instant value of this deformation in a measuring spot can be directly read with  $\mu\text{m}/\text{m}$  units in the software for data collection.

4.4.3 The test output can be recorded in the form of the Table 3. The recommended labels is in the format of *capital letter.Roman numeral.Arabic numeral*, where *capital letter* denotes the monitored section (can be omitted if the measurement is not performed on multiple monitored sections contemporaneously), *Roman numeral* denotes track stationing and *Arabic numeral* denotes measuring spot at given stationing. It is advisable to label measuring spots by increasing Roman numerals in the direction of increasing stationing. If a track in cross section contains four measuring spots (one measuring spot from each side of each rail), there shall be the maximum number of Arabic numeral used for identification of particular measuring spots.

**Table 3** – Recommended Recording Table.

Monitored Section:		Date:	
Measuring Spot	Time [hh.mm]	Rail Temperature [ $^{\circ}\text{C}$ ]	Deformation [ $\mu\text{m}/\text{m}$ ]
X.I.1	hh.mm	xx,x	xxxx
X.I.2	hh.mm	xx,x	xxxx
X.I.3	hh.mm	xx,x	xxxx
X.I.4	hh.mm	xx,x	xxxx
X.II.1	hh.mm	xx,x	xxxx
X.II.2	hh.mm	xx,x	xxxx
X.II.3	hh.mm	xx,x	xxxx
X.II.4	hh.mm	xx,x	xxxx
X.III.1	hh.mm	xx,x	xxxx
X.III.2	hh.mm	xx,x	xxxx
...	...	...	...
x.x.x	hh.mm	xx,x	xxxx

4.4.4 Recording table according to the sample Table 3 can be complemented by a record of information listed in the column of recommended measurements of the Table 1 at every measurement in the monitored section.



#### 4.5 Test Evaluation

- 4.5.1** Every installed strain gauge can show a different value of deformation measured in  $\mu\text{m}/\text{m}$  units upon the installation on rail without axial stress. It is therefore advisable to subtract the value measured in the measurement No. 3 or 4 according to the Table 2 (values from the measurement No. 3 and 4 shall differ in the order of magnitude of single digits at maximum). This procedure ensures leads to gaining a relative value of deformation to the state of CWR rail stressing. Values from the measurement No. 3 or 4 shall be at the level of zero (or nearly zero).
- 4.5.2** Time of measurement shall be added to every measured value of deformation to get a pair of data time–deformation.
- 4.5.3** Measured data pairs shall be pictured in the form of a graph with time being in the independent axis and deformation measured by strain gauges and data acquisition system and processed by a data collection software being in the dependent axis. Obtained points shall be connected into a line graph. It is advisable to depict data from more strain gauges into one graph. It is, however, important to keep in mind parameters which may differ for particular stain gauges. Identification and research into the impact of particular parameters are subject of a further research and exceed the scope of this methodology.
- 4.5.4** Rail deformation changes after stress-controlled rail welding, as illustratively shown in the Figure 6, can be observed from the course of the graph. Length of the consolidation phase depends on tonnes carried in the track section. In the case of a heavy haul corridor line, the consolidation phase ends shortly after the start of operation after the stress-controlled rail welding. In the case of a more regional character of railway operation, this phase can be observed several months after the start of operation after the stress-controlled rail welding. A closer identification of particular phases and parameter that affect their length are subject of a further research and exceed the scope of this methodology.

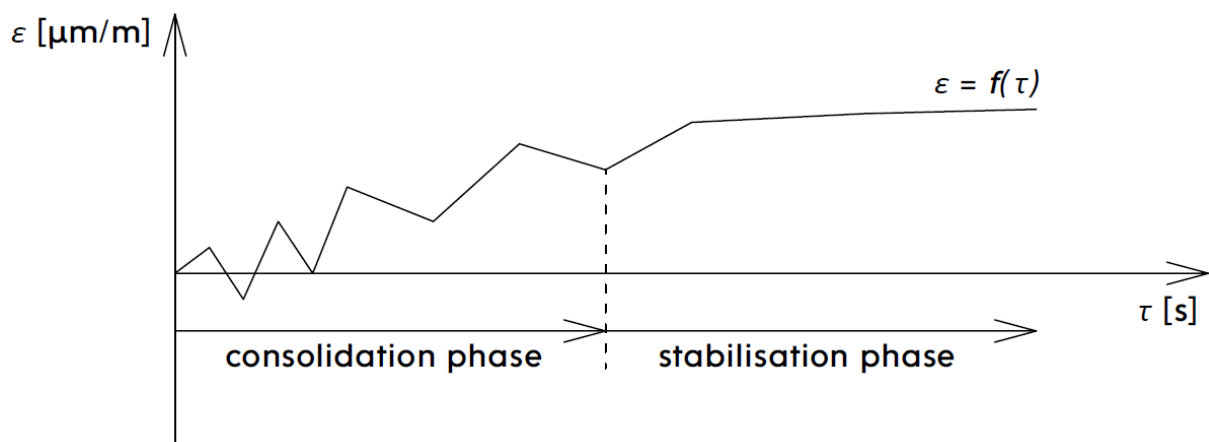


**Figure 6** – Scheme of CWR Deformation Development Gained from Measured Data Pairs Time–Deformation.

**4.5.5** Under no deformation (length change) of CWR, the instant value of normal mechanical stress in rail could be derived from (e. g. in [5]):

$$\sigma = -\alpha \cdot (t - t_0) \cdot E, \quad (2)$$

where  $\sigma$  is stress from thermal loading on rail,  $\alpha$  is the coefficient of linear thermal expansion of steel,  $t$  is the instant value of rail temperature,  $t_0$  is the rail tensioning temperature and  $E$  is the Young's modulus of rail.

**4.5.6** Under CWR deformation (in its central part, i. e. out of a breathing end), however, this deformation appears as a change of neutral temperature in a spot (section) where the deformation occurred. Deformation

$$\varepsilon = \frac{\Delta l}{l} \quad (3)$$

is directly proportional to the stress

$$\sigma = E \cdot \varepsilon \quad (4)$$

and this can be substituted to a formula analogical to the Formula 2, and after modifications, it can be obtained in the form

$$\varepsilon = \alpha \cdot (t_1 - t_0), \quad (5)$$

where  $t_1$  is the instant value of rail neutral temperature and  $t_0$  the original rail neutral temperature (if deformation is subtracted from a value measured just after stress-controlled welding, it is the rail tensioning temperature). The theoretical change of rail neutral temperature is schematically depicted in the Figure 7 (The presented shape of neutral temperature function curve  $t$  is illustrative only.).

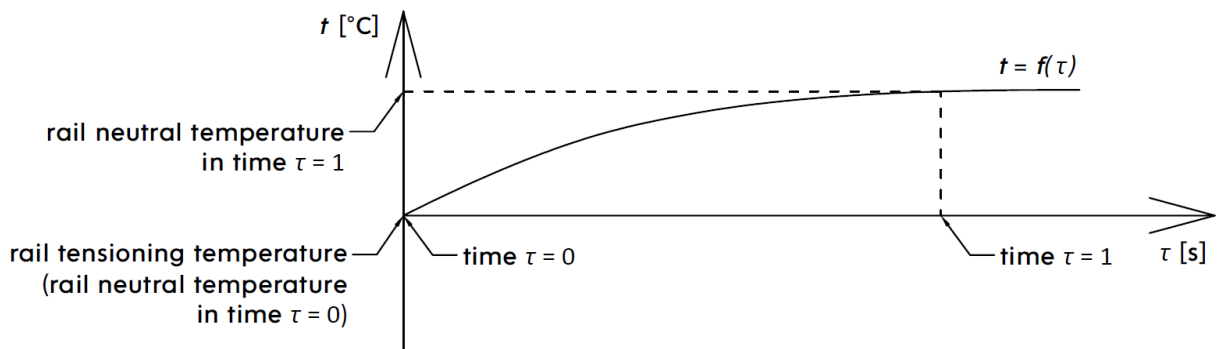


**Figure 7** – Scheme of Rail Neutral Temperature Time Development.

**4.5.7** The instant value of rail neutral temperature, which is the second goal of the methodology, can be easily derived from the Formula 5

$$t_1 = \frac{\varepsilon}{\alpha} + t_0. \quad (6)$$

**4.5.8** If the instant value of rail neutral temperature is substituted for the original  $t_0$  in the Formula 2, a formula for stress calculation in CWR including the impact of its potential deformation after the stress-controlled rail welding is obtained. This formula can be written in the form of

$$\sigma = -\alpha \cdot \left( t - \frac{\varepsilon}{\alpha} - t_0 \right) \cdot E. \quad (7)$$

Determination of the neutral value of mechanical stress in CWR is the third goal of this methodology. Please note that  $\alpha$ ,  $t_0$  and  $E$  are constants in this formula, whereas measured quantities  $t$  and  $\varepsilon$  are variables.

## 4.6 Recommendations

**4.6.1** Areas to be cleaned on the rail web shall be selected in such a way that the resultant position of the protective tube is in the centre of the sleeper spacing. Otherwise the protective tube may collide with rail clamp if the rail longitudinally moves. There is no danger of collision of strain gauge with rail clamp.

**4.6.2** It is advisable to avoid spots with rail marking at measuring spot selections, as it may be challenging to create a smooth and even surface by rust removal.

**4.6.3** 3D printed gauges can be used to easily mark rail neutral axis.



**Figure 8** – 3D Printed Rail Neutral Axis Gauge.

- 4.6.4** It is advisable to orient the strain gauge at installation on rail in such a way that the conductors aim to the opposite side than the protective tube is located. The conductors are then bent by 180° and reach the orientation towards the tube. Complete bending of the conductors can be covered under the snippet of aluminium foil with kneading compound and better protected from mechanical damage.
- 4.6.5** Cable tie holders can be better connected in the way that their edges are parallel, i. e. both holders have the same tilt as is the longitudinal slope of the protective tube. The protective tube shall then better keep the longitudinal slope required for minimizing of water retention inside the tube.
- 4.6.6** It is necessary to take into account the need for a sufficient space for rail grip by a tamping machine roll, mostly at vertically positioning the cable tie holder in the (b) area.
- 4.6.7** It is advisable to keep the directional orientation of the protective tubes in all the measuring spots of a measuring locality. The preferred orientation is with the unplugged end of the protective tube in the direction of decreasing vertical alignment of track. This measure helps water drainage from the protective tubes.
- 4.6.8** Polyurethane foam cube plugging one end of the protective tube can easily freeze to the tube if measurement is performed under freezing weather conditions. In this case, it is advisable to be equipped with a gas burner and propane-butane cartridge to heat up the end of protective tube to melt the freezing connection between the polyurethane foam cube and the protective tube and gain access to the strain gauge cable with RJ11 connector.
- 4.6.9** It is advisable to place the measuring set mobile unit and all other equipment into a transport crate, which enables quick transport along the track, for measurement at more measuring spots of one measuring locality.
- 4.6.10** It is advisable to place the crate on a terrain sack truck and carry it for an access to more remote track sections.
- 4.6.11** It is better to use a surface thermometer for rail temperature measurement, as the rail web surface emissivity, which affects the contactless thermometer measurements, can change over the time.
- 4.6.12** Measuring set track unit structure is made in such a way that it enables track tamping by an automatic tamping machine without any restrictions and the measuring set is kept safe. A restriction comes into effect in the case of a ballast profiling machine ride. Its technology to clean rails from ballast may lead to tearing the measuring set track unit off the rail. It is therefore important to agree on a procedure of measuring set track unit protection with railway infrastructure manager and construction site manager. Possible solutions are marking of measuring spot positions by bold red marks on the upper surface of neighbouring sleepers outside the track channel, or by a sign placed next to the track at the affected stationing.



**Figure 9** – Marking of Stationing with Measuring Spots in the Bezprávi Measuring Locality by Red Colour on the Upper Surface of Sleepers Outside the Track Channel and by a Flag Made from an Orange Reflective Vest.

## 5 Novelty of Procedures

- 5.1 Many non-destructive approaches to determine mechanical stress in CWR are described in the Czech and world literature (selective overview e. g. in [9]). None of them, despite partial successes in laboratory environment, managed to reach a wider application at railway infrastructure managers.
- 5.2 This methodology proceeds from the strain gauge technology, which is known for decades [10], but only the long development of this technology enabled using the products available in the market to perform long-term measurements, especially in a significantly larger scope of rail sections and data collection on the CWR behaviour, which is one of the key aspects of this methodology.
- 5.3 Novelty of procedure described in this methodology resides in the use of *Measuring Set for Diagnostics of Time-Based Development of Stress States in Continuous Welded Rail*, too. This measuring set is an original research result realized within the scope of the TACR TJ04000301 project.
- 5.4 Novelty of procedure, which is a result of experimental development of mentioned measuring set and applied research, resides in recommendation of using only one strain gauge installed on the rail web for one measuring spot, too. This decreases noise of the measured signal, as it was shown in many performed measurements.

## 6 Methodology Applicability Description

- 6.1** Methodology finds a wide applicability in the research of CWR. Because of time-demanding research of effects connected to CWR deformations and normal mechanical stress development, it can be assumed that research comes to further recommendations over time. These recommendations shall proceed out of this methodology, but shall make the information experimentally gained using this methodology more precise.
- 6.2** This methodology reacts to a long-term demand for easily performable investigation of mechanical stress in CWR. Combination of use of established technology that leads to precise measured data and keeping a sufficient simplicity of procedures applicable for practical use is its advantage.
- 6.3** This methodology is applicable at all CWR regardless the track gauge, track order, track speed (the methodology is applicable at high speed railways, too), and other parameters. It is applicable in all countries of the world with a railway network.
- 6.4** Low costs needed for performing measurements are another factor that contributes to the applicability of the methodology. Moreover, the initial investment costs for railway infrastructure managers are relatively low, too, especially upon consideration the scope of the problems connected to the mechanical stress in CWR.
- 6.5** The development of CWR all over the world leads to the idea that world extent of CWR will increase. Therefore, it can be assumed that the applicability of this methodology will increase over time.

## 7 Economic Aspects

### 7.1 Measurement Costs

**7.1.1** Measurement Costs can be divided into

- investment costs of measuring set mobile unit acquisition,
- investment costs of measuring set track unit acquisition,
- costs of measuring set installation and
- costs of performing one measurement.

**7.1.2** It is sufficient to expend the investment costs of measuring set mobile unit acquisition only once, as one measuring set mobile unit can be used for measurement of any number of measuring spots. The most expensive item of the measuring set mobile unit is the data acquisition system. The price of the system depends on the type and producer selection. Another expensive item is the computer and software for data collection. Costs of other items of the measuring set mobile unit are negligible. The total investment costs of measuring set mobile unit can vary based on the instant price of data acquisition system, but it can be estimated as several hundred thousand Czech korunas.

**7.1.3** Investment costs of measuring set track unit acquisition are very low and can be estimated as one thousand Czech korunas. It shall be noted that investigation of a longer track section requires several dozens (e. g. in the case of a hundreds meter long track section) or hundreds (e. g. in the case of a track section of several kilometres) of measuring set track units.

**7.1.4** Costs of measuring set installation comprise of relatively negligible costs of used energy, costs of transport of workers to the installation locality and back, and costs of work of installation workers. For an estimation total number of working hours that can significantly differ based on the planned extent of installation, the Formula 1 can be applied.

**7.1.5** Costs of performing one measurement are, except for costs of workers performing the measurement, negligible, too. In the case of experience workers who work in a pair, the length of measurement at one measuring spot can be estimated as one minute. It is necessary to count with a longer time if the track is intensively operated and must be cleared more often between the measurements or if the measurement is performed during freezing weather. The latter requires melting the connection between the protective tube and the polyurethane foam cube by gas burner. This can be accelerated if more workers are available for the work.



## 7.2 Possible Economic Assets

**7.2.1** At the time of release of this methodology, the authors do not have information on CWR axial forces management costs from the Czech Republic at disposal. Nevertheless, they try to compile an estimation of the economic assets of the methodology based on available information in the following paragraphs.

**7.2.2** According to [6], CWR axial forces management costs in the USA reach the level of 134 million USD annually. Division per particular items is presented in the Table 4.

**Table 4** – Annual CWR Axial Forces Management Costs in the USA. [6]

Costs [mil. USD]	Item
15	Track Buckle Repair
28	Buckle Derailments
51	Slow Orders
40	Destressing

**7.2.3** Table 5 shows the length of tracks (not railway lines) in the Czech Republic in 2020 and in the USA in 2003, i. e. in year to which the data of costs from the Table 4 are related. The data origin from a statistics of the International Union of Railways [11]. For the USA of 2003, the date were calculated by linear extrapolation from available data of the period from 2013 to 2020.

**Table 5** – Length of Tracks in the CZ (2020) and in the USA (2003, Extrapolation from 2013 to 2020). [11]

Length of Tracks [km]	Country
15 189	Czech Republic
267 751	United States of America

**7.2.4** Assuming the same ratio of buckle derailments and track buckle repair in the Czech Republic and the USA, it can be estimated by comparison of the data from the Tables 4 and 5 that the costs connected to buckle derailments and track buckle repair are in the Czech Republic currently approximately 2.4 million USD in prices of 2003. Upon recalculation of the CZK/USD exchange rate from 2003 (an approximate value of 28 Kč [12] was used in the calculation) and involvement of the past inflation to 2003 in aggregate level of approximately 50 % [13], the orientation recalculation of buckle derailments and track buckle repair results in approximately 100 million CZK annually. The authors do not have necessary data for a more precise cost estimation.

**7.2.5** It can be derived out of the estimation presented in the preceding paragraphs that a potential decrease by 10 % in average annual costs of buckle derailments and track buckle repair in the Czech Republic shall lead to financial savings of 10 million CZK. This would significantly overweight the investment and measurement costs. Moreover, it needs to be noted that the application of this methodology is not bound to the area of the Czech Republic and upon involvement of foreign railway networks, the financial savings would significantly increase.

## 8 References

1. ORRINGER, Oscar; ORKISZ, Janusz; ŚWIDERSKI, Zdzisław (eds.). *Residual Stress in Rails: Effects on Rail Integrity and Railroad Economics* [online]. Kluwer Academic Publishers, 1992 [visited on 2022-01-23]. ISBN 978-94-011-1787-6. Available from DOI: 10.1007/978-94-011-1787-6.
2. SZELAŻEK, Jacek. Monitoring of thermal stresses in continuously welded rails with ultrasonic technique. *The e-Journal of Nondestructive Testing & Ultrasonics* [online]. 1997, vol. 3, no. 6 [visited on 2022-01-23]. ISSN 1435-4934. Available from: <https://www.ndt.net/article/dresd97/szelazek/szelazek.htm>.
3. PLÁŠEK, Otto; ZVĚŘINA, Pavel; SVOBODA, Richard; MOCKOVČIAK, Milan. *Železniční stavby. Železniční spodek a svršek*. Brno: Brno University of Technology, Faculty of Civil Engineering, 2004. ISBN 80-214-2620-9.
4. LICHTBERGER, Bernhard. *Track Compendium*. 2nd ed. Hamburg: DVV Media Group, 2011. ISBN 978-3-7771-0421-8.
5. ESVELD, Coenraad. *Modern Railway Track*. 2nd ed. Delft: MRT-Productions, 2001. ISBN 90-800324-3-3.
6. KOOB, Michael J. *The development of a vibration technique for estimation of neutral temperature in continuously welded railroad rail* [online]. Champaign, Illinois, 2005 [visited on 2022-01-23]. Available from: [http://railtec.illinois.edu/wp/wp-content/uploads/pdf-archive/Koob-MS-thesis-\(final\).pdf](http://railtec.illinois.edu/wp/wp-content/uploads/pdf-archive/Koob-MS-thesis-(final).pdf). Dissertation. University of Illinois at Urbana-Champaign. Supervisors: Christopher P. L. Barkan and Richard L. Weaver.
7. UIC. *Code 720 Laying and Maintenance of CWR Track*. Paris, 2005.
8. SPRÁVA ŽELEZNIC. *S3/2 Bezstyková kolej*. Prague, 2013.
9. VNEK, Petr; CULEK, Bohumil. Measurement Methods of Internal Stress in Continuous Welded Rail. *Acta Polytechnica CTU Proceedings* [online]. 2017, vol. 11 [visited on 2022-01-31]. ISBN 978-80-01-06297-5. ISSN 2336-5382. Available from: <https://ojs.cvut.cz/ojs/index.php/APP/issue/view/605>.
10. WINDOW, A. L. (ed.). *Strain Gauge Technology*. 2nd ed. Springer Netherlands, 1993. ISBN 978-1-85166-864-9.
11. UIC. *RAILISA* [online]. 2019. Paris [visited on 2022-02-01]. Available from: <https://uic-stats.uic.org/>.
12. KURZY.CZ. *USD průměrné kurzy 2003, historie kurzů měn* [online]. 2022 [visited on 2022-02-01]. Available from: <https://www.kurzy.cz/kurzy-men/historie/USD-americky-dollar/2003/>.
13. PENÍZE.CZ. *Kalkulačka inflace: jak se znehodnocuje česká koruna?* *Peníze.cz* [online]. 2022 [visited on 2022-02-01]. ISSN 1213-2217. Available from: <https://www.penize.cz/kalkulacky/znehodnoceni-koruny-inflace>.

## 9 Annexes

### 9.1 Complete List of Items for Installation and Measurements Used by the Authors

**9.1.1** The authors used following devices and aids for installation of approximately 50 measuring set track units:

- strain gauges HBM K-CLY4-0060-1-350-4-005-Y (50 pcs + 30 pcs spare ones)
- covering foil with kneading compound HBM ABM75 (2 packages)
- cleaning agent with cleaning pads HBM RMS1 (2 l of agent and 200 pcs of pads)
- last for cleaning pads (can be made e. g. out of wide flat screwdriver)
- spare sanding belts of 9 mm width (10 pcs)
- wire brushes for drill (2 pcs)
- steel brush (1 pcs)
- sandcloth of grit size 180 (10 pcs)
- sandpaper of grit size 400 (6 pcs)
- rail neutral axis gauges (4 pcs, own production in 3D printer)
- thin permanent markers (4 pcs, oil markers can be applied)
- pencils (3 pcs)
- tape measure of 5 m length (2 pcs)
- steel ruler (2 pcs)
- penknife (1 pcs)
- power strips of 5 m length with five sockets (2 pcs)
- cable ties (200 pcs)
- cable tie holders (200 pcs)
- contact adhesive (5 pcs)
- polypropylene tubes HTEM DN 40 of 150 mm length (60 pcs)
- end caps to polypropylene tubes HTEM DN 40 (60 pcs)
- scissors (3 pcs)
- black (3 pcs) and red (3 pcs) electrical insulation tapes
- AA batteries (18 pcs)
- LED torch (1 pcs)
- basic tools (spanners, pliers, screwdrivers) and cloths
- marking spray paints (4 pcs)

*continues from the previous page*

- polyurethane foam cube of 5 cm length edge (60 pcs)
- spatulas (1 pcs)
- work gloves
- polyurethane lacquer HBM PU140 (3 pcs)
- strain gauge adhesive HBM Z70 (3 pcs)
- head torch (1 pcs)
- connecting cable D-Sub 15 pin male/RJ11 female (2 pcs, own production)
- pens (2 pcs)
- notebooks
- recording sheet for measurement results
- strain gauge installation plan
- data acquisition system power cable for connection to 12 V maintenance-free car battery (1 pcs)
- computer power cable for connection to 12 V maintenance-free car battery (1 pcs)
- data acquisition system QuantumX MX840A
- computer with Catman Easy software
- reflective vests
- copy of K-03 certificate of work supervisor
- copy of monitoring contract agreed with the infrastructure manager
- entry to the railway area passes
- 12 V maintenance-free car batteries (2 pcs)
- surface thermometer Testo 905-T2
- belt grinders (3 pcs)
- drills (2 pcs)
- hot air gun
- 10 kg propane-butane cylinder (2 pcs)
- petrol generator
- 20 l petrol can
- 50 m extension cord on cylinder
- knee pads (6 pairs)
- protective tents (2 pcs)
- gas space heater

**9.1.2** The authors used following devices and aids for measurements:

- connecting cable D-Sub 15 pin male/RJ11 female (2 pcs, own production)
- pens (2 pcs)
- notebooks
- recording sheet for measurement results
- strain gauge installation plan
- head torch (1 pcs)
- data acquisition system power cable for connection to 12 V maintenance-free car battery (1 pcs)
- computer power cable for connection to 12 V maintenance-free car battery (1 pcs)
- cable ties (200 pcs)
- cable tie holders (200 pcs)
- contact adhesive (5 pcs)
- data acquisition system QuantumX MX840A
- computer with Catman Easy software
- AA batteries (18 pcs)
- digital radios (6 pcs)
- reflective vests
- entry to the railway area passes
- 12 V maintenance-free car batteries (2 pcs)
- surface thermometer Testo 905-T2
- dust pan and hand brush
- cloth
- gas burner
- gas cartridges for gas burner (2 pcs)
- red electrical insulation tape
- polyurethane foam cube of 5 cm length edge (3 pcs)

## 9.2 Example of Methodology Application – Bezpráví Locality

**9.2.1** Bezpráví locality is a part of the I. and III. railway corridor line of the Czech Republic. It lies between Ústí nad Orlicí and Brandýs nad Orlicí station. The monitored section is in the 1st track in km 260.8 to 261.4. 16 measuring spots are located in the section, always four in four stationings in spacing of 160 m. The total length of the monitored section is 480 m. The Bezpráví locality strain gauge installation scheme is a separate annex of this methodology. Measuring set track units were installed into the monitored section on the 31st August 2021, stress-controlled rail welding was made on the 1st of September 2021.

**9.2.2** The right-hand side rail was welded in km 261.233 on the 1st of September around noon. Before the welding, the rail from the direction of Ústí nad Orlicí was pulled by 14 mm and the rail from the direction of Brandýs nad Orlicí by 7 mm. The rail anchorage section in the direction of Brandýs nad Orlicí started after the measuring spot in the fourth stationing with the measuring set track unit installed (km 261.328). 95 meters of rail was prolonged by 7 mm. Rollers under the rail foot were used by this rail pulling. The average relative prolongation is  $74 \mu\text{m}/\text{m}$  on average. Measurement after the rail release and placing of rollers under the rail foot, and after the required prolongation and fastening was made in the profile of the fourth stationing (km 112.010) Measured values are summarized in the Tables 6 and 7.

**Table 6** – Record of Measured Data from Bezpráví Locality before Rail Pulling.

Monitored Section: Bezpráví			Date: 01 September 2021
Measuring Spot	Time [hh.mm]	Rail Temperature [°C]	Deformation [ $\mu\text{m}/\text{m}$ ]
D.IV.3	10.26	19.9	1699
D.IV.4	10.27	19.5	1776

**Table 7** – Record of Measured Data from Bezpráví Locality after Rail Pulling.

Monitored Section: Bezpráví			Date: 01 September 2021	
Measuring Spot	Time [hh.mm]	Rail Temperature [°C]	Deformation [ $\mu\text{m}/\text{m}$ ]	Relative Deformation [ $\mu\text{m}/\text{m}$ ]
D.IV.3	11.44	21.6	1764	65
D.IV.4	11.45	21.6	1856	80

**9.2.3** Upon comparison of the values from the Tables 6 and 7, it can be seen that the average prolongation of the rail by pulling is  $73 \mu\text{m}/\text{m}$  in the monitored section. This corresponds the expected value (the difference in the order of magnitude of single digits of  $\mu\text{m}/\text{m}$  corresponds the noise of the measurement) very precisely. The measured data show that the prolongation of the 95 m long rail (not counting the anchorage block) placed on rollers under the rail foot by 7 mm was very uniform. It needs to be added that more measuring spots would increase the level of certainty of this conclusion. However, this was not possible due to the limited number of research team members and restricted time allocated for installation.

9.2.4 The complete record of measured values after stress-controlled rail welding in the Bezprávi locality is presented in the Table 8.

Table 8 – Record of Measured Data from Bezprávi Locality after Stress-Controlled Rail Welding.

Monitored Section: Bezprávi			Date: 01 September 2021	
Measuring Spot	Time [hh.mm]	Rail Temperature [°C]	Deformation [ $\mu\text{m}/\text{m}$ ]	
D.I.1	13.47	30.3	1546	
D.I.2	13.48	31.2	1511	
D.I.3	13.50	31.0	1198	
D.I.4	13.51	31.2	1677	
D.II.1	13.57	28.5	2103	
D.II.2	13.58	28.2	2030	
D.II.3	13.59	28.4	2024	
D.II.4	14.00	28.0	2183	
D.III.1	11.50	19.1	1621	
D.III.2	11.51	19.8	1301	
D.III.3	11.52	19.8	1576	
D.III.4	11.53	19.9	1293	
D.IV.1	11.41	22.3	1503	
D.IV.2	11.42	21.5	1694	
D.IV.3	11.44	21.6	1764	
D.IV.4	11.45	21.6	1856	

9.2.5 Figure 10 shows development of measured data of deformation by measuring spots and days, or months respectively, after stress-controlled rail welding. Values presented in both graphs are related to the measurement after rail welding, i. e. to the values from the Table 8.

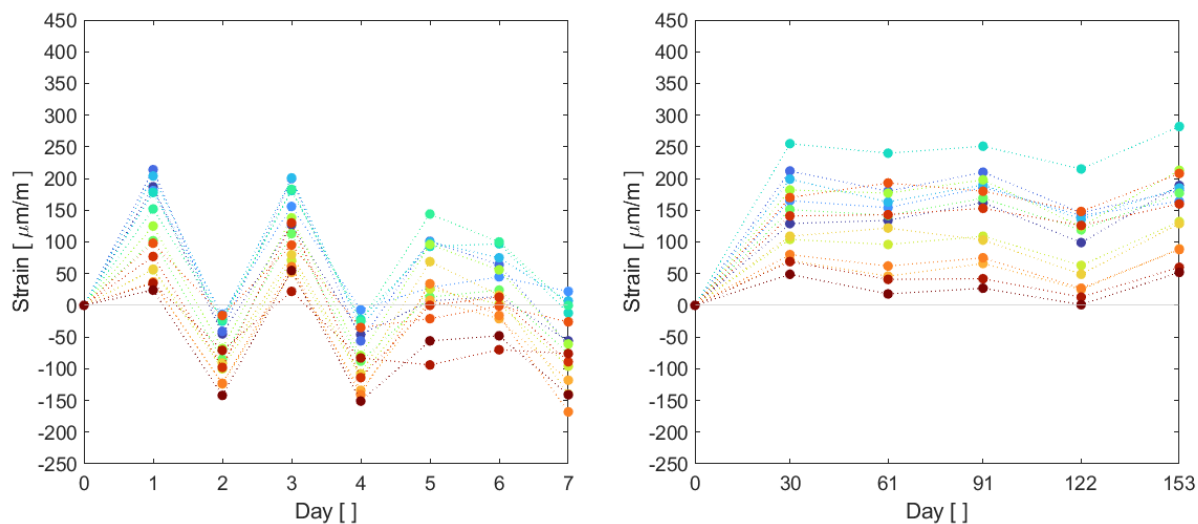


Figure 10 – Development of Measured Deformation Values by Measuring Spots in Bezprávi Locality over the First Days and Months after the Stress-Controlled Rail Welding.

**9.2.6** Comparison of the graphs shows that significant changes of deformation values occur shortly after the stress-controlled rail welding. The tonnes carried, which are significant in the monitored section, stabilise the deformation value afterwards, what corresponds to the phases presented in the Figure 6. The prolongation of the rails after the stress-controlled rail welding is apparent in all the measuring points what corresponds to an increase of neutral temperature in this locality. As an example, values measured in the profile of the third stationing in km 261.168 from the 1st February 2022, i. e. five months after the stress-controlled rail welding, can be shown. These values are presented in the Table 9.

**Table 9** – Record of Measured Data from km 261.168 of the Bezpráví Locality on the 1st February 2022.

Monitored Section: Bezpráví			Date: 01 February 2022	
Measuring Spot	Time [hh.mm]	Rail Temperature [°C]	Deformation [ $\mu\text{m}/\text{m}$ ]	Relative Deformation [ $\mu\text{m}/\text{m}$ ]
D.III.1	12.13	3.4	1753	132
D.III.2	12.14	3.5	1430	129
D.III.3	12.14	4.0	1665	89
D.III.4	12.15	4.0	1381	88

**9.2.7** The average value of relative deformation in comparison to the state after the stress-controlled rail welding in the km 261.168 stationing five months after the welding is 131  $\mu\text{m}/\text{m}$  in the left-hand side rail and 89  $\mu\text{m}/\text{m}$  in the right-hand side rail, as it is visible from the Table 9. Based on the Formula 6, it corresponds to the neutral temperature increase by approximately 11, or 7,5 °C respectively, from the tensioning temperature. The instant value of axial stress in the inspected stationing in the left-hand side rail is approximately 76,5 MPa and in the right-hand side rail 66,5 MPa, according to the Formula 7.

### 9.3 Other Annexes

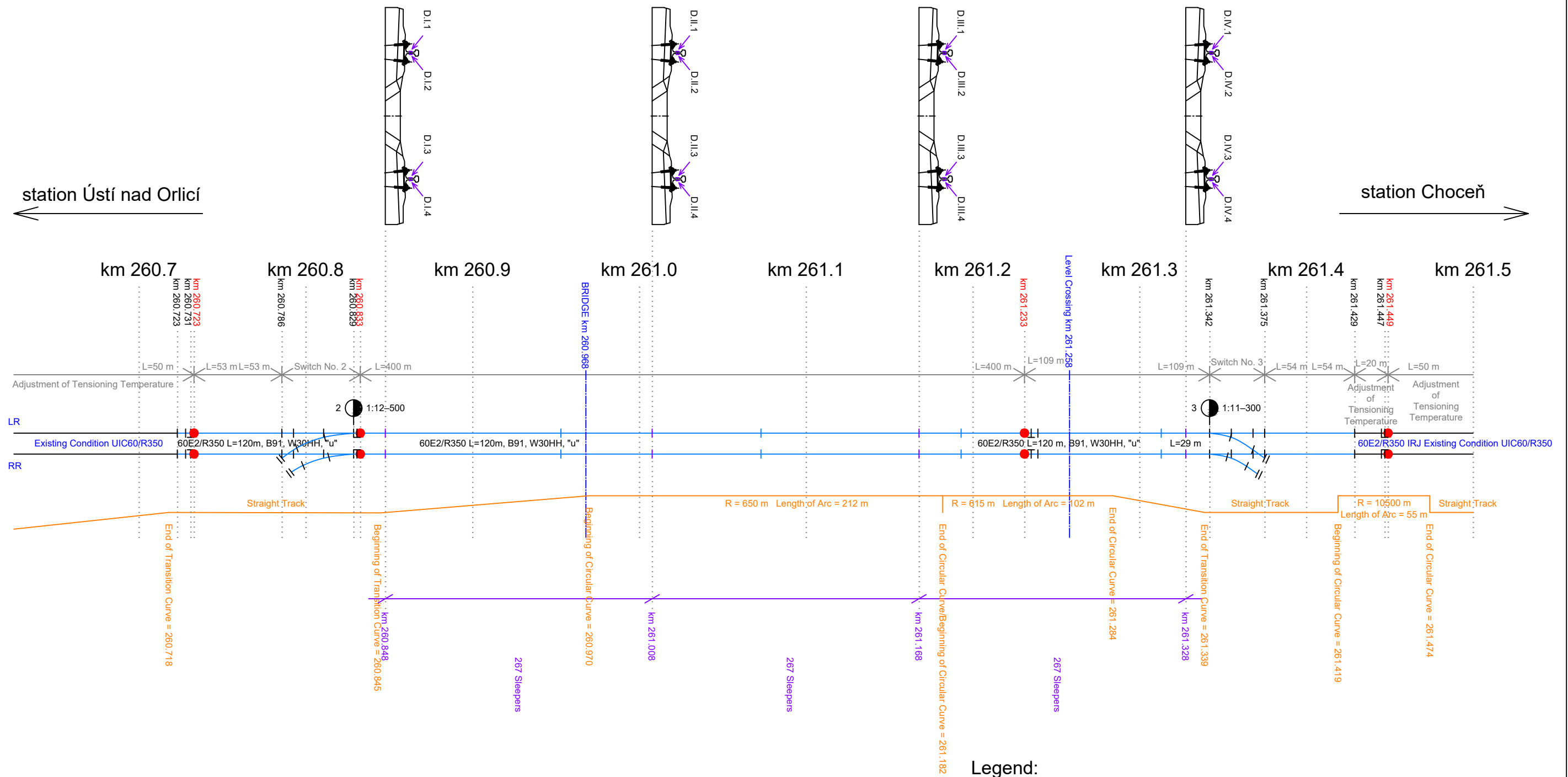
Other annexes to this methodology comprise

- Scheme of Strain Gauge Installation in Bezpráví Locality and
- Documentation of the Functional Sample TJ04000301-V2 *Measuring Set for Diagnostics of Time-Based Development of Stress States in Continuous Welded Rail*, which is an outcome of research performed within the scope of investigation of the TACR TJ04000301 project *Non-Destructive Determination of Mechanical Stress in Continuous Welded Rail*.




station Ústí nad Orlicí ←

→ station Choceň



**Legend:**

- sleeper spacing „u“
- stress-controlled rail weld
- ++ stress-free rail weld
- + strain gauge positioning (from both sides of the rail web)

Workplace FTE-ERCT/DTS	Designed by Petr Vnenk	Document Type Strain Gauge Installation Scheme	Document State Released	Format A3
	Made by Petr Vnenk	Name, Additional Name Strain Gauge Installation State, Bezprávi Locality, TJ04000301, WP1	Document No. 2	Scale -
	Controlled by		Version 2	Release Date 14 Jul 2022
			Sheet 1/1	

## Functioning sample identification

**Name:** Measuring set for diagnostics of time-based development of stress states in continuous welded rail

**Identification code:** TJ04000301-V2

**Project No.:** TJ04000301

**Authors:** Petr Vnenk, Özgür Yurdakul, Ph.D., Jiří Šlapák, Vladimír Suchánek, Ph.D., Assoc. Prof. Bohumil Culek, Ph.D., Assoc. Prof. Ladislav Řoutil, Ph.D., Ondřej Sadílek, Ph.D., Filip Klejch, Zdeněk Sháněl, Karel Suchý, Tadeáš Šustr, Miloš Šula

**Contact person:** Petr Vnenk, petr.vnenk@upce.cz, University of Pardubice, Studentská 95, 532 10 Pardubice, Czech Republic

## Technical specifications

The measuring set was developed within the investigation of the project No. TJ04000301 Non-destructive determination of mechanical stress in continuous welded rail supported by a grant from the ZETA programme of the Technological Agency of the Czech Republic.

The measuring set is composed out of a track and a mobile part. The track part contains a K-CLY4-0060-1-350-4-050-Y strain gauge type produced by HBM, polypropylene tube of length of 150 mm and outer diameter of 40 mm, and a polyurethane foam cube of an edge length of 50 mm. The strain gauge is connected to the investigated rail at its neutral axis with the main axis of the strain gauge being parallel to the neutral axis of the rail. Corresponding area of the rail surface must be cleaned from rust and unevennesses and degreased. Strain gauge is attached by 1-Z70 fast-acting superglue and, after drying, painted over by 1-PU140 polyurethane lacquer, both produced by HBM. After the covering material is dry, the strain gauge is covered by 1-ABM75 aluminium foil coated with kneadable putty produced by HBM, too. The polypropylene tube is attached to the lower part of the rail web by a pair of cable ties and cable ties holders and Chemopren Extreme glue. Strain gauge conductors with RJ male connector are placed into the polypropylene tube closed from one end, while the other end of the tube is plugged by the polyurethane foam cube. Mobile part contains an MX840A data acquisition system and a SCM-SG350 quarter bridge adaptor produced by HBM, a connecting cable and an RJ11 female connector produced by ENCITECH. Mechanical deformation is measured directly by the MX840A data acquisition system.

The track part of the measuring set is currently installed in 44 spots in the Hostinné – Pilníkov railway line section and in 16 spots in the Ústí nad Orlicí – Brandýs nad Orlicí railway line section. Former development stages of the track part of the measuring set were installed in the Mostek – Horka u Staré Paky and Brno-Horní Heršpice – Střelice railway line sections. One specimen of the measuring set is permanently placed in the area of the Educational and Research Centre in Transport, Faculty of Transport Engineering, in Doubravice.

## Economical parameters

Economical asset of the measuring set resides in the ability of continuous and discrete logging of the value of longitudinal deformation of rail, which enables prediction of continuous welded rail failures – rail breaks and track bucklings. Timely prediction of such failures can lead to a modification of operational loading of rail and minimize economical loss.

## Description

The measuring set is in use at regular measurements of longitudinal deformations of continuous welded rail in operated railway lines. Its asset is a very precise determination of rail deformation in the location of track part installation. This accuracy ranges up to  $\mu\text{m}\cdot\text{m}^{-1}$ . Further assets are the lifetime of at least 1 year and no limitations for the use of track maintenance technology, except for ballast profiling and distributing machines. It is necessary to lift the brushes of the ballast profiling and distributing machine in order to save the track part of the measuring set while riding over the spot of installation.

## Figures



Figure 1: Track part of the measuring set.



Figure 2: Mobile part of the measuring set.



Figure 3: Strain gauge attachment by 1-70 fast-acting superglue.



Figure 4: Connection of track and mobile part of the measuring set during measurement.



Ministerstvo dopravy



**v y d á v á**

## **OSVĚDČENÍ**

o uznání uplatněné schválené metodiky

v souladu s podmínkami „Metodiky hodnocení výsledků výzkumných organizací a hodnocení výsledků ukončených programů“ a jejích příloh

*s názvem*

*„Nedestruktivní stanovení mechanického napětí v bezстыkové koleji“*

**ŘEŠITEL**

**Univerzita Pardubice**

**Autoři:**

**Ing. Petr Vnenk, Ing. Özgür Yurdakul, Ph.D., Ing. Jiří Šlapák, Ing. Vladimír Suchánek, Ph.D., Ing. Ondřej Sadílek, Ph.D., Ing. Filip Klejch, doc. Ing. Bohumil Culek, Ph.D., doc. Ing. Ladislav Řoutil, Ph.D.**

Metodika byla vytvořena v rámci programu Zéta, projektu č. TJ04000301, podpořeného Technologickou agenturou České republiky.

**Zpracovatelé 2 nezávislých oponentních posudků:**

- doc. Ing. Otto Plášek, Ph.D., Vysoké učení technické v Brně, Fakulta stavební
- Ing. Petr Szabó, Správa železnic, státní organizace, Generální ředitelství, odbor traťového hospodářství, oddělení železničního svršku

**JUDr. Václav Kobera**

ředitel

Odbor ITS, kosmických aktivit a výzkumu vývoje a inovací